Licensing Report

High Density Spent Fuel Racks

Grand Gulf Nuclear Station
Unit 1

TABLE OF CONTENTS

TABLE OF CONTENTS (Continued)

TABLE OF CONTENTS (Continued)

TABLE OF CONTENTS (continued)

TABLE OF CONTENTS (Continued)

LIST OF FIGURES

LIST OF FIGURES (continued)

LIST OF FIGURES (continued)

LIST OF FIGURES (continued)

LIST OF FIGURES (continued)

LIST OF TABLES

1.0 INTRODUCTION

The purpose of this report is to describe the design, fabrication, and safety analysis of High Density Spent Fuel Racks produced by Joseph Oat Corporation for Grand Gulf Nuclear Station, Unit 1 (GGNS-1). GGNS-1 is a 1250 MWe generating unit containing a General Electric Nuclear Steam Supply System of the BWR-6 Design. It is owned jointly by Middle South Energy, Inc. and Southwest Mississippi Electric Power Association and operated by Mississippi Power and Light Company (MP&L). The spent fuel racks described in this report are intended to replace the existing GGNS-1 spent fuel racks in both the Upper Containment Pool and the Spent Fuel Pool. When installed, these racks will increase the total GGNS-1 spent fuel storage capacity from the current 1440 fuel assemblies to 5148 fuel assemblies (800 in the Upper Containment Pool and 4348 in the Spent Fuel Pool). Based upon the projected GGNS-1 fuel discharge schedule presented in Table 1.1, full core discharge capability will be lost after twenty years of commercial operation with these racks installed.

Joseph Oat Corporation, in conjunction with its nuclear physics consultant Southern Science (a division of Black & Veatch), has performed detailed dynamic, seismic, thermal/hydraulic and criticality analyses of the proposed rack design under both normal and postulated accident conditions. In all cases, the results of these analyses demonstrate that acceptable margins of safety exist with respect to appropriate NRC and ASME acceptance criteria. In addition, Middle South Energy, Inc. has performed an environmental impact evaluation and a cost-benefit comparison of several potential spent fuel disposition alternatives. The results of these analyses demonstrate that reracking of the GGNS-1 Upper Containment and Spent Fuel Pools would not present a significant impact. In addition, it is shown that re-racking is the most cost-effective alternative and that neither the reracking operation nor the

increased storage of irradiated material pose an increased hazard to the Plant Staff or the public.

The following sections provide a synopsis of the design, fabrication, neutronics analysis, thermal/hydraulic analysis, structural analysis, accident analysis, environmental analysis and cost-benefit analysis of the High Density Spent Fuel Racks. In particular, the integrity of the spent fuel pool slab under the specified combinations of inertial, seismic, and mechanical loads and thermal gradient per NUREG-0800 is demonstrated. Also included are concise descriptions of the rack Inservice Surveillance Program and the Joseph Oat Corporation Quality Assurance program. The Joseph Oat Corporation Quality Assurance Program has been reviewed and found acceptable for engineered fabrication of ASME Section III Class 1, 2, 3 and MC components by both ASME and NRC.

Table 1.1 Grand Gulf Unit 1 Fuel Assembly Discharges

Year	Discharge Assemblies	Total Discharged Assemblies in Spent Fuel Pool Following Refueling	Remaining Storage Capability
1986	280	280	4068
1987	240	520	3828
1988	208	728	3620
1989	228	956	3392
1990	228	1184	3164
1991	228	1412	2936
1992	228	1640	2708
1993	228	1868	2480
1994	228	2096	2252
1995	228	2324	2024
1996	228	2552	1796
1997	228	2780	1568
1998	228	3008	1340
1999	228	3236	1112
2000	228	3464	884
2001	228	3692	656
2002	228	3920	428
2003	228	4148	200

Full core discharge in upper containment pool.

2.0 GENERAL ARRANGEMENT

The high density spent fuel racks consist of individual cells with a 6-inch-square cross section, each of which accommodates a single BWR fuel assembly. The cell walls consist of a neutron absorber sandwiched between sheets of stainless steel. The cells are arranged in modules of varying numbers of cells with a 6.26" (nominal) center-to-center spacing.

The high-density racks are engineered to achieve the dual objectives of maximum protection against structural loadings (such as ground motion) and the maximum utilization of available storage volume. In general, a greater width-to-height aspect ratio provides greater margin against rigid body tipping. Hence, the modules are made as wide as possible within the constraints of transportation and site-handling capabilities. The high-density spent fuel racks will be installed in the Unit 1 upper containment and spent fuel pools. The upper containment pool is only for interim cooling of the fuel assemblies discharged from the reactor and does not contain any fuel while the plant is operating. The fuel assemblies are transferred from this pool to the spent fuel pool for long term storage.

The Grand Gulf Unit 1 spent fuel pool will contain 16 high-density fuel racks in 5 different module sizes. The module types are labelled A,B,C,D and H in Figure 2.1, which also shows their relative placement. There will be a total of 4393 storage locations in the spent fuel pool.

The Grand Gulf Unit 1 upper containment pool will contain 8 high-density fuel racks in 3 different module sizes. The module types are labelled E through G in Figure 2.2, which also shows their relative placement. There will be a total of 800 storage locations in the upper containment pool.

Table 2.1 gives the detailed module data (e.g., weight, quantity, and number of storage locations).

Table 2.1 Module Data

Type	Quantity	Pool	Number of Cells/Module	Array Size	Approximate Weight lbs/module
A	12	SFP†	304	19x16	32,400
B	1	SFP	256	16x16	27,360
C	1	SFP	216	12x18	23,160
D	1	SFP	228	12x19	24,420
E	4	UCP††	90	9x10	9,930
F	2	UCP	99	9x11	10,880
G	2	UCP	121	11x11	13,190
H	1	SFP	45	9x5	11,300

† Spent Fuel Pool (SFP)

†† Upper Containment Pool (UCP)

The spent fuel rack modules are free standing, i.e. they are not anchored to the pool floor or connected to the pool walls through snubbers or lateral restraints.

The nominal gap between any two modules is 3 3/4 inches along the top edge for modules in the spent fuel pool and 3 15/16" for modules in the upper containment pool. The minimum gap between the spent fuel pool wall and the modules is 6 1/4 inches and 2 inches between the upper containment pool wall and the modules. Adequate clearance from other pool resident hardware is also provided. In this manner, the possibility of inter-rack impact, or rack collision with other pool hardware during the postulated ground motion events is precluded. Details on rack kinematics under seismic conditions may be found in Section 6.6.

Of the 4393 storage locations in the spent fuel pool, 4348 locations are intended for spent fuel storage. Rack Type H is designated for storage of 27 control rods, 9 control rod blade guides and 9 defective fuel storage canisters.

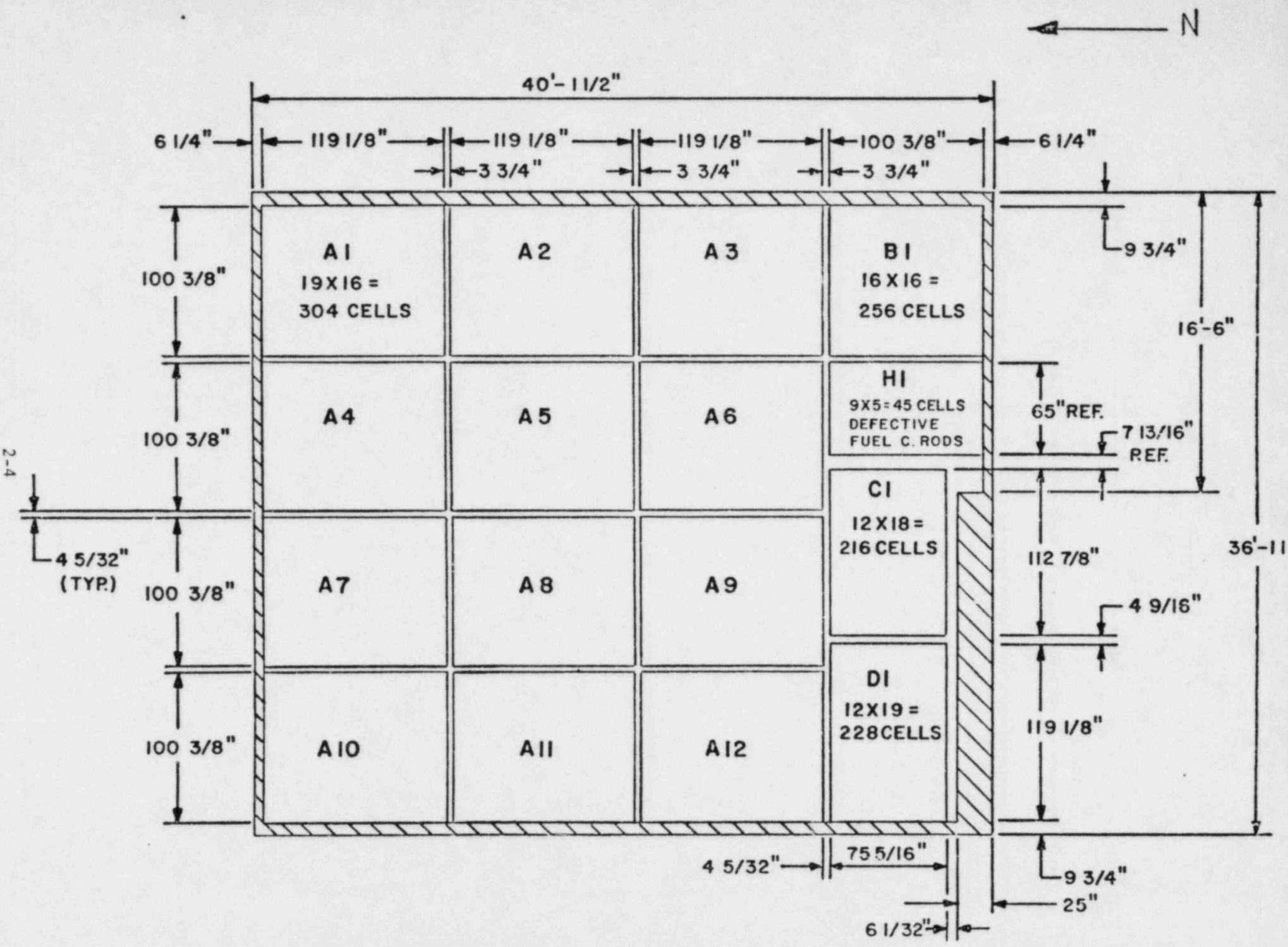

FIG 2.1- RACKS ARRANGEMENT IN SPENT FUEL POOL

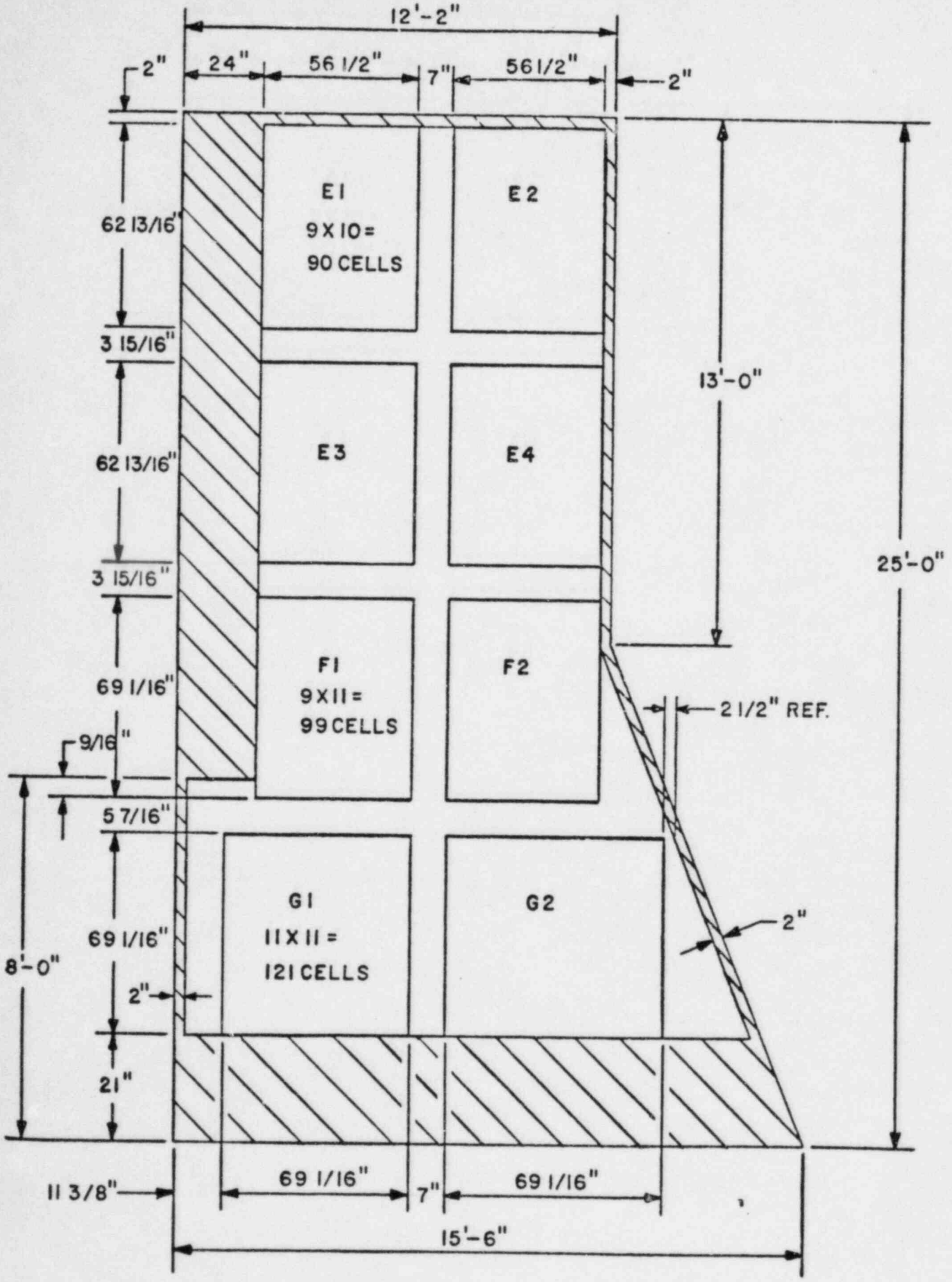

FIG. 2.2 - RACKS ARRANGEMENT IN CONTAINMENT POOL

3.0 RACK CONSTRUCTION

3.1 Construction

The racks are constructed from SA 240, Type 304, austenitic steel sheet material, SA 240, Type 304 austenitic steel plate material, and SA 182, Type F 304 austenitic steel forgings material. Boraflex, a patented brand name product of Bisco* is the neutron absorber material. The detailed radiological properties of Boraflex may be found in Section 4. The experience list of Boraflex is given in Table 3.1.

Figure 3.1 shows a horizontal cross-section of an array of 4x4 cells. As stated in the preceding section, the modules vary in array size from the smallest 9x10 array to the largest array size of 19x16. A typical module contains storage cells which have 6" nominal internal cross-sectional openings.

The cells provide a smooth and continuous surface for lateral contact with the fuel assembly. The construction of the rack modules may be best described by exposing the basic building blocks of this design, namely, the "cruciform", "ell" and "tee" elements, shown in Figure 3.2. The cruciform element is made of 4 angular sub-elements, "A" (Figure 3.3) with the neutron absorber material tightly sandwiched between the

---

* Bisco, a Division of Brand, Inc., 1420 Renaissance Drive, Park Ridge, Illinois

Table 3.1

BORAFLEX EXPERIENCE FOR HIGH DENSITY RACKS

Site	Plant Type	NRC Docket #	Licensing Status
Point Beach - 1 & 2	PWR	50-226 & 301	Issued
Nine Mile Point - 1	BWR	50-220	Issued
Oconee - 1 & 2	PWR	50-269 & 270	Issued
Prairie Island - 1 &2	PWR	50-262 & 306	Issued
Calvert Cliffs _ 2	PWR	50-318	Issued
*Quad Cities - 1 & 2	BWR	50-254 & 265	Issued
Watts Bar - 1 & 2	PWR	50-390 & 391	Pending
Waterford - 3	PWR	50-382	Issued
*Fermi - 2	BWR	50-341	Issued
H. B. Robinson - 2	PWR	50-261	Issued
River Bend - 1	BWR	50-458	Pending
*Rancho Seco - 1	PWR	50-312	Issued
Nine Mile Point - 2	BWR	50-410	Pending
Shearon Harris - 1	PWR	50-400	Pending
Millstone - 3	PWR	50-423	Pending

*Joseph Oat Corporation fabricated racks.

stainless sheets. The long edges of the cruciform are welded using a 3/8" thick stainless steel backing strip as shown in Figure 3.4. The bottom of the cruciform assembly has 7 7/8" high stainless strips, which ensure against slippage of the "poison" material downwards due to gravitational loads or operating conditions. The fabrication procedure leads to one hundred percent surface contact (in a macroscopic sense) between the poison and the stainless sheets. The top of the cruciform is also end welded using a spacer strip as shown in Figure 3.4. Continuous welding of the straight segments of the top edges produces a smooth lead-in surface. Ample venting is available through the roof openings of cell corners. This venting will preclude bulging of the cell walls due to gas entrapments.

The "ell" and "tee" elements are constructed similarly using angular sub-elements "B", and flat sub-elements "C" (Figure 3.5). Other more complicated shapes have also been used to produce the same final "cruciform" & "tee" elements. Having fabricated the required quantities of the "cruciform", "tees", and "ells", the assembly is performed in a specially designed fixture which serves the vital function of maintaining dimensional accuracy while welding all the contiguous spokes of all elements using fillet welds. Figure 3.1 shows the fillet welds. The cells are bonded to each other along their long edges, thus, in effect forming an "egg-crate".

The bottom ends of the cell walls are welded to the baseplate. Machined sleeve elements are positioned concentric with the cell center lines above the holes drilled in the base plate, and attached to the base plate through circular fillet welds (Fig. 3.6). The conical machined surface on the sleeve provides a contoured seating surface for the "nose" of the fuel assembly. Thus, the contact stresses at the fuel assembly nose bearing surface are minimized.

The central hole in the baseplate provides the coolant flow path for heat transport from the fuel assembly cladding. Lateral holes (Nom. dia. = 3/4") in the cell walls (Figure 3.6)

provide the redundant flow path in the unlikely event that the main coolant flow path is clogged. Each module is supported on four "plate-type" supports; a sketch of a typical support is shown in Figure 3.7.

The defective cell container module (module H1, Figure 2.1) employs the same structural assemblage concept, although the physical details are different. Figure 3.8 shows a horizontal cross section of this module. The individual storage locations are composed of 10.5" O.D. x 0.125" wall tubing, except for 9 containers which are 12" schedule 20S pipe (12.75" O.D. x 0.25" wall). The latter type of containers is intended for storing control rod blade guides. These are located at the short sides of the defective cell rack. The cylindrical containers are joined to each other near the top using specially shaped stainless steel stampings and at the mid-span by welding. A suitably machined baseplate provides the bottom support for the module.

The construction of the cell assembly is an integral structure which possesses extremely high flexural rigidity. Thus, the response of the module to seismic excitation simulates that of the Type A modules.

The defective fuel storage rack module is 150" high, thus, a portion of the defective fuel container will be above the module. Redundant flow paths (2 holes 1" diameter in each cell) are provided to alleviate concerns regarding main flow path clogging.

Further construction details may be found in Figures 3.8 to 3.12.

3.2 CODES, STANDARDS, AND PRACTICES FOR THE SPENT FUEL POOL MODIFICATION

The following are the public domain codes, standards, and practices to which the fuel storage racks are designed, constructed and assembled, and/or pool structure analyzed. Additional problem-specific references related to detailed analyses are given at the end of each section.

I. Design Codes

(a) AISC Manual of Steel Construction, 8th edition (1980)

(b) ANSI N210-1976, Design Objectives for Light Water Reactor Spent Fuel Storage Facilities at Nuclear Power Stations.

(c) American Society of Mechanical Engineers (ASME), Boiler & Pressure Vessel Code, Section III, 1980 Edition up to and including Winter 1981 addenda. (Subsection NF)
Note: Where the weld stresses are less than 20% of yield, the vendor visual inspection criteria will apply in lieu of NF visual inspection criteria.

(d) ASNT-TC-1A June, 1980, American Society for Nondestructive Testing (Recommended Practice for Personnel Qualifications)

(e) ANSI N412-1975, The Determination of neutron reaction rate distributions and reactivity of nuclear reactors.

II. Material Codes

(a) American Society for Testing and Materials (ASTM) Standards - A240 & A262, Practice E.

(b) American Society of Mechanical Engineers (ASME), Boiler & Pressure Vessel Code, Section II, Subsection NA, 1980 Edition up to and including Winter 1981 addenda.

III. Welding Codes

(a) ASME Boiler and Pressure Vessel Code, Section IX- Welding and Brazing Qualifications, 1980 Edition up to and including Winter 1981 addenda.

IV. Quality Assurance, Cleanliness, Packaging, Shipping, Receiving, Storage, and Handling Requirements

(a) ANSI 45.2.2, Packaging, Shipping, Receiving, Storage and Handling of Items for Nuclear Power Plants.

(b) ANSI 45.2.1, Cleaning of Fluid Systems and Associated Components During Construction.

(c) ASME Boiler and Pressure Vessel, Section V, Non-destructive Examination, 1980 Edition, including Winter 1981.

V. Other References

(a) NRC Regulatory Guides, Division 1, Regulatory Guides 1.13, 1.29, 1.60, 1.61, 1.71, 1.85, 1.92, and 1.124 (revisions as applicable).

(b) General Design Criteria for Nuclear Power Plants, Code of Federal Regulations, Title 10, Part 50, Appendix A (GDC Nos. 1, 2, 61, 62, and 63).

(c) NUREG-0800, Standard Review Plan (1981).

(d) "NRC Position for Review and Acceptance of Spent Fuel Storage and Handling Applications," dated April 14, 1978, and the modifications to this document of January 18, 1979.

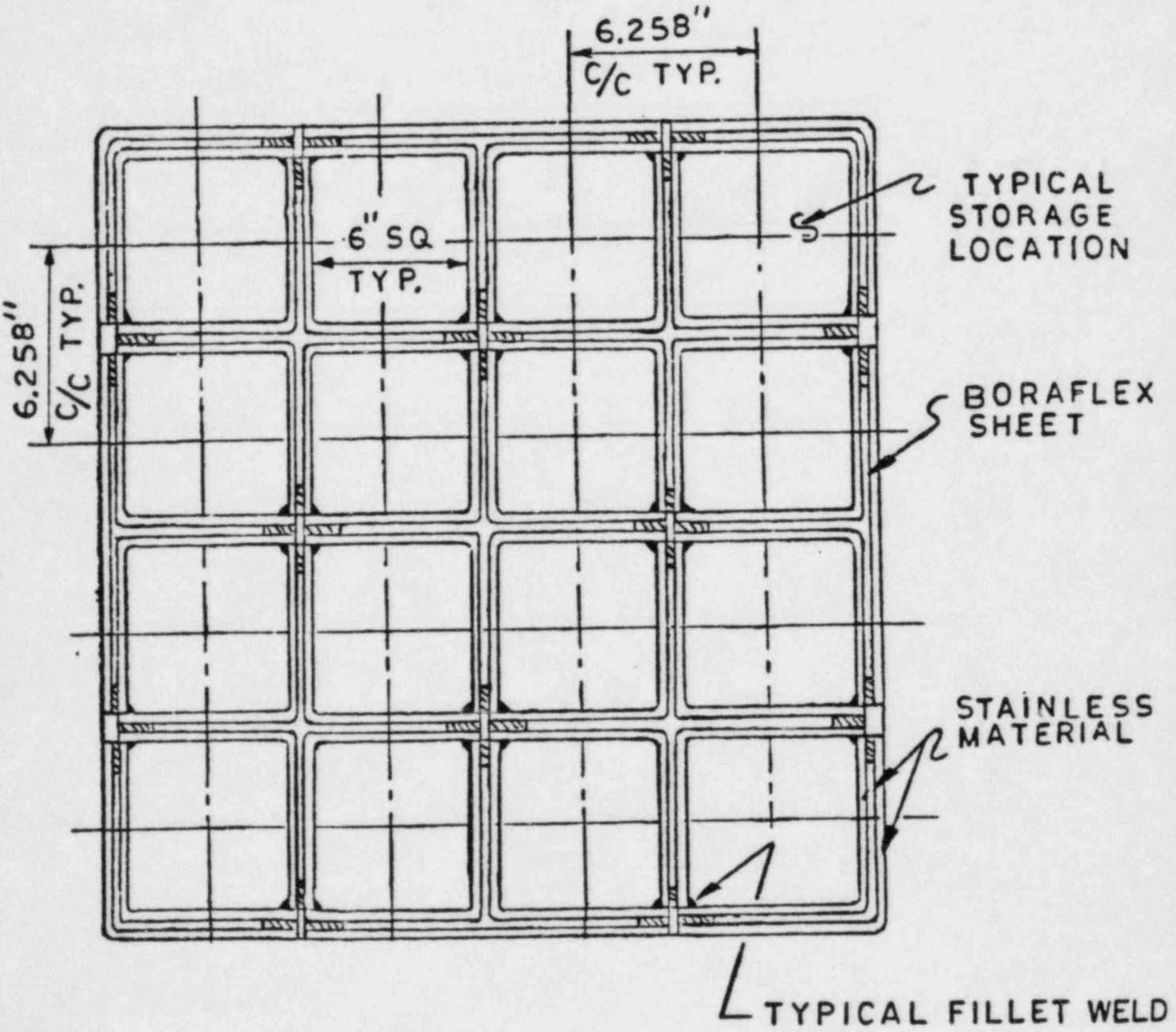

FIG. 3.1 ARRAY OF CELLS (4 X 4)

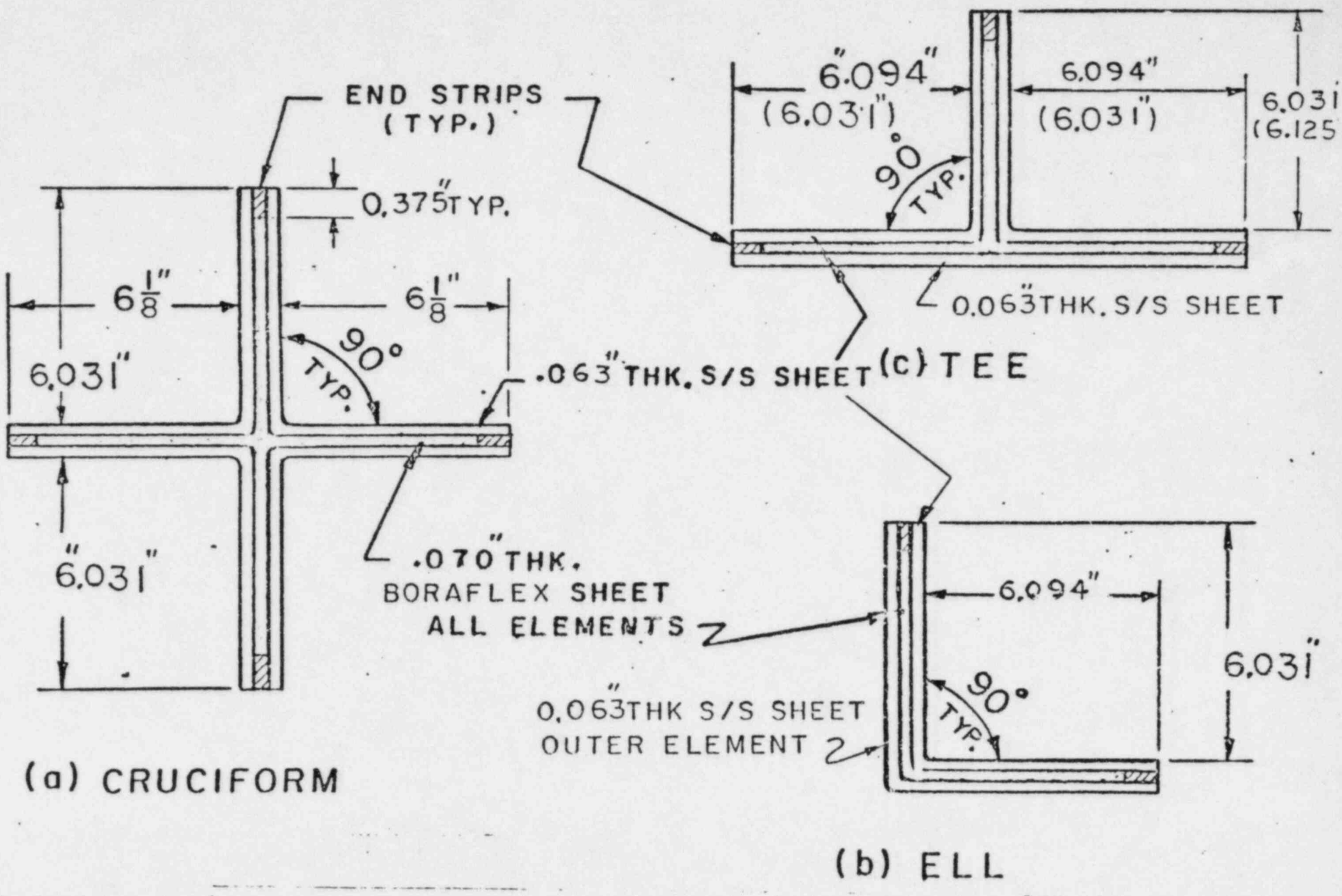

FIGURE 3.2 ELEMENTS CROSS SECTION

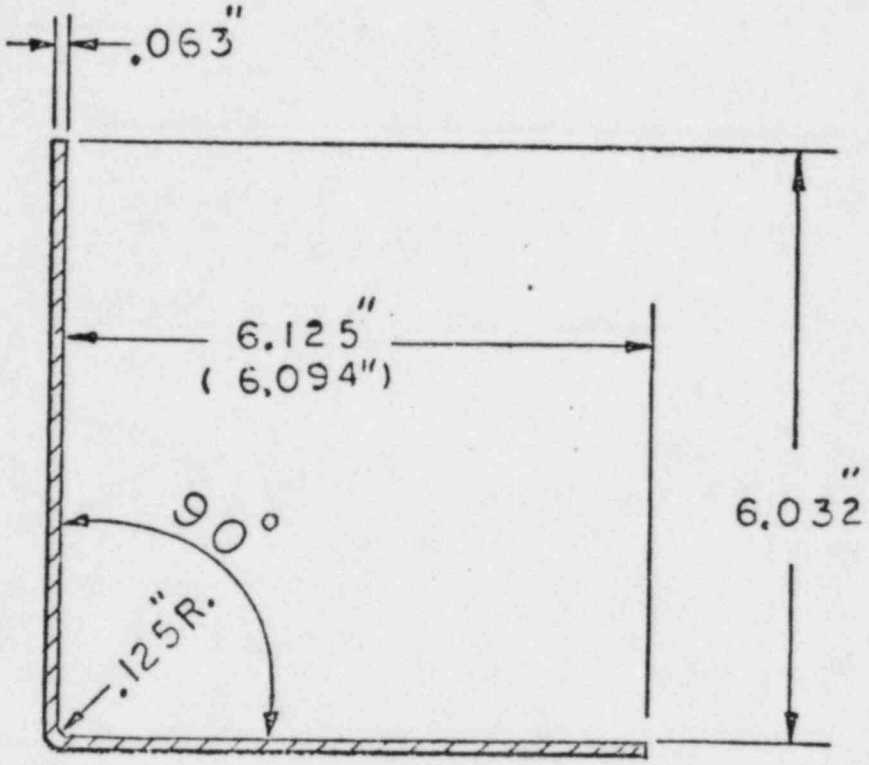

FIG. 3.3 ANGULAR
SUB ELEMENT 'A'

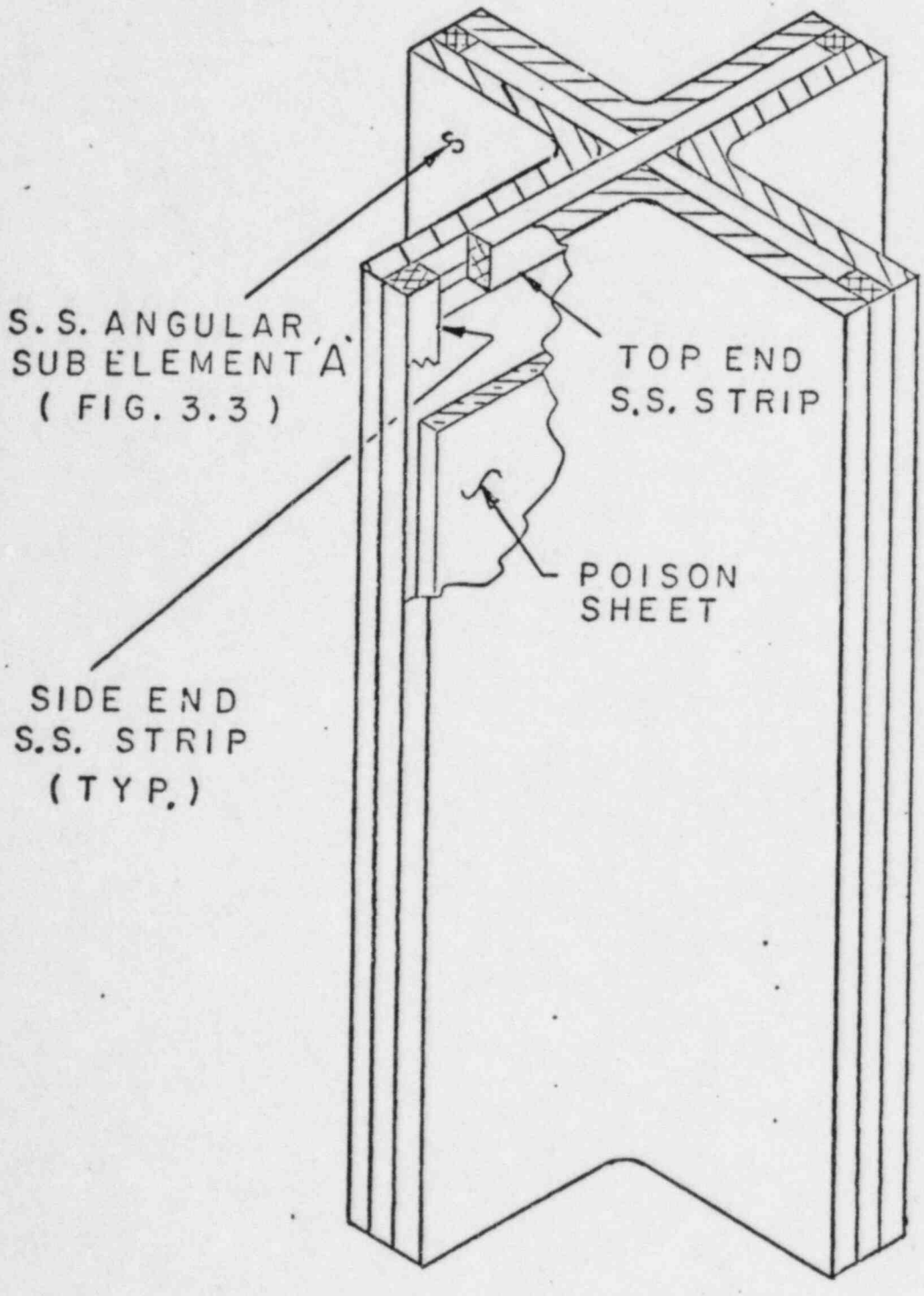

FIG. 3.4 CRUCIFORM ELEMENT (ISOMETRIC VIEW)

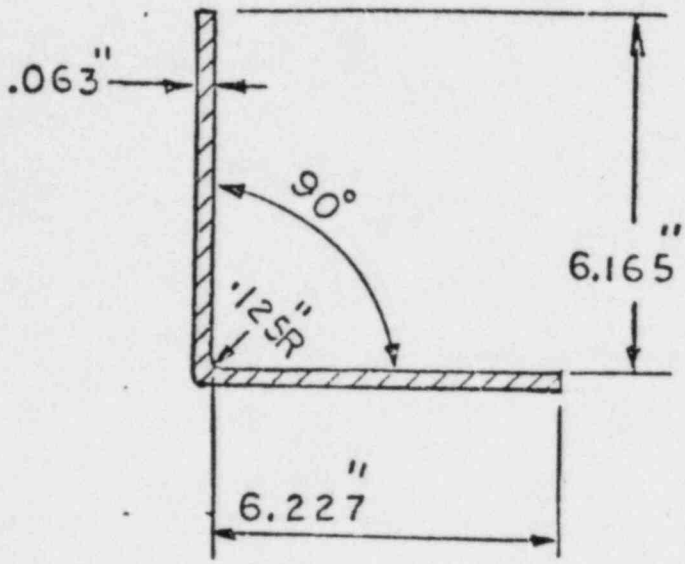

(a) ANGULAR SUB ELEMENT 'B'

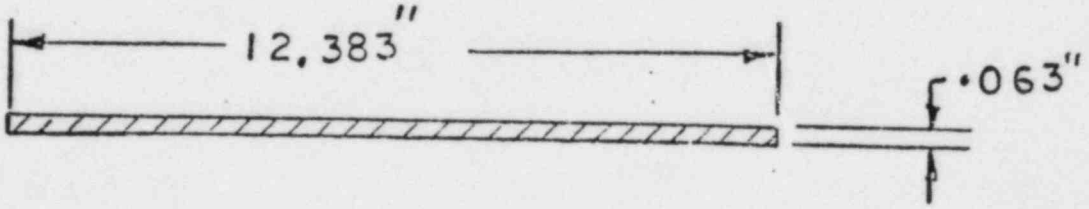

(b) FLAT SUB ELEMENT 'C'

FIG. 3.5 SUB ELEMENTS

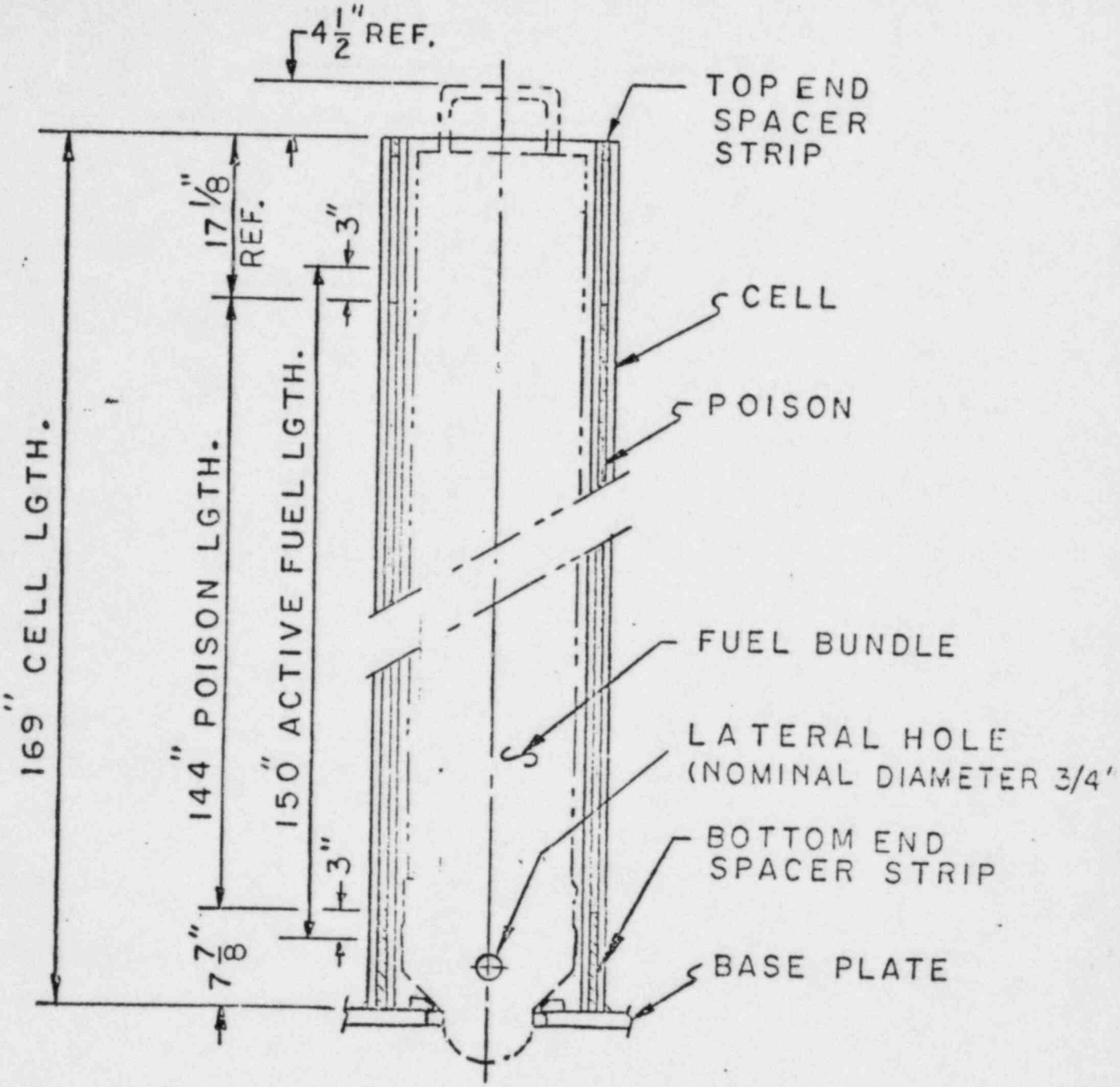

FIG. 3.6 TYPICAL CELL ELEVATION

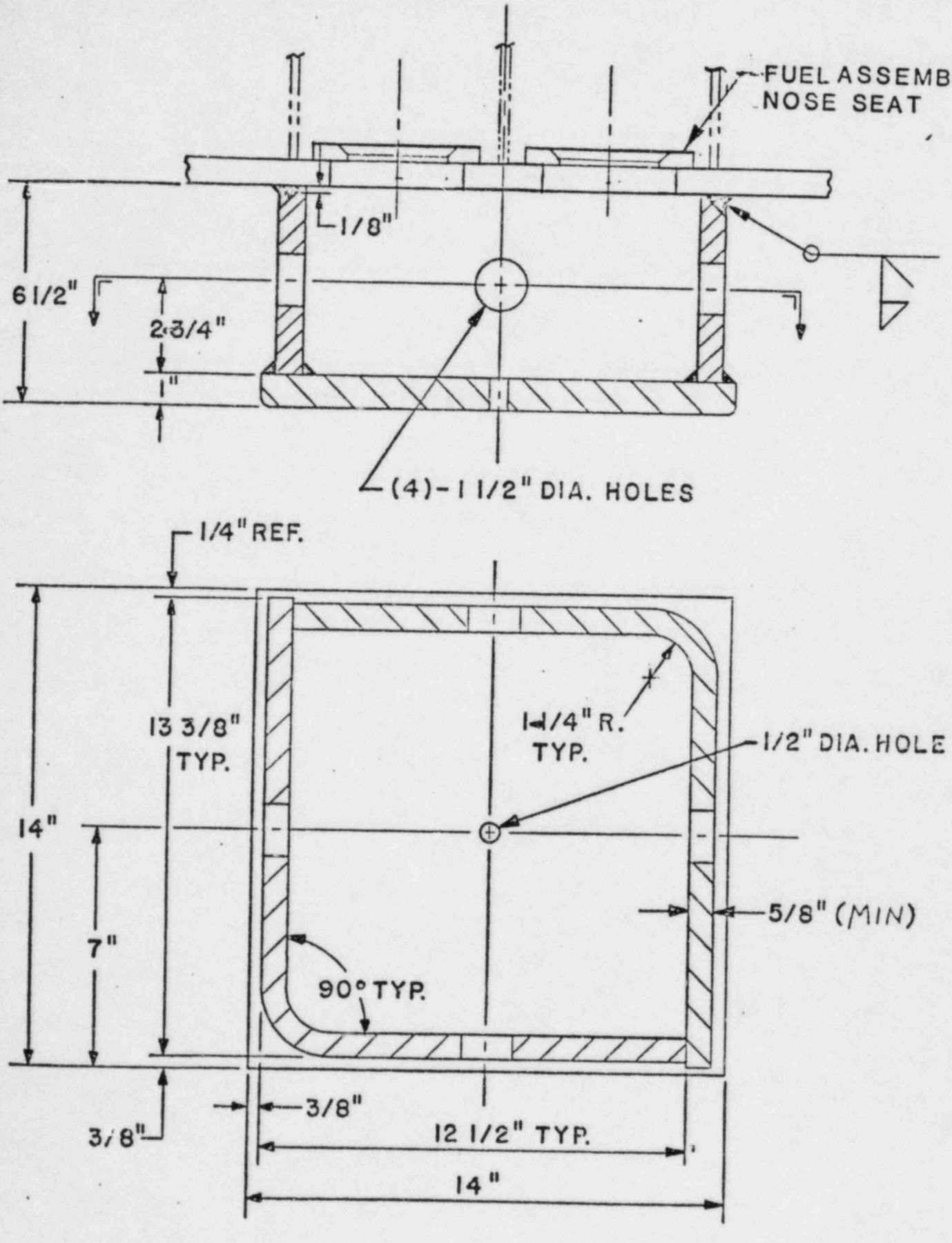

FIG. 3.7 – SUPPORT

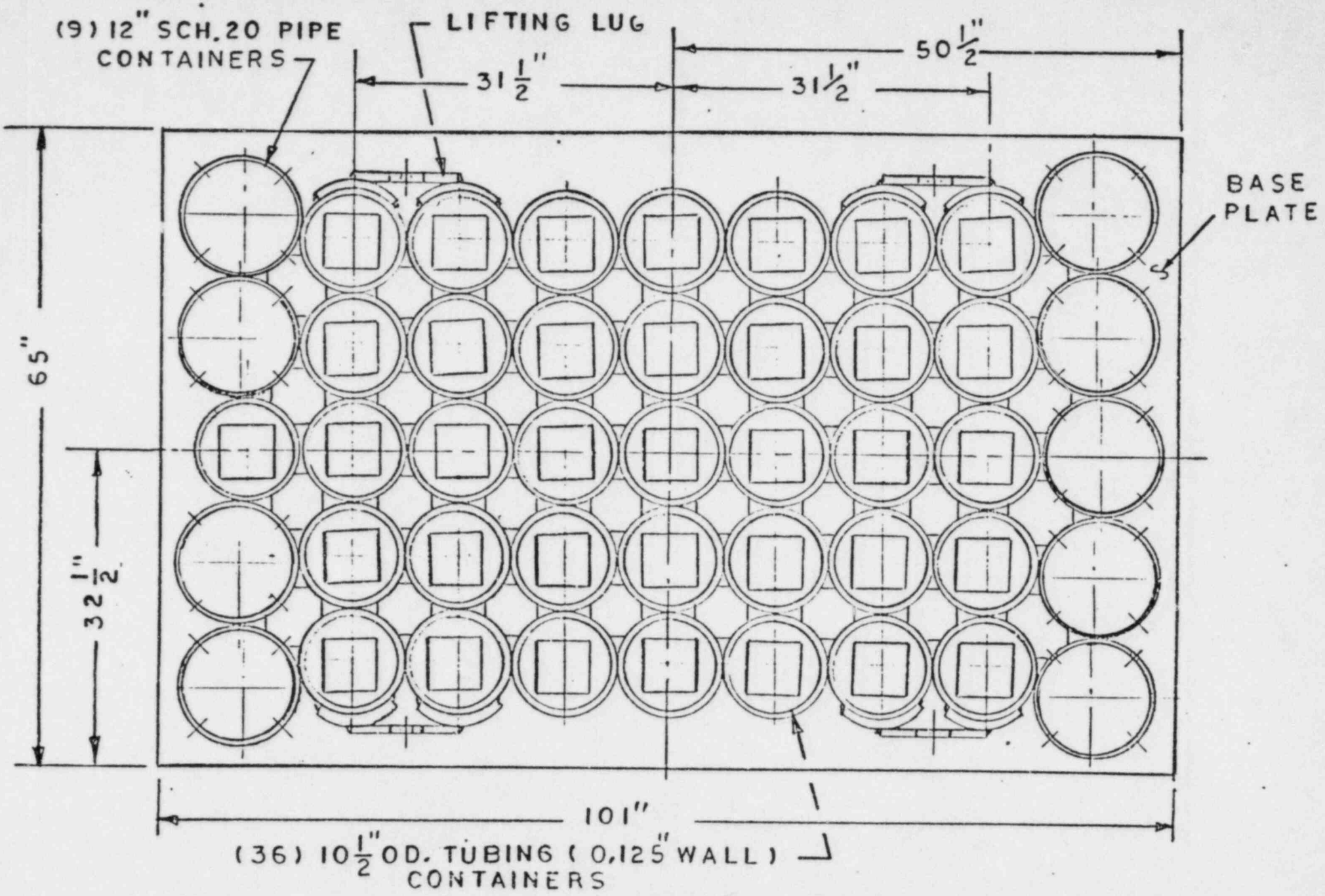

FIG. 3.8 TOP VIEW EQUIP. STORAGE RACK

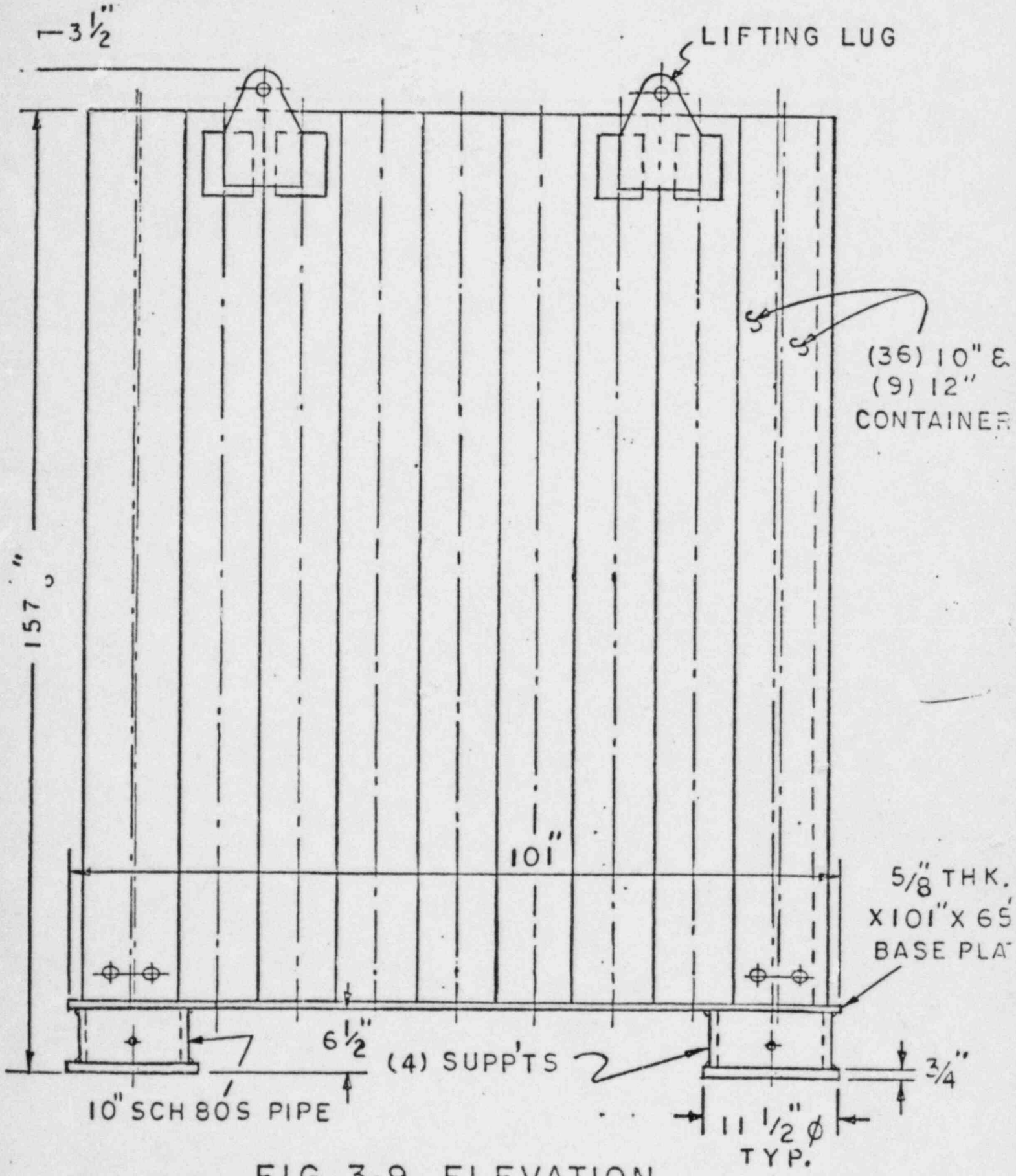

FIG. 3-9 ELEVATION

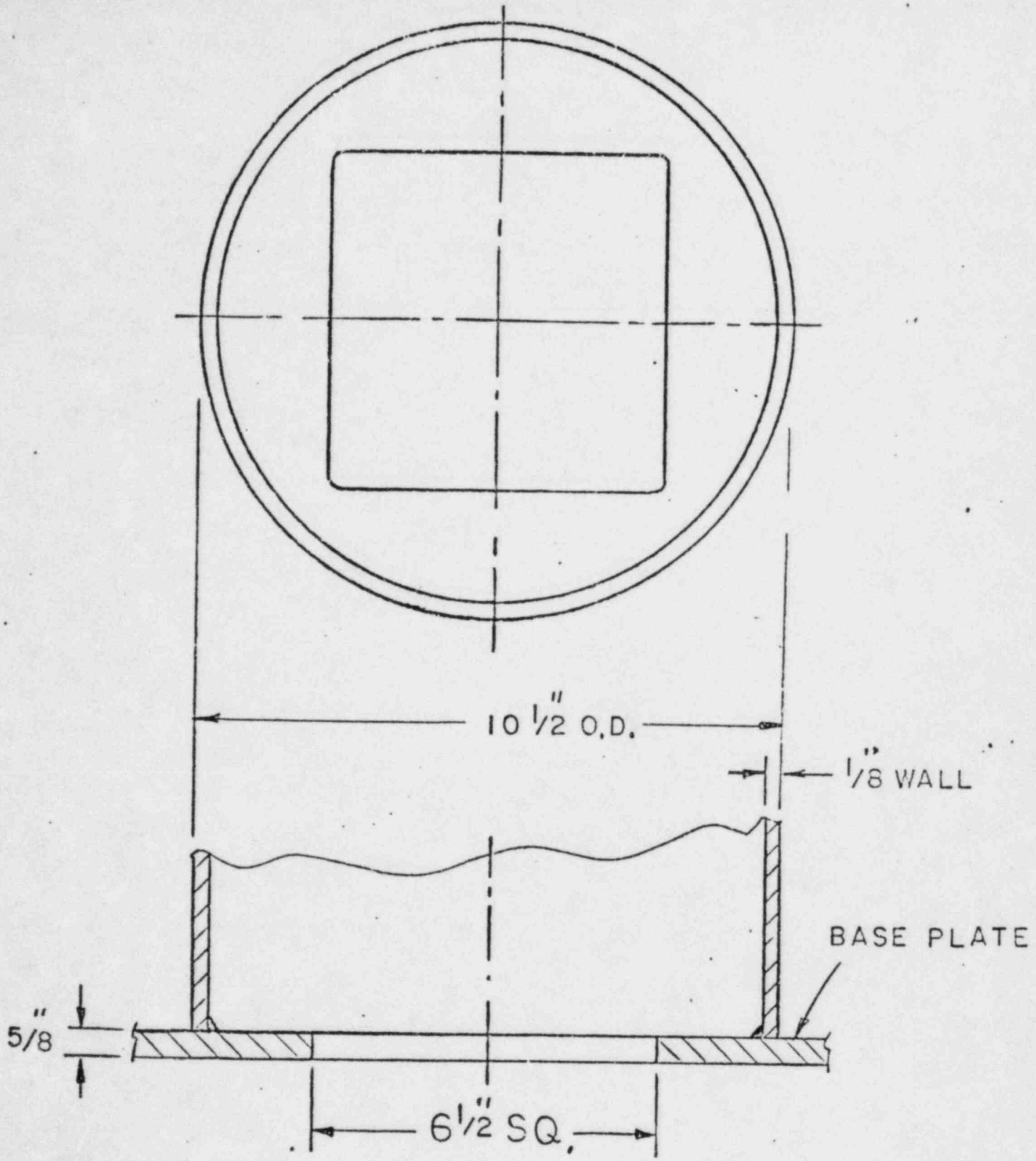

FIG. 3.10 BOTTOM DETAIL
10" SIZE CONTAINER

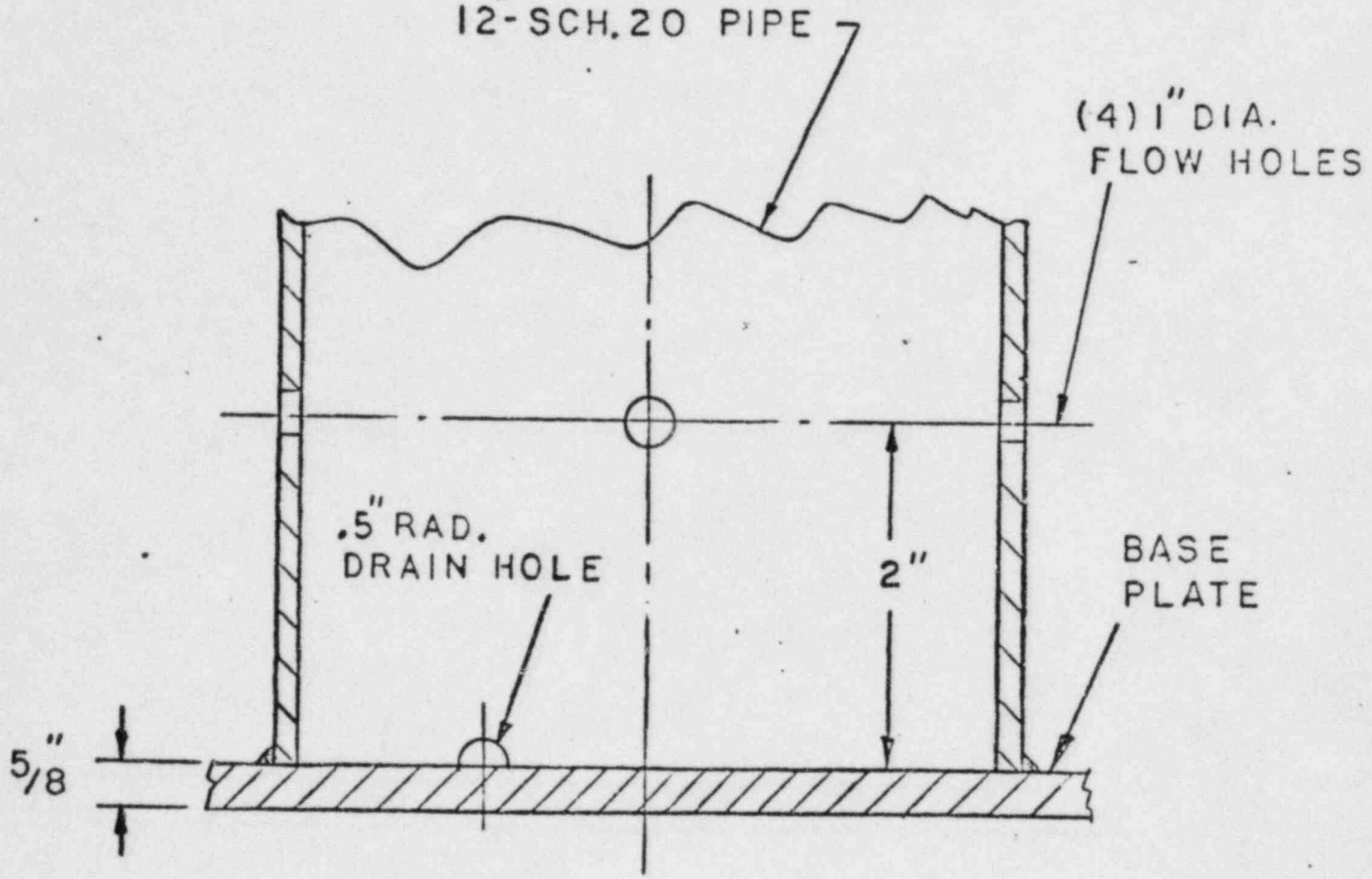

FIG. 3.11 BOTTOM DETAIL
12" SIZE CONTAINER

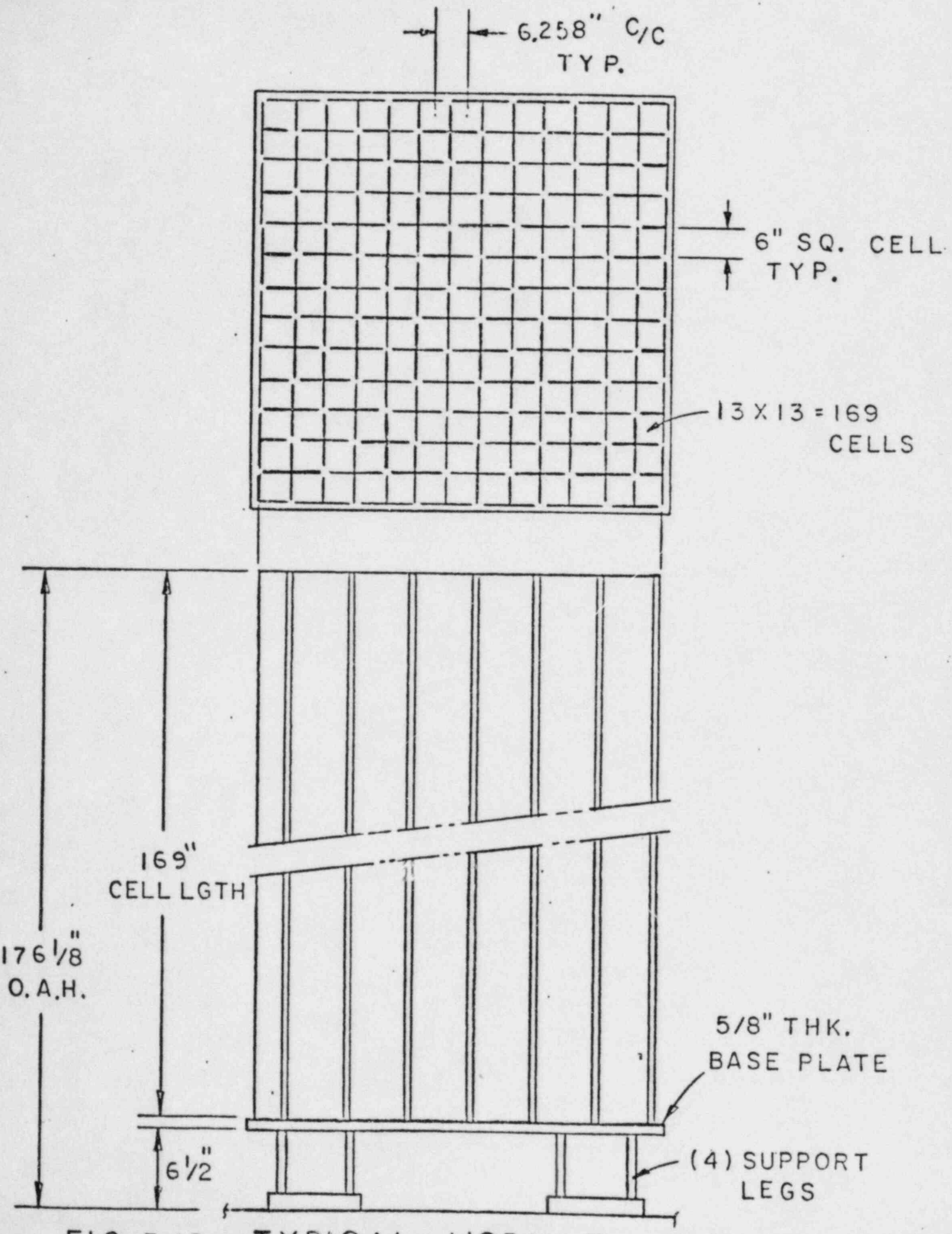

FIG. 3.12 TYPICAL MODULE

4. NEUTRONIC CONSIDERATIONS

4.1 Introduction

The spent fuel storage racks are designed to assure that a k_{eff} equal to or less than 0.95 is maintained with the racks fully loaded with fuel of the highest anticipated reactivity and flooded with unborated water at a temperature corresponding to the highest reactivity. The maximum calculated reactivity includes a margin for uncertainty in reactivity calculations and in mechanical tolerances, statistically combined, such that the true k_{eff} will be equal to or less than 0.95 with a 95% probability at a 95% confidence level.

Applicable codes, standards and regulations or pertinent sections thereof include the following:

- General Design Criterion 62 - Prevention of Criticality in Fuel Storage and Handling.
- NRC letter of April 14, 1978, to all Power Reactor Licensees - OT Position for Review and Acceptance of Spent Fuel Storage and Handling Applications, including modification letter dated January 18, 1979.
- USNRC Standard Review Plan, NUREG-0800, Section 9.1.2, Spent Fuel Storage.
- Regulatory Guide 1.13, Spent Fuel Storage Facility Design Basis (Draft, Revision 2), December 1981.
- Regulatory Guide 3.41, Validation of Calculational Method for Nuclear Criticality Safety (and related ANSI N16.9-1975).
- ANSI N210-1976, Design Objectives for Light Water Reactor Spent Fuel Storage Facilities at Nuclear Power Plants.
- ANSI N18.2-1973, Nuclear Safety Criteria for the Design of Stationary Pressurized Water Reactor Plants.

The design basis fuel assembly is a standard 8 x 8 array of fuel rods (BWR type) containing UO_2 clad in Zircaloy. Fixed neutron absorbing material is used in the spent fuel storage racks to maintain the required margin in subcriticality. The spent fuel racks are designed to safely accommodate fuel assemblies with a maximum infinite multiplication factor (k_∞) of 1.395, as calculated for the standard core configuration in the cold, unrodded condition.

To assure the true reactivity will always be less than the calculated reactivity, the following conservative assumptions were made.

- Moderator is pure, unborated water at a temperature corresponding to the highest reactivity.
- Lattice of storage racks is infinite in all directions; i.e., no credit is taken for axial or radial neutron leakage, except in the evaluation of axial cutback and for certain abnormal conditions where neutron leakage is inherent.
- No credit is taken for the presence of gadolinium burnable poison or for the reduction in reactivity that accompanies fuel burnup.
- Neutron absorption in minor structural members is neglected; i.e., spacers and Inconel springs are replaced by water.
- Pure zirconium is used for cladding and flow channel; i.e., higher neutron absorption of alloying materials in Zircaloy is neglected.

4.1.1 Neutron Multiplication Factor

The nominal design case assumes fuel of uniformly distributed 3.5 wt% U-235 enrichment, corresponding to 16.49 grams U-235 per axial centimeter of fuel assembly. Fixed neutron absorber material (Boraflex) of 0.02041 g/cm^2 boron-10 areal density is positioned between fuel assemblies in an egg-crate

structure that provides a nominal center-to-center lattice spacing of 6.2585 inches for the storage cell locations. The maximum infinite multiplication factor (k_∞) calculated for the nominal design case is 0.936 including all uncertainties (95% probability at a 95% confidence level) for fuel of 3.5% uniform enrichment (k_∞ of fuel assembly in standard core geometry* of 1.3798 ± 0.0037).

With the configuration described above, the spent fuel storage rack can safely accommodate fuel assemblies whose maximum infinite multiplication factor in the standard reactor core geometry (cold conditions) is 1.395, without exceeding the limiting design criterion for spent fuel storage racks (maximum k_∞ of 0.95 including all uncertainties).

The calculations and uncertainties, supporting the criticality safety of the spent fuel storage racks for Grand Gulf Nuclear Station Unit 1, are summarized in Table 4-1, and described in Section 4.4, Criticality Analysis.

4.1.2 Analytical Methods

The reference method for nuclear criticality analyses of the high density spent fuel storage rack is the AMPX[1]-KENO[2] computer package, using the 123-group GAM-THERMOS cross-section set and the NITAWL subroutine for U-238 resonance shielding effects (Nordheim integral treatment). AMPX-KENO has been extensively benchmarked against a number of critical experiments (e.g., Refs. 3, 4, 5 and 6).

---

*In the standard reactor core geometry, fuel assemblies at 39.6°F are located on a 6.00 inch center-to-center spacing, surrounded by full density (ρ=1.0) water, with all control blades removed and with no credit for the presence of gadolinium burnable poison.

Table 4-1 SUMMARY OF CRITICALITY ANALYSIS

		Nominal Design Case	Maximum Storage Capability
k_∞ in standard core geometry		1.3798 ± 0.0037 (1σ)	1.395
k_∞ in spent fuel storage rack		0.9216	0.935
Calculational bias, Δk		0.0036	0.0036
Uncertainties and tolerances			
Calculational bias	±0.0028 Δk		
Calculation (statistical)	±0.0048 Δk		
Boraflex thickness	∓0.0059 Δk		
B-10 concentration	∓0.0027 Δk		
Boraflex width	∓0.0016 Δk		
Fuel enrichment	±0.0032 Δk		
Fuel density	±0.0024 Δk		
Pellet diameter	negligible		
Lattice pitch	∓0.0040 Δk		
SS thickness	±0.0011 Δk		
Flow channel bulge	±0.0047 Δk		
	±0.0114		
Statistical combination		±0.0114	±0.0114
Maximum k_∞		0.937	0.950
Abnormal/accident condition Δk			
Temperature increase			negative Δk
Boiling			negative Δk
Reduced moderator density			negative Δk
Fuel assembly positioning			negative Δk
Assembly outside rack			negligible Δk
Dropped fuel assembly			negligible Δk

For two-dimensional X-Y analysis, a zero current (reflecting) boundary condition was applied in the axial direction and at the centerline through the Boraflex absorber on all four sides of the cell, effectively creating an infinite array of storage cells for analytical purposes.

For investigation of small reactivity effects (e.g., mechanical tolerances), a four-group diffusion/blackness theory method of analysis was used (Ref. 5) to calculate small incremental reactivity changes. This model has been used previously with good results and is normally used only to evaluate trends and small incremental reactivity effects that would otherwise be lost in the KENO statistical variation. Where possible, trends calculated by AMPX-KENO and by diffusion/blackness theory were compared and found to be in good agreement, within the statistical uncertainty of KENO calculations.

4.1.3 Calculational Bias and Uncertainty

Results of benchmark calculations[6] on a series of critical experiments indicate a calculational bias of 0, with an uncertainty of ±0.0028 (95% probability at a 95% confidence level). In addition, a small correction in the calculational bias is necessary to account for the slightly greater gap thickness (1.1 inches) between fuel assemblies in the Grand Gulf spent fuel rack compared to the corresponding thickness (0.644 inch) in the benchmark critical experiments. Based upon the correlation developed in Ref. 6, the correction for water-gap thickness in the Grand Gulf spent fuel storage rack indicates a small underprediction of 0.0036 Δk. Thus, the net calculational bias is taken as 0.0036 ± 0.0028, including the effect of the water-gap thickness.

4.1.4 Trend Analysis

Trend analysis[6] of benchmark calculations on critical experiments with varying boron content in the absorber plate between fuel assemblies indicates a tendency to overpredict k_{eff} with higher reactivity worth of the boron absorber. In the Grand Gulf spent fuel rack, the boron worth is about 40% Δk, or ~2.7 times the highest boron worth (15.9% Δk) in the critical experiments analyzed in Ref. 6. Based upon extrapolation of the trend analysis, AMPX-KENO calculations of the Grand Gulf rack would be expected to overpredict k_∞ by an estimated 3.1% Δk, including allowance for water-gap thickness. Statistically combining the standard deviation of the regression analysis [6] ($\pm 0.003, 1\sigma$) and a typical standard deviation of the KENO variation of the mean ($\pm 0.003, 1\sigma$), the maximum uncertainty would be ± 0.008, including a one-sided tolerance factor[7] of 1.92 (95% probability at a 95% confidence level) for 100 generations in a KENO calculation. Thus, to the extent extrapolation of the linear regression analysis is valid, the AMPX-KENO calculation of the Grand Gulf rack will be high (overprediction) by 0.031 ± 0.008 Δk, or a minimum overprediction of 0.023 Δk including calculational uncertainty. Although extrapolation of the regression trend much beyond the range of the measurements may be questionable, the analysis does indicate that AMPX-KENO calculations would be expected to overpredict k_{eff} when strong boron absorbers are present. No credit is taken for the expected overprediction other than to indicate an additional level of conservatism in the criticality analysis of the Grand Gulf spent fuel storage rack.

4.2 Input Paramaters

4.2.1 Fuel Assembly Design Specifications

Design specifications for the fuel assembly as used in the criticality analysis are given in Table 4-2. Assemblies containing fuel rods of slightly different dimensions or configuration may be safely accommodated in the high density spent fuel storage racks, provided the assembly k_∞ in the standard core geometry is within the limit established in the criticality analysis.

4.2.2 Reference Design Spent Fuel Storage Cell

The nominal spent fuel storage cell model used in the criticality analyses is shown in Fig. 4.1. The rack is composed of Boraflex absorber material sandwiched between 0.063-inch stainless-steel plates. The fuel assemblies are centrally located in each storage cell on a nominal lattice spacing of 6.2585 inches. The Boraflex absorber has a nominal thickness of 0.070 inch and a nominal B-10 areal density of 0.02041 grams B-10 per square centimeter.

Table 4-2 FUEL ASSEMBLY DESIGN SPECIFICATIONS

Fuel Rod Data	
Outside dimension, in.	0.484
Cladding thickness, in.	0.035
Cladding material	Zr-2
Pellet density, g UO_2/cc	10.367 ± 0.165
Pellet diameter, in.	0.4055
Enrichment, wt% U-235	3.50* ± 0.05
Grams U-235 per axial centimeter	16.52
Water Rod Data	
Outside diameter, in.	0.591
Wall thickness	0.030
Material	Zr-2
Number per assembly	2
Fuel Assembly Data	
Number of fuel rods	62
Fuel rod pitch, in.	0.636
Fuel channel outside dimension, in.	5.458 ± 0.0065
Fuel channel wall thickness, in.	0.120
Fuel channel material	Zr-4

* Nominal design case

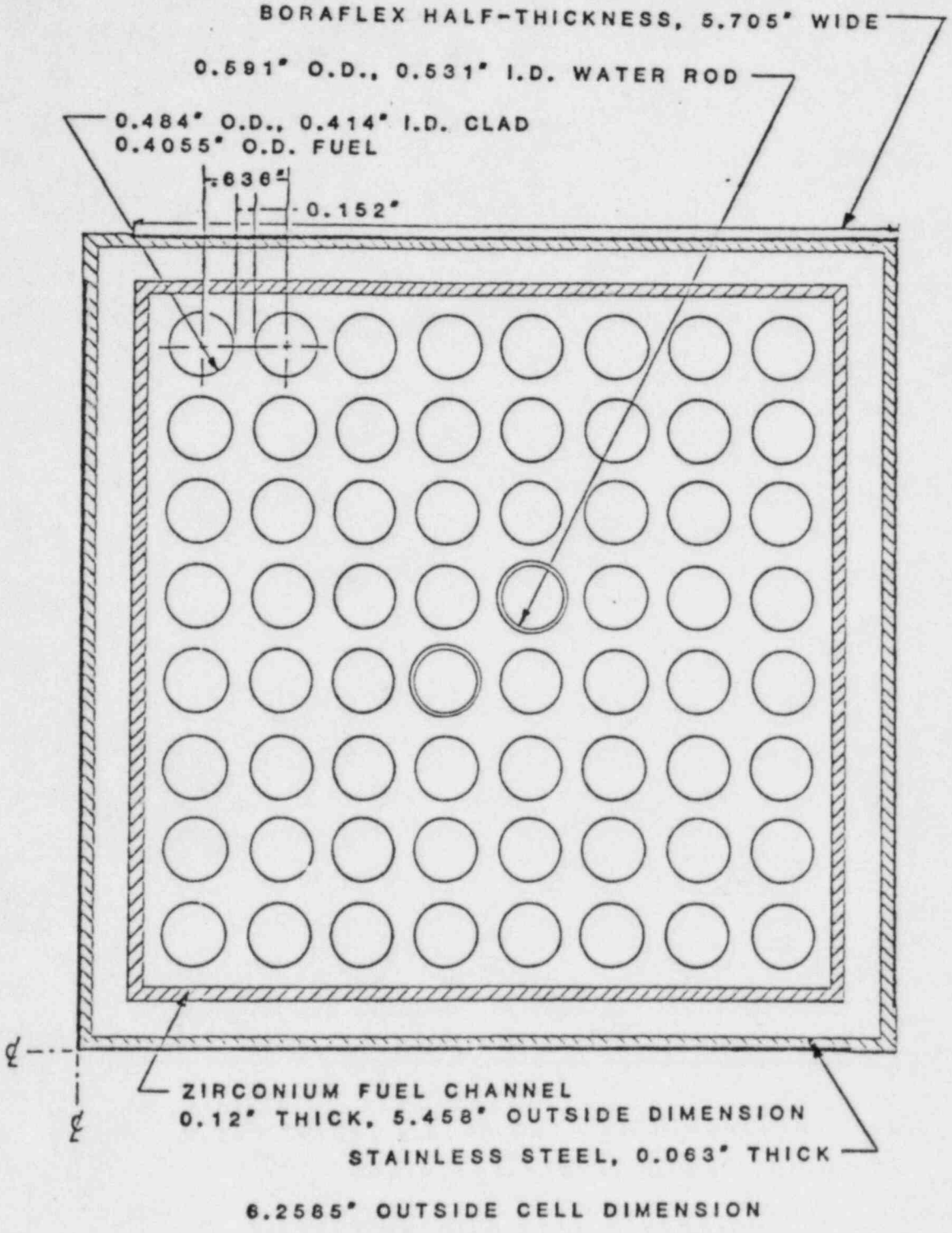

Fig. 4.1 Geometric model of Grand Gulf spent fuel storage rack cell.

4.3 Postulated Accidents and Abnormal Conditions

4.3.1 Temperature and Water Density Effects

The nominal criticality analyses were performed for the maximum water density (ρ=1.0) corresponding to a temperature of ~39°F. As shown in Table 4-3, increasing temperature or introducing void (to simulate boiling) decreased reactivity of the spent fuel storage rack.

Since the storage rack may also accommodate the initial core loading in the dry condition, calculations were made for moderation by water of reduced density to investigate the reactivity effect of hypothetical moderation (foam or spray) of the dry storage cells in conformance with the requirements of SRP 9.1.1. As indicated in Table 4-3, the maximum reactivity occurs for the fully flooded case (reference design configuration) and the reactivity is always substantially lower than the reference k_∞ for all other moderating conditions. As shown in Fig. 4.2, the calculated k_∞ decreases continuously down to 10% moderator density, with no suggestion of a reversal in slope or the appearance of a second maximum in reactivity. These results are consistent with those reported by Cano et al.,[8] who showed, in a parametric study, that the phenomenon of a second maximum in reactivity does not occur in a closely-spaced lattice with a strong neutron absorber present. Thus the spent fuel storage rack will accommodate the initial core loading in the dry condition well within the requirements of SRP 9.1.1.

Table 4-3 EFFECT OF TEMPERATURE AND VOID ON REACTIVITY OF STORAGE RACK

Case	Δk_∞	Comment
39°F (~4°C)	Reference	Maximum water density
68°F (20°C)	-0.0006	$\rho(H_2O) = 0.998$
104°F (40°C)	-0.005	$\rho(H_2O) = 0.992$
176°F (80°C)	-0.015	$\rho(H_2O) = 0.972$
212°F (100°C)	-0.020	$\rho(H_2O) = 0.958$
212°F with 50% void	-0.184	Simulates boiling
39°F (4°C), 50% density	-0.166	Simulates hypothetical reduced density moderation of cells containing an infinite array of fuel assemblies of the nominal enrichment.
39°F (4°C), 40% density	-0.219	
39°F (4°C), 30% density	-0.276	
39°F (4°C), 20% density	-0.340	
39°F (4°C), 10% density	-0.405	

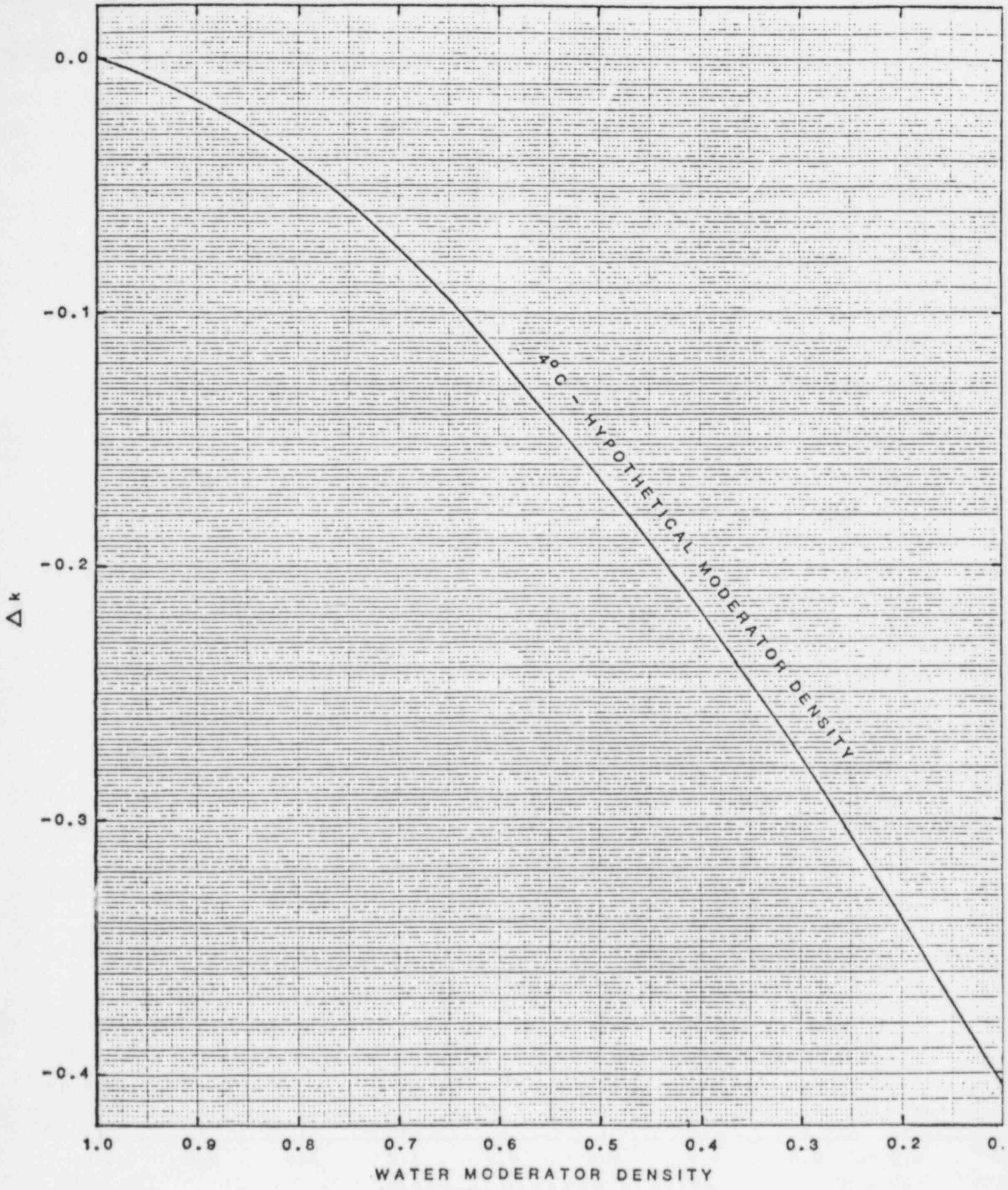

Fig. 4.2 Δk versus H_2O density.

4.3.2 Abnormal Positioning of Fuel Assembly Outside Storage Rack

Since the storage rack criticality calculations were made assuming an infinite array of storage cells with no neutron leakage, positioning a fuel assembly outside and adjacent to the actual finite rack cannot add reactivity, but would, because of neutron leakage, result in a lower k_{eff} than the k_{∞} calculated for the infinite array. This has been confirmed by two-dimensional PDQ analysis of finite racks with a fresh fuel element positioned outside the rack.

4.3.3 Fuel Assembly Positioning in Storage Rack

The fuel assembly is normally located in the center of the storage rack cell with bottom fittings and spacers that mechanically prevent lateral movement of the fuel assemblies. Nevertheless, calculations were made with adjacent fuel assemblies (each assumed to be located on one side of its cell with the zirconium fuel channel touching the SS-Boraflex plate) creating an infinite series of two-assembly clusters separated only by the SS-Boraflex plate. For this case, the calculated reactivity was slightly less than the nominal design case (by 0.010 Δk). Calculations were also made with the fuel assembly moved into the corner of the storage rack cell (four-assembly cluster at closest approach), resulting in an even larger negative reactivity effect (calculated decrease in k_{∞} of 0.015 Δk). With the zirconium fuel channel removed, the reactivity effect of off-set fuel assemblies is even more negative. Thus, the nominal case, with the fuel assembly positioned in the center of the storage rack cell, yields the maximum reactivity.

4.3.4 Effect of Zirconium Fuel Channel Distortion

Consequences of bulging of the zirconium fuel channel are treated as a mechanical deviation in Section 4.4.9 below. Bowing of the zirconium channel (including fuel rods) results in a local negative reactivity effect analogous to that of positioning the fuel asembly toward one side of the storage cell, as described in Section 4.3.3 above. Thus, bowing will result in a reduction in reactivity.

4.3.5 Dropped Fuel Assembly Accident

To investigate the possible reactivity effect of postulated fuel drop accidents, calculations were made for unpoisoned assemblies separated only by water. Figure 4.3 shows the results of these calculations. From these data, the reactivity (k_∞) will be less than 0.95 for any spacing between unpoisoned assemblies greater than ~8 inches. For a dropped fuel assembly lying horizontally on top of the rack, the minimum separation distance is ~14 inches. Maximum expected deformation under seismic or accident conditions (see Section 6) will not reduce the minimum spacing to less than 8 inches. Thus, a dropped fuel assembly will not constitute a criticality hazard, and the storage rack infinite multiplication factor will not be materially altered.

4.3.6 Fuel Rack Lateral Movement

Normally, the individual rack modules in the spent fuel pool are separated by a water-gap of several inches. For finite fuel racks, this separation would reduce the actual maximum reactivity of the racks. Should lateral motion of a fuel rack occur, closing the gap between racks (for whatever reason), the reactivity would, in the limit, only approach the limiting reactivity of the reference infinite array.

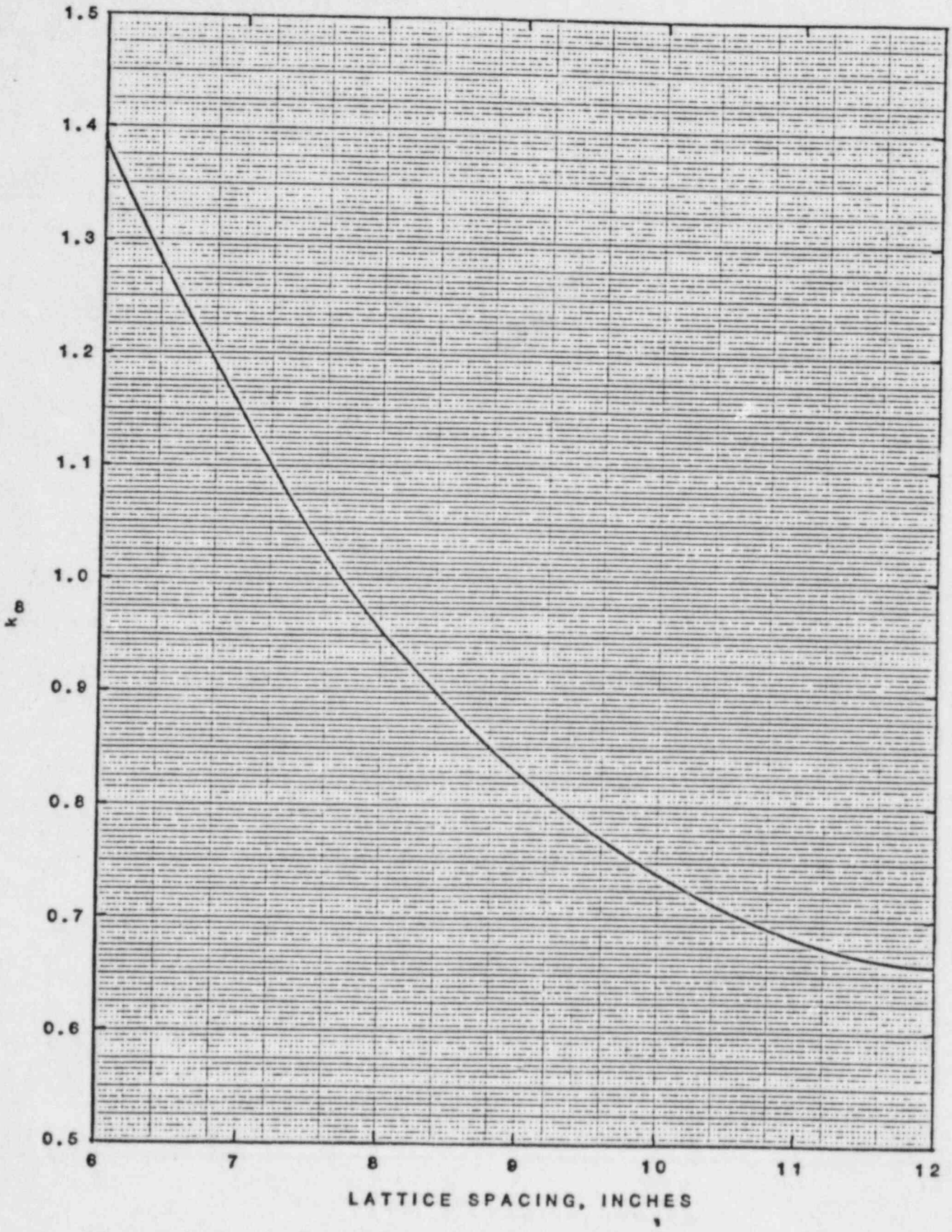

Fig. 4.3 k_∞ of unpoisoned fuel assemblies as a function of assembly spacing.

4.4 Criticality Analysis

4.4.1 Nominal Case

Under normal conditions, with nominal dimensions, the calculated k_∞ is 0.9216 ± 0.0026 (1σ with 150 generations) with fuel of 3.5% uniform enrichment. For a one-sided tolerance factor of 1.868, corresponding to 95% probability at a 95% confidence limit for 150 generations, the maximum deviation of k_∞ is ±0.0048. With the calculational bias and all uncertainties added, the reactivity (k_∞) of the storage racks will always be less than 0.937 with 95% probability at a 95% confidence level. Calculations with fuel of distributed enrichments (average 3.5% enrichment), representative of BWR-type fuel assemblies, showed a lower reactivity than the corresponding calculation with uniform enrichment.

4.4.2 Maximum Reactivity Storage Capability

For uniform enrichment of 3.5 wt% U-235 (k_∞ of 1.3798 in standard core geometry) and the selected Boraflex loading (0.02041 g B-10/cm^2 nominal, 0.0175 g B-10/cm^2 minimum), there is a margin of 0.013 Δk between the limiting reactivity (k_∞ of 0.95) and the calculated reactivity including all uncertainties. Additional calculations were performed to determine the maximum reactivity fuel which the racks could safely accommodate without exceeding the limiting reactivity. Figure 4.4 shows the calculated relationship between the fuel k_∞ (standard core geometry) and the infinite multiplication factor of the spent fuel storage racks. These calculations indicate that fuel with a k_∞ of 1.395 (reactor core geometry) can be safely accommodated and that the maximum k_∞ of the storage rack will not exceed 0.950, including all uncertainties, with 95% probability at a 95% confidence level. A fuel k_∞ of 1.395 in the standard core geometry corresponds to a uniform fuel enrichment of ~3.7 wt% U-235.

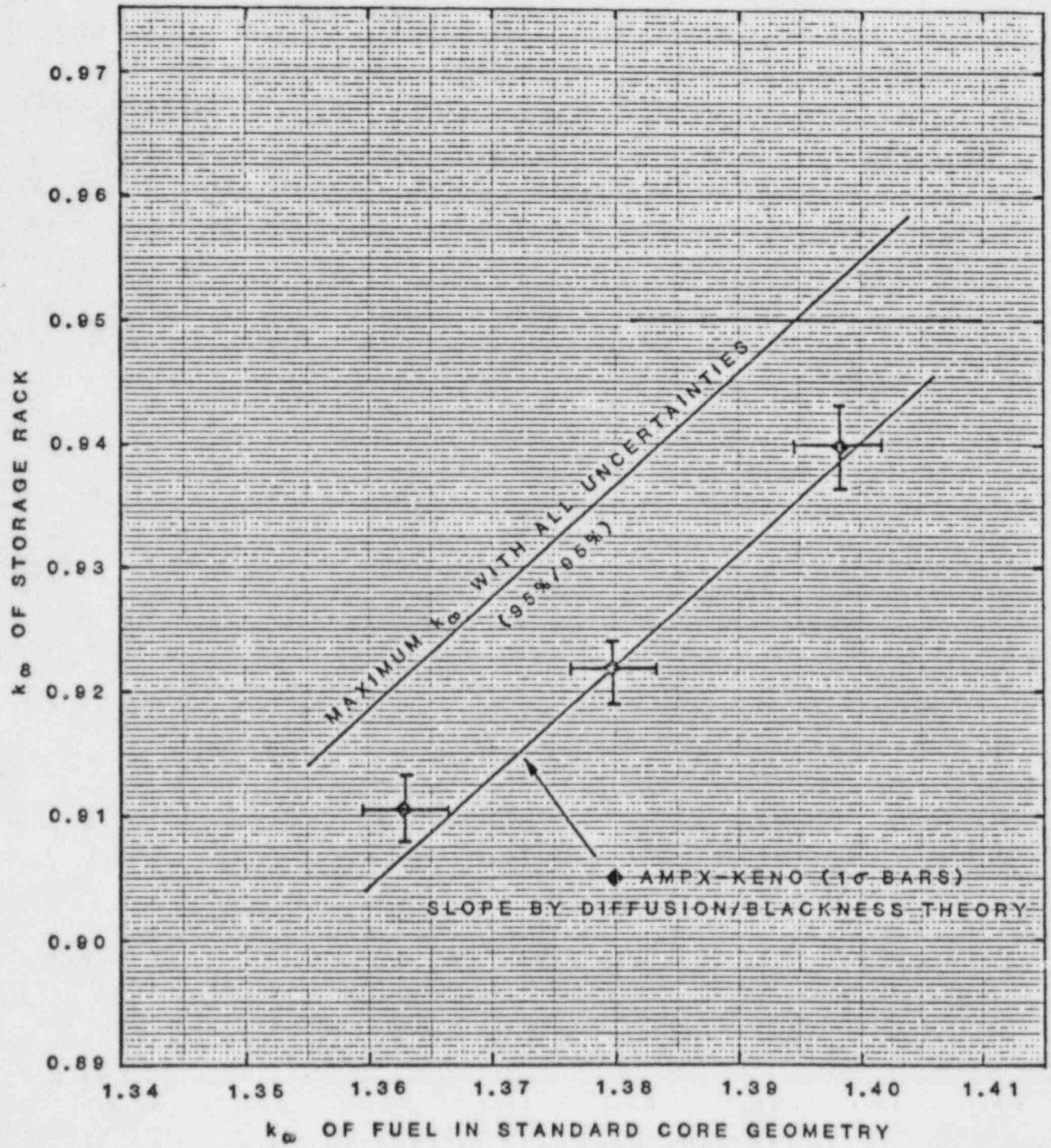

Fig. 4.4 Reactivity of spent fuel storage rack as a function of fuel reactivity in standard reactor core geometry.

In practice, neutron leakage and a higher moderator temperature will reduce the actual storage rack reactivity below the values indicated above. In addition, the presence of gadolinium poison will further reduce the actual rack reactivity by an estimated 0.17 Δk for fresh fuel and by 0.04 Δk for fuel at the point of maximum reactivity in fuel burnup (when the gadolinium has been essentially consumed).

4.4.3 Boron Loading Variation

The Boraflex absorber plate is nominally 0.070 inch thick with a B-10 areal density of 0.02041 g/cm^2. Manufacturing tolerance limits are +0.007 inch in thickness and $\pm$ 0.001 g/cm^2 in boron content. This assures that, at any point where the minimum boron loading (0.01944 g B-10/cm^2) and minimum Boraflex thickness (0.063 inch) may coincide, the boron areal density will not be less than 0.0175 g B-10/cm^2.

Calculations were made of k_∞ with variations in Boraflex absorber loading and thickness. Results of these calculations, shown in Fig. 4.5, indicate that the k_∞ can be described by the following regression fit (least squares) to the data over the range of B-10 loading from 0.010 to 0.030 g/cm^2.

$$k_\infty = 0.7280 \text{ EXP } (-0.0606 \text{ ℓn B-10, } g/cm^2)$$

This relationship indicates that the tolerance limit on boron concentration and Boraflex thickness results in incremental reactivity changes of $\pm$0.0027 Δk and 0.0059 Δk, respectively. The trend calculated both by AMPX-KENO and by diffusion/blackness theory is the same within analytical uncertainty.

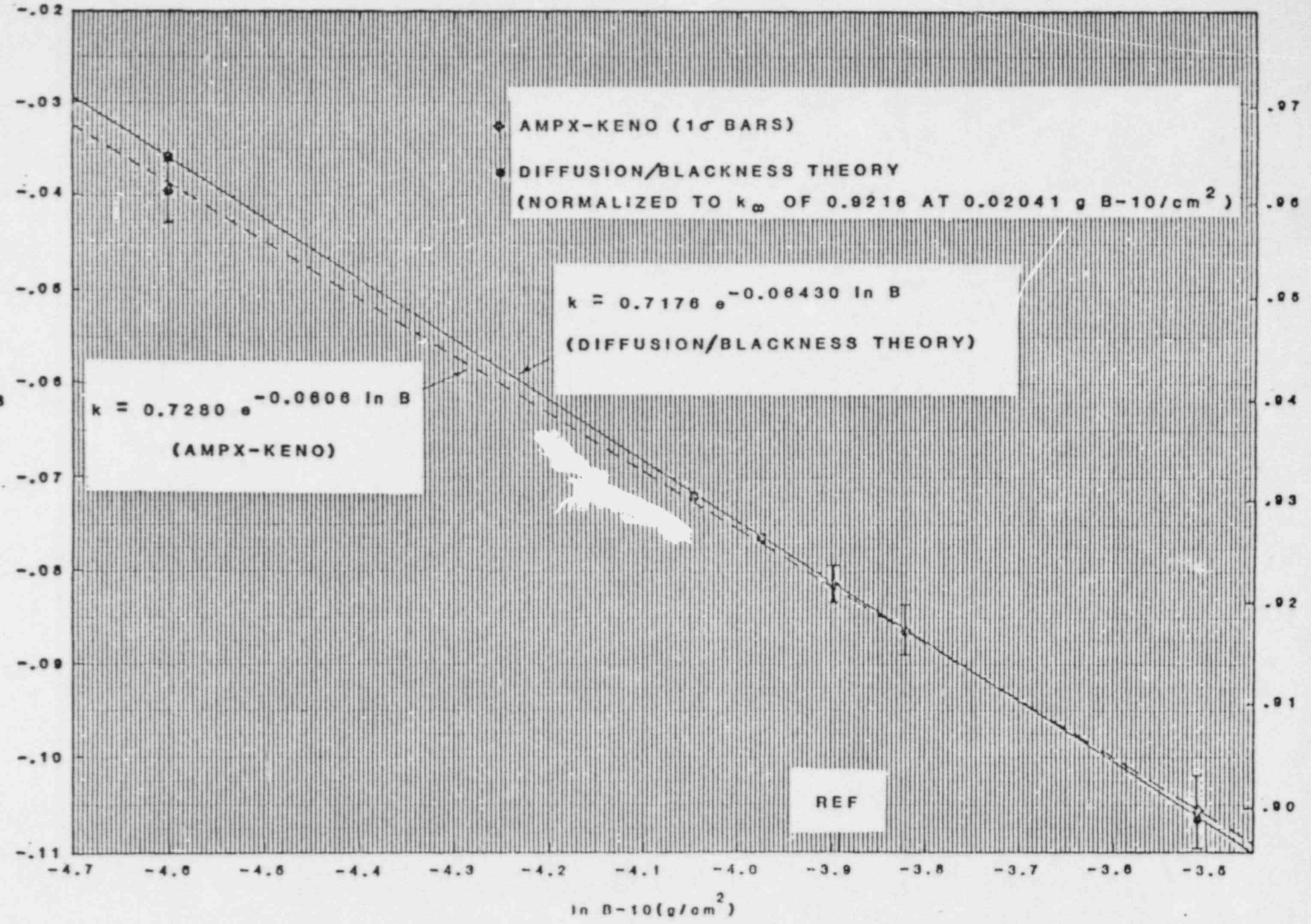

Fig. 4.5 Log log plot of calculated k_∞ versus B-10 loading.

4.4.4 Boraflex Width Tolerance Variation

A decrease in Boraflex plate width increases reactivity. For the manufacturing tolerance limit of ±0.0625 inch on the width of the Boraflex absorber plate, the corresponding uncertainty in reactivity is $\mp 0.0016\ \Delta k$, calculated by diffusion/blackness theory since the reactivity increment is too small to be calculated by AMPX-KENO.

4.4.5 Axial Cutback in Boraflex Length

The axial length of the Boraflex absorber is less than the active fuel length by 3 inches at both the top and bottom of the fuel racks. This axial cutback occurs in the region of high neutron leakage. Axial calculations (1-dimensional) indicate that the incremental reduction in reactivity due to axial leakage ($-0.0023\ \Delta k$) is greater than the increase in reactivity due to the axial cutback ($+0.0013\ \Delta k$). Thus, the infinite multiplication factor (k_∞) used as the reference reactivity is the more conservative condition. The calculations were performed with diffusion/blackness theory since the incremental reactivity effects are too small to be determined by AMPX-KENO calculations.

4.4.6 Storage Cell Lattice Pitch Variation

The design storage cell lattice spacing between fuel assemblies is 6.2585 ± 0.0625 inches. Increasing the lattice pitch reduces reactivity. For the manufacturing tolerance of ±0.0625 inch, the corresponding maximum uncertainty in reactivity is $\mp 0.0040\ \Delta k$, calculated by diffusion/blackness theory, since the reactivity increment is too small to be calculated by AMPX-KENO.

4.4.7 Stainless Steel Thickness Variations

The nominal stainless-steel thickness is 0.063 ± 0.005 inch. The maximum reactivity effect of the expected stainless-steel thickness tolerance variation (0.005 inch) was calculated to be ±0.0011 Δ k by diffusion/blackness theory, since the reactivity increment is too small to be calculated by AMPX-KENO.

4.4.8 Fuel Enrichment and Density Variation

The nominal design enrichment is 3.5 wt% U-235. Calculations of the sensitivity to small enrichment variations by diffusion/blackness theory yielded an average coefficient of 0.0065 Δk per 0.1 wt% U-235. For an estimated tolerance on U-235 enrichment of ±0.05%, the maximum uncertainty is ±0.0032 Δ k due to the tolerance on fuel enrichment.

Calculations were also made to determine the sensitivity to tolerances in UO_2 fuel density. These calculations indicate that the storage rack k_∞ is increased by 0.0024 Δk (diffusion/blackness theory) for the expected tolerance (±1.5% in T.D.) in fuel density. A lower fuel density results in correspondingly lower values of reactivity. Thus, the maximum uncertainty due to the tolerances on UO_2 density is ±0.0024 Δk.

4.4.9 Effect of Zirconium Fuel Channel

Elimination of the zirconium fuel channel results in a small decrease in reactivity (-0.0038 Δ k) as calculated by diffusion/blackness theory. More significant is a small positive reactivity effect resulting from bulging of the zirconium channel, which moves the channel wall outward toward the Boraflex absorber. For the maximum expected bulging (to 5.93 inches outside dimension) uniformly throughout the assembly, an incremental reactivity of +0.0047 Δk would result, as calculated by

diffusion/blackness theory. Since actual bulging of the flow channel would not be the maximum everywhere in all assemblies, the reactivity effect has been statistically combined with the reactivity effect of other mechanical deviations.

Fuel assembly bowing yields a negative reactivity effect and is treated under abnormal conditions (Section 4.3.4 above).

4.5 Acceptance Criteria for Criticality

The USNRC letter of April 14, 1978, to all Power Reactor Licensees, and the draft revision to Regulatory Guide 1.13 specify that the neutron multiplication factor in spent fuel pools shall be less than or equal to 0.95, including all uncertainties, when fully loaded with fuel of the highest anticipated reactivity. For BWR type fuel with an infinite multiplication factor of 1.395 or less in the standard reactor core geometry, the spent fuel storage rack described herein satisfies this criterion.

REFERENCES

1. Green, Lucious, Petrie, Ford, White, Wright, PSR-63/AMPX-1 (code package), AMPX Modular Code System for Generating Coupled Multigroup Neutron-Gamma Libraries from ENDF/B, ORNL-TM-3706, Oak Ridge National Laboratory, March 1976.

2. L. M. Petrie and N. F. Cross, KENO-IV, An Improved Monte Carlo Criticality Program, ORNL-4938, Oak Ridge National Laboratory, November 1975.

3. S. R. Bierman et al., Critical Separation Between Subcritical Clusters of 4.29 wt% U-235 Enriched UO_2 Rods in Water with Fixed Neutron Poisons, NUREG/CR-0073, Battelle Pacific Northwest Laboratories, May 1978, with errata sheet issued by the USNRC August 14, 1979.

4. M. N. Baldwin et al., Critical Experiments Supporting Close Proximity Water Storage of Power Reactor Fuel, BAW-1484-7, The Babcock & Wilcox Company, July 1979.

5. S. E. Turner and M. K. Gurley, Benchmark Calculations for Spent Fuel Storage Racks, Report SSA-127 (Rev. 4), Southern Science Applications, Inc., May 1981.

6. S. E. Turner and M. K. Gurley, Evaluation of AMPX-KENO Benchmark Calculations for High Density Spent Fuel Storage Racks, Nuclear Science and Engineering, Vol. 80, No. 2, pp. 230-237, February 1982.

7. M. G. Natrella, Experimental Statistics, National Bureau of Standards, Handbook 91, August 1963.

8. J. N. Cano et al., Supercriticality Through Optimum Moderation in Nuclear Fuel Storage, Nuclear Technology, Vol. 48, pp. 252-260, May 1980.

5. THERMAL-HYDRAULIC CONSIDERATIONS

A central objective in the design of the high-density fuel rack is to ensure adequate cooling of the fuel assembly cladding. In the following, a brief synopsis of the design basis, the method of analysis, and computed results are given. Similar analysis has been used in previous licensing reports on high density fuel racks for Fermi II (Docket 50-341) and Quad Cities (Docket 50-254/265).

5.1 Forced Circulation Thermal-Hydraulic Analysis

This report section covers requirement III.1.5(2) of the NRC "OT Position for Review and Acceptance of Spent Fuel Storage and Handling Applications" issued on April 14, 1978. This requirement states that calculations for the amount of thermal energy removed by the spent fuel cooling system shall be made in accordance with Branch Technical Position ASB 9-2 "Residual Decay Energy for Light Water Reactors for Long Term Cooling"[1]. The calculations contained herein have been made in accordance with this requirement.

5.1.1 Basis:

The Grand Gulf Unit 1 reactor is rated at 3833 Megawatt-Thermal (MWT). The core contains 800 fuel assemblies. Thus, the average operating power per fuel assembly, P_0, is 4.791 MW. The fuel assemblies are removed from the reactor after the maximum burn-up of 30,000 Megawatt-days per short ton of uranium (MWD/STU).

The Grand Gulf installation has two pools[2] equipped for fuel storage. The pool adjacent to the reactor cavity, hereinafter referred to as the "upper containment pool" has the capacity to accept the entire reactor core (800 fuel assemblies). This pool directly communicates with the reactor cavity and is flooded together with the reactor cavity prior to

initiation of fuel transfer. The second pool, hereinafter referred to as the "spent fuel pool" is located in the Auxiliary Building. Fuel assemblies are transferred to this pool from the containment pool via the Fuel Transfer Canal for long term storage. The upper containment pool does not contain any fuel while the plant is operating. The cooling systems for the two pools are somewhat intertwined. Figure 5.1.1 shows the flow schematic for the two pools. The analytical characterization of this system for thermal analysis purposes is developed later in this section.

The fuel discharge can be made in one of the following two modes:

(i) Normal discharge - Mode (i)
(ii) Full Core discharge - Mode (ii)

As shown in Table 1.1 of Section 1, the equilibrium fuel assembly removal batch size for Mode (i) is 228 fuel assemblies. Mode (ii) corresponds to a full core discharge (800 assemblies). Figure 5.1.1 shows the model for the pool cooling system.

The heat dissipation from the spent fuel pool is accomplished by two independent fuel pool cooler loops, each equipped with a pump rated at 1100 gpm. In addition, two Residual Heat Removal (RHR) heat exchangers, available for supplemental cooling, may be used in conjunction with the fuel pool coolers to boost the heat removal rate. Only one RHR heat exchanger is assumed to be available for supplemental cooling with a pump rated at 7450 gpm for this task. The RHR flow rate in spent fuel pool cooling mode was calculated to be 2550 gpm the other RHR acts as a stand-by unit.

In the following, all relevant performance data for the spent fuel pool and RHR heat exchangers is given.

a. Spent Fuel Pool Heat Exchanger:[3]

TEMA type 26-252 CEU 2087 sq. ft. effective surface on 253 U-tubes; 3/4" diameter x 18 BWG arranged on 0.9375" triangular pitch. Postulated fouling for tube and shellside surfaces is .0005 and 0.0005 sq.ft-°F-Hr/BTU respectively. Shellside pool water and tubeside cooling water flow rates are 550,000 and 532,500 lbs/hr. respectively. The temperature efficiency is 0.5.

b. RHR Heat Exchanger:[2]

The effective surface is 21250 sq. ft. Postulated fouling for the shellside (pool water) of the tube surface is 0.0005 sq.ft-°F-hr/BTU and that for the tubeside (cooling water) is .002 sq.ft.-°F-Hr/BTU. The shellside and tubeside design flow rates are 3.725 x 10^6 lbs/hr. and 3.95 x 10^6 lbs/hr. respectively. The overall heat transfer coefficient is 210 BTU/hr-ft^2-°F. The temperature efficiency is 0.455.

The above data enables complete characterization of the thermal performance of the heat exchangers.

5.1.2 Model Description

Reference (1) is utilized to compute the heat dissipation requirements in the pool. The total decay power consists of "fission products decay" and "heavy elements decay". Total decay power P for a fuel assembly is given as a linear function of P_0 and an exponentional function of t_0 and t_s.

i.e.: $P = P_0 \, f \, (t_0, t_s)$ (5.1.1)

where

P = linear function of P_0

P_0 = average operating power per fuel assembly

t_0 = cumulative exposure time of the fuel assembly in the reactor

t_s = time elapsed since reactor shutdown

The uncertainty factor K, which occurs in the functional relationship $f(t_0, t_s)$ is set equal to 0.1 for $t_s > 10^7$ sec in the interest of conservatism. Furthermore, the operating power P_0 is taken equal to the rated power, even though the reactor may be operating at a fraction of its rated power during most of the period of exposure of the batch of fuel assemblies. The computations and results reported here are based on the discharges at the 13th loading cycle. This approach assures that an asymptotic peak temperature is attained, i.e. highest peak temperature, and the fuel thermal inventory in the spent fuel pool is at its maximum.

The reactor operating time corresponding to 30,000 MWD/STU is less than 3.5 years at the nominal power level. However, since the decay power is a weakly increasing monotonic function of the operating time t_0, we select t_0 = 4 years ($t_0 = 1.26 \times 10^8$ secs) in evaluating the decay power.

Having determined the heat dissipation rate, the next task is to evaluate the time temperature history of the pool water. Table 5.1.1A identifies the loading cases examined. The pool bulk temperature time history is determined using the first law of thermodynamics (conservation of heat). The system to be analyzed is shown in Figure 5.1.1.

A number of simplifying assumptions are made which render the analysis conservative. The principal ones are:

1. The cooling water temperature in the fuel pool heat exchanger (95°F) and the RHR heat exchangers (90°F) are based on the maximum postulated values given in the FSAR.

2. The heat exchangers are assumed to have maximum fouling. Thus, the temperature effectiveness, P, for the heat exchangers utilized in the analysis are the lowest postulated values: P_i = 0.50 for fuel pool coolers (i=1), 0.455 for RHR heat exchangers (i=2). P_i is calculated from FSAR and heat exchanger technical data sheets.

3. No heat loss is assumed to take place through the concrete floor.

4. No credit is taken for the improvement in the film coefficients of the heat exchangers as the operating temperature rises. Thus, the film coefficient used in the computations are lower bounds.

5. No credit is taken for heat loss due to evaporation of the pool water.

- In the model return flow for the RHR system (in the supplemental cooling mode) from the UCP is through the reactor vessel and the re-circulation system.

This is depicted by W_{22} in Fig. 5.1.1. However, should this path not be available , flow arrangement of the RHR system would require mixing of the stream W_{22} (Fig. 5.1.1) with the Spent Fuel Pool water inventory. This represents communication between the two pools through the fuel transfer tube. Since the peak bulk temperature of the water in the UCP is lower than that in the SFP, this assumption has the net effect of over predicting the peak value of the SFP bulk temperature. Thus, the temperature plots presented in Section 5.2.3 are upper bounds.

The basic energy conservation relationship for each pool and heat exchanger system has the form:

$$C \frac{dt}{d\tau} = Q_{IN} - Q_{OUT} \qquad (5.1.2)$$

where

C: Thermal capacity of stored water in the pool.
t: Temperature of pool water at time, τ
Q_{IN}: Heat generation rate due to stored fuel assemblies in the pool. Q_{IN} is a known function of time τ, from the preceding section.
Q_{OUT}: Heat removed via the heat exchangers.

The upper containment pool and the spent fuel pool in the Grand Gulf Unit I installation have total water inventory of 11844 and 51043 cubic feet respectively when all racks are in place in the pools and every storage location is occupied.

The calculations were performed accounting for the interaction between the upper containment pool and the spent fuel pool (see Figure 5.1.1).

Let Q_1 and Q_2 denote the rate of heat generation in Pool 1 (spent fuel pool) and Pool 2 (upper containment pool) respectively. Q_1 and Q_2 are specified functions of time, τ.

Furthermore, let P_1 and P_2 represent the "temperature efficiency"[4] of spent fuel pool heat exchangers and RHR heat exchangers, respectively. Referring to Figure 5.1.1:

$$P_1 = \frac{t_3-t_4}{t_3-\theta_1} = 0.50$$

$$P_2 = \frac{t_5-t_6}{t_5-\theta_2} = 0.455 \qquad (5.1.3)$$

Therefore eq. (5.1.1) for each pool is:

$$C_1 \frac{dt_1}{d\tau} = Q_1 + W_{11}\,(t_4-t_1) + W_{21}\,(t_6-t_1) \qquad (5.1.4)$$

$$C_2 \frac{dt_2}{d\tau} = Q_2 + W_{12}\,(t_4-t_2) + W_{22}(t_6-t_2) \qquad (5.1.5)$$

where C_1 and C_2 are heat capacities of pools 1 and 2, respectively, and W_{ij} (see figure 5.1.1) represents the thermal flow rate from heat exchanger i into pool j (RHR heat exchanger i=2, Fuel Pool Cooler, i=1).
Equations (5.1.4) - (5.1.5) can be cast into the form

$$\frac{dt_i}{d\tau} = \sum_{j=1}^{3} b_{ij}\, t_j \;;\; i = 1,2 \qquad (5.1.6)$$

where t_3 in the RHR has the implied value of unity. The matrix coefficients b_{ij} are functions of W_{ij}, P_i, C_i, etc.

Runge-Kutta first order forward integration scheme is used to solve the two simultaneous first order differential equations (5.1.6).

5.1.3 Results and Discussion

Sixteen typical scenarios (cases) are chosen for the first phase of the analysis. These cases and their underlying assumptions are presented in Table 5.1.1A. The results of the

TABLE 5.1.1A

LIST OF CASES ANALYZED

Case No.	Assumptions and Criteria *		
	I	II	III
1	(a)	(b)	(a)
2	(b)	(b)	(a)
3	(c)	(b)	(a)
4	(a)	(c)	(a)
5	(b)	(c)	(a)
6	(c)	(c)	(a)
7	(c)	(a)	(a)
8	(a)	(a)	(a)
9	(c)	(a)	(b)
10	(a)	(a)	(b)
11†	(c)	(c)	(c)
12†	(a)	(c)	(c)
13†	(c)	(a)	(c)
14†	(a)	(a)	(c)
15	(a)	(b)	(a)
16	(b)	(b)	(a)

* Please see next page for explanation of symbols (a,b, & c) used.

† These cases are analyzed to fulfill the requirements of single failure criterion (i.e. one FPHX and its associated loop is out of service).

TABLE 5.1.1A (Continued)

List of Assumptions and Criteria

I. Time (hrs) for Fuel Movement from Core after Reactor Shutdown (Cool-off time)

(a) 90
(b) 110
(c) 130

II. Rate of fuel discharge

(a) Instantaneous discharge to UCP - hold for 24 hours in UCP and then instantaneous discharge to SFP.
(b) Discharge to UCP @ 4 bundles/hour; 24 hours after start of discharge into UCP, begin transfer from UCP into SFP @ 4 bundles/hour until all required bundles are discharged.
(c) Similar process as in (b) above except that the transfer rate is 2 bundles/hour.

III. Availability of fuel pool heat exchangers (FPHX)

(a) 1 FPHX in continuous service and 1 FPHX put in service at start of refuelling and operating for 60 days thereafter.
(b) 2 FPHX in continuous service
(c) 1 FPHX in continuous service

NOTE:

Cases 1-14: Normal operation - Fuel discharge of 228 bundles for the 12th discharge (or 13th loading cycle). Last refueling outage completed 12 months prior.

Cases 15 & 16: Abnormal operations - Full core discharge of 800 bundles 90 days after the 12th refueling outage (or the 11th discharge)

TABLE 5.1.1B

CASES ANALYZED FOR LONG TERM COOLABILITY

Case	Condition	No. of Fuel Assemblies	No. of Spent Fuel Pool HX's	RHR Availability	Total Time to Transfer Fuel into SFP (hrs)	Cool-Off Time before Transfer begins (hrs)
A	Normal Discharge	228	Note 1	Note 2(a)	57	110
B	Full Core	800	Note 1	Note 2(b)	200	110

Notes: 1 1 SFPHX in continuous service and 1 SFPHX put in service at start of refueling and operates for 60 days thereafter.

2 (a) 1 RHR loop available immediately after shutdown and is in service for 30 days after start of discharge into upper containment pool.

(b) Same as (a) but RHR remains in service.

TABLE 5.1.2A

MAXIMUM SPENT FUEL POOL BULK TEMPERATURE t, COINCIDENT TOTAL POWER Q_1, COINCIDENT TIME AND TIME TO BOILING (Cases 1 - 16)

Case No.	Peak Pool Bulk temp. °F	Coincident time (since initiation of fuel transfer, into UCP), hrs.	$Q_1 \times 10^{-6}$ BTU/hr	Time to Boiling from the instant all cooling is lost, hrs†
1	105.5	84	15.0530	23
2	105.2	86	14.6332	23
3	104.9	86	14.3058	24
4	104.7	140	14.1007	24
5	104.4	142	13.8097	24
6	104.2	142	13.5721	25
7	105.7	36	15.2252	23
8	106.7	36	16.3065	21
9	105.7	36	15.2252	23
10	106.7	36	16.3065	22
11*	106.1	142	13.5721	24
12*	106.6	140	14.1007	24
13*	107.8	38	15.1810	22
14*	109.1	36	16.3065	21
15	126.1	226	37.4520	7
16	125.5	226	36.8038	7

† All cooling is assumed lost at the time instant when pool bulk temperature peaks.
* Single failure criteria cases [see Table 5.1.1A].

TABLE 5.1.2B

MAXIMUM SPENT FUEL POOL BULK TEMPERATURE t, COINCIDENT TOTAL POWER Q_1, COINCIDENT TIME AND TIME TO BOILING (Cases A&B)

Case	No. of Assemblies	Time to Transfer Fuel into Pool, hrs.	Point in Fig. 5.1.2 or 5.1.3	Peak Pool Bulk temp. °F	Coincident time (since initiation of fuel transfer, all into UCP, hrs.	Time to Boiling from the instant all cooling is lost, hrs.	$Q_1 \times 10^{-6}$ BTU/hr
A	228	57	A1	105.2	86	23	14.6632
			A2	121.9	830	29	9.8473
			A3	125.9	1500	30	8.5029
B	800	200	B1	125.5	226	7	36.8038
			B2	113.0	1455	14	21.4858

analyses are presented in Table 5.1.2A. These analyses are performed for an elapsed time (i.e. time since commencement of fuel transfer) of 400 hours. Results obtained from these analyses show that neither cool-off time (i.e. time elapsed between reactor shutdown and before commencement of fuel discharge from the core) nor mode of discharge (ramps or instantaneous) have any significant impact on bulk pool temperatures after 200 hours since commencement of discharge. Therefore, two cases, case 2 and case 16, re-labelled as cases A and B respectively, are chosen for analysis in Phase II for an extended time period so as to study the effect of operational parameters on bulk pool temperatures. The two cases are described in Table 5.1.1B, their results presented in Table 5.1.2B and graphically shown in Figures 5.1.2 and 5.1.3. These plots show that the spent fuel pool water never approaches the boiling point under the most adverse conditions. These figures also give Q_1 as a function of τ.

In addition, an analysis for each loading cycle is performed based on the refueling schedule (ref Table 1.1). These results are plotted in Figure (5.1.4) and (5.1.5).

As stated earlier in this section the upper containment pool serves as a temporary storage pool and therefore the bulk pool temperatures in this pool are generally lower than those in the spent fuel pool. The exception, as can be expected, being for an instantaneous discharge for a normal batch (upper limit fuel discharge rate) where peak temperatures in the upper containment pool are higher. However, even for the most conservative condition (case 14) the calculated peak temperature in the upper containment pool is about 123°F. For the case of an abnormal discharge "Full core discharge (Cases 15 & 16)", discharge rate of 4 bundles/hr is considered. An instantaneous discharge rate, for these cases, is not representative of refueling operations. Therefore, for purposes of analysis, the discharge rate considered coupled with scenario presented above provides an upper bound to bulk pool temperature.

It should be recognized that the analysis described and the results presented herein are conservative and do not represent realistic operational conditions. The purpose of these analyses is to show that under the most conservative scenario acceptable temperature limits will not be exceeded utilizing the available spent fuel pool cooling system with an appropriate backup from the RHR system. Moreover, the licensee intends to monitor the bulk pool temperature subsequent to refueling and take appropriate measures.

5.2 Natural Circulation Thermal-Hydraulics Analysis

This report section covers requirement III.1.5(3) of the NRC "OT Position for Review and Acceptance of Spent Fuel Storage and Handling Applications" issued on April 14, 1978. Conservative methods have been used to calculate the maximum fuel cladding temperature as required therein. Also, it has been determined that nucleate boiling or voiding of coolant on the surface of the fuel rods does not occur.

5.2.1 Basis:

In order to determine an upper bound on the maximum fuel cladding temperature, a series of conservative assumptions are made. The most important assumptions are listed below:

a. As stated above, the fuel pool will contain spent fuel with varying "time-after-shutdown" (t_s). Since the heat emission falls off rapidly with increasing t_s, it is obviously conservative to assume that all fuel assemblies are fresh (t_s = 110 hours), and they all have had 4 years of operating time in the reactor. The heat emission rate of each fuel assembly is assumed to be equal.[2]

b. As shown in Figures 2.1 and 2.2 in Section 2, the modules occupy an irregular floor space in the pool. For purposes of the hydrothermal analysis, a

circle circumscribing the actual rack floor space is drawn. It is further assumed that the cylinder with this circle as its base is packed with fuel assemblies at the nominal pitch of 6.2585 inches (see Figure 5.2.1).

c. The downcomer space around the rack module group varies, as shown in Figure 5.2.1. The minimum downcomer gap (6.25 inches) available in the pool is assumed to be the total gap available around the idealized cylindrical rack; thus, the maximum resistance to downward flow is incorporated into the analysis.

d. No downcomer flow is assumed to exist between the rack modules.

5.2.2 Model Description

In this manner, a conservative idealized model for the rack assemblage is devised. The water flow is axisymmetric about the vertical axis of the circular rack assemblage, and thus, the flow is two-dimensional (axisymmetric three-dimensional). The governing equation to characterize the flow field in the pool can now be written. The resulting integral equation can be solved for the lower plenum velocity field (in the radial direction) and axial velocity (in-cell velocity field), by using the method of collocation. It should be added here that the hydrodynamic loss coefficients which enter into the formulation of the integral equation are also taken from well-recognized sources[5] and wherever discrepancies in reported values exists, the conservative values are consistently used.

After the axial velocity field is evaluated, it is a straight-forward matter to compute the fuel assembly cladding

temperature. The knowledge of the overall flow field enables pinpointing the storage location with the minimum axial flow (i.e. maximum water outlet temperature). This is called the most "choked" location. It is recognized that some storage locations, where rack module supports are located, have some additional hydraulic resistance not encountered in other cells. In order to find an upper bound on the temperature in such a cell, it is asumed that it is located at the most "choked" location. Knowing the global plenum velocity field, the revised axial flow through this choked cell can be calculated by solving the Bernoulli's equation for the flow circuit through this cell. Thus, an absolute upper bound on the water exit temperature and maximum fuel cladding temperature is obtained. In view of the preceding assumption, the temperatures calculated in this manner overestimate the temperature rise that will actually be obtained in the pool.

In this analysis results for cases A and B as presented in Section 5.1.3 were utilized. The radial peaking factor used in the analysis is 1.35[6]. The maximum temperature rise of pool water in the most disadvantageously placed fuel assembly is given in Table 5.2.1 for all loading cases. Having determined the maximum "local" water temperature in the pool, it is now possible to determine the maximum fuel cladding temperature. It is conservatively assumed that the total peaking factor α_T is 1.63. Thus, a fuel rod can produce 1.63 times the average heat emission rate over a small length. The axial heat dissipation in a rod is known to reach a maximum in the central region; and taper off at its two extremities. For the sake of added conservatism it is assumed that the peak heat emission occurs at the top where the local water temperature also reaches its maximum. Furthermore, no credit is taken for axial conduction of heat along the rod. The highly conservative model thus constructed leads to simple algebraic equations which directly give the maximum local cladding temperature, t_c.

5.2.3 Results and Discussion

Table 5.2.1 gives the corresponding maximum local cladding temperature, t_c, at the instances the spent fuel pool bulk temperature peaks. There are three such "peaks" for case A as shown in Figure 5.1.2 and two for case B (only peak B1 is analyzed since peak B2 is significantly lower than peak B1) as indicated in Figure 5.1.3. It is quite possible, however, that the peak cladding temperature occurs at the instant of maximum value of q_r, i.e., at the instant when the fuel assembly is first placed in a storage location. Table 5.2.2 gives the maximum local cladding temperature at τ=24 hours (i.e. the instance when fuel transfer from the upper containment pool to the spent fuel pool begins). It is to be noted that there are wide margins to local boiling in all cases. The local boiling temperature near the top of the fuel cladding is 243°F. Furthermore, the cladding temperature must be somewhat higher than the boiling temperature to initiate and sustain nucleate boiling. The above considerations indicate that a comfortable margin against the initiation of localized boiling exists in all cases.

TABLE 5.2.1

MAXIMUM LOCAL (SPENT FUEL) POOL WATER TEMPERATURE AND LOCAL FUEL CLADDING TEMPERATURE

Case	Point in Fig. 5.1.2 or Fig. 5.1.3	Max. Local Pool Water Temperature °F	Coincident Specific Power q, BTU/sec	Maximum Coincident Local Cladding Temperature °F
A	A1	131.8	12.488	153.62
	A2	138.4	6.741	150.77
	A3	139.7	5.103	149.32
B	B1	147.6	10.509	165.88

TABLE 5.2.2

POOL AND MAXIMUM CLADDING TEMPERATURE AT THE INSTANCE FUEL ASSEMBLY TRANSFER FROM UPPER CONTAINMENT POOL TO SPENT FUEL POOL BEGINS, τ=24

Case	Cladding Temperature °F	Coincident Specific Power, q, BTU/sec	Coincident Pool Temperature, °F	
			Bulk	Local
A	154.6	15.31	98.0	128.5
B	155.6	15.31	99.0	129.5

REFERENCES TO SECTION 5

1. NUREG 0800 U.S. Nuclear Regulatory Commission, Standard Review Plan, Branch Technical Position, ASB 9-2, Rev. 2, July 1981.

2. FSAR, Grand Gulf Unit I, Section 9, Auxiliary and Emergency Systems.

3. "Technical Specifications for Design, Fabrication and Purchase of High Density Spent Fuel Storage Racks", NPE-M-181.1, Rev. 2, Dec., 1982. Mississippi Power & Light Company.

4. "Some Fundamental Relationships for Tubular Heat Exchanger Thermal Performance", K.P. Singh, Journal of Heat Transfer, Transactions of the ASME, Vol. 103, No. 3, August, 1981.

5. General Electric Corporation, R&D Data Books, "Heat Transfer and Fluid Flow", 1974 and updates.

6. T.J. Helbling (ENC) to L.F. Dale (MP&L) "Grand Gulf Nuclear Station FSDD Response", Letter MPEX-82/57, July 3, 1982. (EXXON PROPRIETARY)

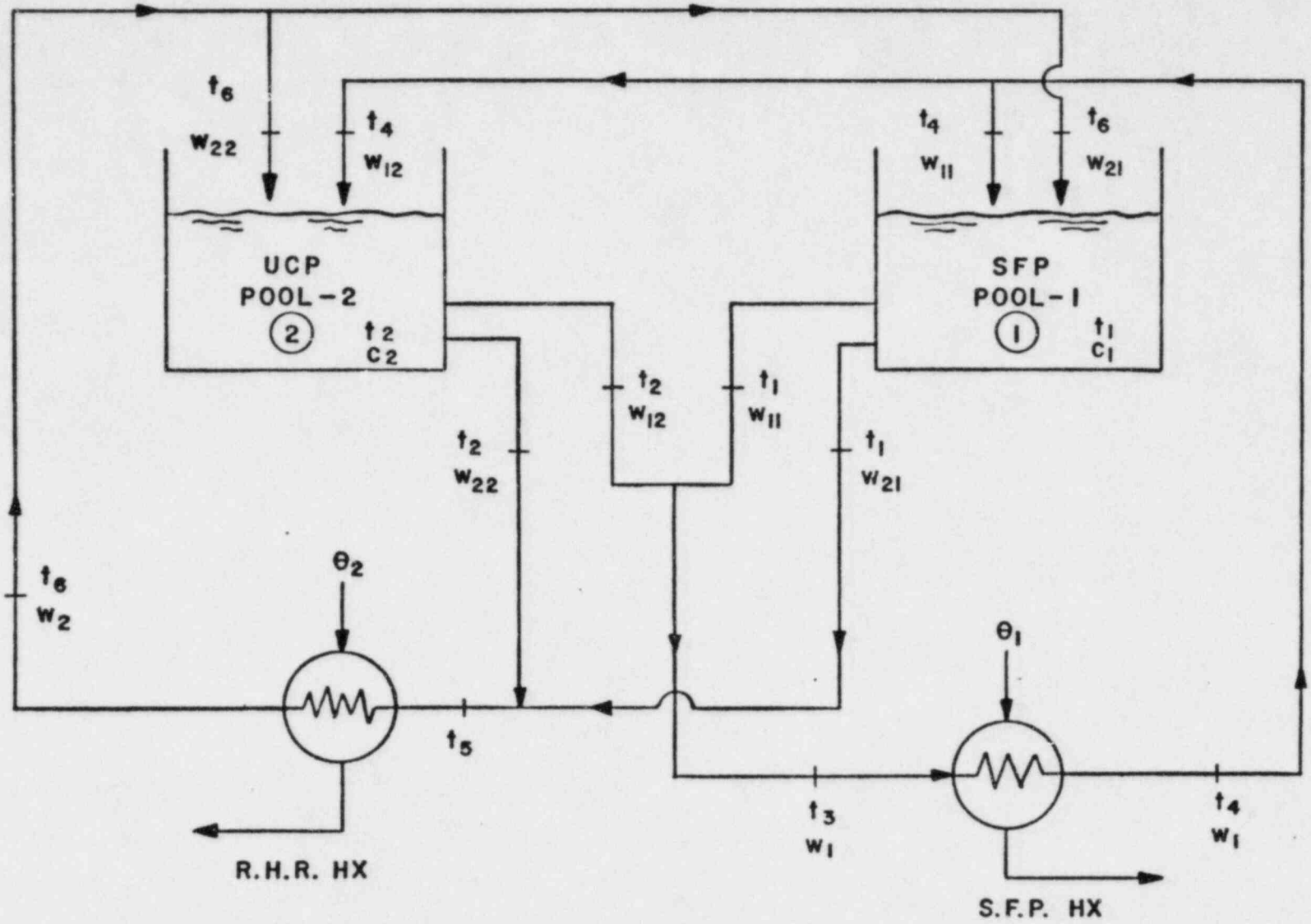

FIG. 5.1.1 – MODEL FOR GRAND GULF POOLS

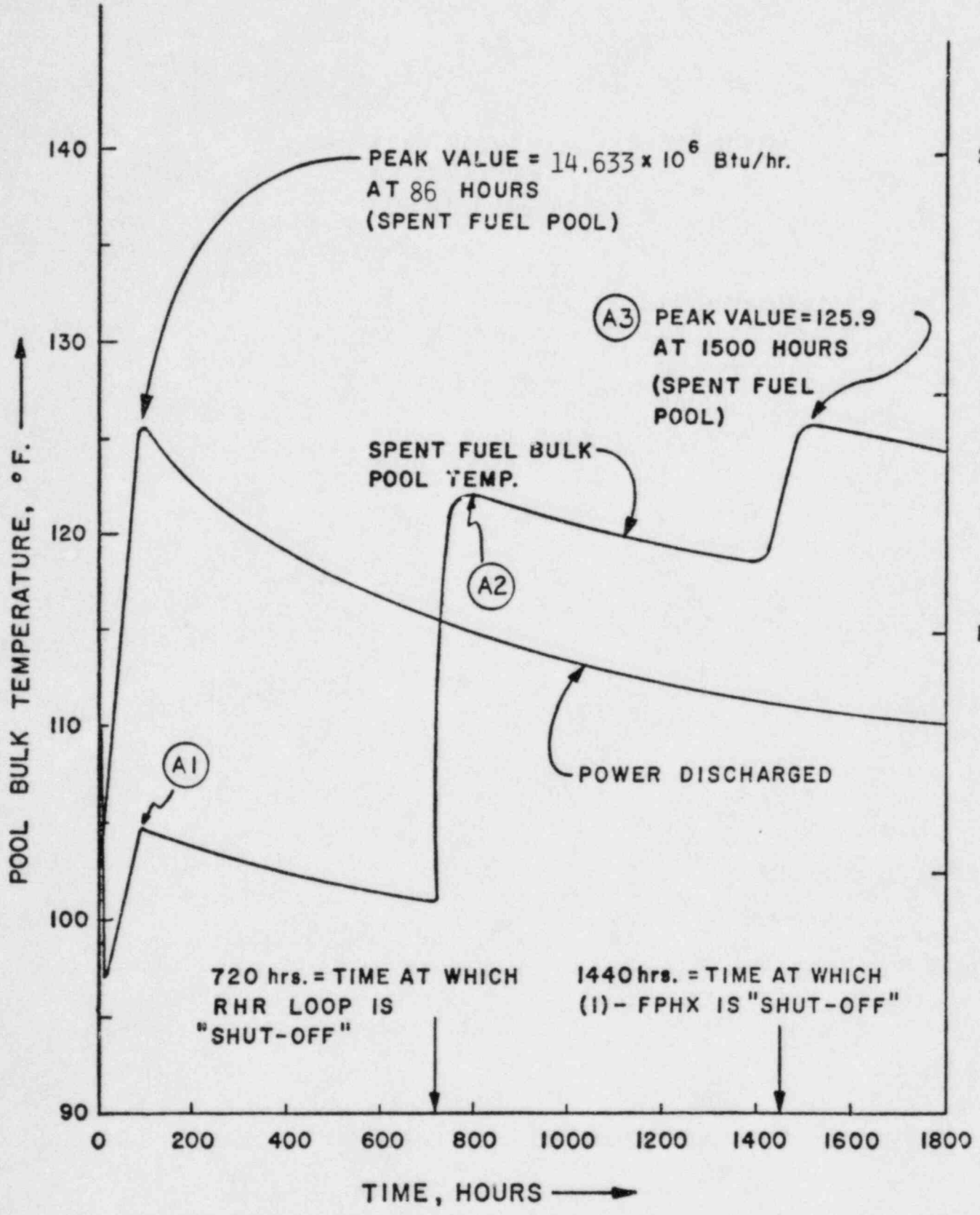

FIG. 5.1.2 – SPENT FUEL POOL BULK TEMPERATURES AND POWER DISCHARGED FOR CASE A (NORMAL DISCHARGE)

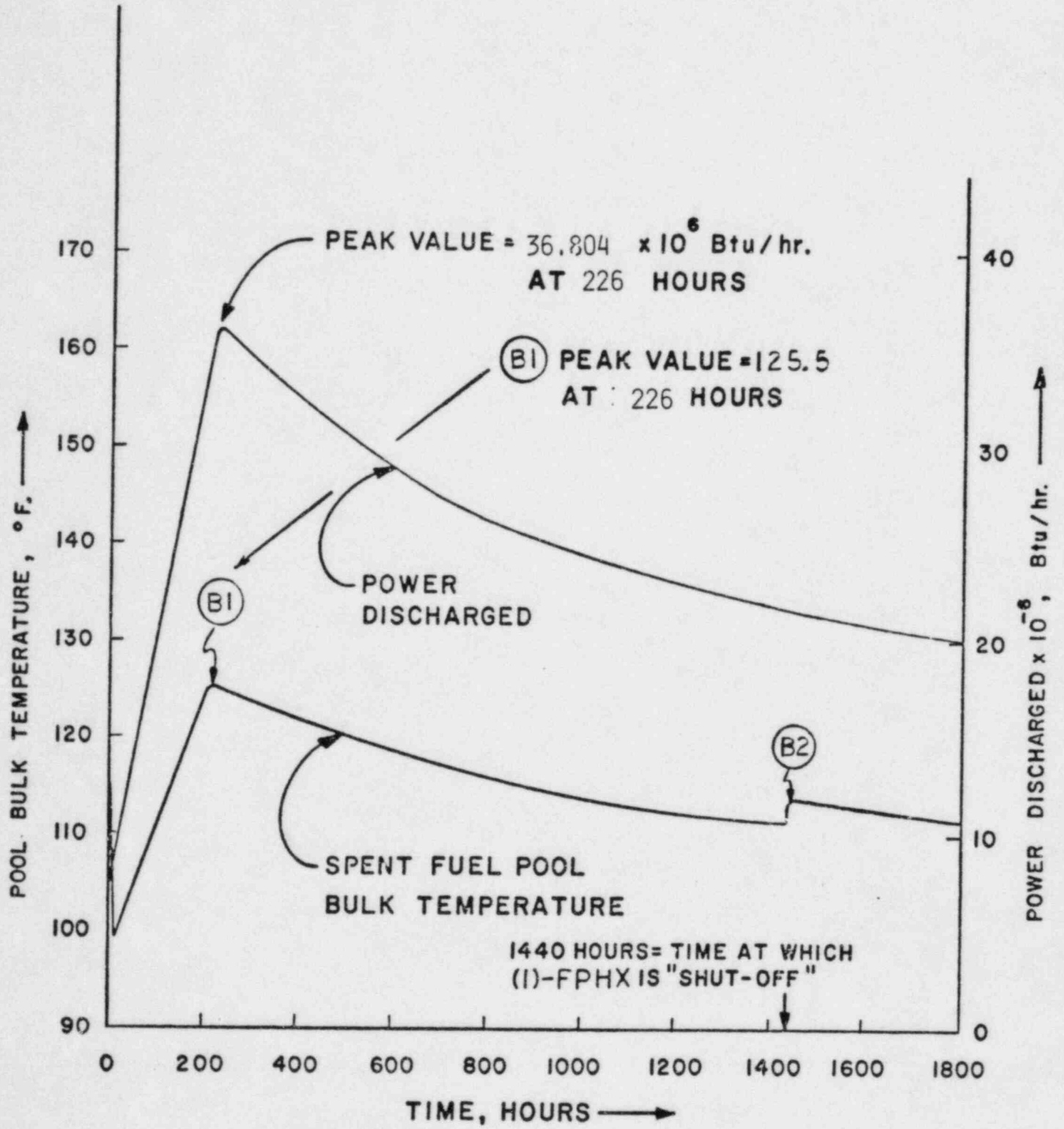

FIG. 5.1.3 – SPENT FUEL POOL BULK TEMPERATURES AND POWER DISCHARGED FOR CASE B (ABNORMAL DISCHARGE)

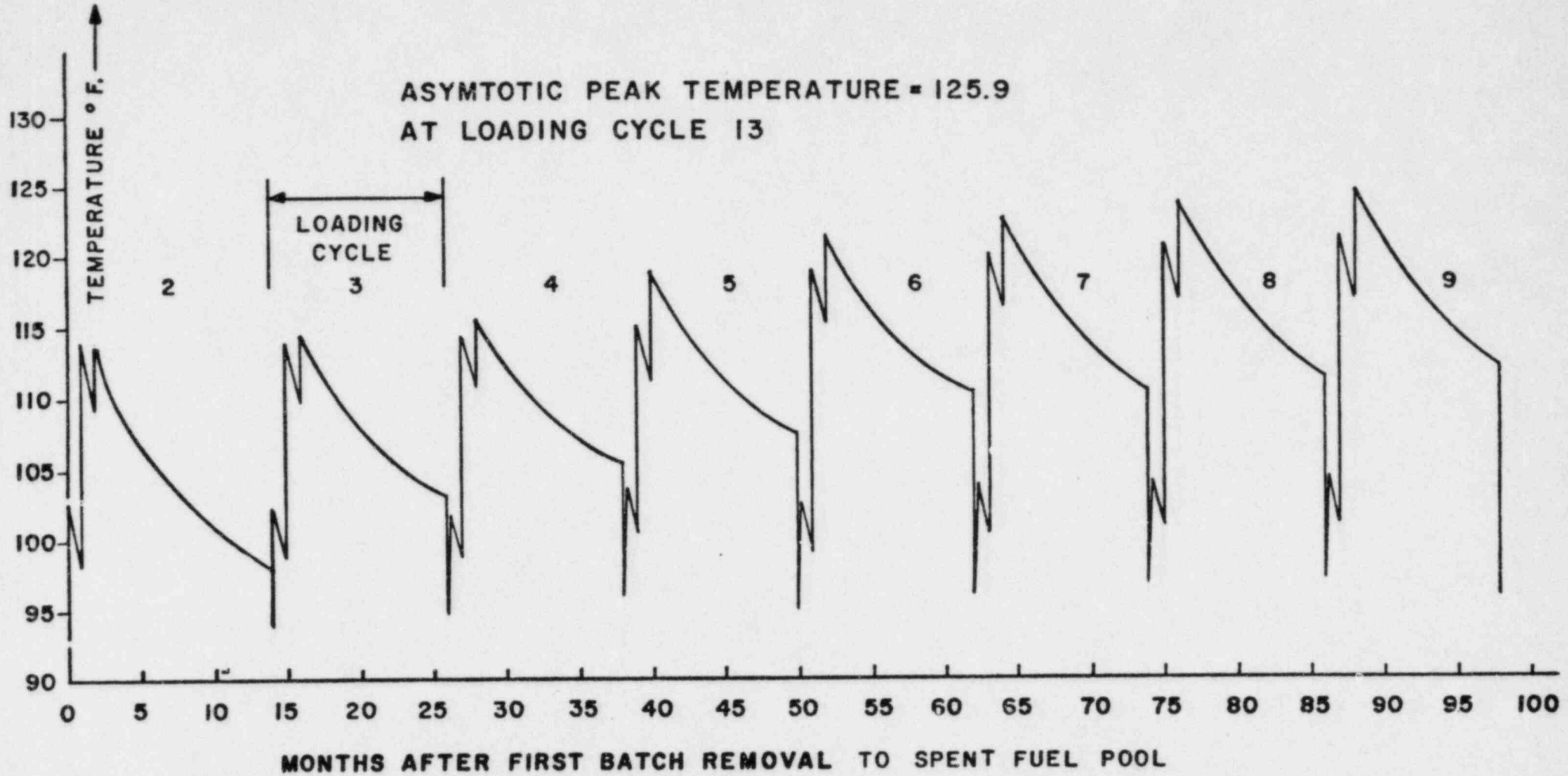

FIG. 5.1.4 – FUEL POOL BULK TEMPERATURE PROFILE USING CRITERIA FROM CASE A

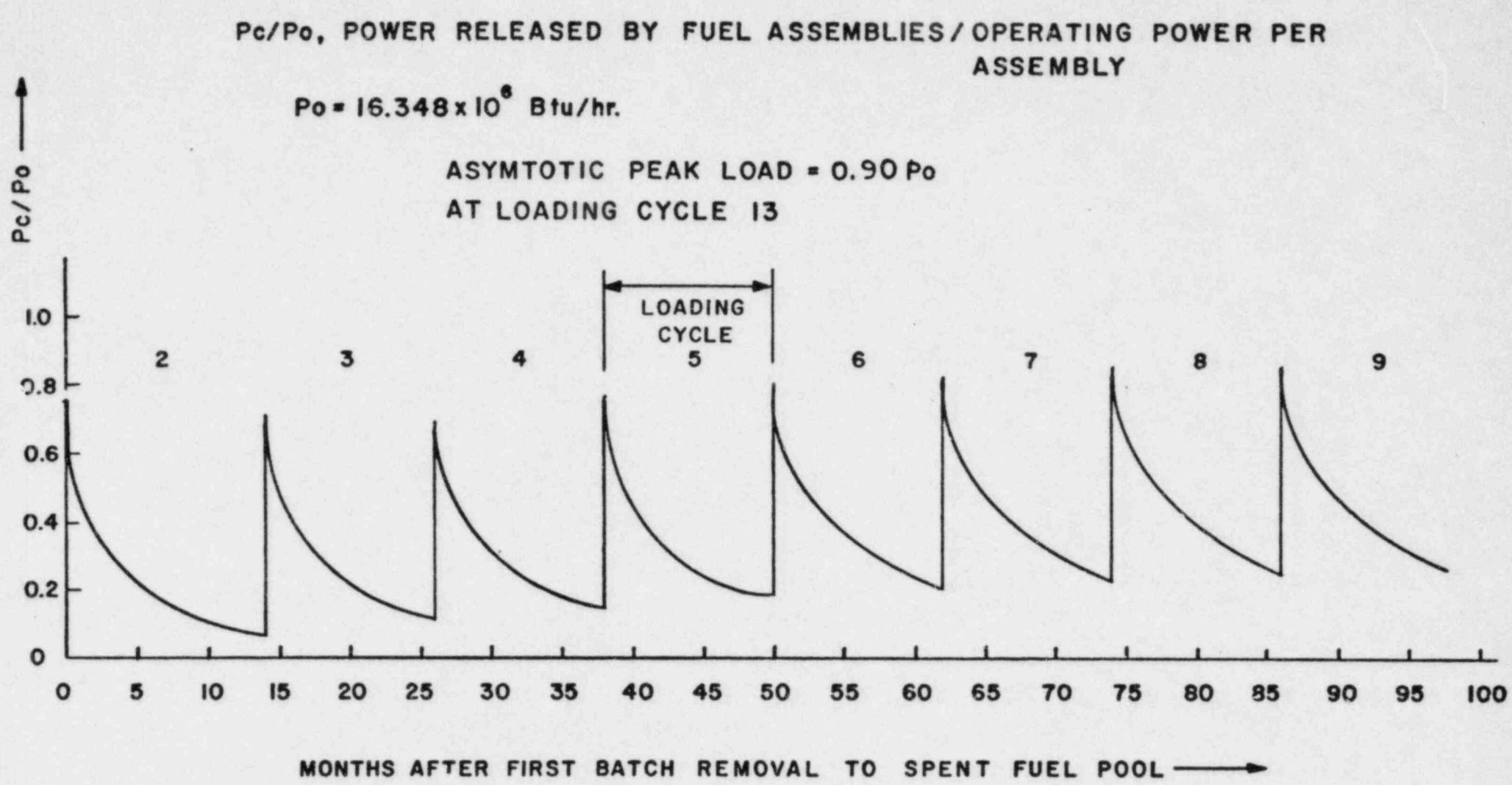

FIG. 5.1.5 – FUEL POOL HEAT LOAD PROFILE USING CRITERIA FROM CASE A

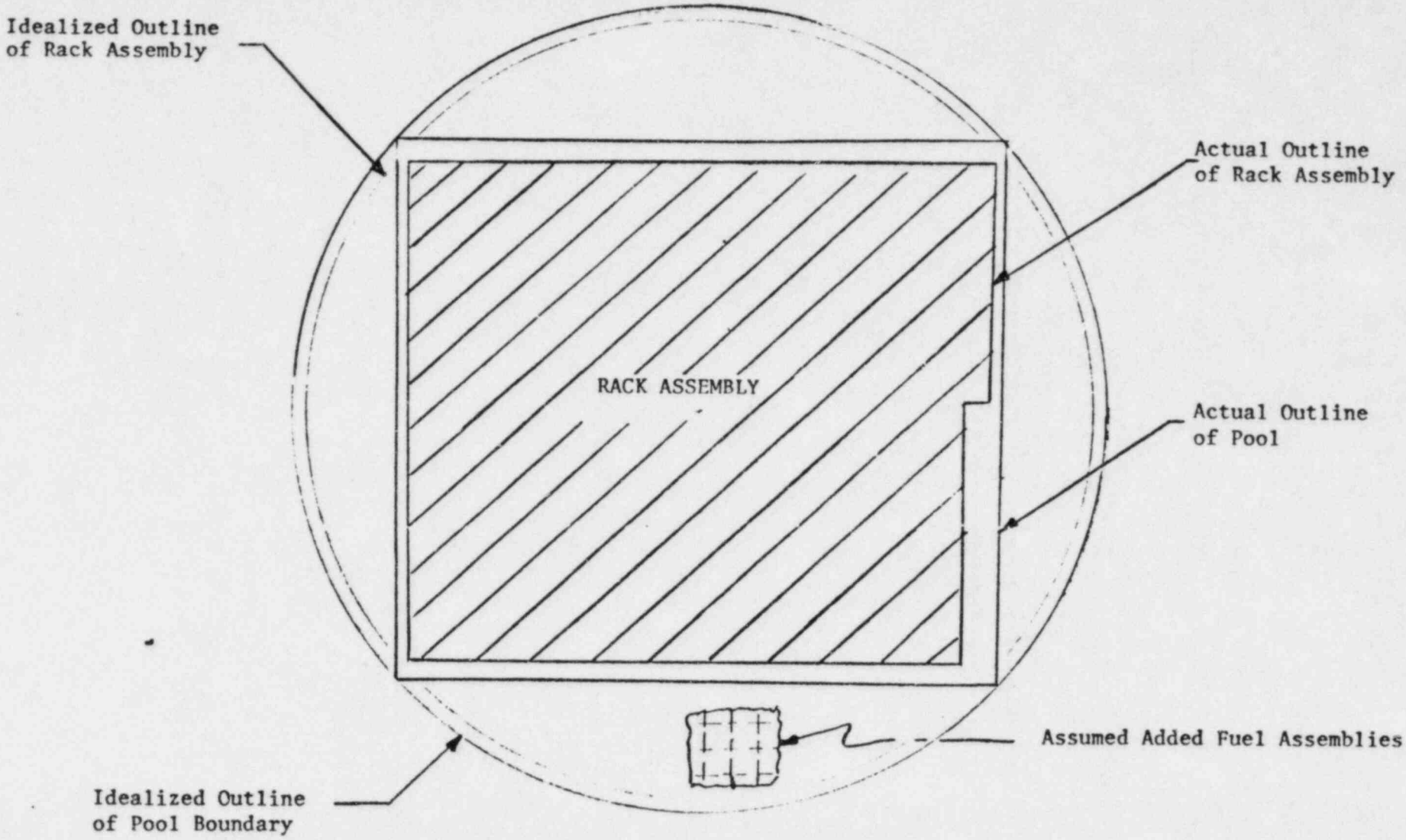

Figure 5.2.1 Rack Space Enveloping Cylinder
(Grand Gulf Unit One)

6. STRUCTURAL ANALYSIS

The purpose of this section is to demonstrate the structural adequacy of the spent fuel rack design under normal and accident loading conditions. The method of analysis presented herein is similar to that previously used in the Licensing Reports on High Density Fuel Racks for Fermi II (Docket 50-341) and Quad Cities (Docket 50-254-265). The results show that the high density spent fuel racks are structurally adequate to resist the postulated stress combinations associated with normal and accident conditions.

6.1 Analysis Outline:

The spent fuel storage racks are Seismic Category I equipment. Thus, they are required to remain functional during and after an SSE (Safe Shutdown Earthquake).[1] As noted previously, these racks are neither anchored to the pool floor, nor are they attached to the side walls. The individual rack modules are not interconnected. Furthermore, a particular rack may be completely loaded with fuel assemblies (which corresponds to greatest rack inertia), or it may be partially loaded so as to produce maximum geometric eccentricity in the structure. The coefficient of friction, μ, between the supports and pool floor is another indeterminate factor. According to Rabinowicz,[2] the results of 199 tests performed on austenitic stainless steel plates submerged in water show a mean value of μ to be 0.503 with a standard deviation of 0.125. The upper and lower bounds ($\mp 2\sigma$) are thus 0.753 and 0.253, respectively. Two separate analyses are performed for this rack assembly with values of μ equal to 0.2 (lower limit) and 0.8 (upper limit) respectively. Initially, the following six separate analyses are performed on the largest rack module (Module A).

1. Fully loaded rack (all storage locations occupied), $\mu = 0.8$ (μ = coefficient of friction).
2. Fully loaded rack, $\mu = 0.2$.

3. Half-loaded rack to produce maximum geometric asymmetry about the major dimension of the rectangular rack, $\mu = 0.8$.
4. Half-loaded rack to produce maximum geometric asymmetry about the major dimension of the rectangular rack, $\mu = 0.2$.
5. Empty rack, $\mu = 0.8$.
6. Empty rack, $\mu = 0.2$.

Based on the results of these runs, additional analyses are performed. The actual studies performed for the different rack modules are summarized in Section 6.6.

The method of analysis employed is the time history method. The pool slab acceleration data are developed from the original plant design as developed by Bechtel Power Corporation, Gaithersburg, Maryland. Bechtel's report is provided as Appendix 1 (proprietary) to this report.

The object of the seismic analysis is to determine the structural response (stresses, deformation, rigid body motion, etc.) due to simultaneous application of the three orthogonal excitations. Thus, recourse to approximate statistical summation techniques such as "Square-Root-of-the-Sum-of-the-Squares" method [3] is avoided and the dependability of computed results is ensured.

The seismic analysis is performed in four steps; namely

1. Development of nonlinear dynamic model consisting of beam, gap, spring, damper and inertial coupling elements.

2. Derivation and computation of element stiffnesses using a sophisticated elastostatic model.

3. Layout of the equations of motion, and inertial decoupling and solution of the equations using the "component element time integration" procedure[4,5] to determine nodal and element forces and displacements of nodes.

4. Computation of the detailed stress field in the rack structure, using the detailed elastostatic model, from the nodal forces calculated in Step III above. Determine if the stress and displacement limits,given in Section 6.5, are satisfied.

A brief description of the dynamic model follows.

6.2 Fuel Rack - Fuel Assembly Model

6.2.1 Assumptions

a. The fuel rack metal structure is represented by five lumped masses connected by appropriate elastic springs as shown in Figure 6.1. The spring rates simulate the elastic behavior of the fuel rack as a beamlike structure.

b. The fuel assemblies are represented by five lumped masses located, relative to the rack, in a manner which simulates either fully or partially loaded conditions.

c. The local flexibility of the rack-support interface is modeled conservatively in the analysis.

d. The rack base support may slide or lift off the pool floor.

e. The pool floor is assumed to have a known time history of accelerations along the three orthogonal directions.

f. Fluid coupling between rack and assemblies, and between rack and adjacent racks is simulated by introducing appropriate inertial coupling into the system kinetic energy.

g. Potential impacts between rack and assemblies are accounted for by appropriate spring gap connectors between masses involved.

h. Fluid damping between rack and assemblies, and between rack and adjacent rack is conservatively neglected.

i. The supports are modeled as extensional elements for dynamic analysis. The bottom of a support leg is attached to a frictional spring as described in Section 6.2.2. The cross section properties of the support beams are derived and used in the final computations to determine support leg stresses.

j. The effect of sloshing can be shown to be negligible at the bottom of a pool and is hence neglected.

k. Deformation due to shear is included in the rack springs, but neglected in the fuel assembly springs.

6.2.2 Model Description

The absolute degrees of freedom associated with each of the mass locations i, i* are as follows (see Figure 6.1):

Table 6.1 Degrees of Freedom

Location (Node)	Displacement u_x	u_y	u_z	Rotation θ_x	θ_y	θ_z
1	p_1	p_2	p_3	q_4	q_5	q_6
1*	Point is assumed fixed to base at $X_B, Y_B, Z=0$					
2	p_7	p_9		q_{11}	q_{12}	
2*	p_8	p_{10}				
3	p_{13}	p_{15}		q_{17}	q_{18}	
3*	p_{14}	p_{16}				
4	p_{19}	p_{21}		q_{23}	q_{24}	
4*	p_{20}	p_{22}				
5	p_{25}	p_{27}	p_{32}	q_{29}	q_{30}	q_{31}
5*	p_{26}	p_{28}				

Thus, there are 32 degrees of freedom in the system. Note that elastic motion of the rack in extension is represented by generalized coordinates p_3 and p_{32}. This is due to the relatively high axial rigidity of the rack. Torsional motion of the rack relative to its base is governed by q_{31}.

The members joining nodes 1 to 2, 2 to 3, etc., are the beam elements with deflection due to bending and shear capability (see Reference 4,pp. 156-161.). The elements of the stiffness matrix of these beam elements are readily computed if the effective flexure modulus, torsion modulus, etc., for the rack structure are known. These coefficients follow from the elastostatic model as described later. The nodal points i (i = 1,2...5) denote the fuel rack mass at the 5 elevations. The node points i^* (i^* = 1,2...5) denote the cumulative mass for all the fuel assemblies distributed at 5 elevations. The element stiffnesses of the fuel assembly are obtained from its geometry. The nodes i^* are located at $x = X_B$, $Y = Y_B$ in the global coordinate system shown in Figure 6.1.

6.2.3 Fluid Coupling

An effect of some significance requiring careful modeling is the so-called "fluid coupling effect." If one body of mass m_1 vibrates adjacent to another body (mass m_2), and both bodies are submerged in a frictionless fluid medium, then the Newton's

equations of motion for the two bodies have the form

$$(m_1 + M_{11})\ddot{X}_1 - M_{12}\ddot{X}_2 = \text{applied forces on mass } m_1$$
$$-M_{21}\ddot{X}_1 + (m_2 + M_{22})\ddot{X}_2 = \text{applied forces on mass } m_2$$

M_{11}, M_{12}, M_{21}, and M_{22} are fluid coupling coefficients which depend on the shape of the two bodies, their relatives disposition, etc. Fritz[6] gives data for M_{ij} for various body shapes and arrangements. It is to be noted that the above equation indicates that effect of the fluid is to add a certain amount of mass to the body (M_{11} to body 1), and an external force which is proportional to the acceleration of the adjacent body (mass m_2). Thus, the acceleration of one body affects the force field on another. This force is a strong function of the interbody gap, reaching large values forms very small gaps. This inertial coupling is called fluid coupling. It has an important effect in rack dynamics. The lateral motion of a fuel assembly inside the storage location will encounter this effect. So will the motion of a rack adjacent to another rack. These effects are included in the equations of motion. The fluid coupling is between nodes i and i* (i =2,3...5) in Figure 6.1. Furthermore, nodal masses i contain coupling terms which model the effect of fluid in the gaps between adjacent racks.

Finally, fluid virtual mass is included in vertical direction vibration equations of the rack; virtual inertia is added to the governing equations corresponding to rotational degrees of freedom, such as q_4, q_5, q_6, q_{11}, etc.

6.2.4 Damping

In reality, damping of the rack motion arises from material hysteresis (material damping), relative intercomponent motion in structures (structural damping), and fluid drag effects (fluid damping). The fluid damping acts on the i and i* nodal masses. In

the analysis, a maximum of 4% structural damping is imposed on elements of the rack structure during SSE seismic simulations. Actual structural damping values used in the analysis are provided in Table 6.4. This is in accordance with the Grand Gulf Nuclear Station Units 1 & 2 FSAR and NRC guidelines [7]. Material and fluid damping are conservatively neglected.

6.2.5 Impact

The fuel assembly nodes i* will impact the corresponding structural mass node i. To simulate this impact, 4 impact springs around each fuel assembly node are provided (see Figure 6.2). The fluid dampers are also provided in parallel with the springs. The spring constant of the impact springs is assumed equal to the local stiffness of the vertical panel computed by evaluating the peak deflection of a six inch diameter circular plate subject to a specified uniform pressure, and built in around the edge. The spring constant calculated in this manner should provide an upper bound on the local stiffnesses of the structure.

6.2.6 Assembly of the Dynamic Model

The dynamic model of the rack, rack base plus supports, and internal fuel assemblies, is modeled for the general three dimensional (3-D) motion simulation, by five lumped masses and inertial nodes for the rack, base, and supports, and by five lumped masses for the assemblage of fuel assemblies. To simulate the connectivity and the elasticity of the configuration, a total of 18 linear spring dampers, 20 nonlinear gap elements, and 18 nonlinear friction elements are used. A summary of spring-damper, gap, and friction elements with their connectivity and purpose is presented in Table 6.2.

If we restrict the simulation model to two dimensions (one horizontal motion plus vertical motion, for example) for the purposes of model clarification only, then a descriptive model of the simulated structure which includes all necessary spring, gap,

and friction elements is shown in Figure 6.3. The beam springs, K_Δ, K_B at each level, which represent a rack segment treated as a structural beam,[4] are located in Table 6.2 as linear springs 2, 3, 6, 7, 10, 14, and 15. The extensional spring, K_e, which simulates the lowest elastic motion of the rack in extension relative to the rack base, is given by linear spring 37 in Table 6.2. The remaining spring-dampers either have zero coefficients (fluid damping is neglected), or do not enter into the two-dimensional (2-D) motion shown in Figure 6.3. The rack mass and inertia, active in rack bending, is apportioned to the five levels of rack mass; the rack mass active for vertical motions is apportioned to locations 1 and 5 in the ratio 2 to 1. The mass and inertia of the rack base and the support legs is concentrated at node 1.

The impacts between fuel assemblies and rack show up in the gap elements, having local stiffness K_I, in Figure 6.3. In Table 6.2, these elements are gap elements 3, 4, 7, 8, 15, 16, 19 and 20. The support leg spring rates K_S are modelled by elements 9 and 10 in Table 6.2 for the 2-D case. Note that the local elasticity of the concrete floor is included in K_Δ. To simulate sliding potential, friction elements 2 plus 8 and 4 plus 6 (Table 6.2) are shown in Figure 6.3. The local spring rates K_f reflect the lateral elasticity of the support legs. Finally, the support rotational friction springs K_R, reflect the rotational elasticity of the foundation. The nonlinearity of these springs (friction elements 9 plus 15 and 11 plus 13 in Table 6.2) reflects the edging limitation imposed on the base of the rack support legs.

For the 3-D simulation, carried out in detail for this analysis, additional springs and support elements (listed in Table 6.2), are included in the model. Coupling between the two horizontal seismic motions is provided by the offset of the fuel assembly group centroid which causes the rotation of the entire rack. The potential exists for the assemblage to be supported on 1

Table 6.2 Numbering System for Springs, Gap Elements, Friction Elements

I. Spring Dampers (18 total)

Number	Node Location	Description
1	1-2	X-Z rack shear spring
2	1-2	Y-Z rack shear
3	1-2	Y-Z rack bending spring
4	1-2	X-Z rack bending
5	2-3	X-Z rack shear
6	2-3	Y-Z
7	2-3	Y-Z rack bending
8	2-3	X-Z
9	3-4	X-Z rack shear
10	3-4	Y-Z
11	3-4	Y-Z rack bending
12	3-4	X-Z
13	4-5	X-Z rack shear
14	4-5	Y-Z
15	4-5	Y-Z rack bending
16	4-5	X-Z
17	1-5	Rack torsion spring
18	1-5	z rack extensional spring

Table 6.2 (continued)

II. Nonlinear Springs (Gap Elements) (20 total)

Number	Node Location	Description
1	2,2*	X rack/fuel assembly impact spring
2	2,2*	X rack/fuel assembly impact
3	2,2*	Y rack/fuel assembly impact
4	2,2*	Y rack/fuel assembly impact
5	3,3*	X rack/fuel assembly impact
6	3,3*	X rack/fuel assembly impact
7	3,3*	Y rack/fuel assembly impact
8	3,3*	Y rack/fuel assemlby impact
9	Support S1	Z compression spring
10	Support S2	Z compression spring
11	Support S3	Z compression spring
12	Support S4	Z compression spring
13	4,4*	X rack/fuel assembly impact spring
14	4,4*	X rack/fuel assembly impact spring
15	4,4*	Y rack/fuel assembly impact spring
16	4,4*	Y rack/fuel assembly impact spring
17	5,5*	X rack/fuel assembly impact spring
18	5,5*	X rack/fuel assembly impact spring
19	5,5*	Y rack/fuel assembly impact spring
20	5,5*	Y rack/fuel assembly impact spring

III. Friction Elements (16 total)

Number	Node Location	Description
1	Support S1	X direction support friction
2	Support S1	Y direction friction
3	Support S2	X direction friction
4	Support S2	Y direction friction
5	Support S3	X direction friction
6	Support S3	Y direction friction
7	Support S4	X direction friction
8	Support S4	Y direction friction
9	S1	X Floor Moment
10	S1	Y Floor Moment
11	S2	X Floor Moment
12	S2	Y Floor Moment
13	S3	X Floor Moment
14	S3	Y Floor Moment
15	S4	X Floor Moment
16	S4	Y Floor Moment

to 4 rack supports during any instant of a complex 3-D seismic event. All of these potential events may be simulated during a 3-D motion and have been observed in the results.

A brief description of the elastostatic model now follows. This detailed model is used to obtain overall beam stiffness formulae for the rack dynamic model, and to determine detailed stress distributions in the rack from a knowledge of the results of the time history analysis.

6.3 Stress Analysis

6.3.1 Stiffness Characteristics:

The fuel rack is a multicell, folded-plate structure which has what is colloquially called a "honey-comb" configuration. This type of construction is very similar to the so-called "stressed-skin" construction of ribs, spars, and cover plates which are widely used in aircraft construction. Techniques developed in the field of aircraft structural analysis are utilized herein to find the stresses and deformations in such structures. These methods have been thoroughly tested and their reliability has been documented in a number of publications.[8-12]

Figure 6.4 shows two cross-sections of the fuel rack which is modeled as a rectangular network of plates interconnected along nodal lines shown as points in Figure 6.1. An arbitrary load with components F_xi, F_yi, F_zi acts at an arbitrary elevation on one of the nodal lines. We find the displacements and stresses due to such a typical load according to the stressed-skin model as follows.

The torsional deformations are solved for by using the classical theory of torsion for multicelled, thin-walled, cross sections.[13]

The bending deformation is found by using the theory of shear flow[12] wherein all axial stresses are carried by the effective flanges (or stringers) formed by the intersections of the plates and all transverse shears are carried by the plates modeled as shear panels.

From a knowledge of the shear flows, the bending and torsional deformations, it is possible to provide a set of influence functions or the following section properties for the fuel rack as a whole:

$(EI)_{eq}$	=	Bending rigidity (in two places)
$(GJ)_{eq}$	=	Torsional rigidity
$(AE)_{eqs}$	=	Extensional rigidity
k_s	=	Shear deformation coefficient

Such properties are used for the dynamic analysis of seismic loads and serve to establish values for the spring rates of the elastic beam elements representing each rack section.

6.3.2 Combined Stresses and Corner Displacements

The cross-sectional properties and the Timoshenko shear correction factor calculated in the previous section are fed into a dynamic analysis of the system shown in Figure 6.5, with a specified ground motion simulating earthquake loading. From the dynamic analysis, the stress resultants (F_x, F_y, F_z, M_x, M_y, M_z) act as shown in Figure 6.6 are computed for a large number of times $t = \Delta t, 2\Delta t$, etc., at a selected number of cross sections. The displacements (U_x, U_y, U_z) at selected nodal points on the z axis are also provided by the dynamic analysis as well as the rotations (θ_x, θ_y, θ_z) of the cross sections at the nodes.

Figure 6.7 shows a typical subdivision of the structure into elements, nodes, and sections. The stresses are calculated at all sections and the displacements at all four corners of the racks are calculated at these elevations.

Since the axial stress varies linearly over the cross section and achieves its extreme values at one of the four corners of the rack, the shear stresses due to torsional loads (M_Z) achieve their extreme values near the middle of each side. The shear stresses due to lateral forces (F_X, F_Y) will achieve their extreme values at the center of the cross section or at the middle of each side. Thus, candidates for the most critical point on any section will be the points labelled 1 through 9 in Figure 6.8. The expression for the combined stress and kinematic displacement for each of these points is written out. Similarly, the stresses in the support legs are evaluated.

A validated Joseph Oat Corporation proprietary computer program "EGELAST"† computes the stresses at the candidate points at each level. It sorts out the most stressed location in space as well as time. The highest stress and maximum kinematic displacements are thus readily found.

6.4 Time Integration of the Equations of Motion

Having assembled the structural model, the dynamic equations of motion corresponding to each degree of freedom can be written by using Newton's second law of motion; or using Lagrange's equation. For example, the motion of node 2 in y-direction (governed by the generalized coordinate p_9) is written as follows:

---

† This code has been previously utilized in licensing of similar racks for Fermi II (Docket No. 50-341), and Quad Cities I and II (Docket Nos. 50-254 and 265).

The inertial mass is:

$$m_{22} + A_{211} + B_{211}$$

where m_{22} is the mass of node 2 for y-directional motion.

A_{211} is the fluid coupling mass due to interaction with node 2*, and

B_{211} is the fluid coupling mass due to interaction of node 2 with the reference frame (interaction between adjacent racks).

Hence, Newton's law gives

$$(m_{22} + A_{211} + B_{211}) \ddot{p}_9 + A_{212} \ddot{p}_{10} + B_{212} \ddot{u} = Q_9$$

where Q_9 represents all the beam spring and damper forces on node 2, and A_{212} is the cross term fluid coupling effect of node 2*; B_{212} is the cross term fluid coupling effect of the adjacent racks, and u represents ground acceleration.

Let

$$q_9 = p_9 - u$$

$$q_{10} = p_{10} - u$$

That is, q_9 is the relative displacement of node 2 in x-direction with respect to the ground. Substituting in the above equation, and rearranging, we have:

$$(m_{22} + A_{211} + B_{211}) \ddot{q}_9 + A_{212} \ddot{q}_{10} = Q_9 - (m_{22} + A_{211} + B_{211} + A_{212} + B_{212}) \ddot{u}$$

A similar equation for each one of the 32 degrees of freedom can be written. The system of equations can be represented in matrix notation as:

$$[M]\{\ddot{q}\} = [Q] + \{G\}$$

where the vector $[Q]$ is a function of nodal displacements and velocities, and $\{G\}$ depends on the coupling inertia and the ground acceleration. Premultiplying above equation by $[M]^{-1}$ renders the resulting equations uncoupled in mass.

We have:

$$\{\ddot{q}\} = [M]^{-1}[Q] + [M]^{-1}\{G\}$$

The generalized force Q_9, which contains the effects of all spring elements acting on node 2 in the "direction" of coordinate q_9 (the relative displacement of node 2 in the y direction), can easily be obtained from a free body analysis of node 2. For example, in the 2-D model shown in Figure 6.3, contributions to Q_9 are obtained from the two shear springs of the rack structure, and the two impact springs which couple node 2* and node 2. Since each of these four spring elements contain couplings with other component deformations through the spring force-deformation relations, considerable static coupling of the complete set of equations results. The level of static coupling of the equations further increases when 3-D motions are considered due to the inclusion of rack torsion and general fuel assembly group centroid effect.

For example, referring to Figure 6.3, and Table 6.1, a 2-D simulation introduces static coupling between coordinates 2,9 and 15 in the expression for Q_9; this coupling comes from the shear springs simulating the rack elasticity which have constitutive relations of the form $|F| = K_S\,|(q_9 - q_2)|$, $K_S\,|(q_{15} - q_9)|$. Further, the impact springs introduce two additional forces having constitutive equations of the form $|F| = K_I\,|(q_9 - q_{10})|$. Of course, at any instant, these forces may be zero if the local gap is open. The local gap depends on the current value of $|q_9 - q_{10}|$.

It should be noted that in the numerical simulations run to verify structural integrity during a seismic event all elements of the fuel assemblies are assumed to move in phase. This will provide maximum impact force level, and hence induce additional conservatism in the time history analysis.

This equation set is mass uncoupled, displacement coupled, and is ideally suited for numerical solution using the central difference scheme. The computer program named "DYNAHIS"†, developed by General Electric Company, performs this task in an efficient manner.

Having determined the internal forces as a function of time, the computer program "EGELAST" computes the detailed stress and displacement fields for the rack structure as described in the preceding section.

6.5 Structural Acceptance Criteria

There are two sets of criteria to be satisfied by the rack modules:

(a) Kinematic Criterion: This criterion seeks to ensure that adjacent racks will not impact during SSE (condition E'[14]) assuming the lower bound value of the pool floor surface friction coefficient. It is further required that the factors of safety against tilting[15] are met (1.5 for OBE, 1.1 for SSE).

(b) Stress Limits

(1) The stress limits of the ASME Code, Section III, Subsection NF, 1980 Edition up to and including Winter 1981 addenda were chosen to be met, since

---

† This code has been previously utilized in licensing of similar racks for Fermi II (Docket No. 50-341), and Quad Cities I and II (Docket Nos. 50-254 and 265).

this Code provides the most consistent set of limits for various stress types, and various loading conditions. The following loading cases[14] have been analyzed.

	SRP Designation	ASME Designation
(i)	$D + L$	Level A
(ii)	$D + L + T_o$	Level A
(iii)	$D + L + T_o + E$	Level B
(iv)	$D + L + T_a + E$	Level B
(v)	$D + L + T_o + P_f$	Level D
(vi)	$D + L + T_a + E'$	Level D
	$D + L + F_d$	Level D

These loads have the following connotation with respect to the fuel rack analysis:

D	=	Dead weight of rack and contained fuel assemblies.
L	=	Live load = 0
T_o	=	Stresses due to differential thermal expansion in the body of the rack. It is further explained below.
E	=	Operating basis earthquake
T_a	=	Identical to T_o
E'	=	Safe shutdown earthquake
P_f	=	Upward force on the racks caused by postulated stuck fuel assembly
F_d	=	Force caused by accidental drop of the heaviest load for the maximum possible height.

The conditions T_a and T_o cause local thermal stresses to be produced. The worst situation will be obtained when an isolated storage location has a fuel assembly which is generating heat at the maximum postulated rate. The surrounding storage locations are assumed to contain no fuel. Furthermore, the loaded storage location is assumed to have unchanneled fuel. Thus, the heated water makes unobstructed contact with the inside of the storage walls, thereby producing maximum possible temperature difference between the adjacent cells. The secondary stresses thus produced are limited to the body of the rack; that is, the support legs do not experience the secondary (thermal) stresses.

(2) Basic Data: The following data on the physical properties of the rack material are obtained from the ASME Codes, Section III, appendices.

Table 6.3 Physical Property Data*

Property	Young's Modulus @ 200°F E	Yield Strength @200°F S_y	Ultimate Strength @200°F S_u	Allowable Stress @ 200°F S
Value	28.3 x 10^6 psi	25 KSI	71 KSI	17.8 KSI
Section III Reference	Table I-6.0	Table I-2.2	Table I-3.2	Table I-7.2

*Evaluated at 200°F. This temperature is higher than the pool water bulk temperature under any of the loading conditions under consideration.

(3.1) Normal and upset conditions (level A or level B):

(i) Allowable stress in tension on a net section $=F_t = 0.6\ S_y$ or

$F_t = (0.6)\ (25000) = 15000$ psi

F_t is equivalent to primary membrane stresses

(ii) On the gross section, allowable stress in shear is $F_v = 0.4\ S_y$

$= (0.4)\ (25000) = 10000$ psi

(iii) Allowable stress in compression, F_a

$$F_a = \frac{[1 - (\frac{kl}{r})^2 / 2C_c^2]S_y}{[(\frac{5}{3}) + [3(\frac{kl}{r})/8C_c] - [(\frac{kl}{r})^3 / 8C_c^3]}$$

where

$$C_c = [\frac{2\pi^2 E}{S_y}]^{1/2}$$

Substituting numbers, we obtain, for both support leg and "honey-comb" region:

F_a = 15000 psi

(iv) Maximum bending stress at the outermost fiber due to flexure about one plane of symmetry:

$F_b = 0.60\ S_y$ = 15000 psi

(v) Combined flexure and compression:

$$\frac{f_a}{F_a} + \frac{C_{mx} f_{bx}}{D_x F_{bx}} + \frac{C_{my} f_{by}}{D_y F_{by}} < 1$$

where

f_a: Direct compressive stress in the section.

f_{bx}: Maximum flexural stress along x-axis

F_{by}: Maximum flexural stress along y-axis

$C_{mx} = C_{my} = 0.85$

$$D_x = 1 - \frac{f_a}{F_{\acute{e}x}}$$

$$D_y = 1 - \frac{f_a}{F_{\acute{e}y}}$$

where

$$F_{ex} = \frac{12\pi^2 E}{23\left(\frac{kl_b}{r_b}\right)^2}$$

(vi) Combined flexure and compression (or tension)

$$\frac{f_a}{0.6\ S_y} + \frac{f_{bx}}{F_{bx}} + \frac{f_{by}}{F_{by}} < 1.0$$

The above requirement should be met for both direct tension or compression case.

(3.2) Faulted Condition:

F-1370 (Section III, Appendix F), states that the limits for the faulted condition are 1.2 (S_y/F_t) times the corresponding limits for normal condition. Thus, the multiplication factor is

$$\text{Factor} = (1.2)\ \frac{25000}{15000} = 2.0$$

(3.3) Thermal Stresses:

There are no stress limits for thermal (self-limiting) stresses in Class 3-NF Structures for linear-type supports. However, the range of primary and secondary stress intensity is required to be limited to 3 S_m in the manner of Class 1 components; S_m is the allowable stress intensity of the rack material at the maximum operating temperature.

6.6 RESULTS

The input time history accelerations for seismic motion were developed by Bechtel Corporation (see Appendix 1). Plots of the time history motions, utilized in the present analysis are shown in in Figure 6.9 through Figure 6.14. These plots correspond to the Safe Shutdown Earthquake (SSE) with 5% damping.

Since there are several rack module configurations (Figs. 2.1 and 2.2) it was decided to make an exhaustive analysis of one rack type. We note that rack A is an above-average size module, and hence will produce above-average floor reaction and support stress levels. Rack type A is also most numerous. Hence rack A is chosen for performing extensive analyses. Appropriate simulations are also carried out for other limiting rack geometries (e.g. tipping study for rack with low cross section to height aspect ratio, stress evaluations for the heaviest module, etc.). To determine the magnitude of structural dampers, free lateral vibration plots of the top of rack A (in X and Y directions) for fully loaded and empty conditions were developed. The dominant natural frequency of vibration thus evaluated enables computations of the linear structural dampers. The maximum percentage structural damping for SSE condition is assumed to be 4% and modifications to the stiffness matrix to incorporate damping is based on the dominant frequency of 12.75 cps. Having determined the damper characteristic data, the dynamic analysis of the rack module is performed using the computer program DYNAHIS. Two components of the SSE horizontal acceleration are applied in two orthogonal directions concurrently with the vertical seismic acceleration. Abstracted results for all simulations carried out are reported in Table 6.4. Table 6.5 gives the maximum values of stress factors R_i (i = 1,2,3,4,5,6). The values given in the tables are the maximum values in time and space (all sections of the rack). The various stress factors are listed below for convenience of reference.

R_1: Ratio of tensile stress on a net section to its allowable OBE value

R_2: Ratio of maximum gross shear on a net section to its allowable OBE value

R_3: Ratio of maximum bending stress in one plane (x-y) to its allowable OBE value for the section

R_4: Ratio of maximum bending stress in one plane (y-z) to its allowable value in OBE

R_5: Combined flexure and compressive factor

R_6: Combined flexure and tension (or compression) factor

The allowable value of R_i ($i = 1,2,3,4,5,6$) is 1 for OBE condition, and is 2 for SSE condition (see Section 6.5).

The displacement and stress tables given herein are for the SSE conditon. If necessary, OBE studies are run to qualify the rack when the SSE simulation with damping of 2% does not yield stress factors that would clearly indicate a safe margin under OBE conditions. Seismic simulations for the tipping conditions are carried out by increasing the horizontal SSE accelerations by 50%[15]. These calculations indicate that the rack remains stable, and the gross movement remains within the limit of small motion theory.

For rack type A (304 cells), the gap between racks is 4 5/32" in the x direction and 3 3/4" in the y direction. The maximum displacement in either direction for any case considered is 0.62" which is less than 50% of the spacing. Note that the direction along the smallest side is the local X direction of the rack.

For rack D1, the critical spacing is 4 5/32" in the local x direction and 4 9/16" in the y direction. The critical deflection for all cases considered is 1.64".

For rack type G in the containment pool, the critical dimensions are 5 7/16" and 7" respectively. Referring to Table 6.4, the maximum displacements for rack G under all cases is less than 1.6", although the artificial tipping analysis (1.5 x SSE on orizontal earthquake) gives 3.02". However, the purpose of the tipping analysis is simply to show the safety factor against overturning.

For rack type F, the critical spacings are 7" and 3 15/16" respectively with the maximum displacement of 1.17 obtained being less than 50% of the inter-rack spacing. Note that all of the rack displacements presented in Table 6.4 are quoted for the top of the rack.

Table 6.5 shows the maximum values of the stress factors obtained. For rack types A, D1, all stress factors are less than 1.0 even using the SSE earthquake if we exclude the cases simulated for tipping. Even under 1.5 SSE horizontal, 1.0 vertical earthquakes, the stress factors remain under 2.0 for an SSE event.

For racks G and F, the stress factors are below 2.0 for all SSE events simulated, even when only 2% damping is considered. The one OBE simulation shows that stress factors drop considerably when the less severe earthquake is used.

It is noted that all of the stress factors shown are maximum in the rack supports. Stress coefficients in the rack proper are usually about 10% or less than the values quoted for the rack supports.

As noted above, seismic simulations for the tipping conditions are carried out by increasing the horizontal SSE accelerations by 50% [15]. The calculations indicate that the rack remains stable, and that the gross movement remains within the limit of small motion theory. Thus, the rack module is seen to satisfy both kinematic and stress criteria with large margins of safety.

Analysis of the rack for damaged fuel modules shows comparable results, and an analysis of the welded joints in the rack also indicates acceptable safety margins.

Cases Considered (All SSE Events except Case 11)

Case Number	Description
1	Full rack, Damping > 2% μ = .8
2	Tipping Analysis (1.5 SSE horizontal quake) 2% damping, μ = .8
3	Full rack, μ = .8, 2% damping
4	Full Rack, μ = .2, 2% Damping
5	Half load, Diag. Fill, μ = .8 2% Damping
6	Half Load, Diag. Fill, μ = .2 2% Damping
7	Half Load, Positive X Quadrant, μ = .8, 2% Damping
8	Empty Rack, μ = .8 2% or 4% Damping
9	Empty Rack, μ = .2 2% or 4% Damping
10	Half load; Positive X Quadrant μ = .2, 2% Damping
11	Full Rack, μ = .8 2% Damping, OBE Quake

Table 6.4

Maximum Rack Module Displacements
(Damping = 2% except where noted)

Module Type	Case No.	μ	Max. X - Dispt. & Time U_x (max) (inch)	Time Instant (sec)	Max Y - Dispt. & Time U_y (max) (inch)	Time Instant (sec)	Comments
A	1	.8	.034	6.54	.027	10.51	Full rack 4% Damping SSE
A	2	.8	.063	8.07	.121	10.88	Full Rack (1.5 SSE)
A	3	.8	.038	8.9	.033	10.98	Full Rack (SSE)
A	4	.2	.167	15.21	.184	10.42	Full Rack (SSE)
A	5	.8	.050	7.66	.016	6.76	Half full-diag. loading
A	6	.2	.174	10.53	.114	5.0	Half full- dia. loading
A	7	.8	.056	10.6	.020	10.44	Half full Pos. x loading
A	8	.8	.59	13.37	.62	9.04	Empty rack 4% Damping SSE
D1	3	.8	.045	10.3	.021	8.38	Full Rack SSE
D1	2	.8	.122	10.5	.042	10.5	Full Rack 1.5 SSE
D1	4	.2	.206	10.4	.200	10.5	Full rack SSE
D1	8	.8	1.64	9.38	.611	7.31	Empty Rack 4% damping SSE
D1	9	.2	.552	5.25	.650	6.75	Empty rack 4% Damping SSE

Table 6.4 (Continued)

Maximum Rack Module Displacements
(Damping = 2% except where noted)

Module Type	Case No.	μ	Max. X - Dispt. & Time U_x (max) (inch)	Time Instant (sec)	Max Y - Dispt.& Time U_y (max) (inch)	Time Instant (sec)	Comments
D1	5	.8	.215	10.53	.032	10.57	Half full diag. loading
D1	6	.2	.244	10.43	.361	10.51	Half full diag. loading
D1	7	.8	.053	9.31	.019	7.23	Half full pos. x loading
D1	10	.2	.179	10.6	.230	10.52	Half full pos. x loading
G	1	.8	.257	7.44	1.27	11.31	Full rack 4% damping, SSE
G	4	.2	.581	10.55	.612	10.48	Full rack SSE
G	2	.8	2.305	10.56	3.02	10.73	Full rack 1.5 SSE
G	5	.8	1.52	11.86	1.55	11.22	Half full SSE diag. loading
G	6	.2	1.042	8.20	.812	10.94	Half full, SSE, diag. loading
G	10	.2	1.10	8.59	.791	10.48	Half full pos. x loading
G	9	.2	1.452	8.63	0.774	8.86	Empty rack, SSE (2% damping)

Table 6.4 (Continued)

Maximum Rack Module Displacements
(Damping = 2% except where noted)

Module Type	Case No.	μ	Max. X - Dispt. & Time U_x (max) (inch)	Time Instant (sec)	Max Y - Dispt.& Time U_y (max) (inch)	Time Instant (sec)	Comments
G	11	.8	.027	5.03	.024	4.79	Full rack OBE Quake 2% Damping
F	1	.8	.147	11.36	1.52	11.35	Full rack 4% damping SSES
F	8	.8	.951	15.57	1.17	10.49	Empty rack 4% damping SSE
F	9	.2	.62	8.63	.74	10.72	Empty rack 4% damping SSE
H	1	.8	.494	11.63	.012	5.98	Full rack, 4% damping 1.5 X SSE
H	2	.8	1.42	10.74	.38	10.52	Full rack 4% damping 1.5 x SSE
H	8	.8	1.402	14.20	1.147	11.62	Empty Rack

Table 6.5

Maximum Values of Stress Factors R_1-R_6

Module Type	Case No.	μ	R_1	R_2	R_3	R_4	R_5	R_6	Comments
A	1	.8	.285	.195	.293	.306	.649	.713	Full rack 4% damping (SSE)
A	2	.8	.439	.374	.706	.597	1.44	1.62	Full Rack (1.5 SSE)
A	3	.8	.321	.209	.334	.363	.647	.849	Full Rack (SSES)
A	4	.2	.246	.064	.124	.149	.4353	.469	Full Rack SSE
A	5	.8	.223	.179	.215	.386	.635	.712	Half full diag. loading
A	6	.2	.172	.049	.081	.097	.280	.299	Half full diag. loading
A	7	.8	.197	.151	.262	.304	.635	.713	Half full - pos. x loading
A	8	.8	.154	.176	.292	.231	.458	.516	Empty rack (4%) damping SSE
D1	3	.8	.239	.184	.263	.317	.599	.666	Full rack SSE
D1	2	.8	.348	.267	.462	.723	1.28	1.45	Full rack 1.5 SSE
D1	4	.2	.206	.056	.123	.217	.422	.460	Full rack SSE
D1	8	.8	.222	.192	.319	.213	.671	.750	Empty rack (4% Damping) SSE
D1	9	.2	.025	.007	.014	.032	.050	.061	Empty rack (4% Damping) SSE
D1	5	.8	.209	.148	.254	.409	.624	.698	Half Full diag. loading
D1	7	.8	.185	.137	.227	.227	.539	.601	Half full pos. x loading

Table 6.5 (Continued)

Maximum Values of Stress Factors R_1-R_6

Module Type	Case No.	μ	R_1	R_2	R_3	R_4	R_5	R_6	Comments
D1	10	.2	.132	.039	.062	.172	.299	.328	Half full pos. x loading
G	1	.8	.250	.208	.565	.447	.768	.866	Full rack 4% Damping SSE
G	4	.2	.165	.045	.224	.282	.454	.508	Full Rack SSE
G	5	.8	.453	.216	.697	.342	1.081	1.192	Half full, SSE, diag. loading
G	7	.8	.172	.094	.403	.251	.549	.622	Half full, pos. x loading
G	10	.2	.099	.029	.130	.143	.297	.308	Half full pos. x loading
G	9	.2	.022	.006	.025	.026	.060	.067	Empty rack sSE
G	11	.8	.135	.039	.123	.151	.273	.303	Full rack OBE Quake 2% damping
F	1	.8	.385	.220	.743	.480	1.069	1.189	Full rack 4% damping SSE
F	8	.8	.134	.067	.305	.105	.462	.520	Empty 4% damping
F	9	.2	.025	.007	.028	.047	.071	.077	Empty 4% Damping
H	1	.8	.184	.173	.207	.487	.588	.618	Full rack 4% damping
H	2	.8							1.5 SSE - 2% Damping
H	8	.8	.376	.496	.529	.577	.853	.854	Empty rack 2% damping

REFERENCES TO SECTION 6

1. USNRC Regulatory Guide 1.29, "Seismic Design Classification," Rev. 3, 1978.

2. "Friction Coefficients of Water Lubricated Stainless Steels for a Spent Fuel Rack Facility," by Prof. Ernest Rabinowicz, MIT, a report for Boston Edison Company, 1976.

3. U.S. Nuclear Regulatory Commission, Regulatory Guide 1.92, "Combining Modal Responses and Spatial Components in Seismic Response Analysis," Rev. 1, February 1976.

4. "The Component Element Method in Dynamics with Application to Earthquake and Vehicle Engineering" by S. Levy and J.P.D. Wilkinson, McGraw Hill, 1976.

5. "Dynamics of Structures" R.W. Clough & J. Penzien, McGraw Hill (1975).

6. R.J. Fritz, "The Effects of Liquids on the Dynamic Motions of Immersed Solids," Journal of Engineering for Industry, Trans. of the ASME, February 1972, pp. 167-172.

7. USNRC Regulatory Guide 1.61, Damping Values for Seismic Design of Nuclear Power Plants, 1973.

8. J.T. Oden, "Mechanics of Elastic Structures," McGraw Hill, N.Y., 1967.

9. R.M. Rivello, "Theory and Analysis of Flight Structures," McGraw-Hill, N.Y., 1969.

10. M.F. Rubinstein, "Matrix Computer Analysis of Structures," Prentice-Hall, Englewood Cliffs, N.J., 1966.

11. J.S. Przemienicki, "Theory of Matrix Structural Analysis," McGraw-Hill, N.Y., 1966.

12. P. Kuhn, "Stresses in Aircraft and Shell Structures," McGraw-Hill, N.Y., 1956.

13. S.P. Timoshenko and J.N. Goodier, "Theory of Elasticity," McGraw-Hill, N.Y., 1970, Chapter 10.

14. U.S. Nuclear Regulatory Commission, Standard Review Plan, NUREG-0800 (1981).

15. U.S. Nuclear Regulatory Commission, Standard Review Plan, Section 3.8.5, Rev. 1, 1981.

16. U.S. Nuclear Regulatory Commission, Regulatory Guide 1.124, "Design Limits and Loading Combinations for Class 1 Linear-Type Component Supports, November 1976.

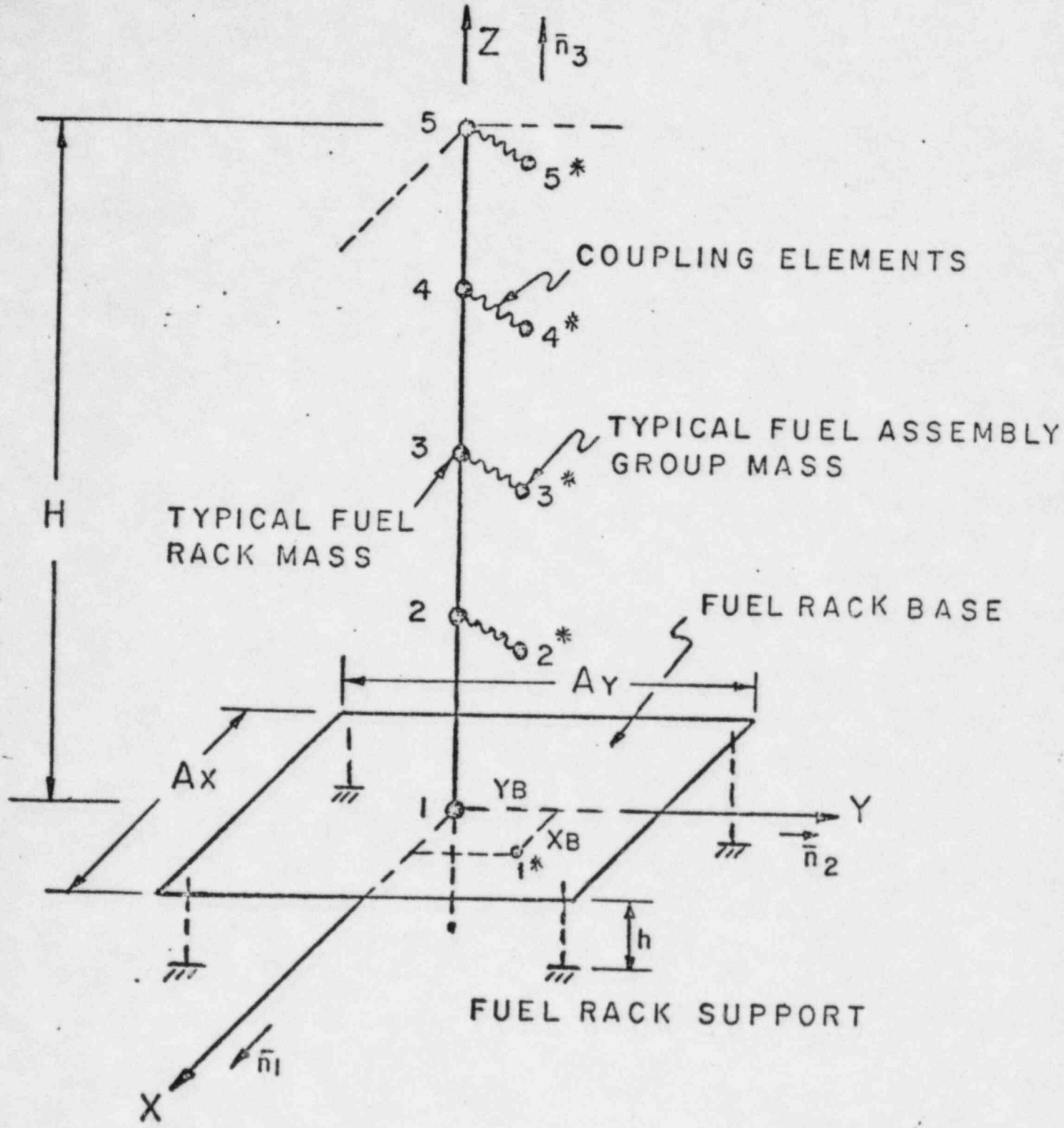

XB, YB - LOCATION OF CENTROID OF FUEL ROD GROUP MASSES - RELATIVE TO CENTER OF FUEL RACK

n_i = UNIT VECTORS

FIG. 6.1 DYNAMIC MODEL

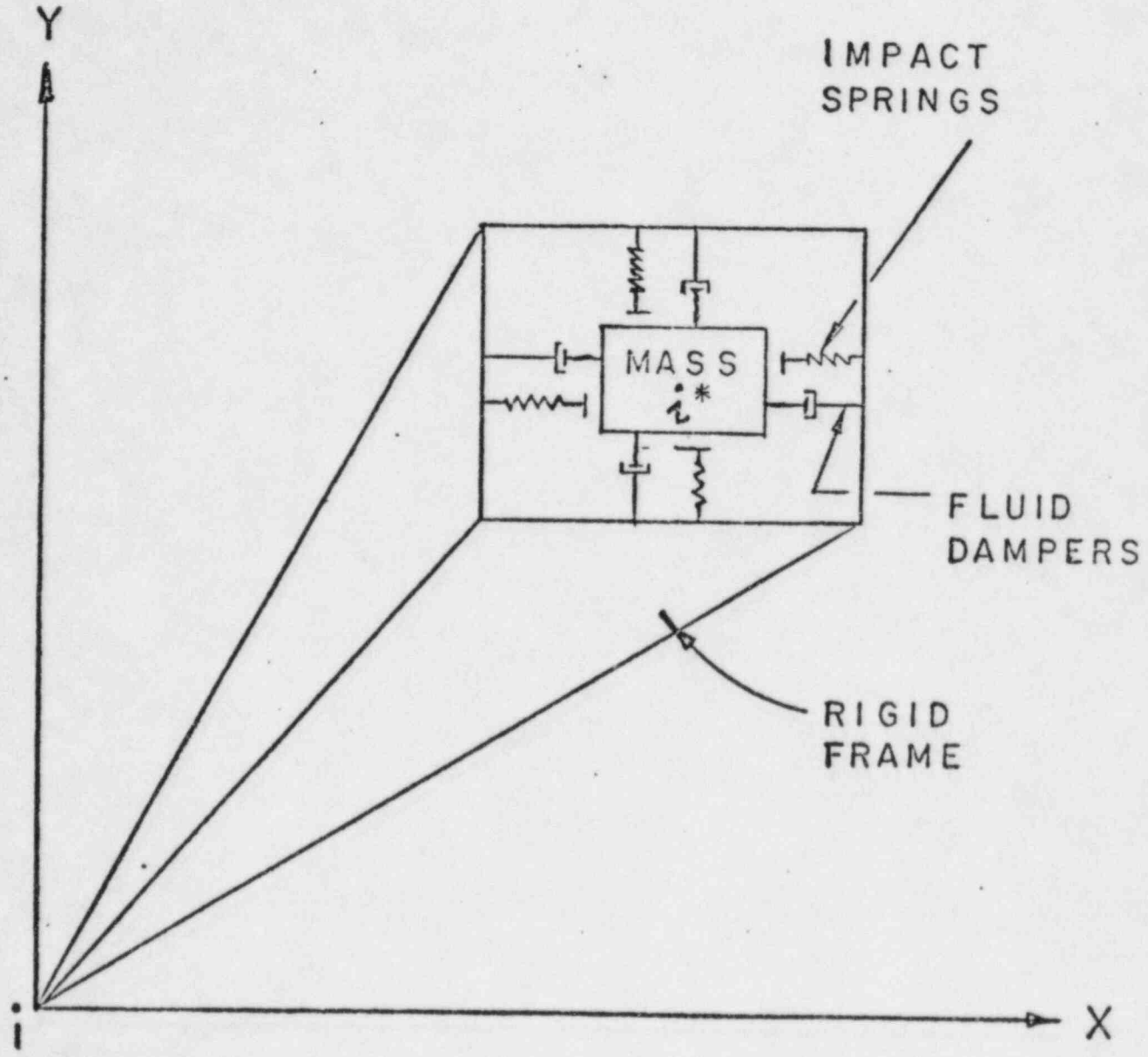

FIG. 6.2 IMPACT SPRINGS AND FLUID DAMPERS

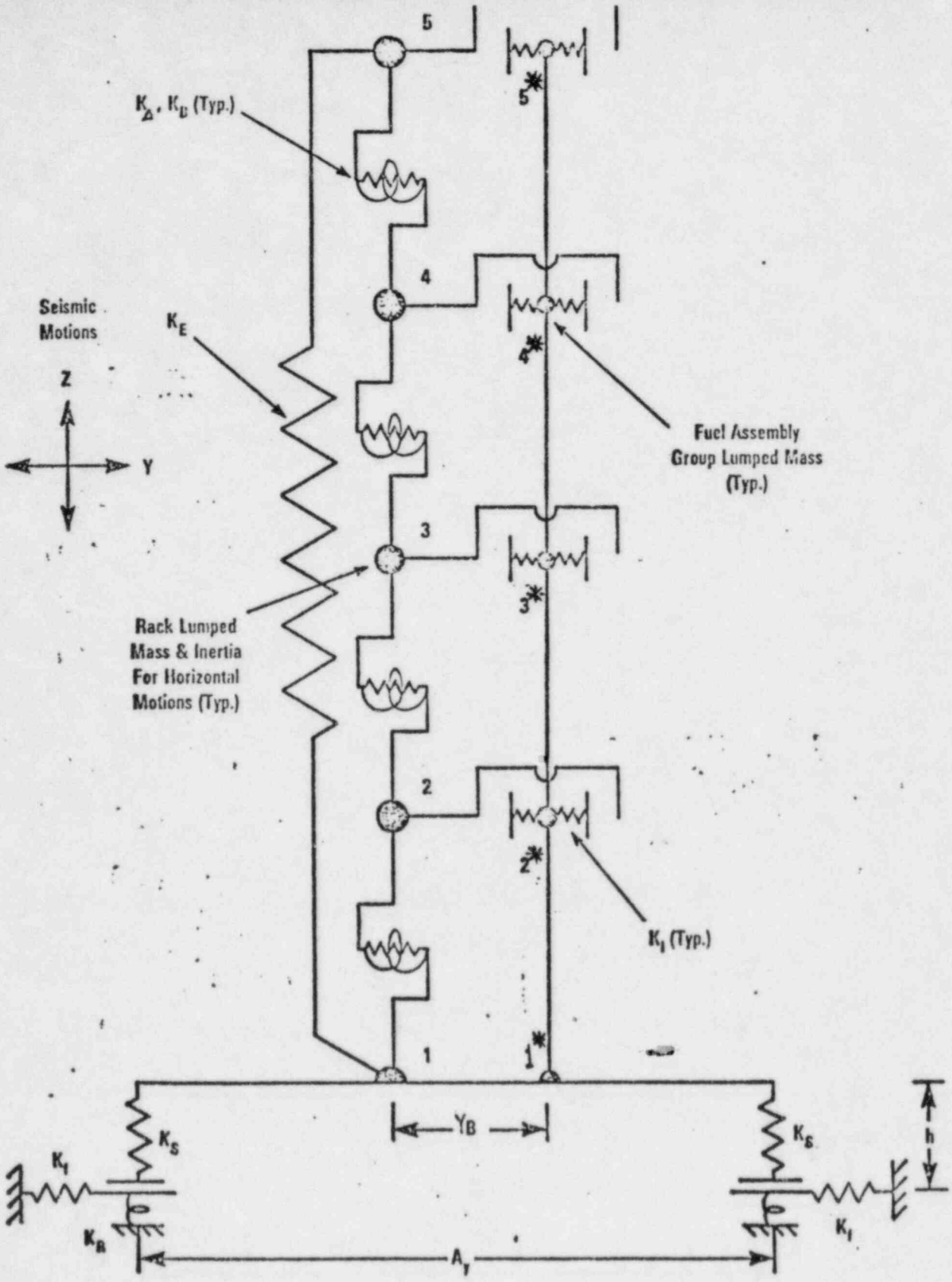

Figure 6.3 Spring Mass Simulation For A Two Dimensional Motion

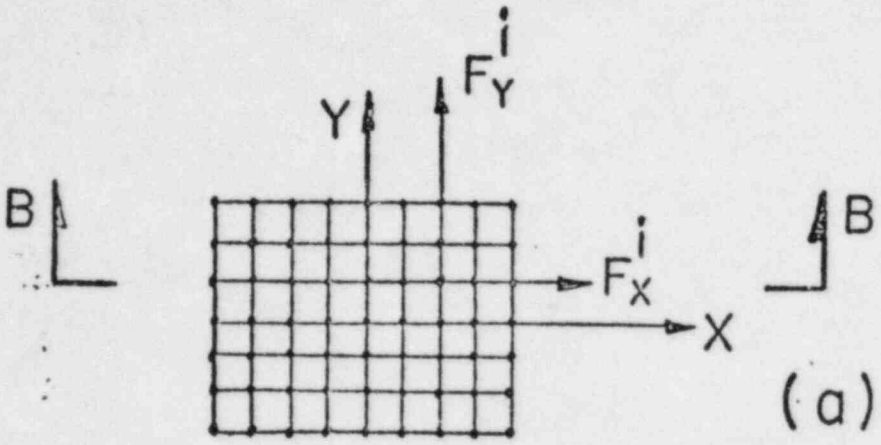

(a) TOP VIEW

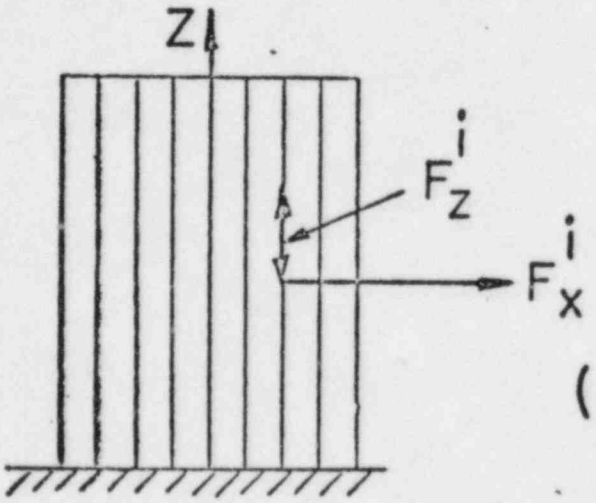

(b) AXIAL CROSS SECTION (B-B

FIG. 6.4 (a) HORIZONTAL CROSS SECTION OF RACK
(b) VERTICAL CROSS SECTION OF RACK

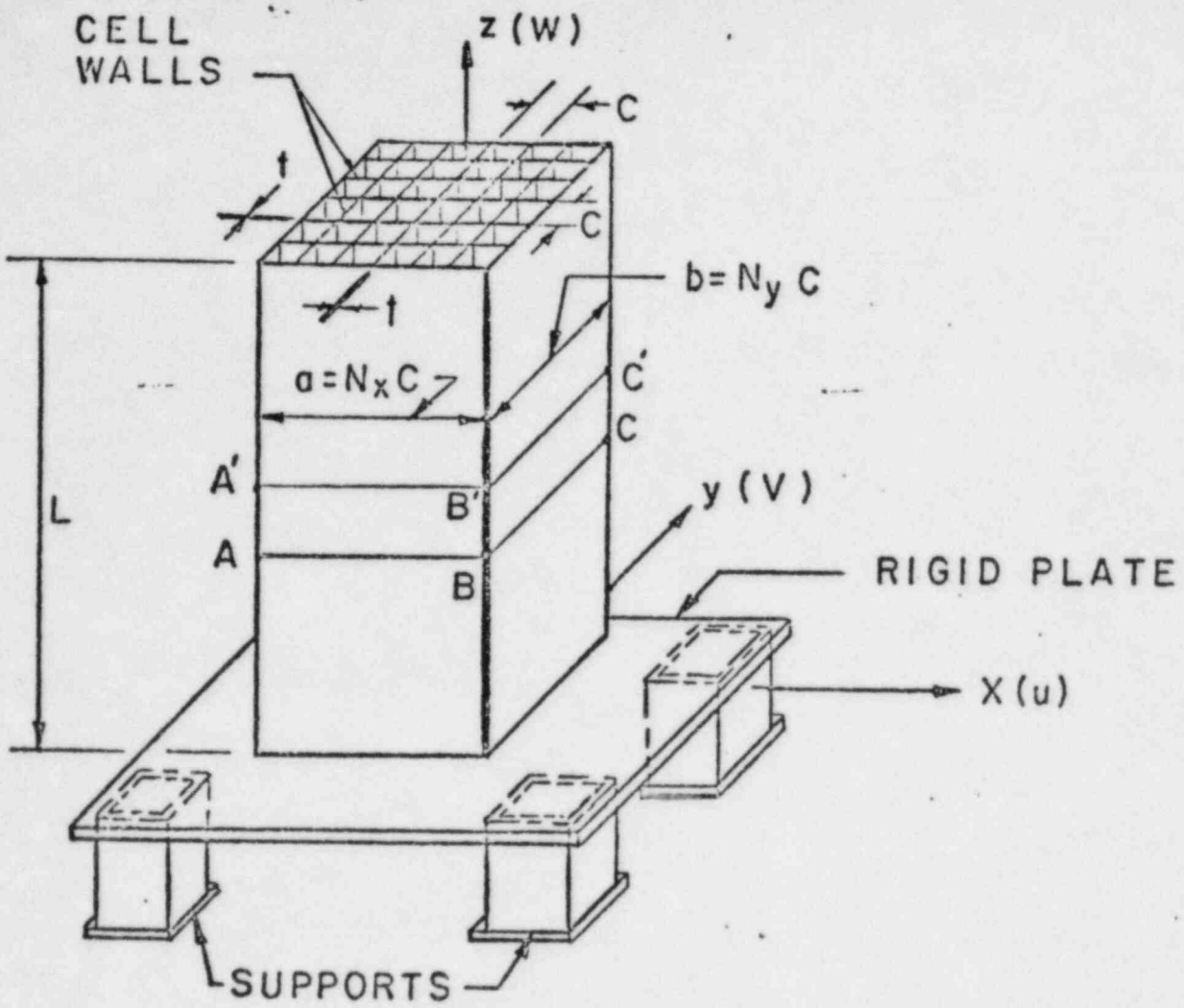

FIG 6.5 DYNAMIC MODEL (RACK)

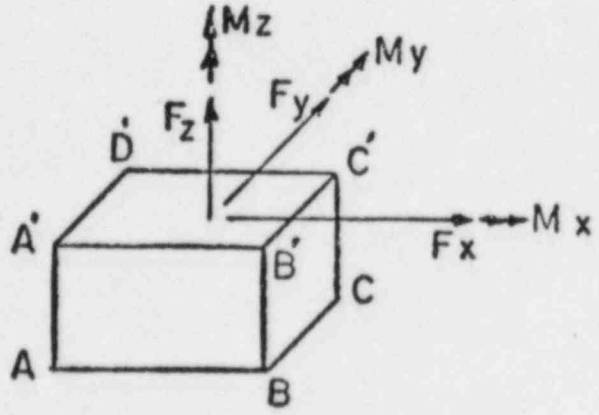

FIG 6.6 STRESS RESULTANTS ORIENTATION

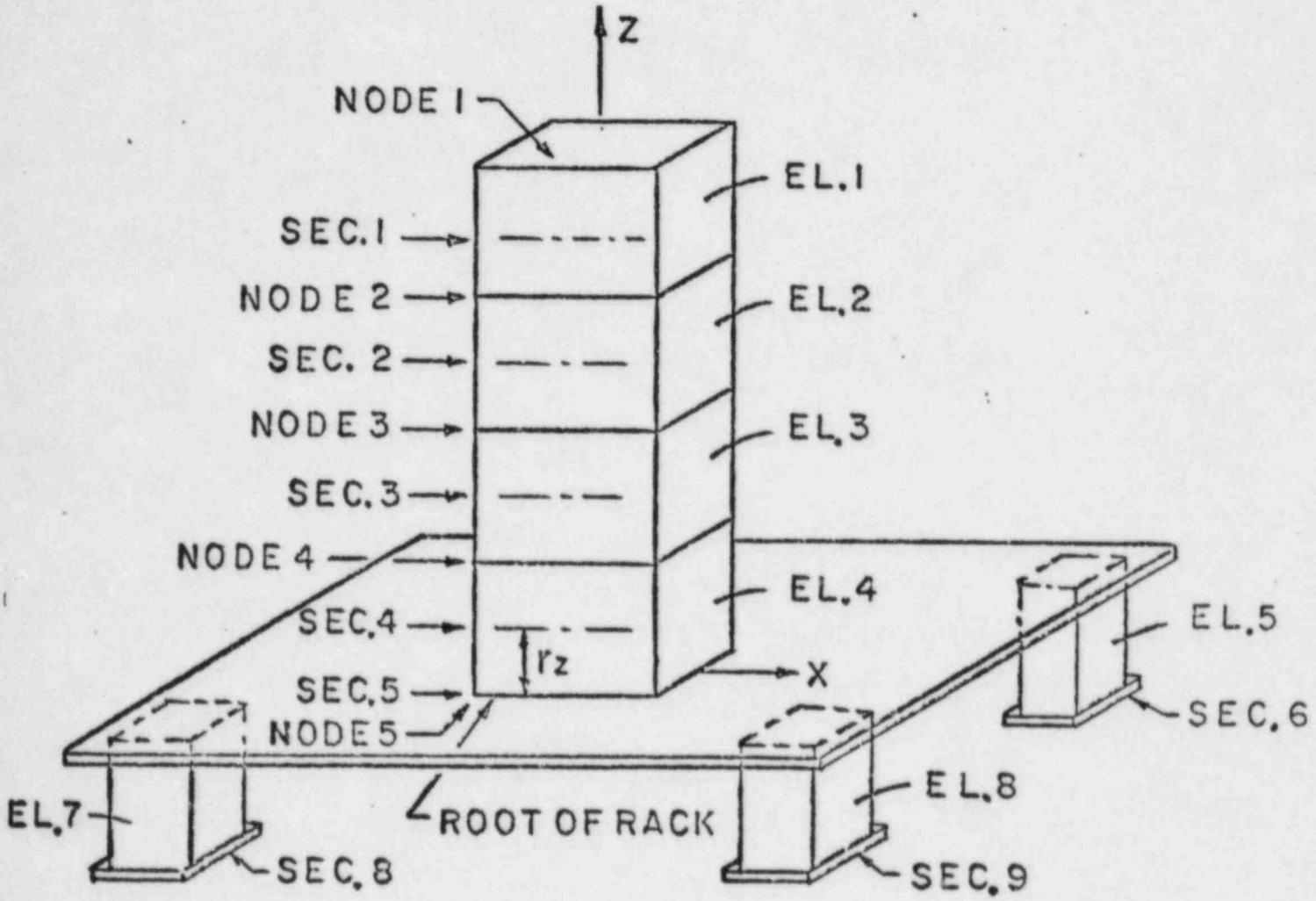

NO. OF ELEMENTS = 8
NO. OF SECTIONS = 9
NO. OF NODES = 5

FIG 6.7 SUBDIVISION OF A TYP. RACK

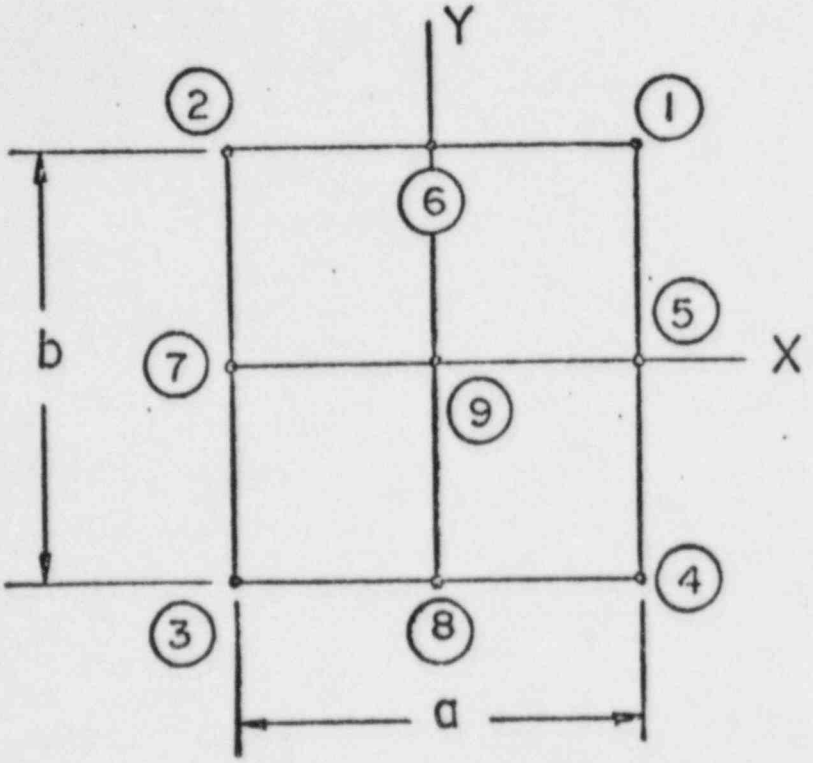

FIG 6.8 FINITE ELEMENT MODEL CROSS SECTION

FIG. 6.9

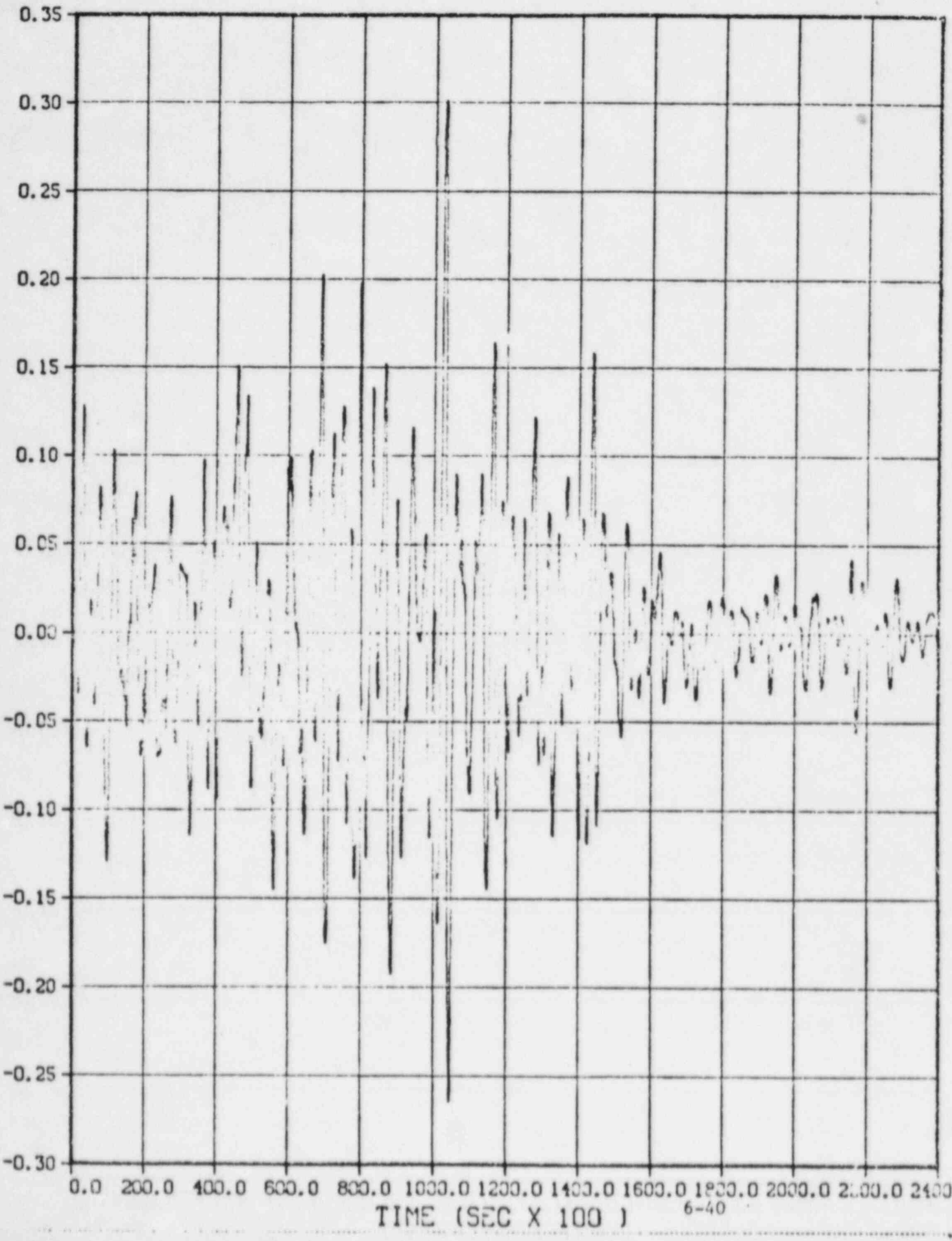
N-S EXCITATION (SSE)
0.35
0.30
0.25
0.20
0.15
0.10
0.05
0.00
-0.05
-0.10
-0.15
-0.20
-0.25
-0.30
ACCELERATION (G)
0.0
200.0
400.0
600.0
800.0
1000.0
1200.0
1400.0
1600.0
1800.0
2000.0
2200.0
2400.0
TIME (SEC X 100)

AUXILLIARY POOL

FIG. 6-10

E-W EXCITATION (SSE)

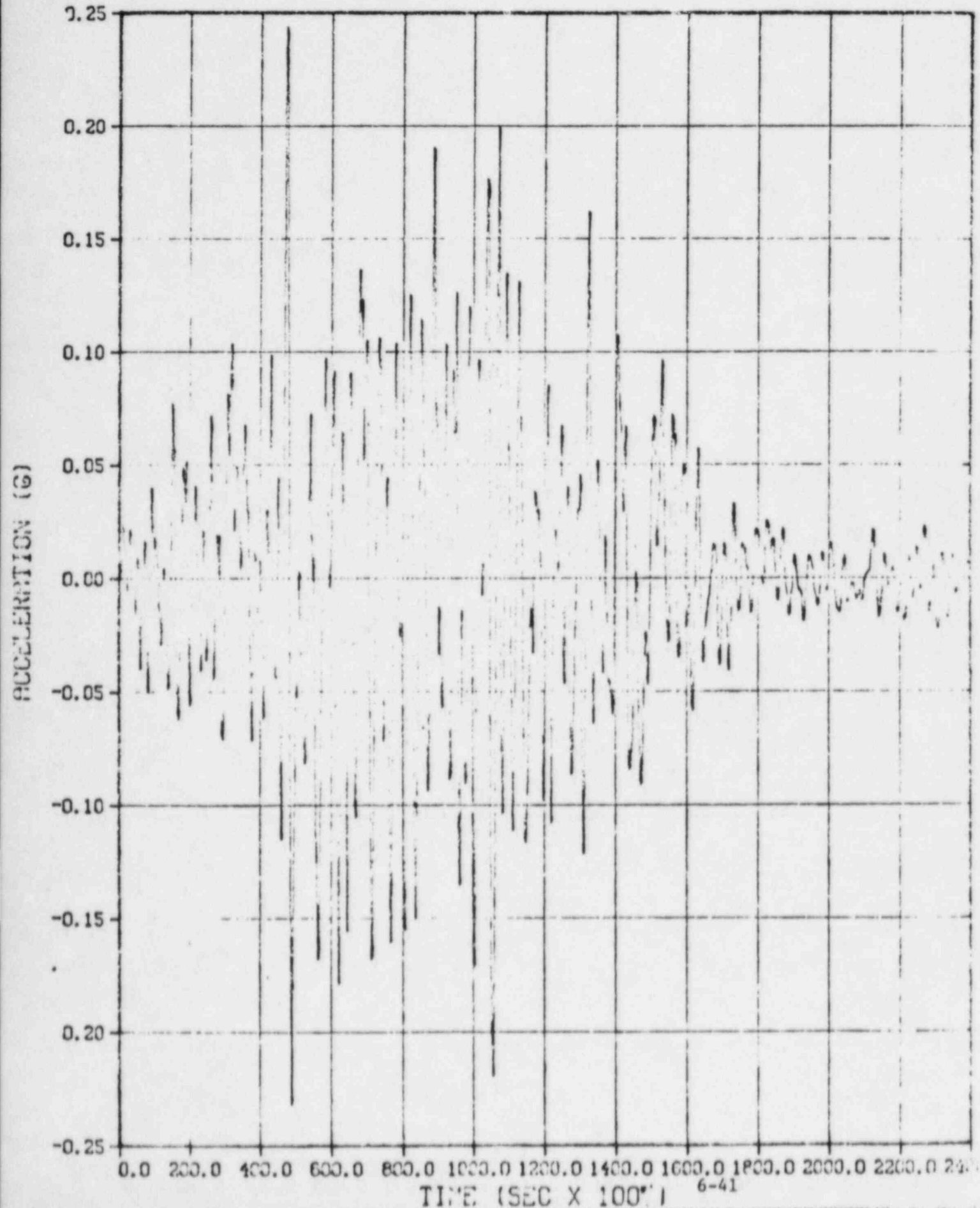

FIG. 6-11

VERTICAL EXCITATION (SSE)

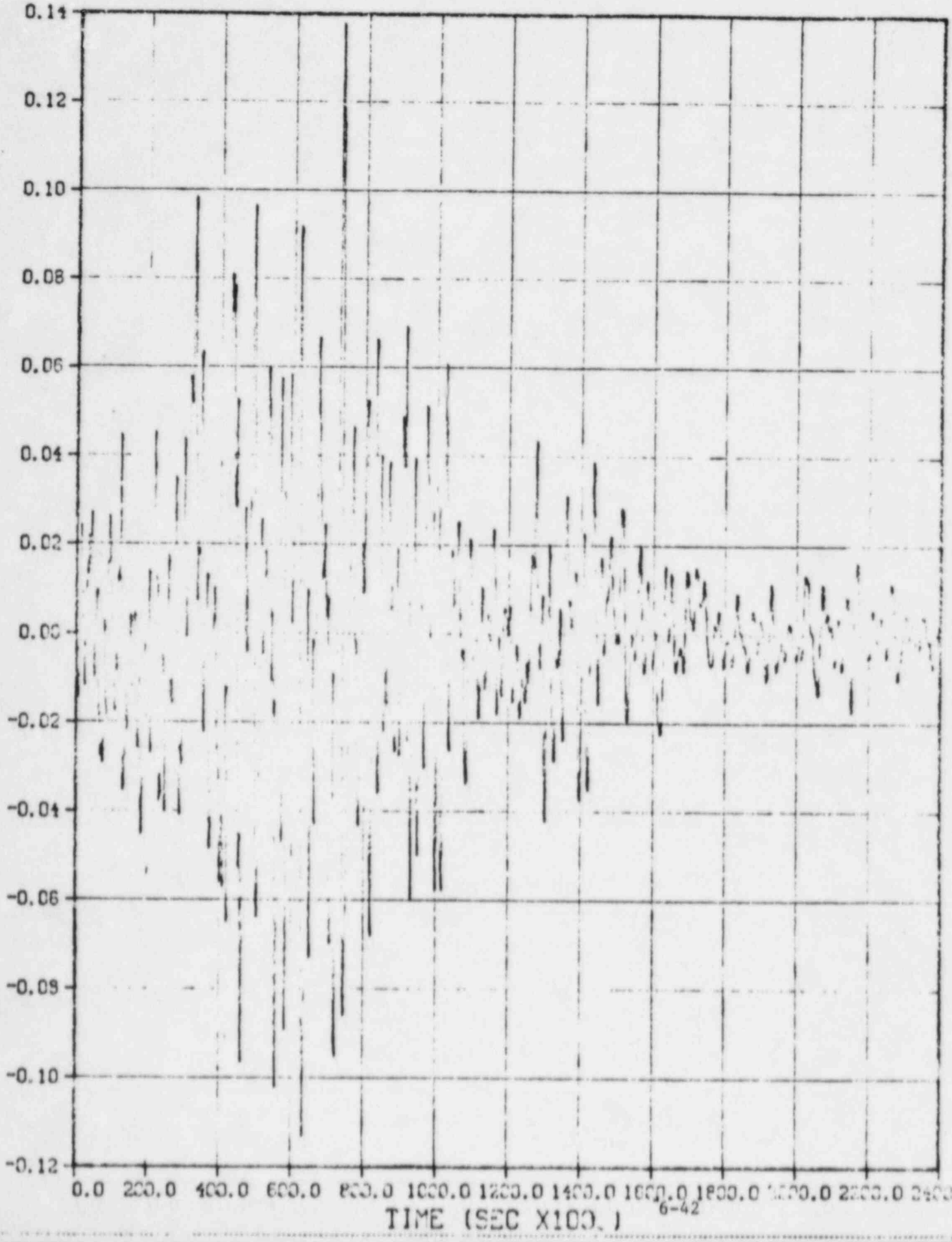

FIG. 6-12

N-S EXCITATION (SSE)

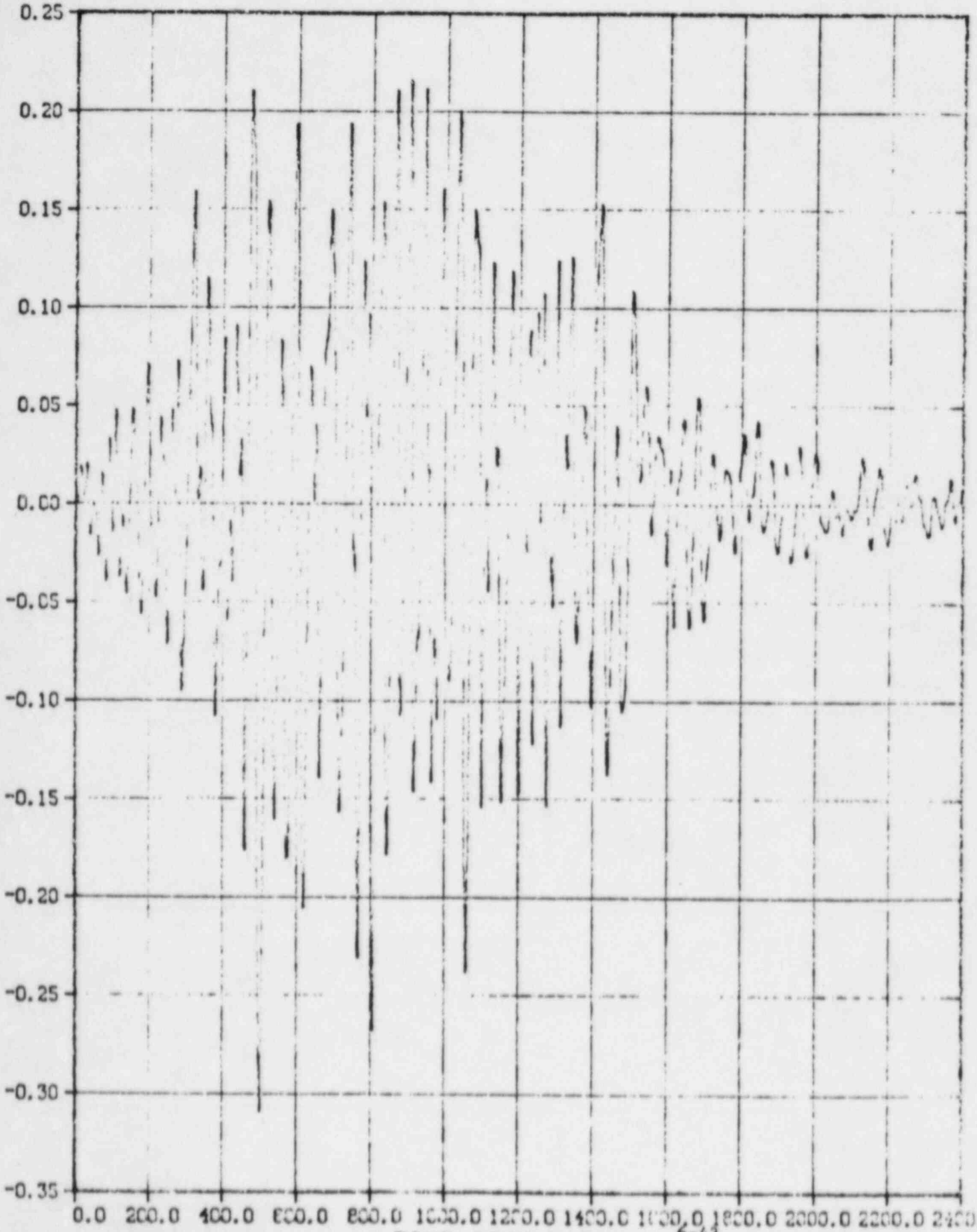

FIG. 6-13

E-W EXCITATION (SSE)

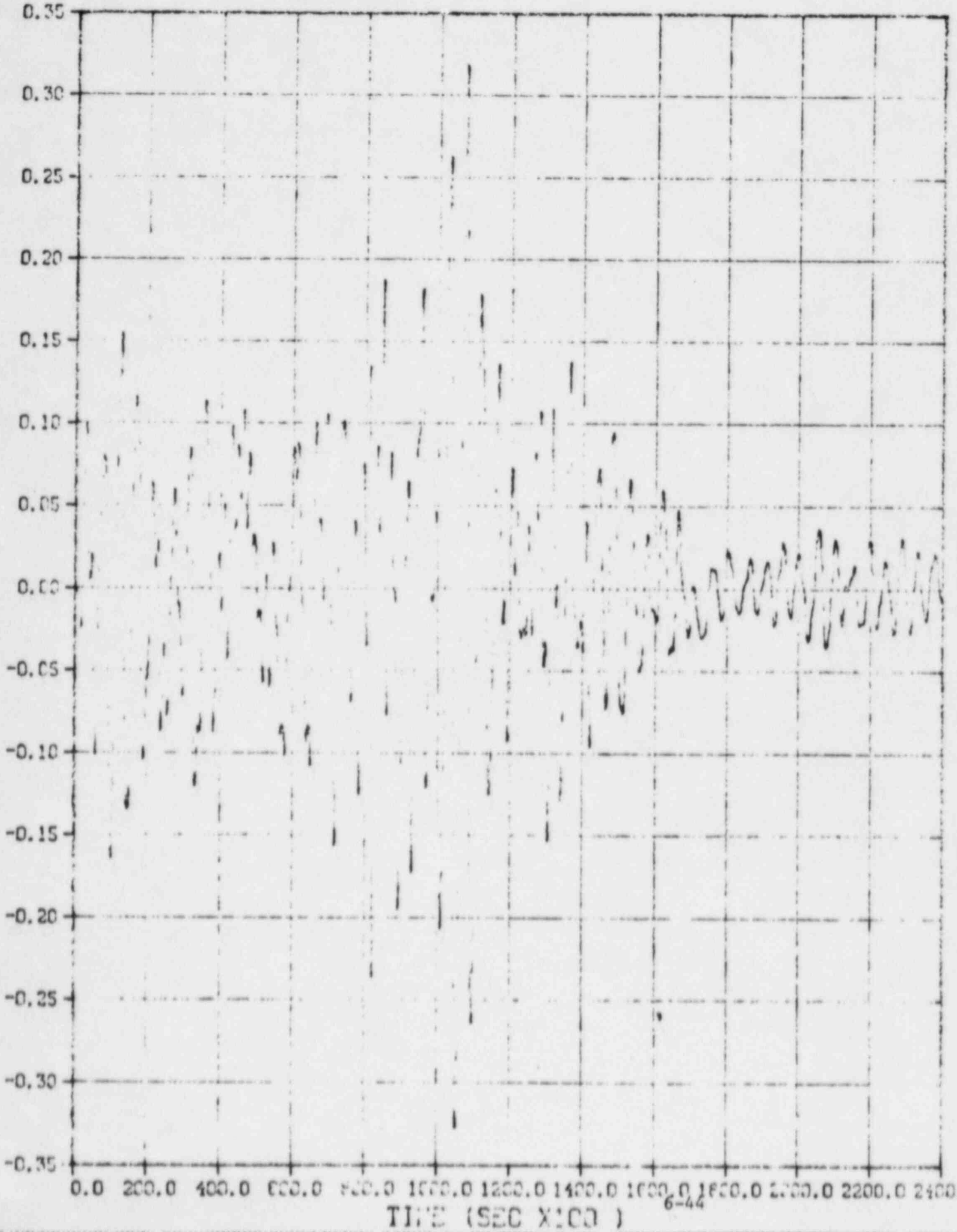

FIG. 6-14

VERTICAL EXCITATION (SSE)

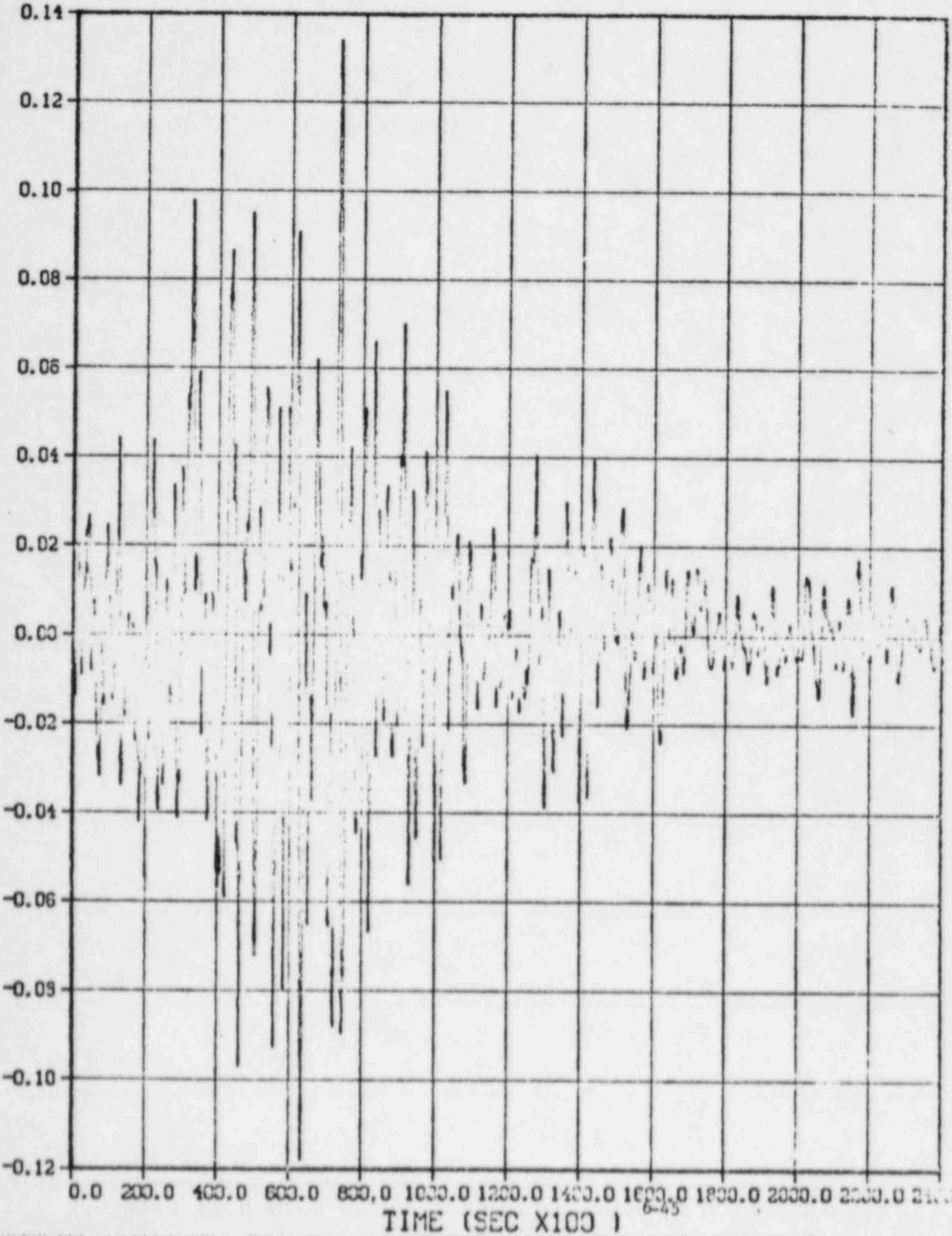

7. ACCIDENTS ASSOCIATED WITH RACK INTEGRITY AND LINER PLATE INTEGRITY

In addition to the seismic analysis presented ir Section 6, the following computations for mechanical loads are also performed.

7.1 Dropped Fuel Accident I

A fuel assembly (weight - 600 pounds) dropping from 36 inches above a storage location and impacting the base. Local failure of the baseplate is acceptable; however, the rack design should preclude impact with the pool liner. The subcriticality of the adjacent fuel assemblies is not to be violated. Calculated results show that the baseplate is not pierced and the rack feet loading on the liner is well below those caused by seismic loads. The maximum depth of baseplate penetration is conservatively estimated to be 0.446" (vs. 0.625" baseplate nominal thickness).

7.2 Dropped Fuel Accident II

One fuel assembly dropping from 36 inches above the rack and hitting the top of the rack. Permanent deformation of the rack is acceptable, but is required to be limited to the top region such that the rack cross-sectional geometry at the level of the top of the active fuel (and below) is not altered. Analysis indicates that the maximum local stress at the top of the rack is limited to 21000 psi which is less than material yield point. Thus, the functionality of the rack is not affected.

7.3 Jammed Fuel-Handling Equipment and Horizontal Force

A 4000-pound uplift force and a 1000-pound horizontal force are applied at the top of the rack at the "weakest" storage locations. The force is assumed to be applied on one wall of the storage cell boundary as an upward edge force over length ℓ. It is shown that if the length ℓ is over 2.46" then no yielding will occur. If ℓ is smaller than 2.46", the damage is limited to the region above the top of the active fuel. Horizontal force of 1000-pounds applied at the top edge of a cell wall produces plastic deformation over 2" depth - well removed from the zone of active fuel.

7.4 Liner Integrity Analysis

The floor liner in both pools is 1/4" thick, ASTM 240-Type 304 plate material. Since the auxiliary pool has heavier rack modules, the liner loads developed in the auxiliary pool bound the problem. The time history loading of the liner due to shear between rack module and liner plate (pool floor) is obtained as a by-product of the seismic analysis (described in Chapter 6). To investigate liner integrity, two load cases - cases 1 & 5 from Chapter 6 - for rack A (heaviest rack module) are examined in detail. Case 1 refers to the condition when all storage locations are occupied, and the coefficient of friction μ between liner and rack support feet is 0.8. Case 5 refers to the condition when all storage locations on one side of the diagonal (in plan form) are loaded leading to a highly asymmetric rack loading. These two cases were identified in

Chapter 6 to be the most limiting in a kinematic and a structural sense.) Tables 7.1 and 7.2 give the instantaneous loadings (two shear and vertical) at each of the four support feet when x-shear and y-shear, respectively, at a support foot reach maximax value. Referring to Table 7.1, maximum x-shear develops at foot 4 at 11.29 seconds. Similarly, maximum y-shear develops at foot 2 at 10.52 seconds into the earthquake. Tables 7.3 and 7.4 give similar data for loading cases 5 (diagonally loaded rack).

In actuality, the shear loading of the liner due to ground excitation is a self-limiting loading since the liner displacement is kinematically limited. However, treating it as a primary loading, the maximum tensile stress in the liner can be calculated in a very conservative manner by considering the equilibrium of a 14" wide (width of support foot) strip. To add to the conservatism, friction between the liner and concrete grout is neglected. Table 7.5 gives the computed liner direct stress for data of Tables 7.1 thru 7.4 which are labeled Cases a thru d in Table 7.5.

Table 7.1

Support reactions at the instant when x-shear is maximax (t=11.29 seconds, Rack A, μ = 0.8, fully loaded, loading Case 1)

Support Foot No.	X-Shear G_x(lb)	Y-Shear G_y(lb)	Vertical G_z(lb)	Notes
1	0	0	0	Foot #1 has lifted off
2	-3437	-4007	-24590	-
3	26650	4648	-63280	-
4	51430	26520	-137600	Maximax reaction this foot

Table 7.2

Support Reactions at the instant when y-shear is maximax. (t=10.52 seconds, Rack A, μ = 0.8, fully loaded)

Support Foot No.	X-Shear G_x(lb)	Y-Shear G_y(lb)	Vertical G_z(lb)	Notes
1	0	0	0	Support foot 1 has lifted off
2	-15410	-65660	-144200	Maximax reaction in this foot
3	-15000	-27090	-53970	-
4	-9393	5126	-14610	-

Table 7.3

Support reactions at the time instant when x-shear is maximax (t=13.61 seconds, Case 5 loading)

Support Foot No.	X-Shear G_x(lb)	Y-Shear G_y(lb)	Vertical G_z(lb)	Notes
1	2546	6113	8277	-
2	0	0	0	Support foot 2 has lifted off.
3	17250	2543	-51390	-
4	41320	19910	-67180	This foot has maximax reaction.

Table 7.4

Support reactions at the time instant when y-shear is maximax (t=14.74 seconds, Case 5 loading)

Support Foot No.	X-Shear G_x(lb)	Y-Shear G_y(lb)	Vertical G_z(lb)	Notes
1	0	0	0	Support foot one has lifted off.
2	10700	14340	-55100	-
3	12540	-46640	-70520	This foot has maximax y-shear
4	7823	-3640	-10790	-

Table 7.5

Liner Direct Stress

Case	Foot #	Vectorial Sum of shear (lb)	Max. Liner Direct direct stress (psi
a	4	57741	16497
b	2	67444	19270
c	4	45866	13105
d	3	48296	13798

Table 7.5 shows that the maximum liner stress is less than 19300 psi. The minimum tensile strength of 304 S.S. is 75000 psi @ 100°F. Therefore, the factor of safety against tearing is over 3.8.

These new results based on conservative analyses make consideration of liner strain analysis and cyclic loading unnecessary.

7.5 Dropped Gate

The transfer canal gate is approximately four feet wide and weighs 7,000 lbs. The consequences of accidentally dropping this gate from a height of 15" (h=15") are considered. The gate is assumed to fall with its fluid drag working on its smallest cross-sectional dimension. Furthermore, the impact on the top of the rack is assumed to take place along a lineal edge.

Localized plastic deformation is not of concern here; however, gross buckling of cruciform panels is not acceptable. The following additional assumptions are made to render the analysis conservative.

(i) The vertical walls of the cells are modeled as long ribbed plate columns 169" high x .063" wall. In reality, it is a composite ribbed plate column consisting of two plates .063" thick sandwiching an elastomeric material. The ribs are assumed to be 3" long and .063" thick at 6.26" pitch.

(ii) The virtual mass of the gate in water is assumed to be equal to its displaced mass.

(iii) Form and viscous drag of water is neglected.

(iv) Top 1.25" of the cruciform walls under impact is considered to be crushed by the impact of the gate. With these assumptions, the equation of motion of the gate is given by

$$(m + m_v) \frac{dv}{dt} = (m - m_v)\, g$$

where

v: downward velocity at time t
t: time coordinate
m : mass of gate
m_v: virtual mass
g: Acceleration due to gravity.

Integrating these equations and utilizing the theory of impact loading of linear springs, the equivalent static load due to gate drop assuming no crushing of the top of the cruciform walls is given by

$$F_{ST} = (2kE_0)^{1/2}$$

where $$E_0 = (m-m_v)gh$$

and,

k = spring constant of the "column" under consideration.

However, the deformation of

$$\delta = \left(\frac{2E}{k} \right)^{1/2} = 0.63$$

and a strain of $\epsilon = 0.5$ results in part of the energy E being absorbed.

Replacing E_0 by the remaining energy E_0^* (= 3281 lb-in) and using $k = .926 \times 10^6$ lb/in, the pseudo static force is given by

$$F_{ST}^* = (2kE_0^*)^{1/2}$$

$$= 55120 \text{ lbs.}$$

We now determine the critical buckling load using Eq. 3.75 p. 108 of "Buckling of Bars, Plates and Shells" by D.O. Brush, B.O. Almroth, McGraw Hill, 1975.

$$\frac{P_x}{b} = \left(\frac{\pi a}{m}\right)^2 \left[\left(\frac{m}{a}\right)^4 C_{44} + 2\left(\frac{m}{ab}\right)^2 (C_{45} + C_{66}) + \left(\frac{1}{b}\right)^4 C_{55}\right]$$

with

$$C_{44} = D + \frac{EI_x}{d_x}$$

$$C_{55} = D$$

$$C_{66} = (1-\nu)\, D + \frac{1}{2}\left(\frac{GJ_x}{d_x}\right)$$

$$C_{45} = \nu D$$

$$D \equiv \frac{Eh^3}{12(1-\nu^2)}$$

$$G = \frac{E}{2(1+\nu)}$$

where

- D = bending stiffness parameter
- G = shear modulus
- E = Young's modulus
- I_x = stiffener moment of inertia relative to the plate middle plane
- J_x = torsional constant
- ν = Poisson ratio

For this composite ribbed plate column, we have $E=27.6 \times 10^6$ psi, $\nu=0.3$, the plate length $a=169"$, the width $b=48"$, the thickness $h=0.063"$, the stiffener or rib spacing $d_x=6.26"$ and the stiffener height and width equals 6" and 0.063", respectively.

Using the above set of equations and data, we obtain the lowest critical load (with m=1) of

$$P_{cr} = 85008 \text{ lb.}$$

The analysis presented in this section thus precludes the buckling of the rack under the impact of a gate drop from a height of 15" above the rack. Moreover, the licensee intends to develop and put in place administrative control for gate movement across the rack areas. In addition, redundant measures will be taken to preclude a gate drop.

8.0 SPENT FUEL POOL FLOOR STRUCTURAL ANALYSIS

8.1 Introduction

The high density rack modules for long term fuel storage described in Section 2 are located in the spent fuel pool (auxiliary building). An overall schematic of the pool structure is given in Appendix I. In essence, the Grand Gulf Unit I fuel pool slab is a reinforced concrete plate-type structure buttressed by a centrally located girder (I-beam). There are two column supports underneath the girder over the pool floor plan. The slab is further reinforced by imbedded I-beams in the lateral direction. Figure 8.1 shows a pictorial view of the slab cross section.

Upper containment pool slab section has a considerably higher bending and shear strength than the spent fuel pool section. A comparison of Figures 2.1 and 2.2 shows that the loading intensity on the U.C.P. slab is significantly lower than that on the S.F.P. slab. Therefore, the analysis of the S.F.P. slab bounds the problem.

In this section, pertinent results of pool slab analysis are presented to demonstrate its structural integrity for all postulated loading conditions. In particular, compliance with the strengh limits and load combination of ACI-349 [1] and NUREG-0800 [2] ,respectively, is shown.

8.2 Assumptions

Seismic qualification of Spent Fuel Pool floor is carried out using the following conservative assumptions:

1. The pool floor is analyzed as a, simply supported, composite rectangular plate; no credit is taken for

structural resistance offered by the adjacent pool walls. Cross beams and girders are modelled by plate elements.

2. Calculation of the stiffness and strength properties for the concrete is based on the assumption of complete cracking of the concrete in tension over the entire floor plan area.

3. The loading used to qualify the pool floor assumes that all racks are fully loaded with channelled fuel assemblies.

4. The ANSYS finite element code[3] is used to determine the static stress state under a uniform pressure load on the floor.

The input loading for dynamic analysis of the pool floor is obtained from the results of detailed dynamic analysis of a single fuel rack. The dynamic mass used on the floor slab analysis includes the concrete mass, the reinforcement mass, and the virtual mass of the water set in motion by the pool floor. The pool floor stiffness properties assume that concrete is fully active on the compression side of the neutral axis, and is fully cracked on the tension side. The time history analysis of the pool floor is carried out using the Joseph Oat proprietary computer code DYNAHIS. Output floor loads, obtained from a time history analysis of an individual fuel rack, are converted to a floor pressure load time history acting on the entire floor slab, and used as the input dynamic load for the time history analysis of the pool floor. The results of the pool floor analysis are scanned during computations, and the maximum floor deformation obtained during the complete seismic event is considered as the primary output for further analysis. An equivalent static load, that yields the same value of maximum

deformation, is then computed and used to perform the structural integrity checks by using a detailed finite element model of the floor under a static pressure. The finite element representation of the slab may be found in Figures 8.2-8.4. This effective static pressure is combined with the dead load pressure due to weight of the racks, the fuel assemblies, and the 40 foot head of water.

8.3 Dynamic Analysis of Pool Floor Slab to Obtain Maximum Floor Displacements

With the dynamic model of the pool floor slab, considered as a simply supported rectangular orthotropic plate, a dynamic load history can be applied to the floor and be used to obtain the maximum displacements of the pool floor from the horizontal position. By equating the maximum displacements, obtained from an analysis over the total time of the seismic event, with the finite element solution for the static deformation of the floor configuration, we obtain a conservative estimate of the effective static pressure load on the pool floor slab. This effective pressure load can then be used in a standard strength qualification of the pool floor as outlined in SRP 3.8.4. The frequencies for the transient analysis are obtained from a detailed modal analysis of the pool floor using ANSYS.

The dynamic load histories applied to the pool floor have been obtained from the results of dynamic analyses of a fully loaded Type A rack. The resulting load represents the algebraic sum, at each time point, of the loads in the four supports, and includes the dead load of the rack and fuel assemblies. This dead load is subtracted out prior to the floor transient analysis.

For the purpose of a floor dynamic analysis, it is assumed that these load histories are representative of the averaged

pool floor loads from all of the different rack types, acting concurrently. This load is converted into a time history of floor pressure by dividing by the base area of a single rack A after removing the dead load component. Using the obtained pressures as input to the floor slab time history analysis, the program DYNAHIS determines the pool floor displacement as a function of time, and as part of the output, gives the maximum displacement of the floor slab, δ_{max}. Structural damping, based on the lowest calculated pool floor natural frequency $f_1 \approx 13$ HZ, is incorporated into the model by modification of the structural stiffness matrix according to standard practices.

To derive an effective static uniform pressure load, for subsequent strength analysis, δ_{max} is compared with the finite element solution for the statically loaded floor. The effective pressure associated with the maximum dynamic deflection δ_{max} is then obtained from the equation

$$q_e = \left(\frac{q_s}{w_s}\right) \delta_{max} \quad ; \quad \begin{array}{l} q_s = 40 \text{ psi} \\ w_s = \text{max. deflection under 40 psi} \end{array}$$

The following effective static pressures are obtained from the floor slab dynamic results:

$$q_e \text{ (SSE)} = 2.92 \text{ psi}$$

8.4 Results and Discussions

Table 8.1 summarizes the loadings used in the qualification of the pool floor. The pressures are calculated based on a rack footprint 122.5" x 104.25" = 12770.625 sq. in.

Table 8.1 Loading Data

Loading Type	Computed Value (Pounds)
1. Dead weight of racks	22270
2. Weight of fuel assemblies (racks fully loaded)	202544
3. Weight of 40' head of water	227062
4. Dead weight of floor slab	60187.96
Total dead load pressure (Area = 12770.625 sq. in.)	40.093 psi
5. SSE Seismic load due to racks	1.57 psi
6. SSE Seismic load due to dead weight of floor slab	1.35 psi

The time histories developed by Bechtel Power Corporation used a slightly smaller value of the dead loads on the slab (2 Ksf (Appendix I) vs. 2.53 Ksf given by above data). This difference, however, has an imperceptible effect on the pool floor time histories.

The fuel assembly weight utilized in the present analysis includes the weight of the fuel channel. Furthermore, all available fuel storage locations are considered to be occupied. In this manner, the total inertial mass of the fuel assembly is maximized and is treated as dead load (D) conjunctively with the pool slab mass and pool water mass. Using the notation of SRP 3.8.4, the following load combinations are deemed critical for the qualification of the pool floor.

Load Combinations

Concrete: The section moments and shear due to the following load combinations should not exceed the design strength, U.

1.4 D
1.05 (D + T_0)
1.05 (D + T_0) + (.75)(1.9)E
D + T_0 + 1.25 E'*

Steel: The section moment and shear due to the following load combinations should not exceed the plastic moment, M_p for the beam section.

1.7 (D + E)
1.3 (D + T_0 + E)
D + T_0 + E'

(See section 6 for definitions of above terms)

Note that the dynamic impact loads on the pool floor, due to motion of the fuel racks, has been accurately included in the loadings E'. We conservatively assume E = .667 E'.

Table 8.2 shows a sampling of the structural integrity results that have been obtained for the pool floor.

8.5 Conclusion

The pool floor has been shown to meet all structural acceptance requirements when conservatively analyzed as a simply supported rectangular plate with no credit taken for the supporting effects of the adjacent walls, or for the effect of hydrostatic loading on the walls causing a load reducing uplift on the floor.

---

* It is widely recognized that the term E' in this equation should be E. However, E' is used herein following the current text of SRP-3.8.4. This renders this load combination quite conservative.

Table 8.2

Synposis of Structural Acceptance Checks for Spent Fuel Pool Floor

Item	Governing Load Condition	Calculated Section Loadings	Allowable Strength	Location
Steel beams or girders	1.7 (D + E) 1.7 (D + E)	67.58×10^6 in.# 5.86×10^6 in.#	100.125×10^6 in# 20.88×10^6 in.#	Girder "Y" W36x150
Concrete slab	$1.05(D+T_0)+1.425E$	196 KIP in/in	306 KIP in/in	Element #4 (Fig. 8.3)
Column Compression	1.05D + 1.425E	5911 psi	16841 psi	Column at G&X function
Girder shear	1.4D	679,610#	899100#	Girder X
Average edge shear	1.4D (concrete edge)	3381#/in	5751#/in†	Slab wall junction
Edge shear on beam	1.4D	63245	307128#	Beam W36 x 135
Shear Transfer from concrete to beams (allowable panel pressure)	———	———	172 psi	

† Capacity based on concrete alone.

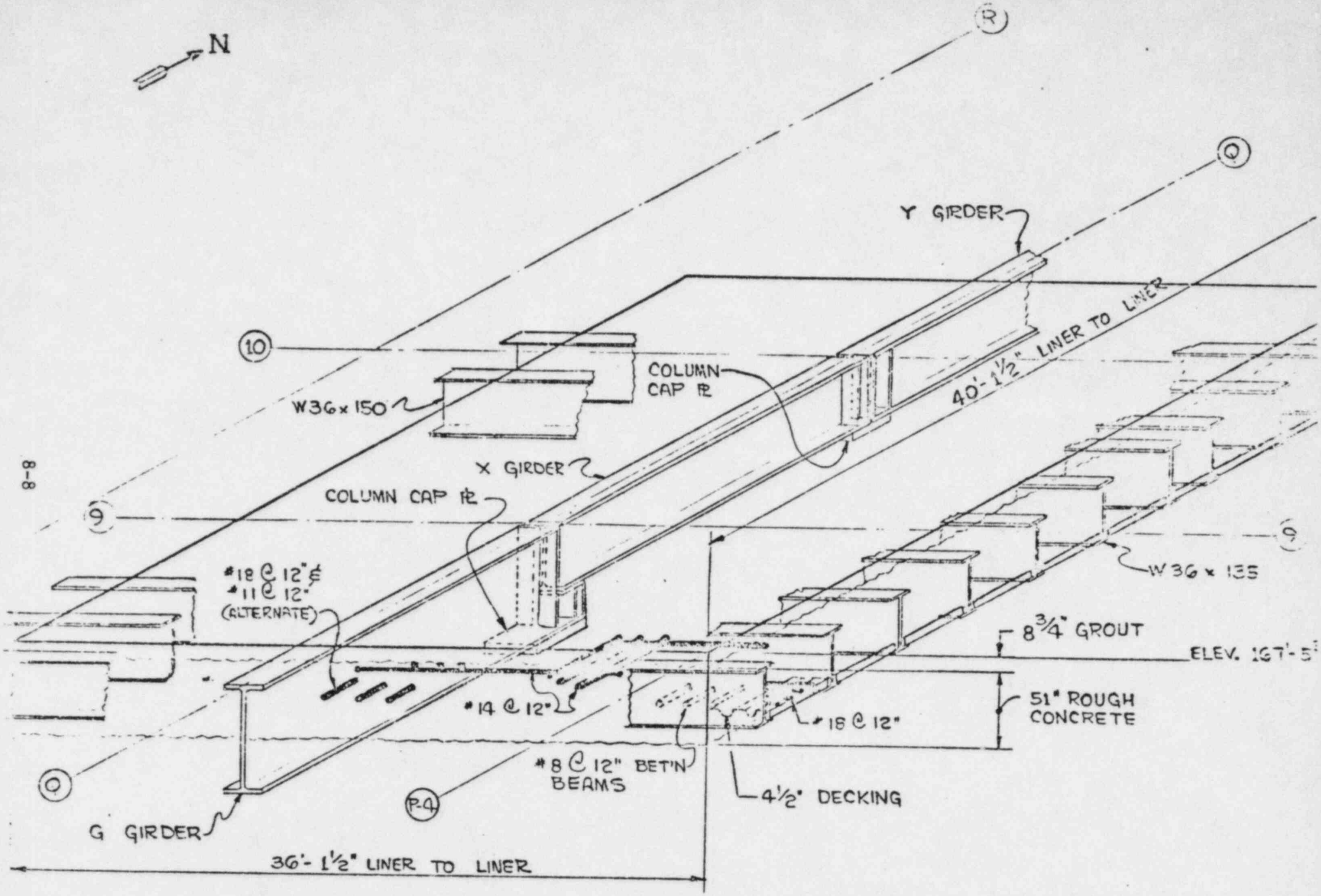

FIG. 8.1 : POOL SLAB PICTORIAL VIEW

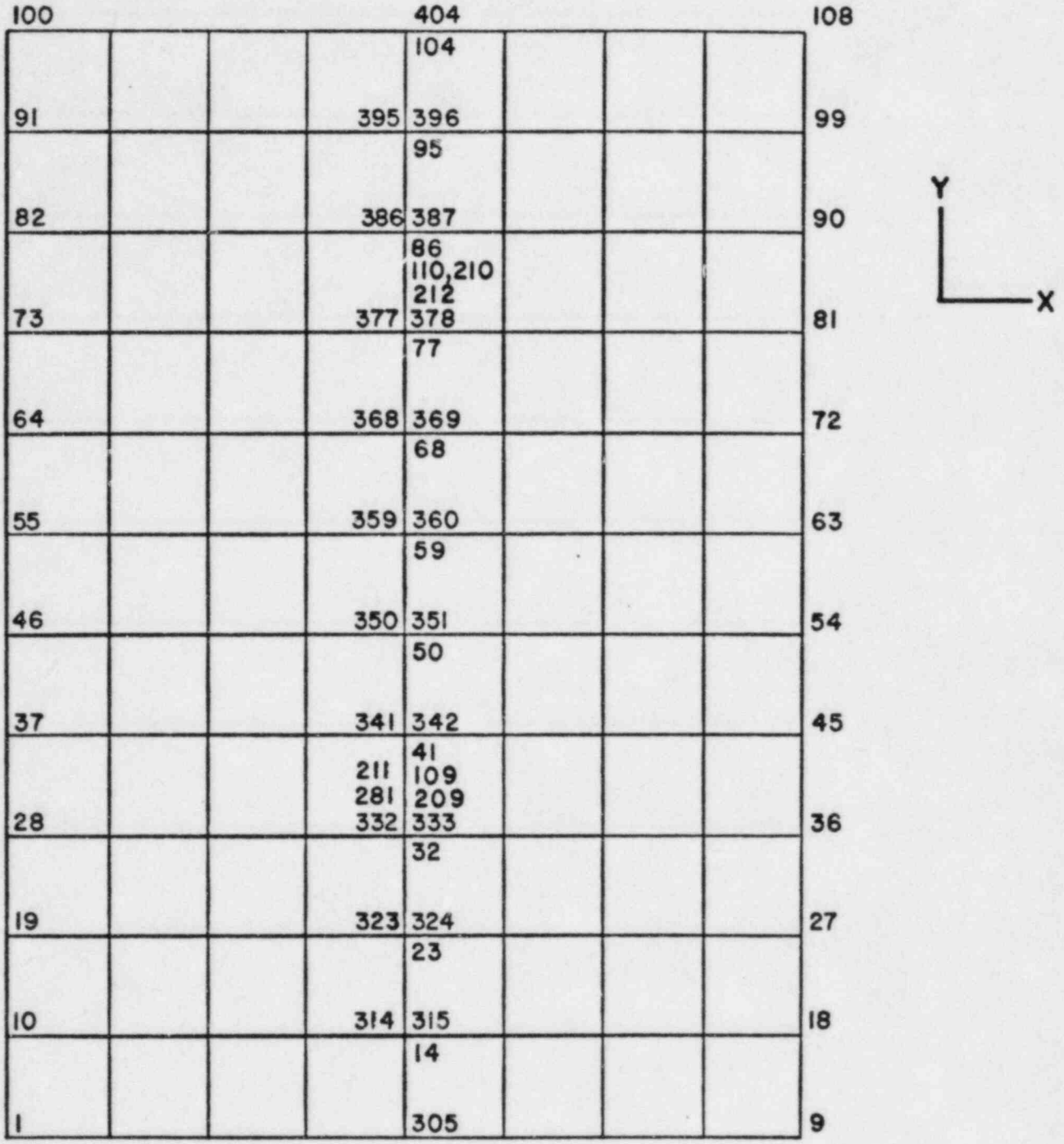

FIG. 8.2– NODE NUMBERS

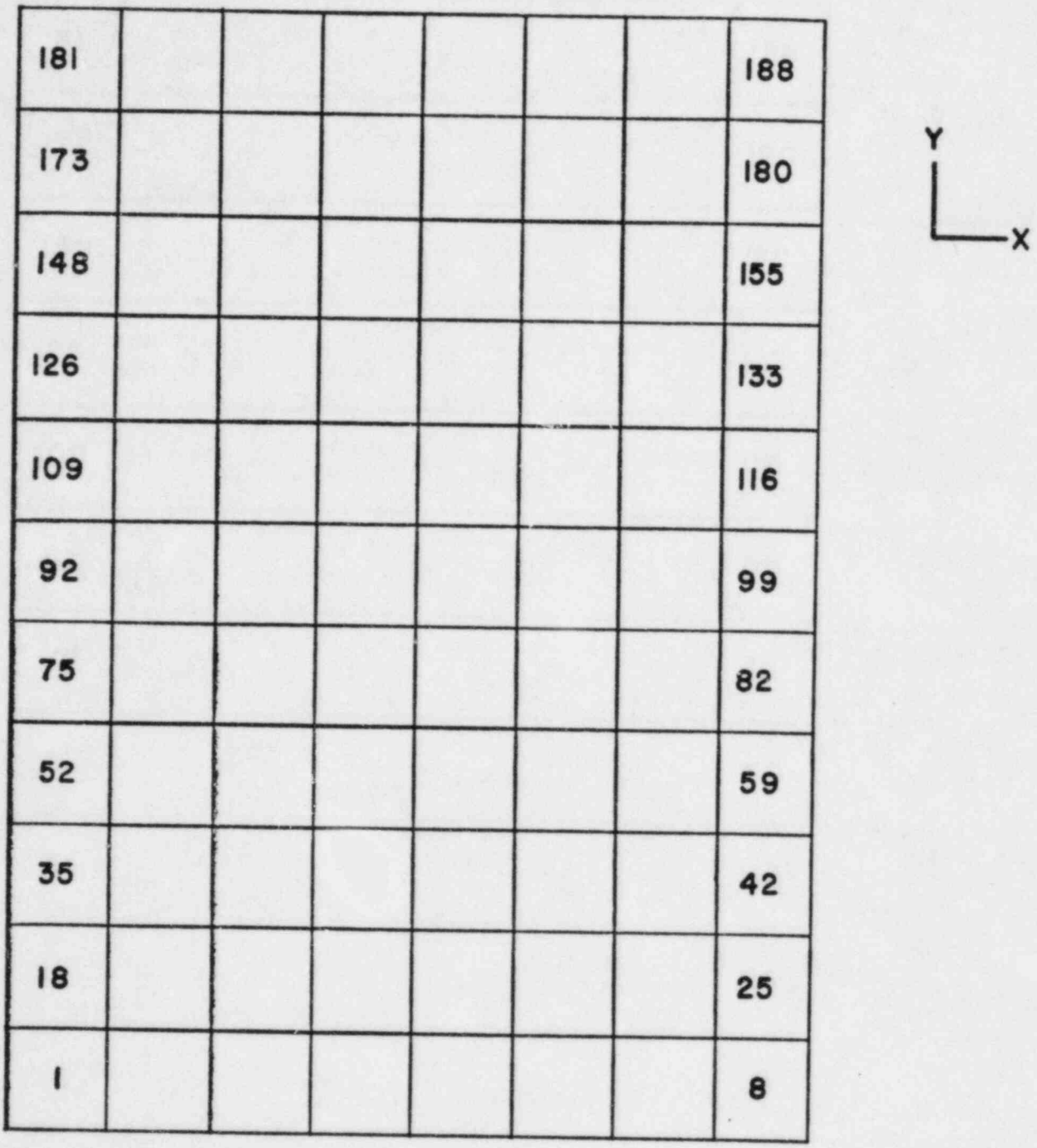

FIG. 8.3 PLATE ELEMENTS

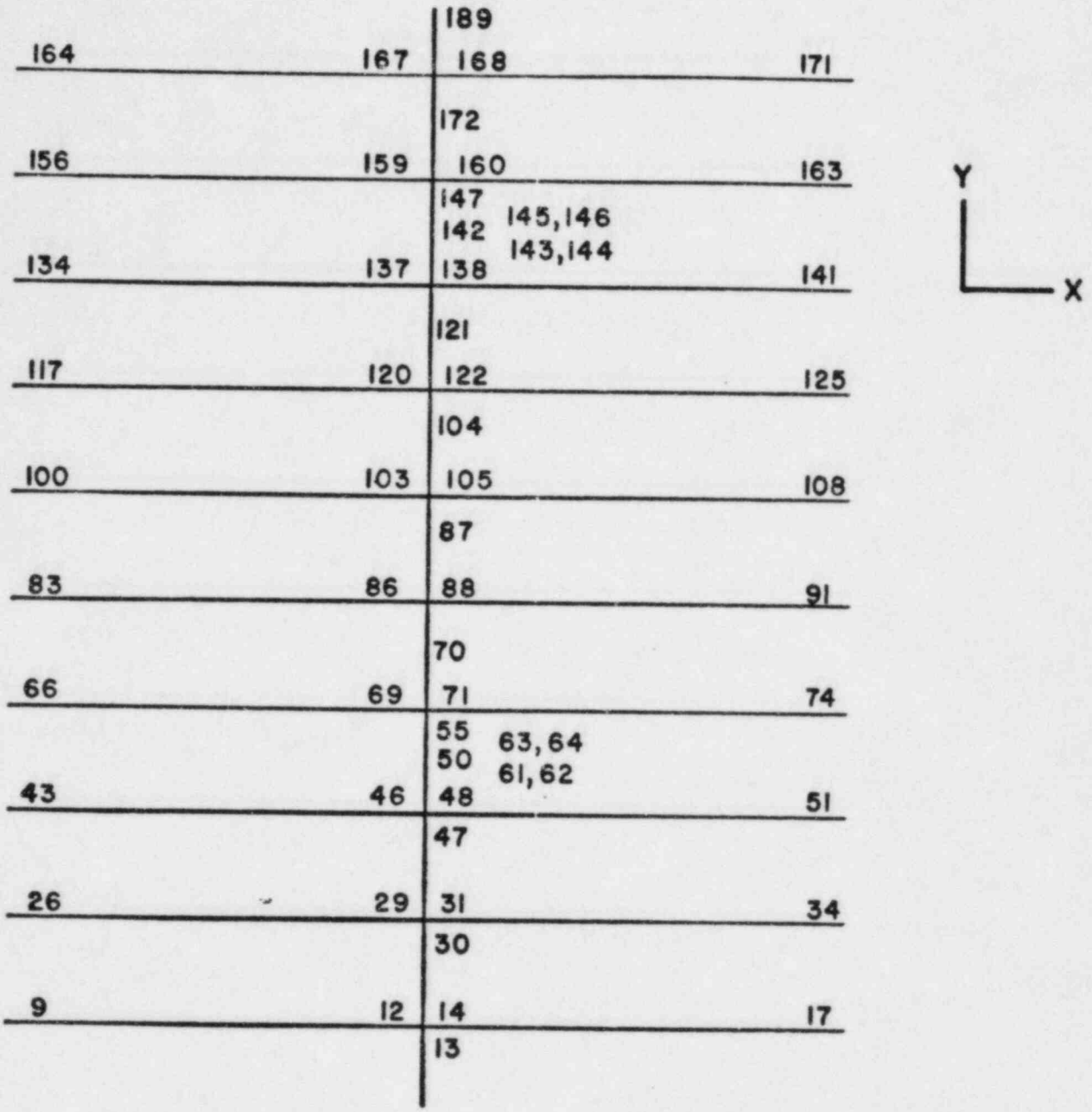

FIG. 8.4 – BEAM ELEMENTS; SPRINGS

References:

[1] American Concrete Institute, Code Requirements for Nuclear Safety Related Concrete Structures (ACI-349-76).

[2] U.S. Nuclear Regulatory Commission, NUREG-0800, SRP 3.8.4., July, 1981.

[3] Swanson Analysis Systems, Inc., ANSYS-User Manual, February 1982.

9.0 ENVIRONMENTAL EVALUATION

An environmental evaluation for the existing storage racks has been presented to the NRC[1] and has been approved.[2] MP&L concludes that the expansion of storage capacity of the spent fuel pools will not have a significant radiological or non-radiological impact on the environment.

9.1 SUMMARY

Installation of High Density Spent Fuel Storage Racks at Grand Gulf Nuclear Station Unit-1, will increase the storage capacity of the spent fuel from 1270 to 4348 assemblies. In addition 45 defective fuel assemblies or control rod blades storage locations are provided. The upper containment pool temporary storage capacity is increased from 170 to 800 assemblies. Radiological consequences of expanding the capacity have been evaluated with the objective of determining if there is significant additional on site or off site radiological impact relative to that previously reviewed and evaluated[1-2]. In addition, radiological impact to operating personnel has been evaluated to ensure that exposures remain As Low As is Reasonably Achievable (ALARA).

The decay heat loading and the radiological burden to the spent fuel pool water are determined almost entirely by refueling operations. The frequency of refueling operations and the conduct of refueling are independent of the increased capacity of the storage pool, except that the increased capacity will reduce fuel movements and allow continued normal operation. Since the fuel assemblies which will utilize the bulk of the storage capacity (and

will ultimately fill all incremental capacity above that of the existing design) are aged, their contribution to either the peak decay-heat load or the increased radiological impact, in terms of increased dose, would be negligibly small. A study performed by the NRC[3] supports this conclusion. Consequently, the increase in the storage capacity of both the spent fuel pool and the upper containment pool will neither significantly alter the operating characteristics of the current pool nor result in a measurable change in impact on the environment.

9.2 CHARACTERISTICS OF STORED FUEL

The currently authorized storage capacity of the spent fuel storage pool is 1270 assemblies and that of the upper containment pool is 170 assemblies. This capacity allows for two normal refueling discharges plus a full core discharge of 800 assemblies. The planned expansion of both the upper containment pool and the spent fuel pool would permit storage of 800 and 4348 assemblies in the respective pools. This expansion would allow storage of 18 annual discharges (see Table 1.1, Section 1) in the spent fuel pool with the capability to store a full core discharge in the upper containment pool.

The decay heat generation rate after about 4 years of cooling[6] is only a small fraction (less than 2%) of the rate at 110 hours (the time at which fuel transfer from the core is assumed to commence) after shutdown. As shown in Figures 5.1.4 and 5.1.5 (Section 5), the highest decay heat loading and the corresponding peak temperatures in the spent fuel pool occur during the refueling period. At this time the Residual Heat Removal System provides additional heat removal such that the bulk temperatures remain within acceptable limits. Following discharge, the stored fuel

decay heat rate falls off substantially, hence the spent fuel pool cooling system adequately handles the heat load. Because the majority of heat loading is due to freshly discharged fuel and since aged fuel contributes very little to the total heat load, the effect of expanding the spent fuel storage capacity is insignificant. Therefore, it is not expected that this expansion will significantly increase the thermal dissipation to the environment.

Since the intensity of gamma radiation follows the decline in decay heat generation rate, it is similarly concluded, that there would be no significant increase in gamma radiation due to the expanded storage.

It is important to note that the aged fuel in the expanded storage capacity pool will not contain significant amounts of radioactive iodine or short-lived gaseous fission products, since these would have decayed during the refueling period. The Krypton-85 which might escape from defective fuel assemblies has been shown to do so quickly[3] (i.e. within a short time after discharge from the core). Further, the residual Krypton-85 will be contained within the fuel pellet matrix and hence any leakage would occur at very low rates[3]. Cesium 134/137[3] is strongly bound within the fuel pellet matrix and its dissolution rate in water is extremely small. Any cesium dissolved in the pool water is easily controllable in the clean up system (demineralizer-ion exchange resin bed)[3]. Thus the planned storage expansion will not significantly increase the release of gaseous radionuclides.

9.3 RELATED INDUSTRY EXPERIENCE

Experience with storing spent fuel underwater has been

substantial[3,7,8]. These references show that the pool water activity, normally low, during refueling periods experiences a small increase which decays rapidly with time. References 3 and 7 also state that the increase in pool water activity during refueling can be attributed to:

a. dislodging (sloughing off) of corrosion products on the fuel assembly during transfer and handling operations.

b. the possible short-term exposure of fuel pellets to pool water via a cladding defect, and

c. mixing of the spent fuel pool water with the higher activity reactor coolant. Upon cessation of the refueling operations the fuel pool water and the reactor coolant system would be isolated from each other, thereby terminating transport of corrosion products from the Reactor Coolant System. Thus, deposition of crud is a function of refuelling operations and is not impacted by the expanded storage.

Furthermore, it has been shown[9] that release of fission products from failed fuel decreases rapidly after shutdown to essentially negligible levels. The fuel pellets are made of inert UO_2 that have very low solubility in water and the propensity for corrosion of the cladding (Zircaloy 2) at spent fuel pool water temperatures is virtually nil.[3,7] Thus the only mechanism available for the release of the gaseous fission matrix is diffusion through the UO_2 pellet. It has been shown that at low water temperatures (<150°F) the diffusion coefficient is

extremely small[10]. Therefore, the small increase in activity of the spent fuel pool water is due to either crud transport, fission products release, or cross flow from the reactor coolant system and is only a function of refuelling operations. It is reasonable to assume that the increased capacity of the spent fuel pool will reduce fuel handling operations, since fuel assemblies will not have to be consolidated or shipped for an extended period, thereby reducing the probability of increased pool water activity due to crud dislodging. Thus, the expansion of fuel pool storage capacity will not cause a significant increase in dose either on site or off site.

The corrosion properties of irradiated Zircalloy-2 cladding have been reviewed[3,8] and the conclusion is drawn that the corrosion of the cladding in spent fuel pool water is negligibly small. The minor incremental heating of pool water, due to the expansion of storage capacity, is far too small to materially affect the corrosion properties of Zircalloy-2 cladding.

9.4 OPERATING EXPERIENCE

Grand Gulf Nuclear Station Unit 1 is not currently a commerical operating plant and, since no spent fuel has been discharged, an experience data base is not yet available.

9.5 SPENT FUEL POOL COOLING AND CLEANUP (FPCC) SYSTEM

The fuel pool cleanup system at Grand Gulf Nuclear Station

Unit 1 is described in Section 9.1.3 of Reference 1. Radiological considerations are described in Chapters 11 and 12 and Section 15.7 of Reference 1.

It has been shown previously (Section 5) that the cooling systems at GGNS-1 are adequate to handle the expected heat loads with the additional heat removal capacity from the RHR system that would be required during refueling periods to maintain the temperature peaks within acceptable limits. The use of the RHR system to provide additional heat removal capability has been discussed for the GGNS-2 high density spent fuel storage pool[1] and was accepted by the NRC[2]. It has been shown earlier in this section that the small increase in heat load due to the storage capacity expansion of Unit-1 will neither significantly increase the thermal dissipation to the environment nor increase the propensity for corrosion of the cladding.

It has been shown that the crud deposition in the spent fuel pool water occurs during refueling outages and that the planned expansion will not increase crud deposition. The fuel pool clean up system (filter and demineralizer) is designed to maintain fuel pool water clarity and is operated and maintained per Grand Gulf Nuclear Station Unit-1 operation procedures.

The spent fuel pool filter demineralizer is backwashed and precoated when one of the two limits, either differential pressure or conductivity, is reached. The differential pressure set point is 25 psid and conductivity set point is 0.1μ mhos. When these set points are exceeded an alarm sounds in the control room and the system operations procedure directs the operator to appropriate procedures for backwash and precoat. Furthermore, the Plant Chemistry

program at Grand Gulf Nuclear Station Unit 1, has a reading/recording schedule for differential pressure and conductivity. Neither impact on the existing procedures nor a significant increase in activity of the cleanup system filters or resins is anticipated.

9.6 RADIOLOGICAL CONSEQUENCES

As stated earlier and confirmed by other studies [3,4,5,7,8,9] it can be shown that there will be no significant increase in activity due to Krypton-85, Cesium 134/137 or crud buildup on pool walls. It is concluded that the incremental impact from the release of either volatile fission products or crud with the expanded capacity of the spent fuel pool will be negligibly small.

9.7 RERACKING OPERATION

The existing spent fuel racks, in the upper containment and spent fuel pool, are to be removed prior to the discharge of any spent fuel from the core. These racks have not been exposed to spent fuel and are not contaminated. Therefore, it is concluded that significant radiation dose to individuals involved in the reracking is not anticipated.

9.8 CONCLUSIONS

Based upon the industry experience and evaluations discussed in previous sections, the following conclusions can be supported.

- Minor increases in radiological burden to the pool water, if any, can be adequately handled by the fuel pool clean up system (filter and demineralizer), thereby maintaining the radionuclide concentration in the water at an acceptably low level.

- No appreciable increase in solid radioactive wastes (i.e., filter media and demineralizer resin) is anticipated.

- No increase in release of radioactive gases is expected, since any long-lived inert radioactive gas potentially available for release (i.e., Kr-85) will have leaked from the fuel either in the reactor core during operation or during the first few months of residence in the pool. Further, Vol. 1, Ref. 3 (pp. 4-16) has shown that airborne activity to be considerably lower than that allowable by Table 1 of 10CFR Part 20, Appendix B. Therefore, the planned expansion will not significantly increase the release of radioactive gases.

- Based on industry experience to date, [References 4 & 5 and the findings cited in Reference 3, pp. 6-16], no increase in radiological impact due to crud buildup either on the pool walls or by suspension in pool water is expected.

- The existing spent fuel pool cooling system, along with the added cooling capability achieved by the operation of the Residual Heat Removal System (RHR) during refuelling outages, will keep the pool water temperature at an acceptable level [see Section 5 - Thermal Hydraulic Considerations]

- The existing radiation protection monitoring systems and program are adequate to detect and warn of any unexpected abnormal increases in radiation level. This provides sufficient assurance that personnel exposures can be maintained As Low As is Reasonably Achievable.

- Since the re-racking operations will be performed prior to any spent fuel being placed in either pools, the existing racks are not expected to be contaminated. Hence removal and disposal of the existing racks will have no radiological impact.

- Expanding the storage capacity of the spent fuel pool and the upper containment pool will not significantly increase the onsite or offsite radiological impact above that of the currently authorized storage capacity, nor is any significant increase in environmental radiological or non-radiological impact anticipated.

REFERENCES

1. "FSAR", Grand Gulf Nuclear Station Units 1 & 2," Chapters 9, 11, 12 & 15, Docket No. 50-416 and 417.

2. NUREG 0831 "Safety Evaluation Report Related to the Operation of Grand Gulf Nuclear Station, Units 1 and 2". Docket Nos. 50-416 and 50-417, Issued by USNRC, Office of Nuclear Regulation, Sept. 1981.

3. NUREG 0575, "Handling and Storage of Spent Light Water Power Reactor Fuel, Vol. 1, Executive Summary and Text, USNRC August 1979.

4. "Licensing Report on High-Density Spent Fuel Racks for Quad-Cities Units 1 and 2," Docket Nos. 50-254 and 50-265, Commonwealth Edison Company, June 1981.

5. "Licensing Report for High Density Spent Fuel Storage Racks", Rancho Seco Nuclear Generating Station, Sacramento Municipal Utilities District, Docket No. 50-312, June 1982.

6. NUREG 0800, USNRC Standard Review Plan - Branch Technical Position ASB9-2, Rev. 2, July 1981.

7. A.B. Johnson, Jr., "Behavior of Spent Nuclear Fuel in Water Pool Storage,:" BNWL-2256, September 1977.

8. J.R. Weeks, "Corrosion of Materials in Spent Fuel Storage Pools", BNL-NUREG-2021, July 1977.

9. J.M. Wright, "Expected Air and Water Activities in the Fuel Storage Canal", WAPD-PWR-CP 1723, (with addendum) undated.

10. ANS 5.4 Proposed Standard, "Method for Calculating the Fractional Release of Volatile Fission Products from Oxide Fuel," American Nuclear Society, issued for review 1981.

10. INSERVICE SURVEILLANCE PROGRAM FOR BORAFLEX NEUTRON ABSORBING MATERIAL

10.1 Program Intent:

A sampling program to verify the integrity of the neutron absorber material employed in the high-density fuel racks in the long-term environment is described in this section.

The surveillance program is designed for the spent fuel pool since the Boraflex used in these racks will experience long term radiation. No surveillance program is planned for the Boraflex used in the upper containment (UCP) pool racks. These UCP racks are planned to be used for interim (short term) storage of spent fuels; therefore, they are not subject to long term radiation.

The program is intended to be conducted in a manner which allows access to the representative absorber material samples without disrupting the integrity of the entire fuel storage system. The program is tailored to evaluate the material in normal use mode, and to forecast future changes using the data base developed. The surveillance program is to be utilized in the spent fuel racks auxiliary building pool. Since the spent fuel racks in the upper containment pool are utilized for interim (transitory) storage, a surveillance program for these racks is not needed.

10.2 Description of Specimens:

The absorber material, henceforth referred to as "poison", used in the surveillance program must be representative of the material used within the storage system. It must be of the same composition, produced by the same method, and certified to the same criteria as the production lot poison. The sample coupon must be of similar thickness as the poison used within the storage system and not less than 5 3/4 x 3 inches on a side. Figure 10.1 shows a typical coupon. Each poison specimen must be encased in a stainless steel jacket of an identical alloy to that used in the storage system, formed so as to encase the poison material and fix it in a position and with tolerances similar to that design used for the storage system. The jacket has to be closed by tack welding.

10.3 Test:

The test conditions represent the vented conditions of the box elements. The samples are to be located adjacent to the fuel racks and suspended from the spent fuel pool wall. Eighteen test samples are to be fabricated in accordance with Figure 10.1 and installed in the pool when the racks are installed.

The procedure for fabrication and testing of samples is as given below:

a. The samples should be cut to size and weighed carefully in milligrams.
b. The length, width, and the average thickness of each specimen is to be measured and recorded.
c. The samples should be fabricated in accordance with Figure 10.1 and installed in the pool.
d. Two samples should be removed at each time interval according to the schedule shown in Table 10.1.

10.4 Specimen Evaluation:

After the removal of the jacketed poison specimen from the fuel pool at a designated time, a careful evaluation of that specimen should be made to determine its actual condition as well as its apparent durability for continued function. Separation of the poison from the stainless steel specimen jacket must be performed carefully to avoid mechanical damage to the poison specimen. Immediately after the removal, the specimen and jacket section should visually be examined for any effects of environmental exposure. Specific attention should be directed to the examination of the stainless steel jacket for any evidence of physical degradation. Functional evaluation of the poison material can be accomplished by the following measurements:

a. A neutron radiograph of the poison specimen aids in the determination of the maintenance of uniformity of the boron distribution.

b. Neutron attenuation measurements will allow evaluation of the continued nuclear effectiveness of the poison. Consideration must be given, in the analysis of the attenuation measurements, for the level of accuracy of such measurements as indicated by the degree of repeatability normally observed by the testing agency.

c. A measurement of the hardness of the poison material will establish the continuance of physical and structural durability. The hardness acceptability criterion requires that the specimen hardness will not exceed the hardness listed in the qualifying test document for laboratory test specimen irradiated to 10^{11} rads. The actual hardness measurement should be made after the specimen has been withdrawn from the pool and allowed to air dry for not less than 48 hours to allow for a meaningful correlation with the preirradiated sample.

d. Measurement of the length, the width, and the average thickness and comparison with the pre-exposure data will indicate dimensional stability within the variation range reported in the Boraflex laboratory test reports.

A detailed procedure paraphrasing the intent of this program will be prepared for step-by-step execution of the test procedure and interpretation of the test data.

TABLE 10.1

Date Installed _____

	SCHEDULE	INITIAL WEIGHT (mg/Cm^2-Yr)	FINAL WEIGHT (mg/Cm^2-Yr)	WEIGHT CHANGE (mg/Cm^2-Yr)	PIT PENETRATION mil/Yr
1					
2	90 day				
3					
4	180 day				
5					
6	1 Year				
7					
8	5 Year				
9					
10	10 Year				
11					
12	15 Year				
13					
14	20 Year				
15					
16	30 Year				
17					
18	40 Year				

TIME SCHEDULE FOR REMOVING COUPONS

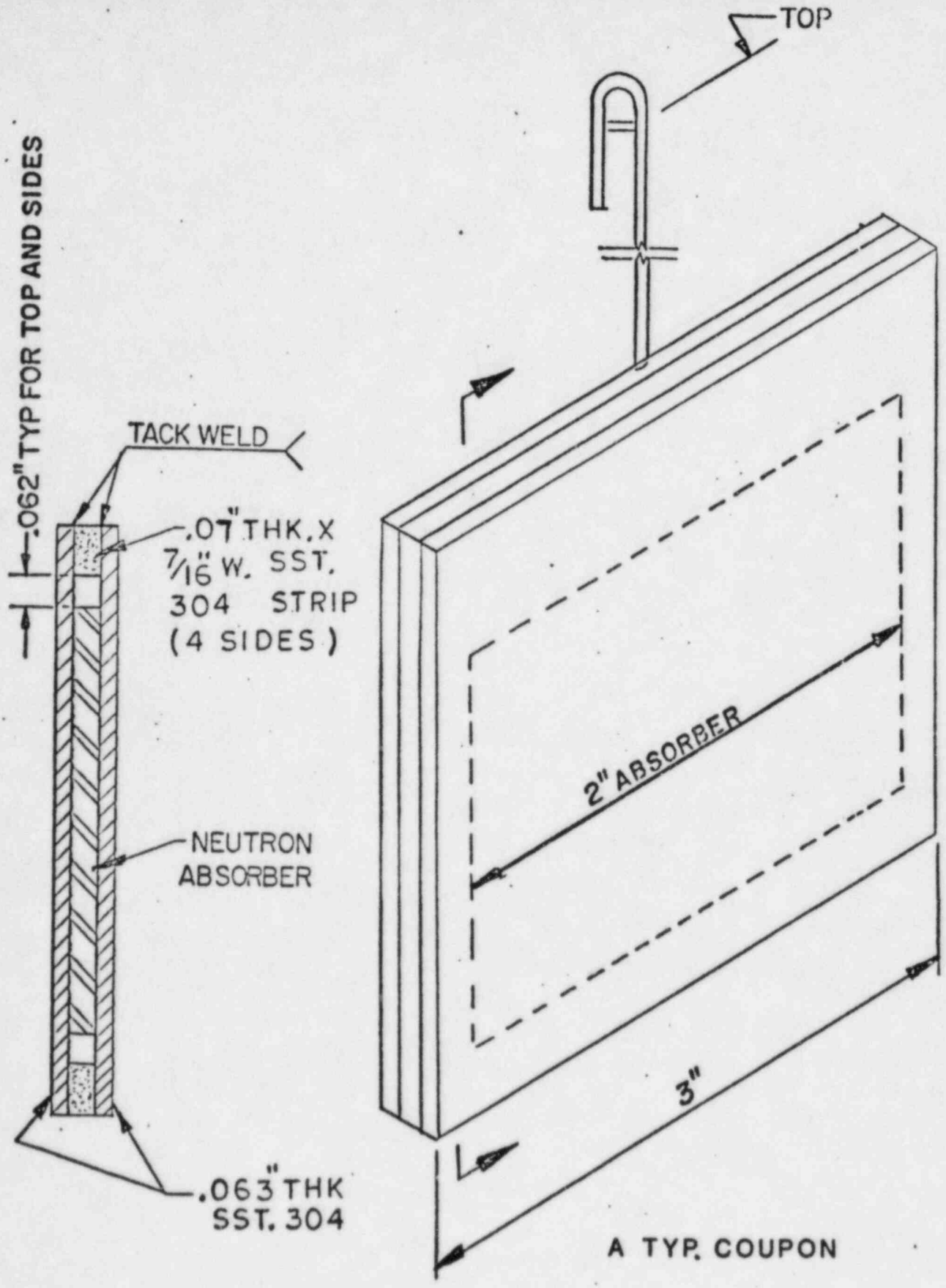

FIG. 10.1 — TEST COUPON

11.0 COST/BENEFIT ASSESSMENT

A cost/benefit assessment has been prepared in accordance with the requirements of reference 1 Section V, Part 1. The purpose of the assessment is to demonstrate that the installation of high-density spent fuel storage racks is the most advantageous means of handling spent fuel, considering the needs of our customers for a dependable source of electric power.

The material is presented to satisfy the NRC's need for information; it is the position of MP&L that no environmental impact statement need be prepared in support of the request, because there will be no significant impact on the human environment. NRC precedent establishes that alternatives and economic costs need not be discussed when there is no significant environmental impact. However, for the sake of completeness, alternatives to re-racking, for additional spent fuel storage capacity, are discussed in Section 11.3.

11.1 Specific Needs for Spent Fuel Storage

Disposal of Grand Gulf spent nuclear fuel is scheduled to be carried out by the Department of Energy in or after 1998 in accordance with Public Law 97-425; Nuclear Waste Policy Act of 1982. As Grand Gulf spent fuel may not be accorded a high priority under the DOE program, MP&L is seeking to provide a spent fuel storage capacity to support approximately twenty years of nominal operation. No other contractual arrangements exist for the interim storage or reprocessing of spent fuel from Grand Gulf; therefore, increased storage capacity in the Grand Gulf fuel pool is the only viable option under consideration. Table 1.1, the fuel discharge schedule, indicates that with the high density spent fuel racks, loss of full core discharge capability (FCDC) will occur in 2003.

In addition to spent fuel, storage is available in the Grand Gulf Unit 1 spent fuel storage pool for other types of materials (see Section 1), namely,

- o Control rods
- o Control rod guide tubes.
- o Defective fuel

11.2 Cost of Spent Fuel Storage

The design and manufacture of the spent fuel storage racks will be undertaken by the organizations described in Section 1. It is expected that the total project cost will be between 3.3 and 3.5 million dollars.

11.3 Alternatives to Spent Fuel Storage

Mississippi Power & Light has considered the various alternatives to the proposed onsite spent fuel storage. These alternatives are as follows:

- o Shipment of fuel to a reprocessing or independent spent fuel storage/disposal facility

  No commercial spent fuel reprocessing facilities are presently operating in the United States. MSEI and MP&L have a contractual arrangement whereby spent nuclear fuel and/or high level nuclear waste will be accepted and disposed of by the U.S. Department of Energy. However, such acceptance and disposal is not expected to begin before 1998; the Grand Gulf Unit 1 existing fuel storage capacity will not provide full core discharge capability beyond 1987. Spent fuel acceptance and disposal by the Department of Energy is not, therefore, an alternative to increased on-site pool storage capacity.

- o Shipment of fuel to another reactor site

  Shipment of Grand Gulf-1 fuel to another reactor site

could provide short term relief to the storage capacity problem. However, transshipment of spent fuel merely serves to transfer the problem to another site and does not result in any additional net long-term storage capacity. Accordingly, MP&L does not consider the transshipment of spent fuel to be an appropriate alternative to high-density spent fuel storage at the site.

- o Not completing the reactor plant/not operating the plant after the current spent fuel storage capacity is exhausted

  As indicated in NUREG-0575, "Final Environmental Impact Statement on Handling and Storage of Spent Light Water Power Reactor Fuel," the replacement of nuclear power by coal-generating capacity would cause excess mortality to rise from 0.59-1.70 to 15-120 per year for 0.8 GWY(e). Based on these facts, not operating the plant or shutting down the plant after exhaustion of spent fuel discharge capacity are not viable alternatives to high density storage in the spent fuel pool. The prospective 1983 expenditure of approximately $3.5 million for the high density racks is small compared to the estimated value of replacement power equivalent to the plant's energy output: $590,000 per day in 1983 and $2,000,000 per day in 1990-1991.

The subject of the comparative economics associated with various spent fuel options is the subject of Chapter 6 of NUREG-0575. Although the material presented is generic, it is of value in comparing the costs of the various options. Of the options presented in Chapter 6 of NUREG-0575[2], high-density spent fuel storage at the site is the most economic option at $18 per

KgU. The price of "Away From Reactor (AFR)" fuel storage, if available, would be $115 per KgU. This corresponds to 0.5 mill/Kwh from a 1000 MWe power reactor for AFR storage. The marginal cost per KgU of high density spent fuel racks for Grand Gulf-1 is $5.18.

11.4 Resource Commitments

The expansion of the Grand Gulf-1 spent fuel storage capacity will require the following primary resources:

- Stainless steel - 522,000 pounds
- Boraflex neutron absorber - 41,000 pounds - of which 2800 pounds is Boron Carbide (B_4C) powder.

The requirement for stainless steel represents a small fraction of the total domestic production for 1983.[3] Although the fraction of domestic production of B_4C, required for the fabrication, is somewhat higher than that for stainless steel, it is unlikely that the commitment of B_4C to this project will affect other alternatives. Experience has shown that the production of B_4C is highly variable and depends on need, but could easily be expanded to accommodate additional domestic needs.

REFERENCES TO SECTION 11

1. B.K. Grimes, "OT Position for Review and Acceptance of Spent Fuel Storages and Handling Applications," April 14, 1978.

2. NUREG-0575, "Handling and Storage of Spent Light Water Power Reactor Fuel", Vol. 1-3, USNRC, August, 1979.

3. "Mineral Facts and Problems," Bureau of Mines Bulletin 671, 1980.

12. QUALITY ASSURANCE PROGRAM

12.1 Introduction

This chapter provides a general description of the Quality Assurance Program that is implemented to assure that the quality objectives of the contract specification are met.

12.2 General

The Quality Assurance Program used on this project is based upon the system described in Joseph Oat's Nuclear Quality Assurance Manual; both of these meet the intent of 10CFR, Part 50, Appendix B. This system is designed to provide a controlled system for the design, manufacture and testing of customized components in accordance with various Codes, specifications, and regulatory requirements. The Joseph Oat Nuclear Quality Assurance Program has been accepted by ASME and found to be adequate by NRC audit team.

The philosophy behind Oat's Quality Assurance System is that it shall provide for all controls necessary to fulfill the contract requirements with sufficient simplicity to make it functional on a day to day basis. As this system is applied to most of the contracts which Joseph Oat obtains, implementation of it is almost second nature to Oat's personnel. The system readily adapts to different designs and component configurations, making possible the construction of many varied forms of equipment. The highlights of this system, as addressed in the following paragraphs, provide an overview of the system and how it has been applied to the customer specifications and regulations.

12.3 System Highlights:

Design control is organized to provide for careful review of all contract requirements to extract each individual design and quality criteria. These criteria are translated into design and quality control documents customized to the contract requirements and completely reviewed and approved by responsible personnel.

The system for control of purchased material entails generating detailed descriptions of each individual item of material along with specifications for any special requirements such as impact testing, corrosion testing, monitoring, or witnessing of chemical analysis, provision of overcheck specimens, special treatments or conditioning of material, source inspection, and provision of documentation of performance of any of the above.

Material receipt inspection includes a complete check of all material and its documentation. Upon acceptance, each item of material is individually listed on a control sheet issued once a week to assure that only accepted material goes into fabrication.

The fabrication control system provides that a shop traveler is prepared for each subassembly and assembly in each contract. The traveler is generated specifically to provide step by step instructions for fabrication, inspection, testing, cleaning, packaging, etc. which address all standard and special requirements of the contract specifications. Special attention is given to deployment of fabrication sequence and inspection steps to preclude the possibility of missing poison sheets or incorrect sheets (incorrect B^{10} loading).

Due to the tendency of contract specifications to require special examination techniques or test procedures, all nondestructive examination procedures and test procedures are custom written to apply to each given component within a contract.

The system provides for qualification and written certification of personnel performing quality related activities including nondestructive examination and fabrication inspection, welding, engineering, production supervision and auditing.

Other requirements of a solid quality control system are fully covered as specified in the Quality Assurance Manual including

document control, control of measuring and test equipment, control of nonconforming material and parts, corrective action auditing and other areas as specified.

12.4 Summary:

Joseph Oat Corporation's Quality Assurance System provides the full measure of quality assurance required by the contract. All special requirements of the specifications are covered including source inspection of material and witnessing of material testing by the Engineer, furnishing of material certifications and test reports within five days of shipment, and obtaining verification of qualification testing of poison materials. Oat has a long history of providing excellent quality control over a wide range of equipment types such as the high density fuel racks.

APPENDIX I

REPORT ON

SEISMIC ANALYSIS OF SPENT FUEL POOLS

FOR

HIGH DENSITY SPENT FUEL RACKS

December 1982

GRAND GULF NUCLEAR POWER STATION, UNIT 1

MISSISSIPPI POWER AND LIGHT COMPANY

SEISMIC ANALYSIS OF SPENT FUEL POOLS FOR HIGH DENSITY SPENT FUEL RACKS

1. Introduction

MP&L has decided to install High Density Spent Fuel Racks (HDSFR) in the auxiliary building spent fuel pool at floor elevation 167'-6" and in the containment building upper pool at floor elevation 167'-6" in Grand Gulf Nuclear Station (GGNS) Unit 1 (see Reference 1).

Seismic response time histories at the spent fuel pool floor level are required in three orthogonal directions (i.e., two horizontal and one vertical) for the design of HDSFR to withstand OBE and SSE loadings.

To enable algebraic addition of the rack responses in the three directions, the earthquake motions specified in these directions will have to be statistically independent (Reference 2, Section 3.7.2). Also, the time histories will have to be in compliance with the Regulatory Guide 1.60 (Reference 3) for Regulatory Guide 1.61 (Reference 4) dampings to be applicable.

Bechtel computer programs CE786, and CE917, CE931, CE920, and CE921 were used to modify input earthquake motion and to generate and verify the response time histories.

2. Mathematical Model

2.1 Auxiliary Building

The lumped mass models shown in Figures 1 and 2 are obtained from the GGNS FSAR (Reference 5), Figures 3.7-19, and 3.7-20. All properties of these models are essentially the same as in the original models (Reference 6). Sloshing effects of water in the spent fuel pool subjected to horizontal excitations and new loads of the high density racks and fuel bundles (2000 psf per Reference 7) have been included in the models.

Figure 3A shows the actual lumped masses with W_0 and W_1 which represent the equivalent weight of fluid to produce impulsive force and equivalent oscillating weight to produce the convective force on the tank respectively.

This model is simplified to the model on Figure 3B by lumping W_0 to M_5 and W_1 to M_6 and ignoring the spring stiffness that represent the effect of sloshing water. This simplified model will give structural response slightly more conservative than that of Figure 3A since the centroid of W_1 and W_0 in Figure 3A is slightly lower than the one on Figure 3B. The weight of the racks have been applied at the mass point 4 (elevation 166'-0").

For vertical excitation, since there is no sloshing effect of water, the only change in mass 4 from the original model is the new weight of racks and fuel bundles.

2.2 Containment Building

Figure 4 shows the lumped mass model of the containment building as obtained from the GGNS FSAR Figure 3.7-18. All properties of this model are essentially the same as in the original model (Reference 8). The only change in the model is the additional weight of the racks and fuel bundles to mass point 15 at elevation 161'-10" (2200 psf, per Reference 7). This elevation is four inches higher than the bottom of pool floor slab which has top of floor at elevation 167'-6" and bottom of floor at elevation 161'-6". Since the slab is rigid and has thickness of six feet, the displacements of top of floor and bottom of floor are almost identical. Thus, the response time histories at mass 15 represent the response at top of floor slab at elevation 167'-6" as required for design of the racks.

3. Ground Motion

The basic ground motions have been derived from the Bechtel standard ground motions for two horizontal and one vertical directions, namely, H1, H2 and V as mentioned in the Bechtel Design Guide C-2.44 (Reference 9) "Seismic Analysis of Structures and Equipment for Nuclear Power Plants." These input ground motions are spectrum consistent in that they envelope the respective Regulatory Guide 1.60 Spectra. The ground motions were further evaluated to determine if they would envelope the Grand Gulf Design Spectra to comply with GGNS Licensing requirements. Also, it was determined that these Ground motions are statistically independent.

The spectra of the horizontal ground motions H1 and H2 normalized to 1 g for 2%, 4%, 5%, and 7% damping values are examined against the Grand Gulf Design Spectra as defined in the GGNS FSAR. The results showed that these horizontal ground motions will envelope the Grand Gulf Design Spectra designated as GGNS and the Regulatory Guide 1.60 Spectra, as shown in Figures 5 through 12.

For vertical excitation, however, the ground motion V had to be modified to envelope the Grand Gulf Design Spectra. This is done by using a spectrum raising procedure in accordance with Bechtel Computer Program CE 786. By using this program, the new vertical ground motion is obtained. The corresponding spectra are shown in Figures 13 through 16.

The three ground motions, i.e., H1, H2, and modified V, are named HORQUAKE 1, HORQUAKE 2, and VERTQUAKE for the two horizontals and one vertical directions respectively. Each time history has 4800 data points with an earthquake duration of 24 seconds (Time step = 0.005 sec) and scaled to 1 g (see Figures 17, 18, and 19).

The statistical independence between the three components of the earthquake ground acceleration time history has been verified by using the absolute values of correlation coefficients among the three components. Namely, in order to accept the three generated components as being statistically independent, the absolute values of all of the correlation coefficients must be less than or equal to 0.16 per Reference 6 of Regulatory Guide 1.92 (Reference 10).

Absolute values of correlation coefficients of these Ground Motions were computed as shown below:

CORRELATION COEFFICIENT FOR H_1-H_2 = .02413

CORRELATION COEFFICIENT FOR H_2-V = .03309

CORRELATION COEFFICIENT FOR V-H_1 = .12468

These values show that the input ground motions are statistically independent.

4. Analysis

The time history analyses were performed by using the following Bechtel computer programs as shown in the flow chart below. The details of the analyses are given in Reference 11.

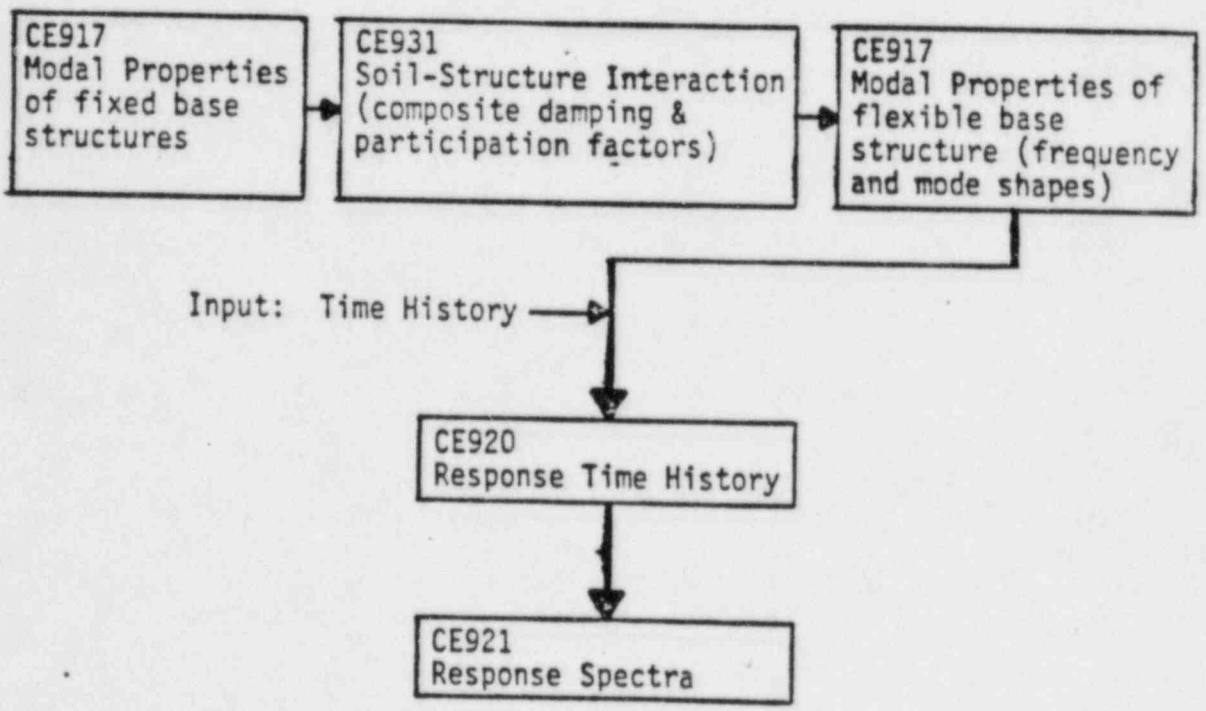

The modal properties, i.e., natural frequencies, participation factors and mode shapes, of the lumped mass model with the bases considered fixed were obtained from CE 917. These modal properties together with appropriate structural damping are utilized in CE 931 to obtain the composite modal damping and the participation factors due for soil structure interaction (see Section 3.7 of Reference 5 for details). The composite modal damping have been evaluated for two sets of structural damping, i.e., 2% and 4% for OBE and

5% and 7% for SSE events. The lower value of damping for each event (i.e., 2% and 5%) has been specified in the Section 3.7 of the GGNS FSAR while the higher values (4% and 7%) have been obtained from the Regulatory Guide 1.61. The results of the analyses presented in the following sections indicate that the composite modal damping is rather insensitive to the indicated variations in the structural damping.

The composite modal damping and the participation factors obtained from CE 931 are used in combination with the modal properties (frequencies and mode shapes) obtained from a flexible base analysis of the lumped mass model to determine the response time history for the input ground motion. However, Section 3.7.2.4 of the GGNS FSAR stipulates that, for the sake of conservatism, the computed composite modal dampings need not exceed 10% of critical except for those modes that are clearly associated with rigid body translation or rotation of the structure. Since the input ground motions are consistent with Regulatory Guide 1.60 and the spectra used in the present analysis are clearly more conservative than that stipulated in the GGNS FSAR, it was decided that an exception to the GGNS FSAR may be considered if it were to be shown by analysis that the effect of the arbitrary cut off of damping at 10% is critical.

The input ground motions are scaled to peak acceleration of 0.075g and 0.15g for OBE and SSE events.

4.1 Auxiliary Building

4.1.1 Free Vibration Analysis

E-W Excitation:

Mode	Freq (cps)	Participation Factor
1	4.01	69.42
2	8.69	-26.11
3	12.24	-1.06

N-S Excitation:

Mode	Freq (cps)	Participation Factor
1	3.65	67.70
2	8.91	29.78
3	14.46	-7.95

Vertical Excitation:

Mode	Freq (cps)	Participation Factor
1	6.08	74.45
2	25.64	-5.93
3	38.84	1.76

4.1.2 Composite Modal Damping for Auxiliary Building

E-W Excitation

	Structural Damping			
Mode	2% Damp.	4% Damp.	5% Damp.	7% Damp.
1	0.256	0.260	0.262	0.266
2	0.115*	0.120*	0.123*	0.128*
3	0.004	0.005	0.006	0.007

N-S Excitation

	Structural Damping			
Mode	2% Damp.	4% Damp.	5% Damp.	7% Damp.
1	0.197	0.201	0.204	0.209
2	0.203*	0.209*	0.211*	0.217*
3	0.023	0.025	0.027	0.031

Vertical Excitation

	Structural Damping			
Mode	2% Damp.	4% Damp.	5% Damp.	7% Damp.
1	0.585	0.586	0.587	0.589
2	0.044	0.046	0.047	0.050
3	0.012	0.015	0.016	0.020

*The damping is suppressed to 10% for nonrigid body translations.

4.2 Containment Building

4.2.1 Free Vibration Analysis

E-W Excitation

	Mode	Freq (cps)	Participation Factor
*	1	0.21	8.98
	2	2.49	50.15
	3	4.80	4.86
	4	5.34	21.78
	5	6.54	6.97
	6	7.57	-25.39

N-S Excitation

	Mode	Freq (cps)	Participation Factor
*	1	0.21	7.38
	2	2.49	50.22
	3	4.80	4.80
	4	5.34	21.39
	5	6.54	7.06
	6	7.60	-25.20

Vertical Excitation

Mode	Freq (cps)	Participation Factor
1	4.74	6.11
2	5.05	61.80
3	14.46	0.69
4	18.19	2.53

*Water Sloshing Mode

4.2.2 Composite Modal Damping for Containment

E-W Excitation

	Structural Damping			
Mode	2% Damp.	4% Damp.	5% Damp.	7% Damp.
1	.0128	.0123	.0121	.0118
2	.070	.0728	.0739	.0761
3	.0848	.0860	.0855	.0868
4	.0859	.9110	.1066	.1203
5	.0346	.0438	.0474	.0548
6	.2232	.2277	.2300	.2354

N-S Excitation

	Structural Damping			
Mode	2% Damp.	4% Damp.	5% Damp.	7% Damp.
1	.0273	.0223	.0209	.0194
2	.0704	.0726	.0737	.0759
3	.0844	.0855	.0849	.0863
4	.0823	.0889	.1048	.1174
5	.0344	.0436	.0472	.0548
6	.2222	.2269	.2292	.2348

Vertical Excitation

	Structural Damping			
Mode	2% Damp.	4% Damp.	5% Damp.	7% Damp.
1	.0229	.0452	.0562	.0780
2	.6548	.6560	.6572	.6590
3	.0058	.0093	.0104	.0120
4	.0141	.0190	.0215	.0270

5. Results

The seismic response time histories for the auxiliary building and the containment at the specified locations for SSE with 5% and 7% structural dampings and OBE with 2% and 4% structural dampings are shown in Figures 20 to 43.

The effect of cut off of composite model damping to 10% for nonrigid body modes was rather small in increasing the response time histories. Although the acceleration response time histories were computed both with and without cut off of composite modal damping, only the ones with cut off damping are shown here. It should be noted that for the containment building the composite modal dampings, which exceed 10%, are all associated with rigid body modes.

References:

1. Letter from J. F. Pinto to R. S. Trickovic, BMP-82/224, dated June 23, 1982.

2. USNRC Standard Review Plan (NUREG 0800)

3. USNRC Regulatory Guide 1.60, Rev. 1

4. USNRC Regulatory Guide 1.61.

5. Grand Gulf Nuclear Station Final Safety Analysis Report.

6. Bechtel Civil/Structural Calculation No. C-H002.5, Rev. 0 for Grand Gulf Nuclear Station.

7. Letter from J. F. Pinto to R. S. Trickovic, BMP-82/263, dated July 28, 1982.

8. Bechtel Civil/Structural Calculation No. C-G711.0, Rev. 1, for Grand Gulf Nuclear Station.

9. Bechtel Power Corporation Design Guide C-2.44, Rev. 0, dated August 1980.

10. USNRC Regulatory Guide 1.92, Rev. 1.

11. Bechtel Civil/Structural Calculation No. C-K600.0, Rev. 0 for Grand Gulf Nuclear Station.

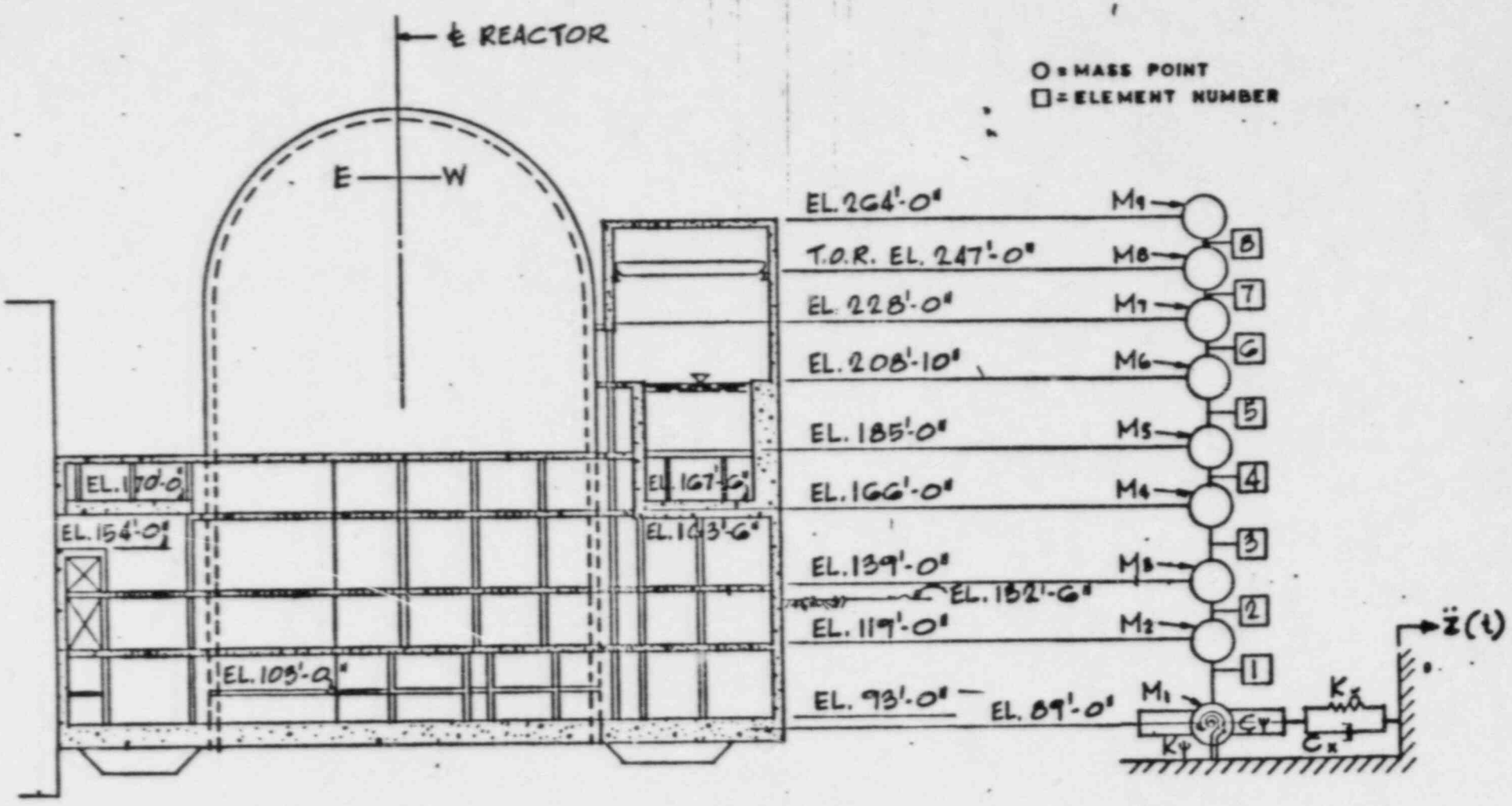

SECTION
LOOKING SOUTH

Figure 1 AUXILIARY BUILDING LUMPED MASS MODEL (EAST-WEST DIRECTION)

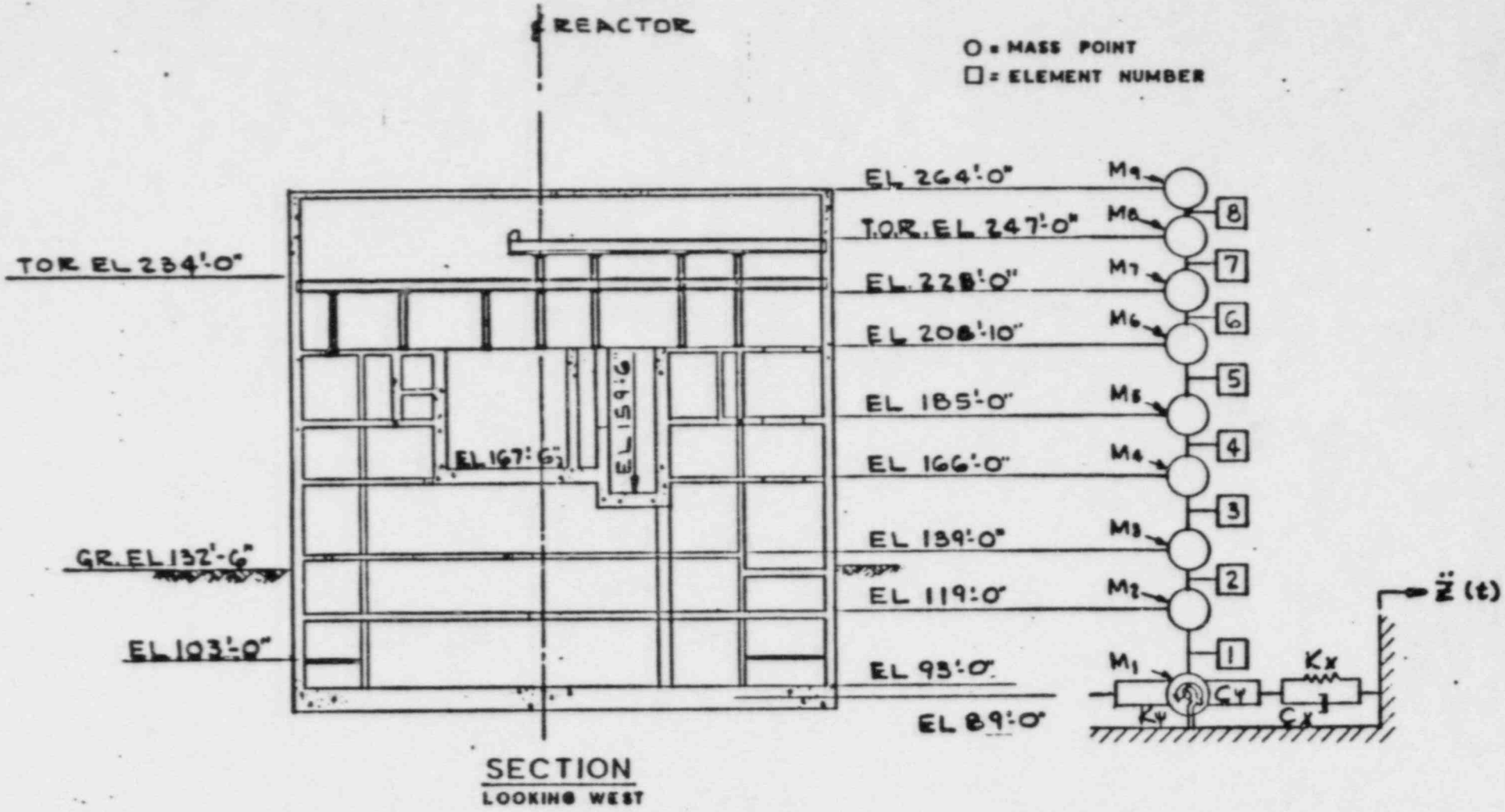

Figure 2 AUXILIARY BUILDING LUMPED MASS MODEL (NORTH-SOUTH DIRECTION)

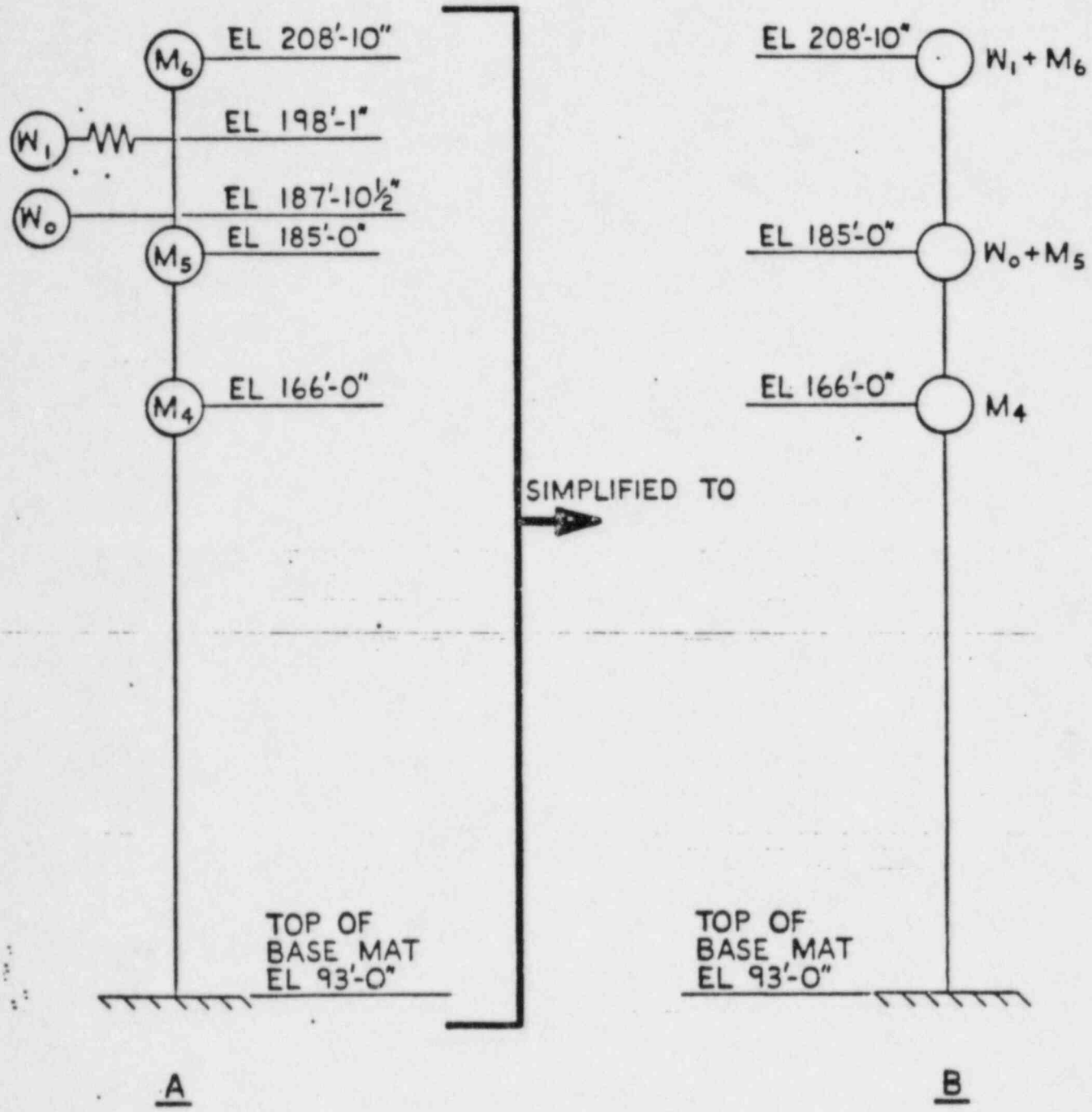

FIGURE 3 IDEAL VS SIMPLIFIED LUMPED MASS MODEL AUXILIARY BUILDING (PARTIAL)

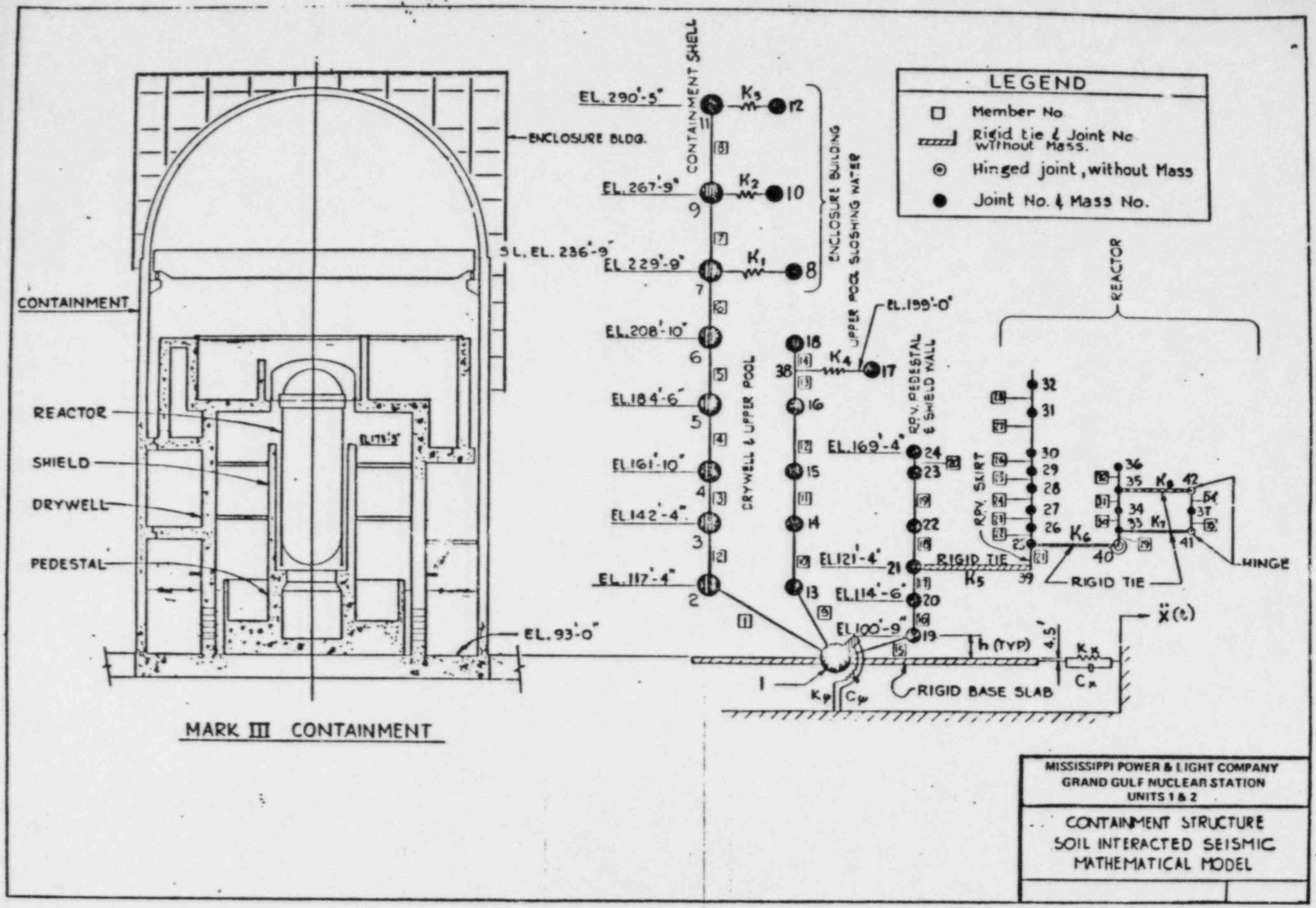

Figure 4 CONTAINMENT BUILDING LUMPED MASS MODEL

MISSISSIPPI POWER & LIGHT COMPANY
GRAND GULF NUCLEAR STATION
UNITS 1 & 2

CONTAINMENT STRUCTURE
SOIL INTERACTED SEISMIC
MATHEMATICAL MODEL

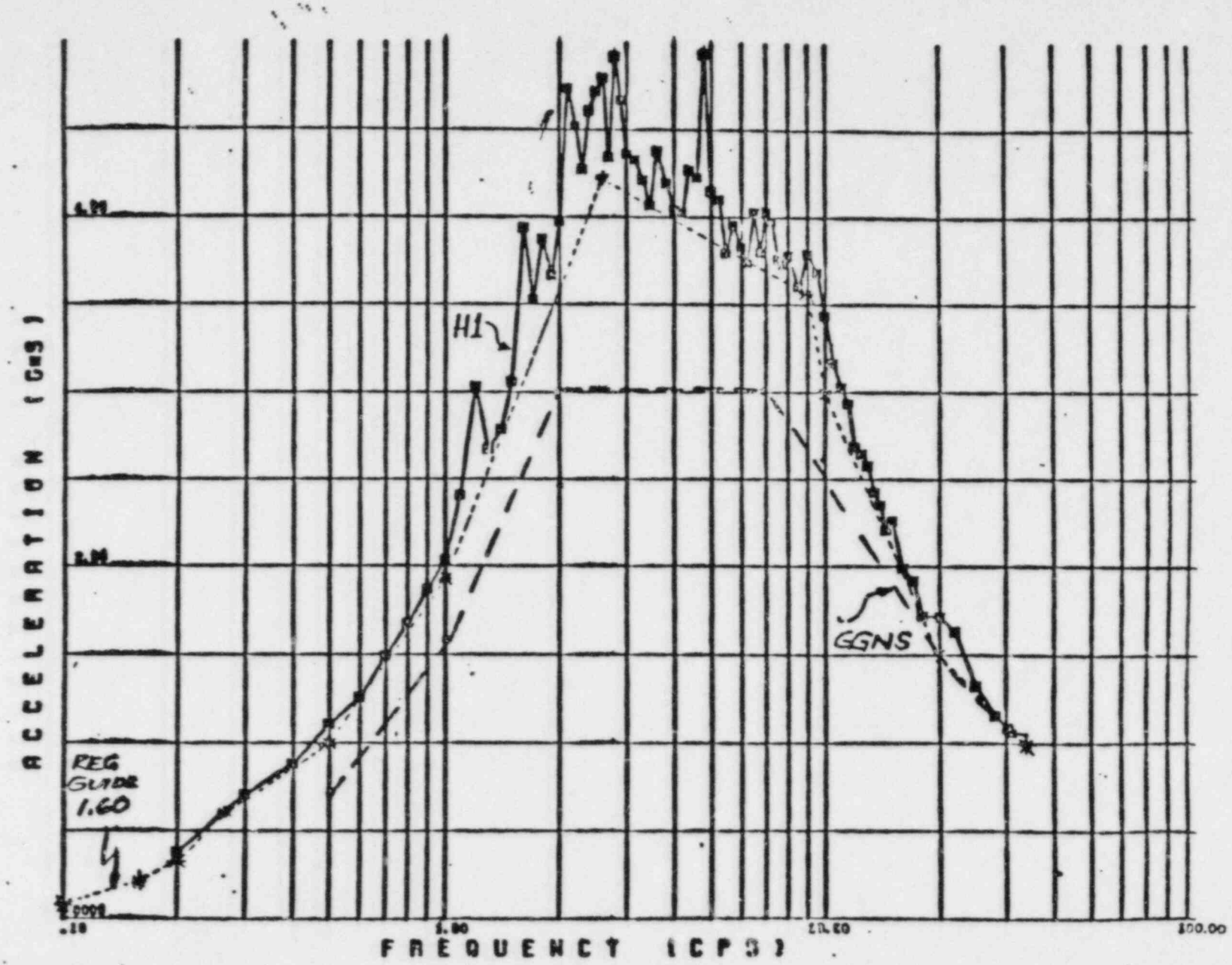

SPECTRA PLOT OF TIME HISTORY H1

FIGURE-5: SPECTRA OF HORIZONTAL MOTION 'H1' (DAMPING 2%)

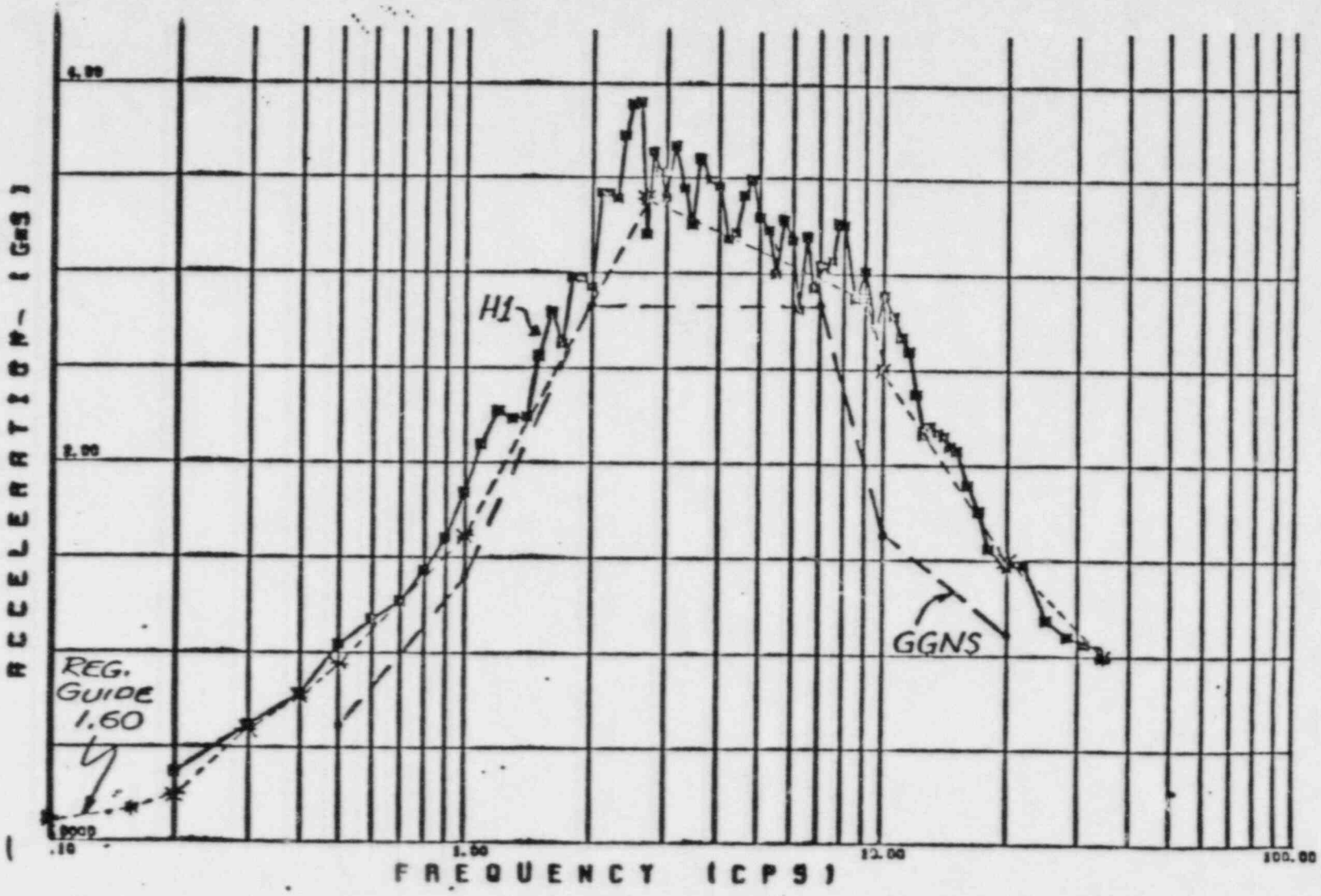

FIGURE-6: SPECTRA OF HORIZONTAL MOTION 'H1' (DAMPING 4%)

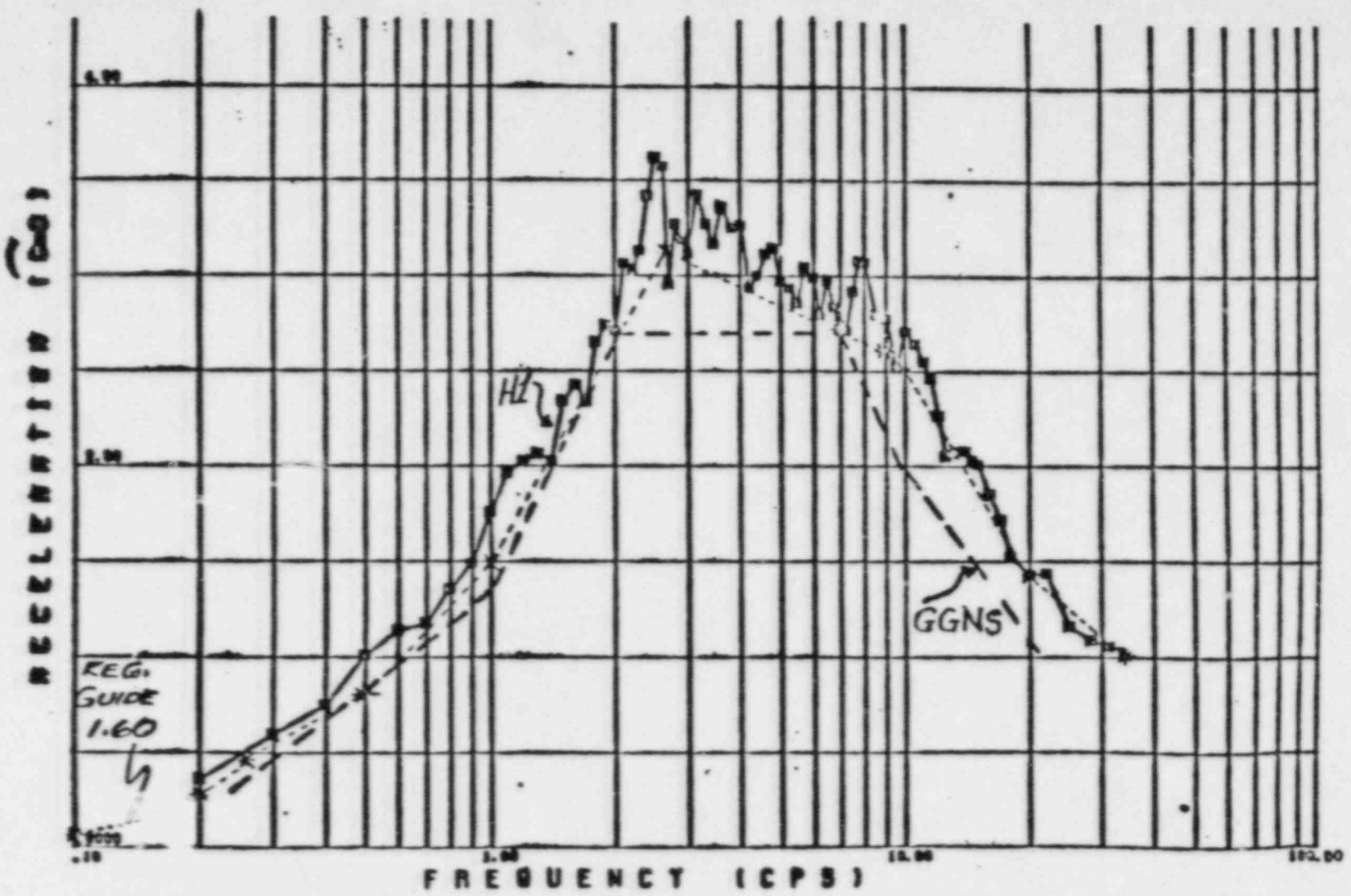

SPECTRA PLOT OF TIME HISTORY H1

FIGURE-7: SPECTRA OF HORIZONTAL MOTION 'H1' (DAMPING 5%)

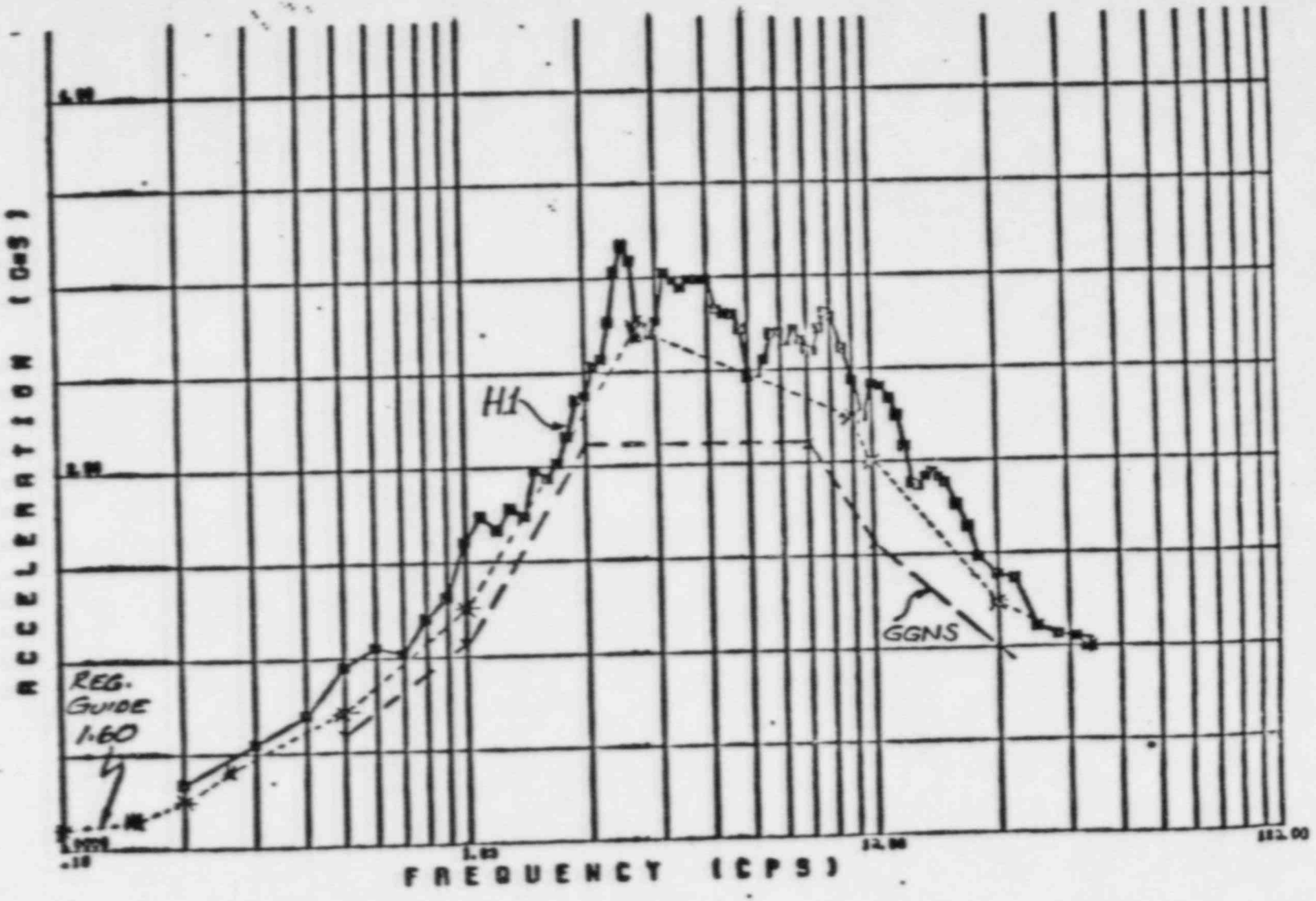

SPECTRA PLOT OF TIME HISTORY H1

FIGURE-8: SPECTRA OF HORIZONTAL MOTION 'H 1' (DAMPING 7%)

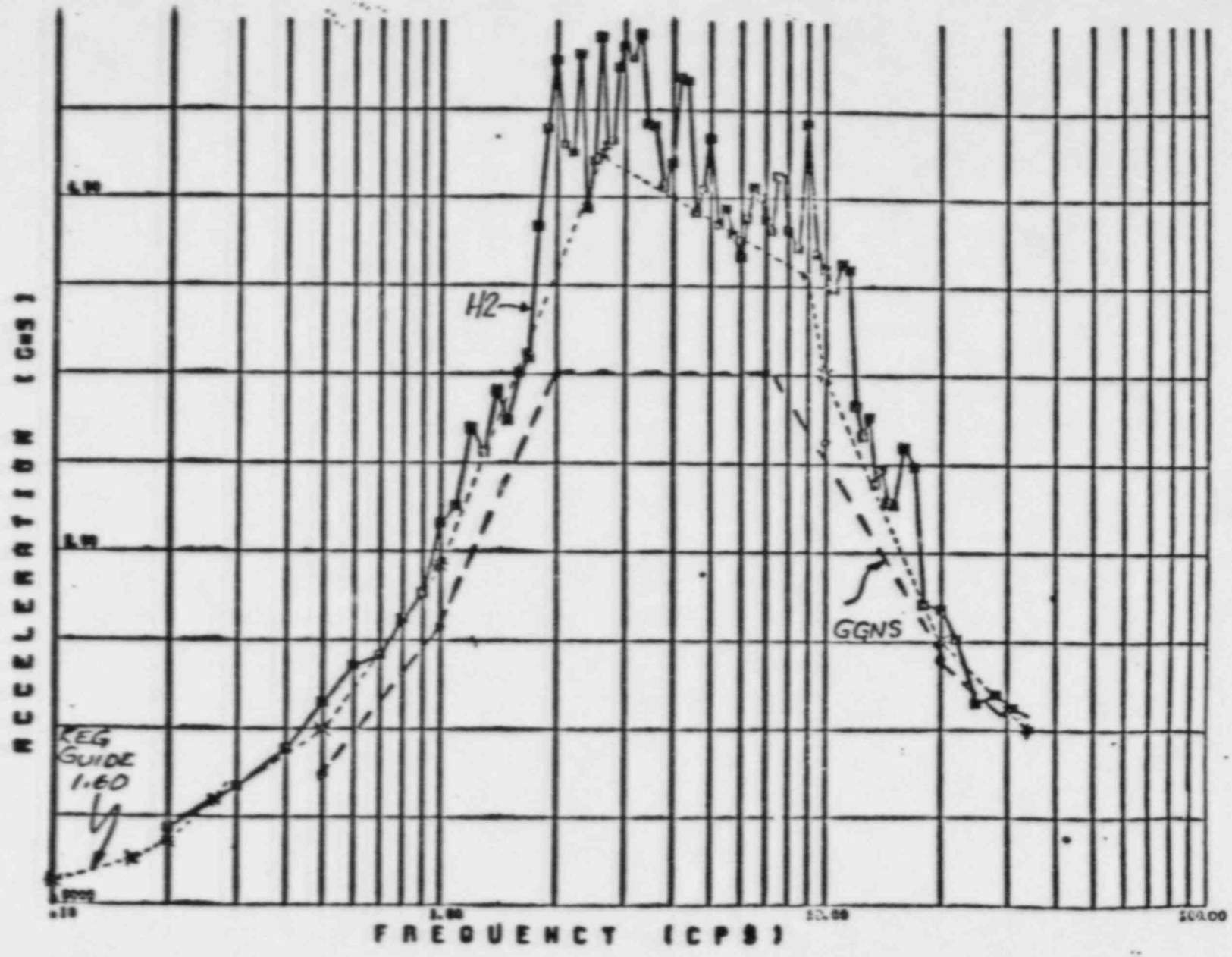

FIGURE-9: SPECTRA OF HORIZONTAL MOTION 'H2' (DAMPING 2%)

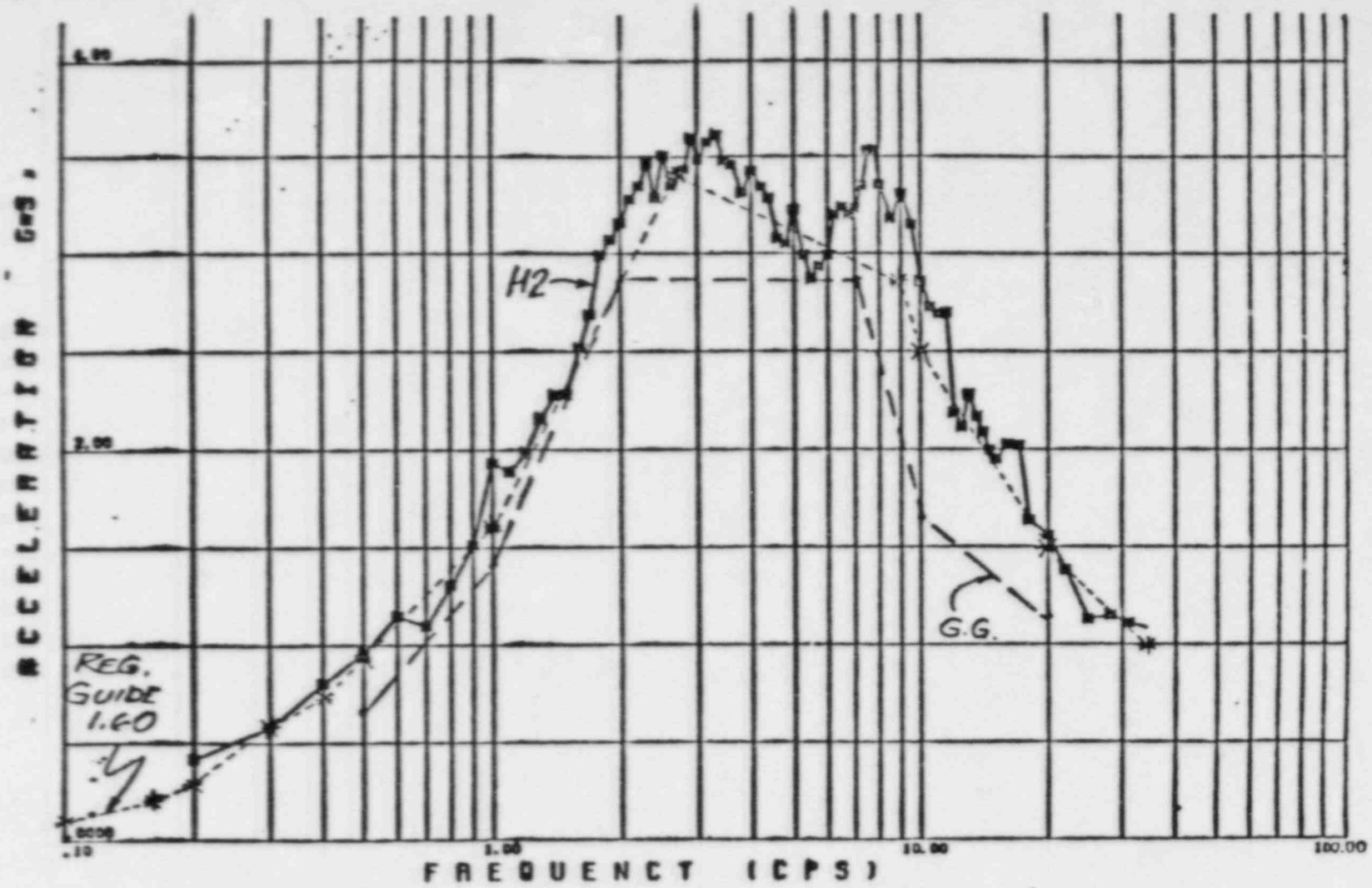

SPECTRA PLOT OF TIME HISTORY H2

FIGURE-10: SPECTRA OF HORIZONTAL MOTION 'H2' (DAMPING 4%)

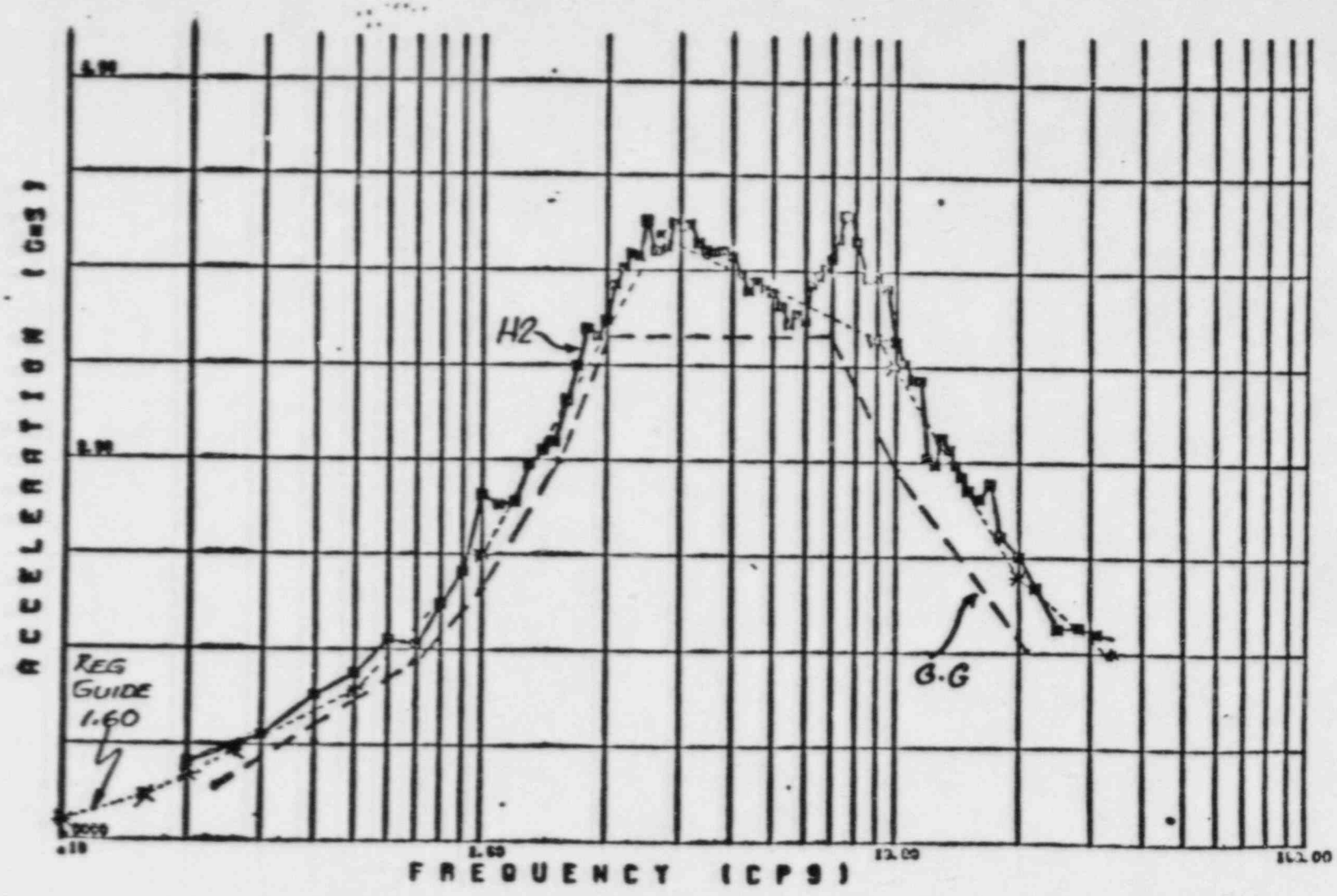

FIGURE-11: SPECTRA OF HORIZONTAL MOTION 'H2' (DAMPING 5%)

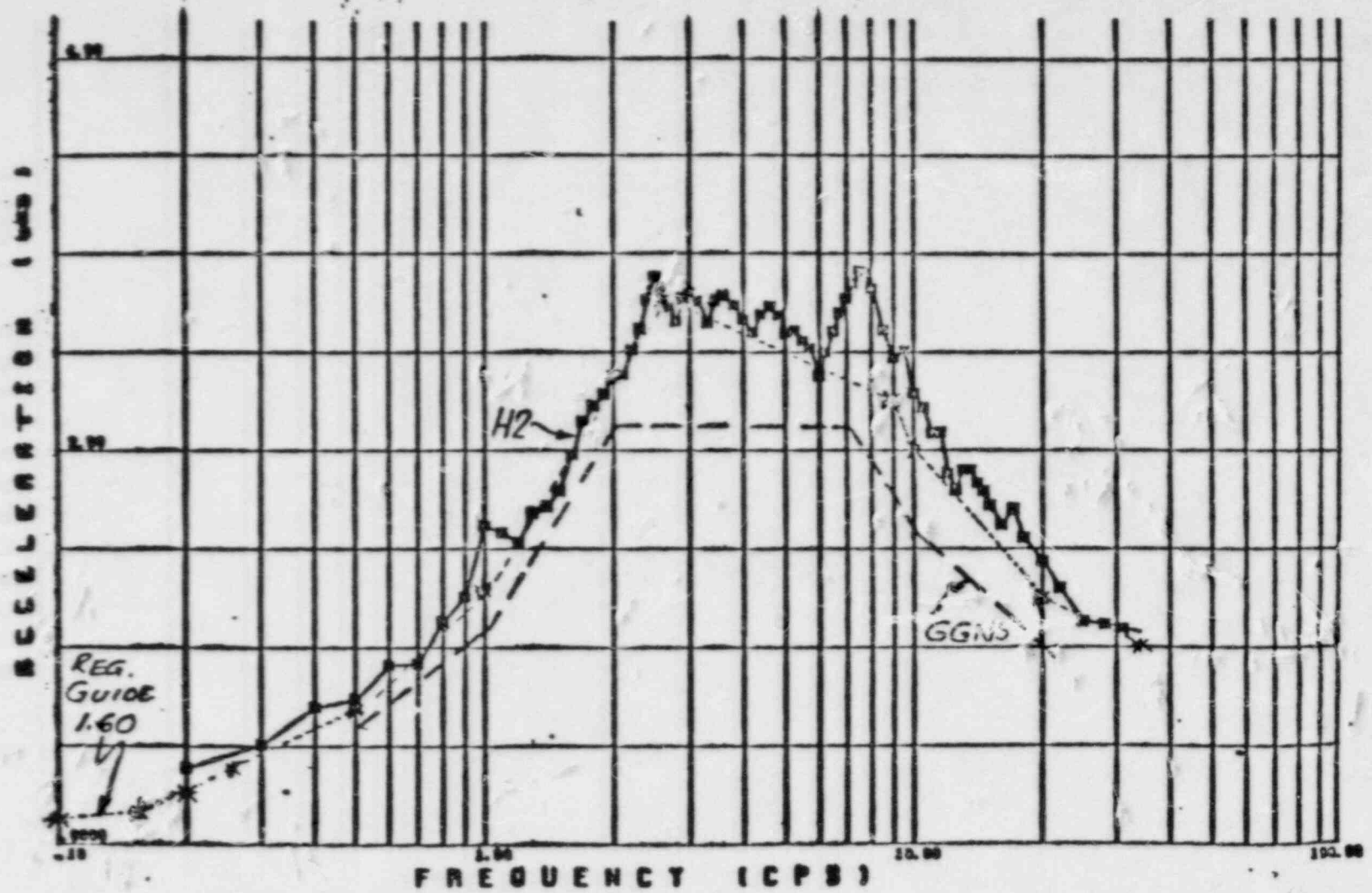

SPECTRA PLOT OF TIME HISTORY H2

FIGURE-12: SPECTRA OF HORIZONTAL MOTION 'H2' (DAMPING 7%)

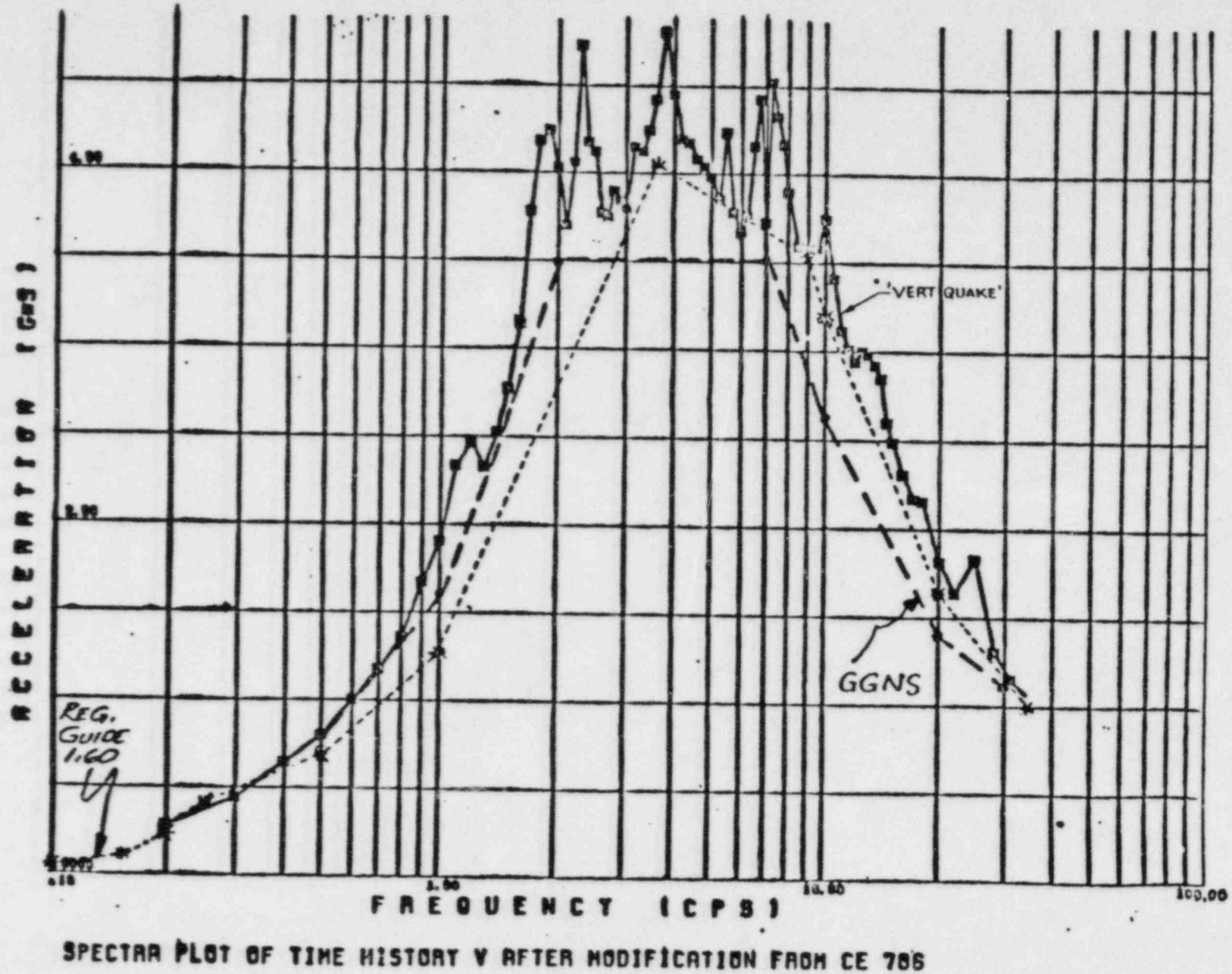

FIGURE-13: SPECTRA OF VERTICAL MOTION 'VERTQUAKE' (DAMPING 2%)

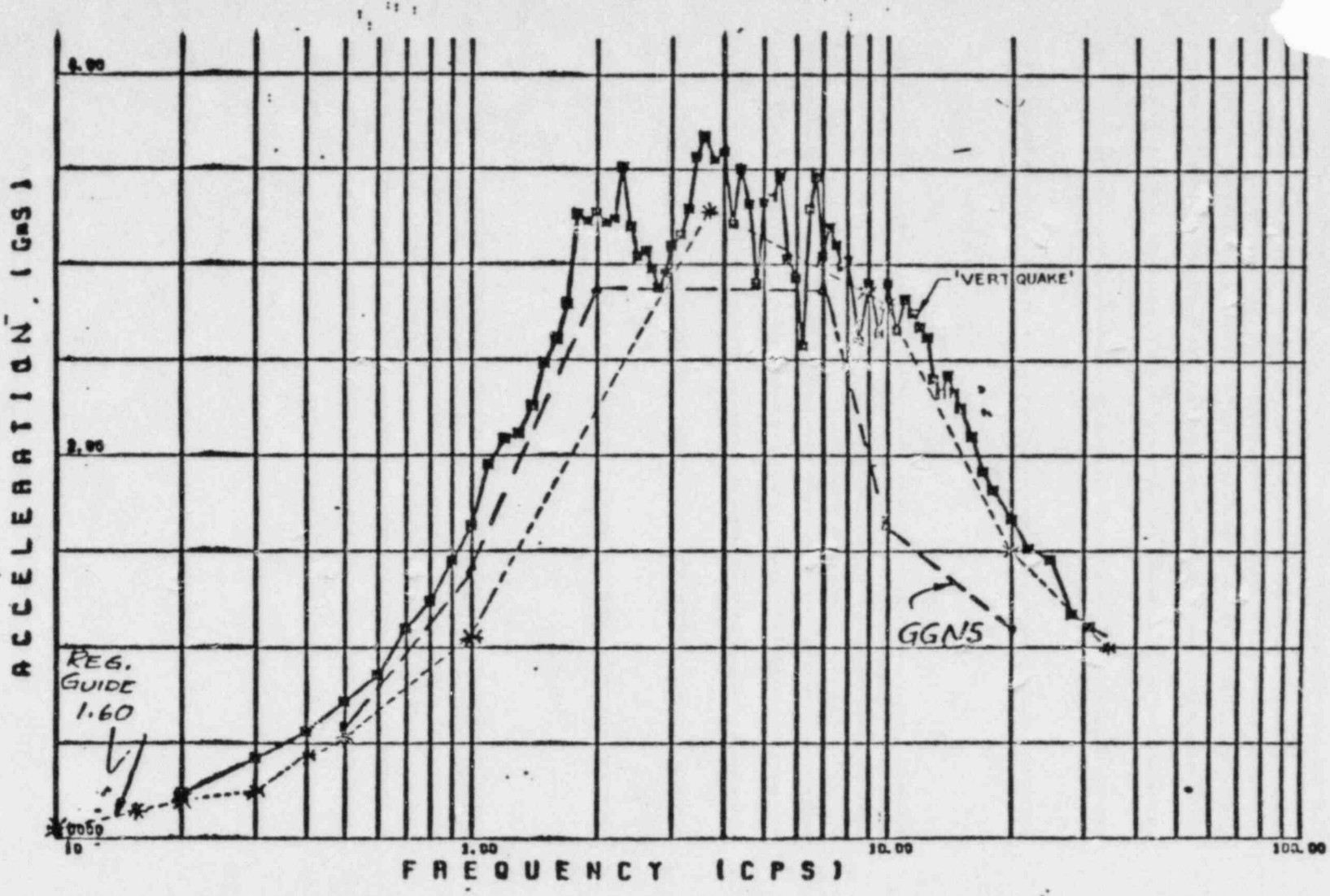

FIGURE-14: SPECTRA OF VERTICAL MOTION 'VERTQUAKE' (DAMPING 4%)

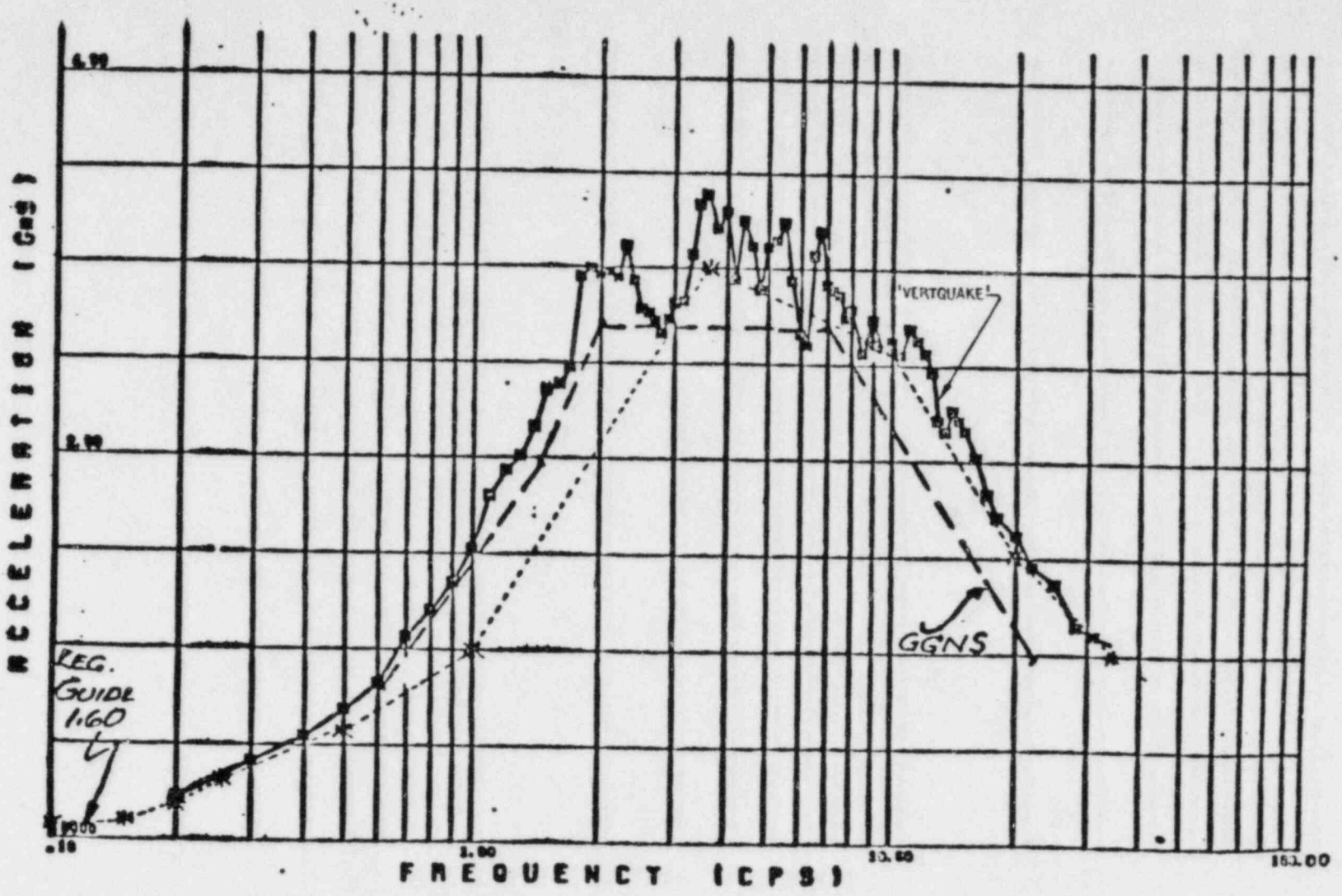

SPECTRA PLOT OF TIME HISTORY V AFTER MODIFICATION FROM CE 788

FIGURE-15: SPECTRA OF VERTICAL MOTION 'VERTQUAKE' (DAMPING 5%)

CE201811-1 T30304 072382

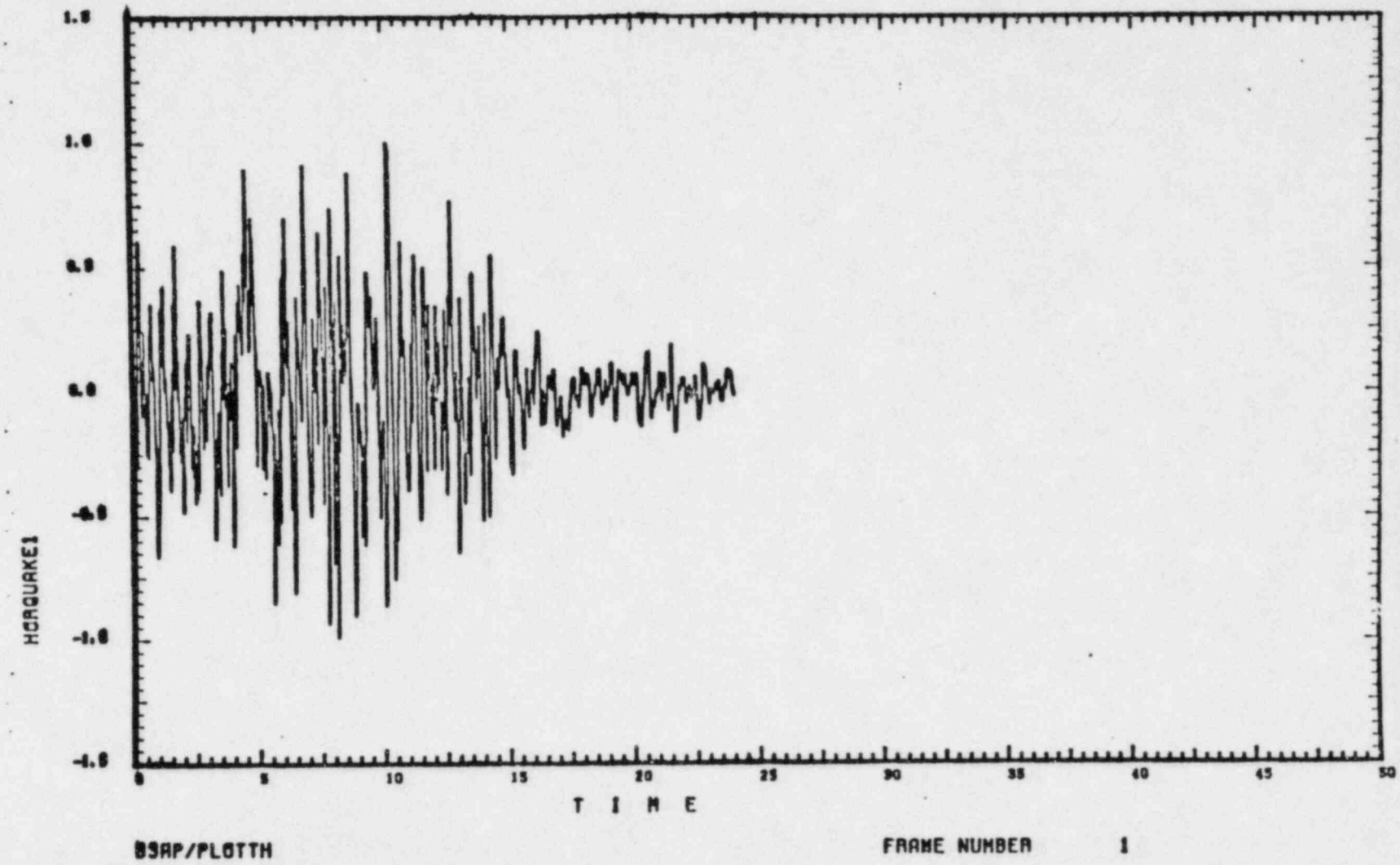

Figure 17 HORIZONTAL GROUND MOTION HORQUAKE1

CE201811-1 T70000 072782

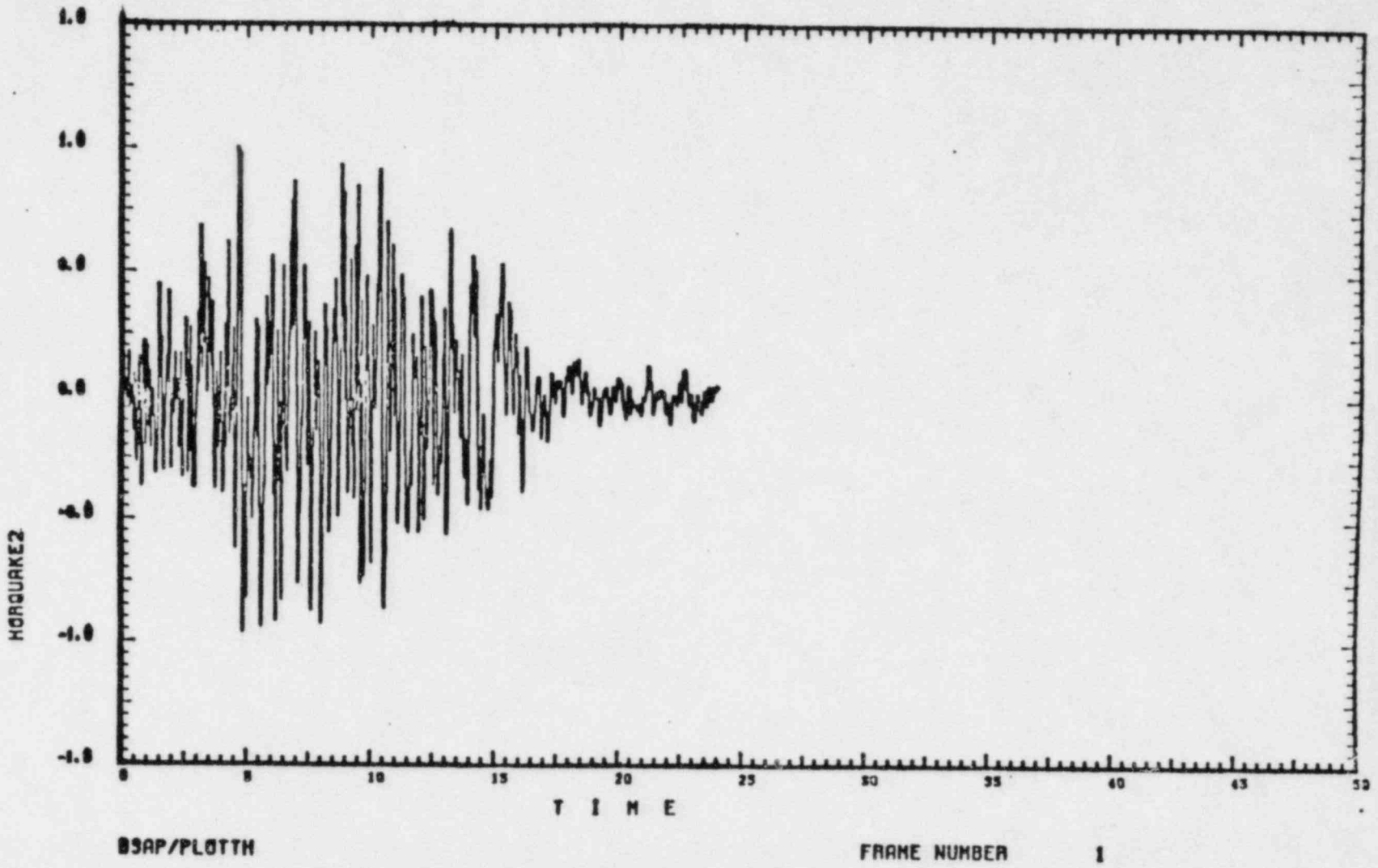

Figure 18 HORIZONTAL GROUND MOTION HORQUAKE2

CE201811-1 T70024 072782

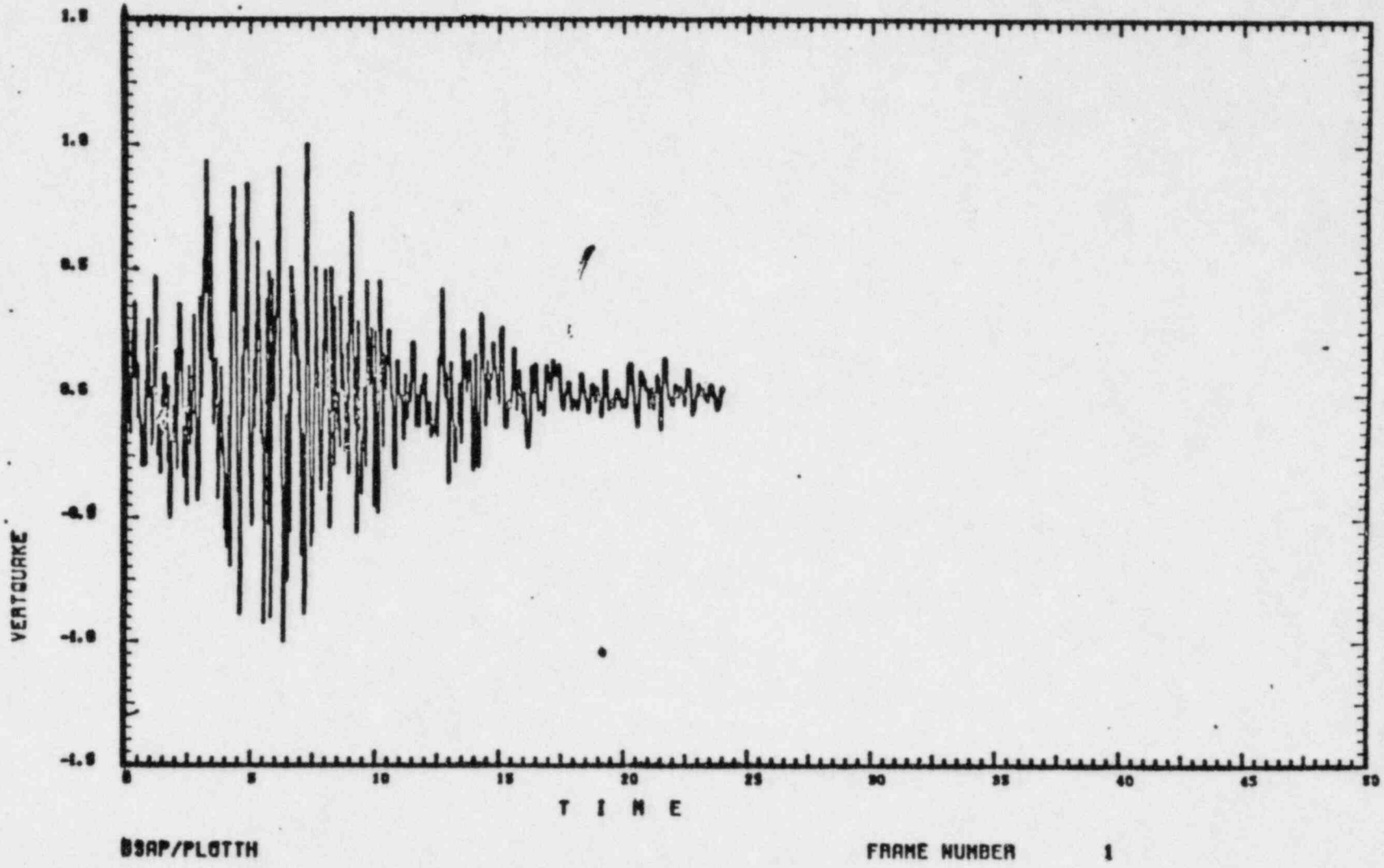

Figure 19 VERTICAL GROUND MOTION VERTQUAKE

CE201811-1 X3055 081382

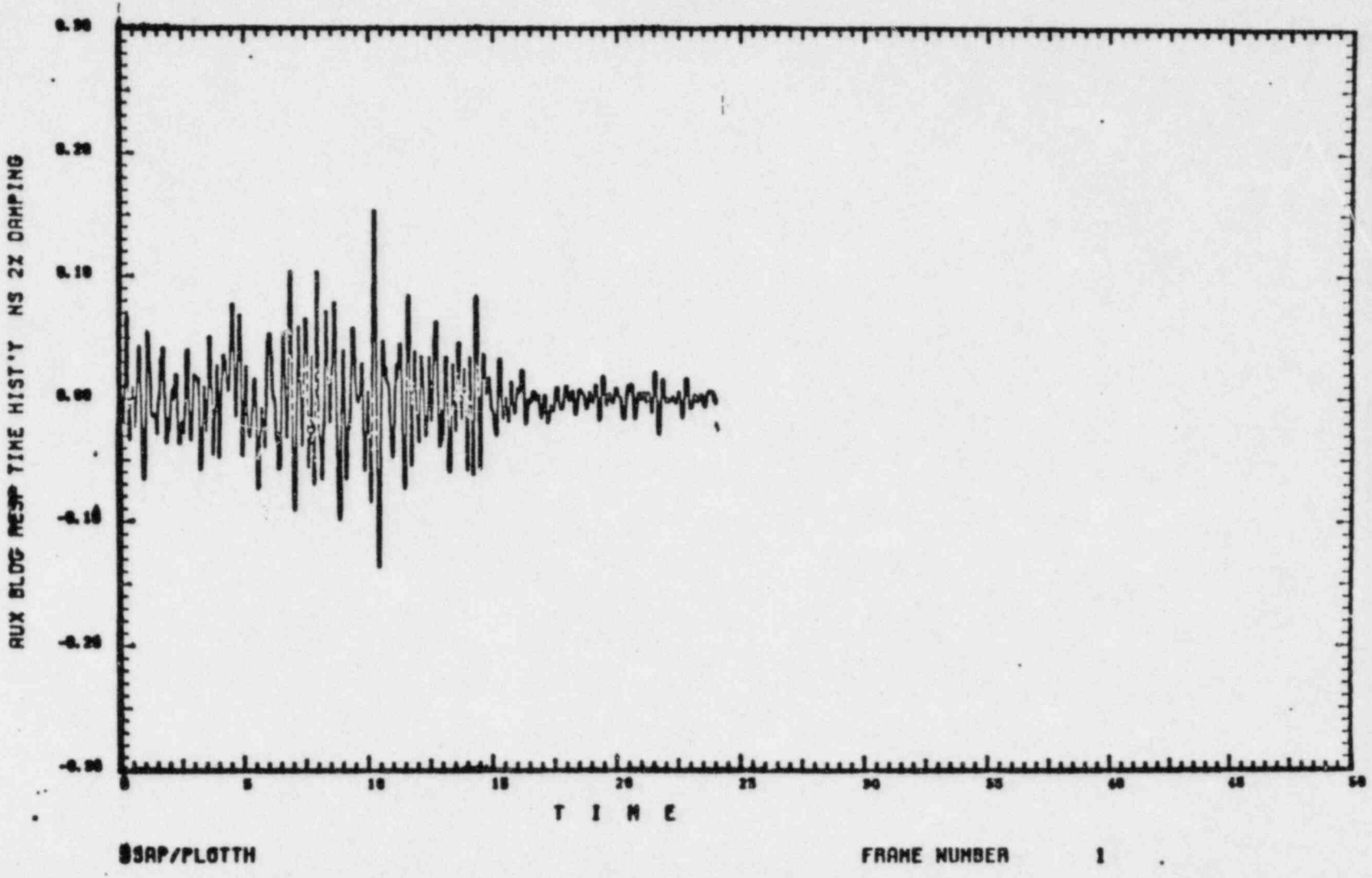

Figure 20 SEISMIC RESPONSE TIME HISTORY AT EL 166'-0" OF AUX BLDG SPENT FUEL POOL (HORIZONTAL N-S OBE 2% DAMPING)

CE201811-1 X3058 081382

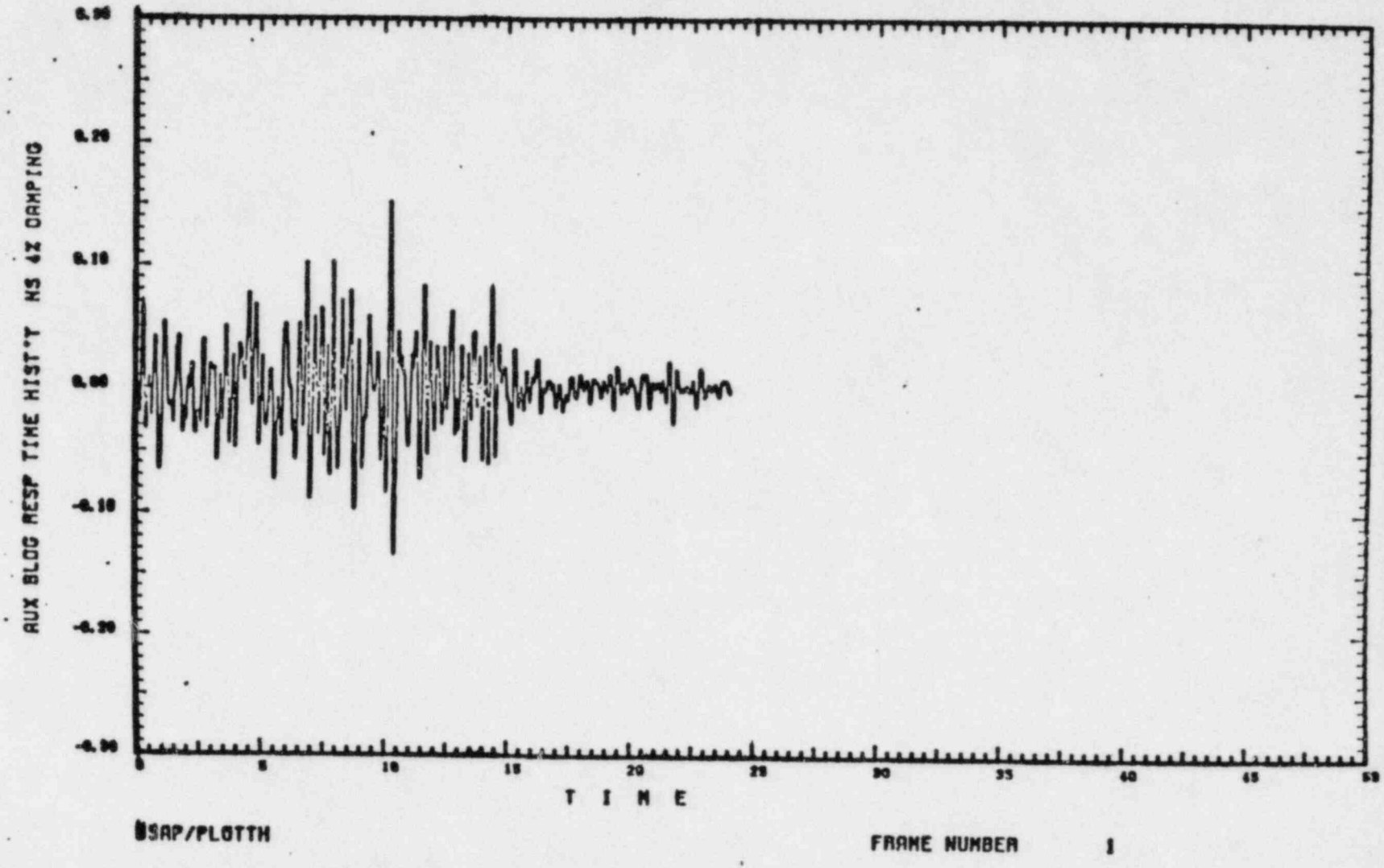

Figure 21 SEISMIC RESPONSE TIME HISTORY AT EL 166'-0" OF AUX BLDG SPENT FUEL POOL (HORIZONTAL N-S OBE 4% DAMPING)

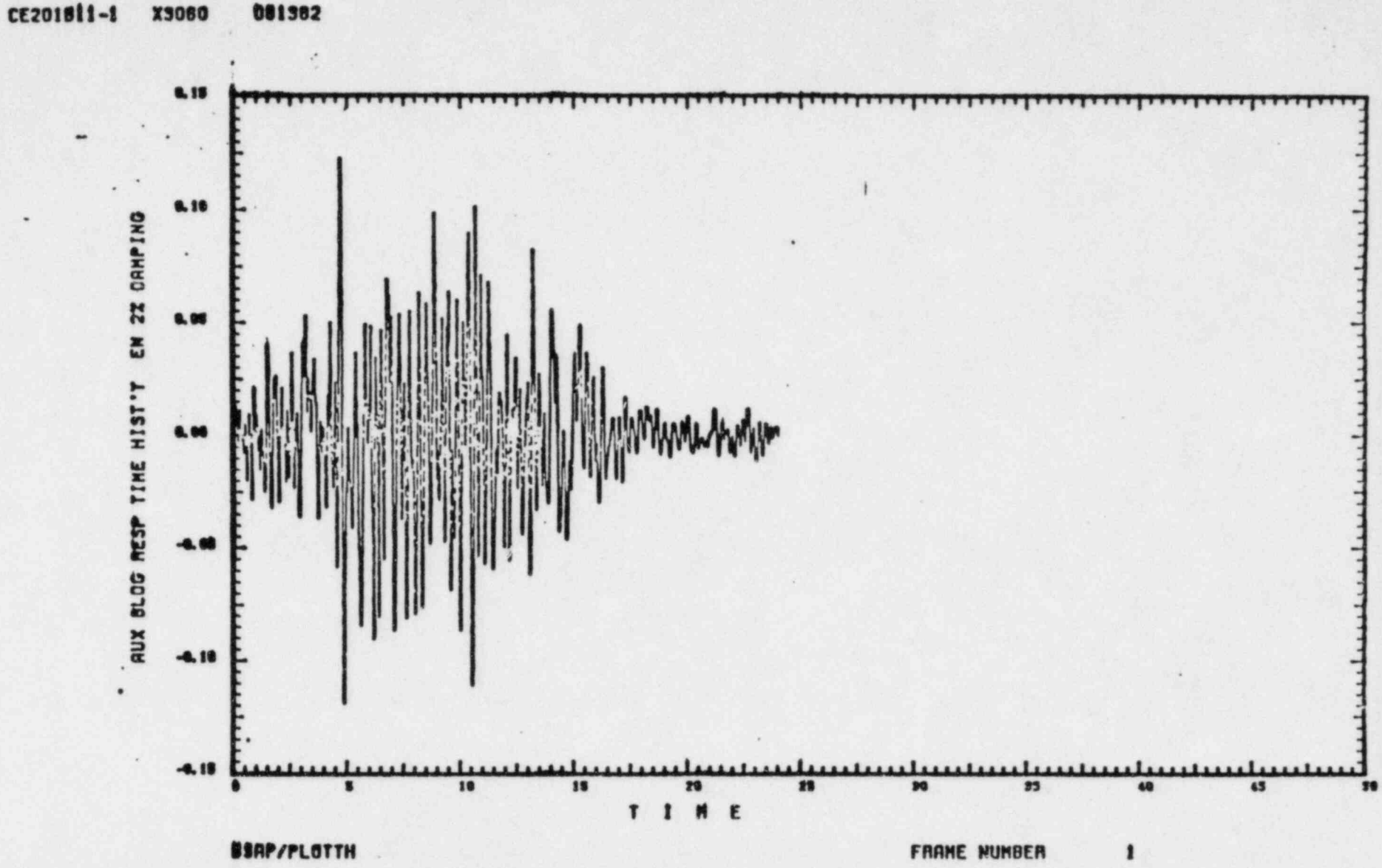

Figure 22 SEISMIC RESPONSE TIME HISTORY AT EL 166'-0" OF AUX BLDG SPENT FUEL POOL (HORIZONTAL E-W OBE 2% DAMPING)

CE201811-1 X3081 081382

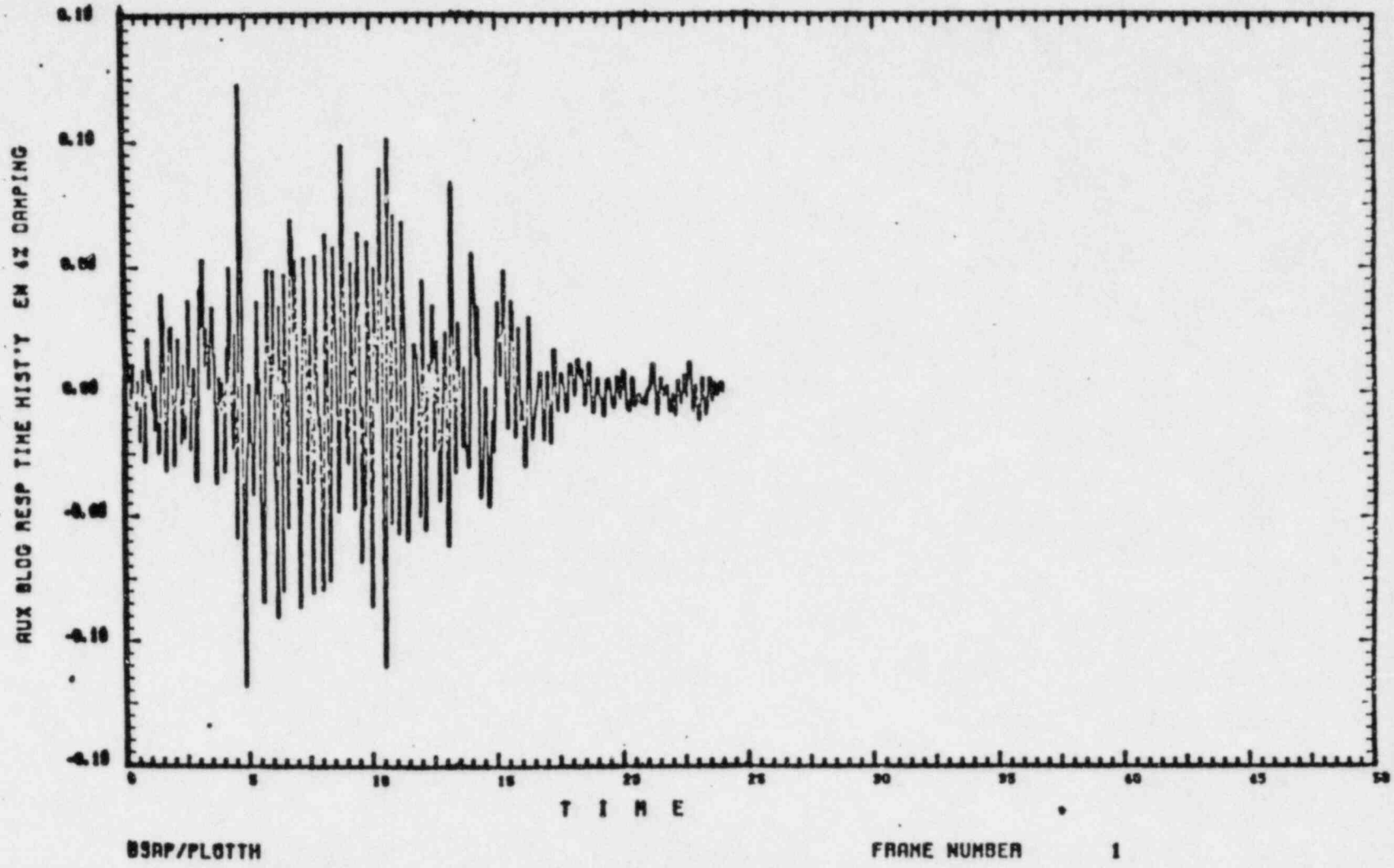

Figure 23 SEISMIC RESPONSE TIME HISTORY AT EL 166'-0" OF AUX BLDG SPENT FUEL POOL (HORIZONTAL E-W OBE 4% DAMPING)

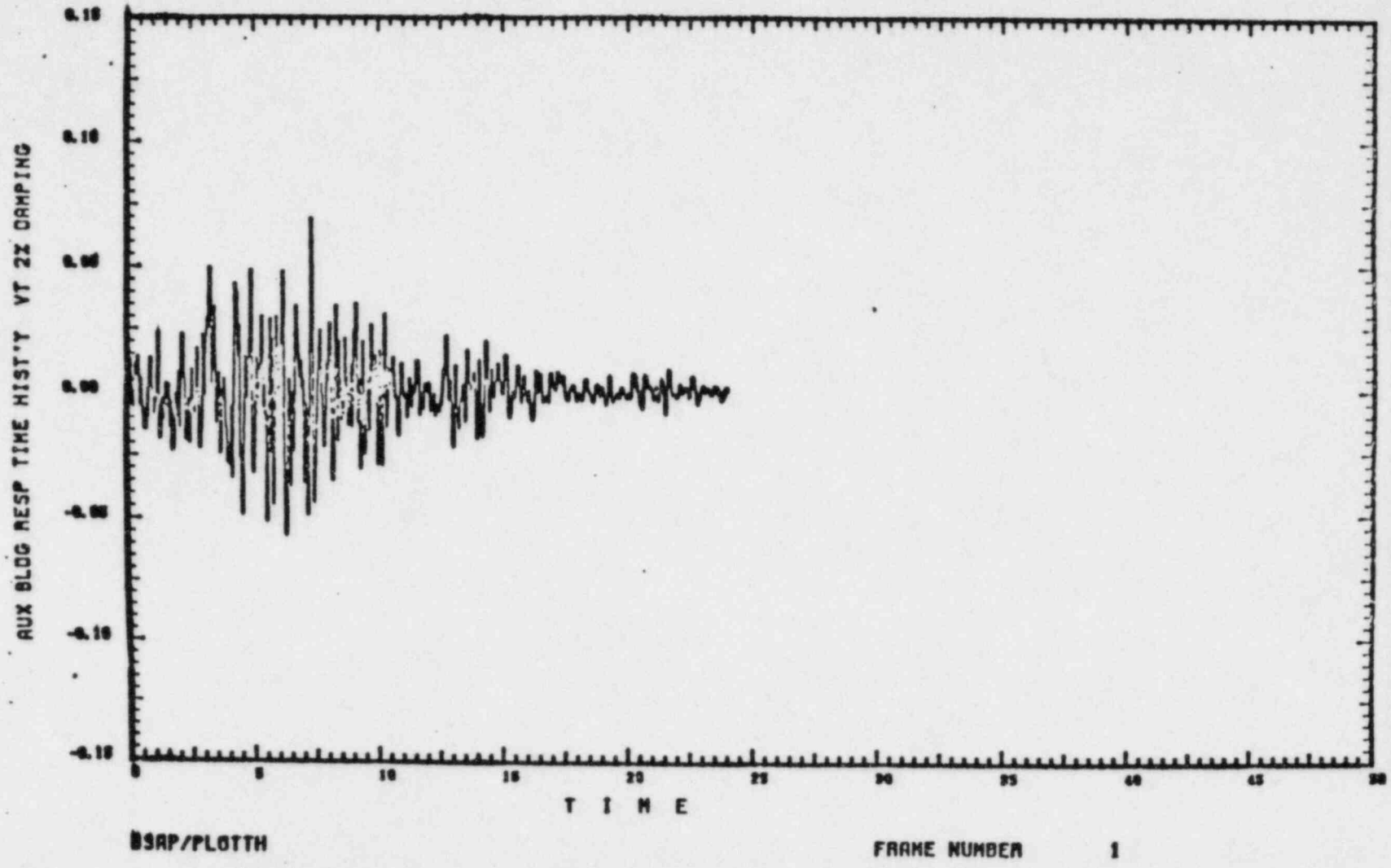

Figure 24, SEISMIC RESPONSE TIME HISTORY AT EL 166'-0" OF AUX BLDG SPENT FUEL POOL (VERTICAL OBE 2% DAMPING)

CE201811-1 X3069 081382

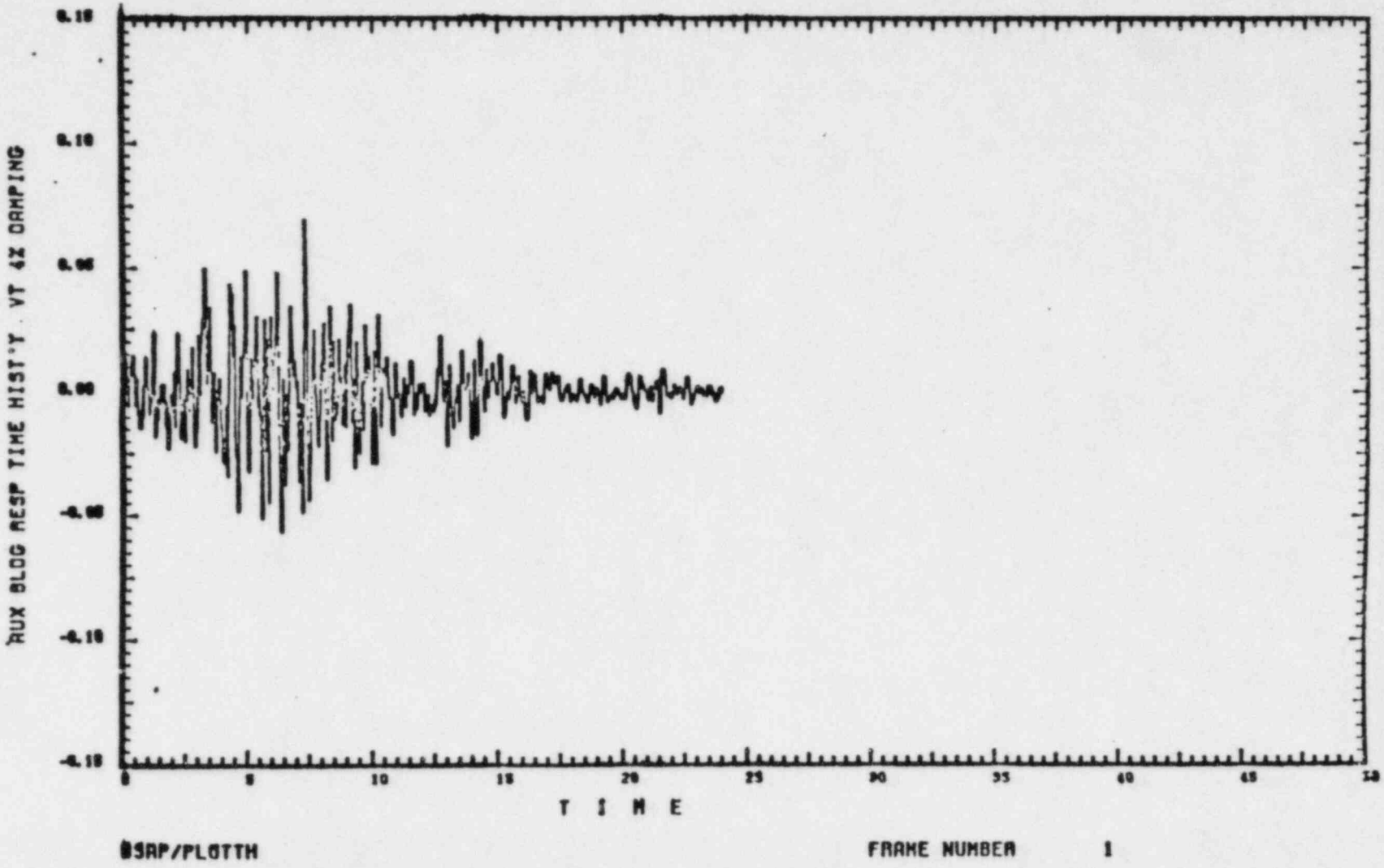

Figure 25 SEISMIC RESPONSE TIME HISTORY AT EL 166'-0" OF AUX BLDG SPENT FUEL POOL (VERTICAL OBE 4% DAMPING)

CE201811-1 X3058 081382

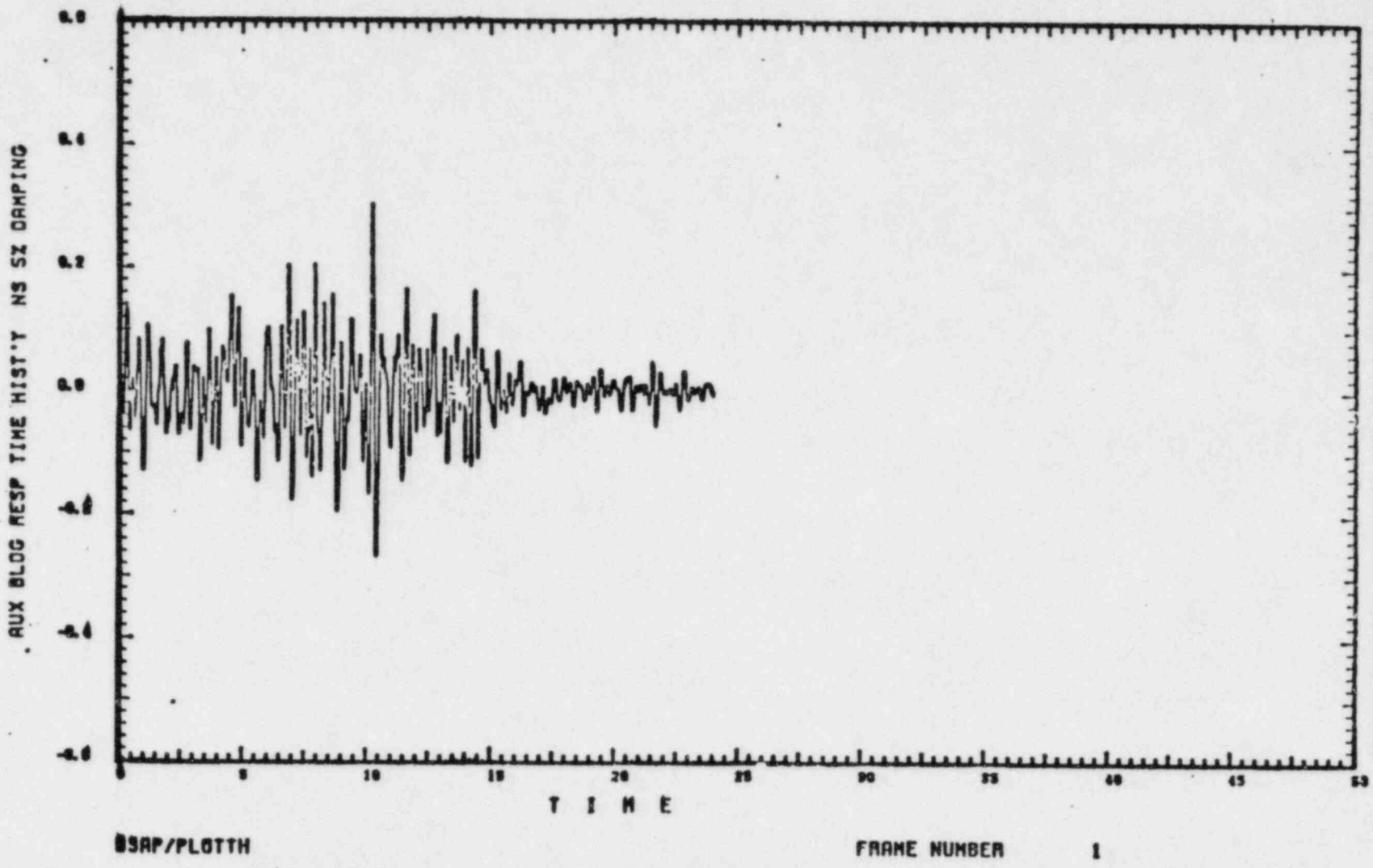

Figure 26 SEISMIC RESPONSE TIME HISTORY AT EL 166'-0" OF AUX BLDG SPENT FUEL POOL (HORIZONTAL N-S SSE 5% DAMPING)

CE201811-1 X9059 081982

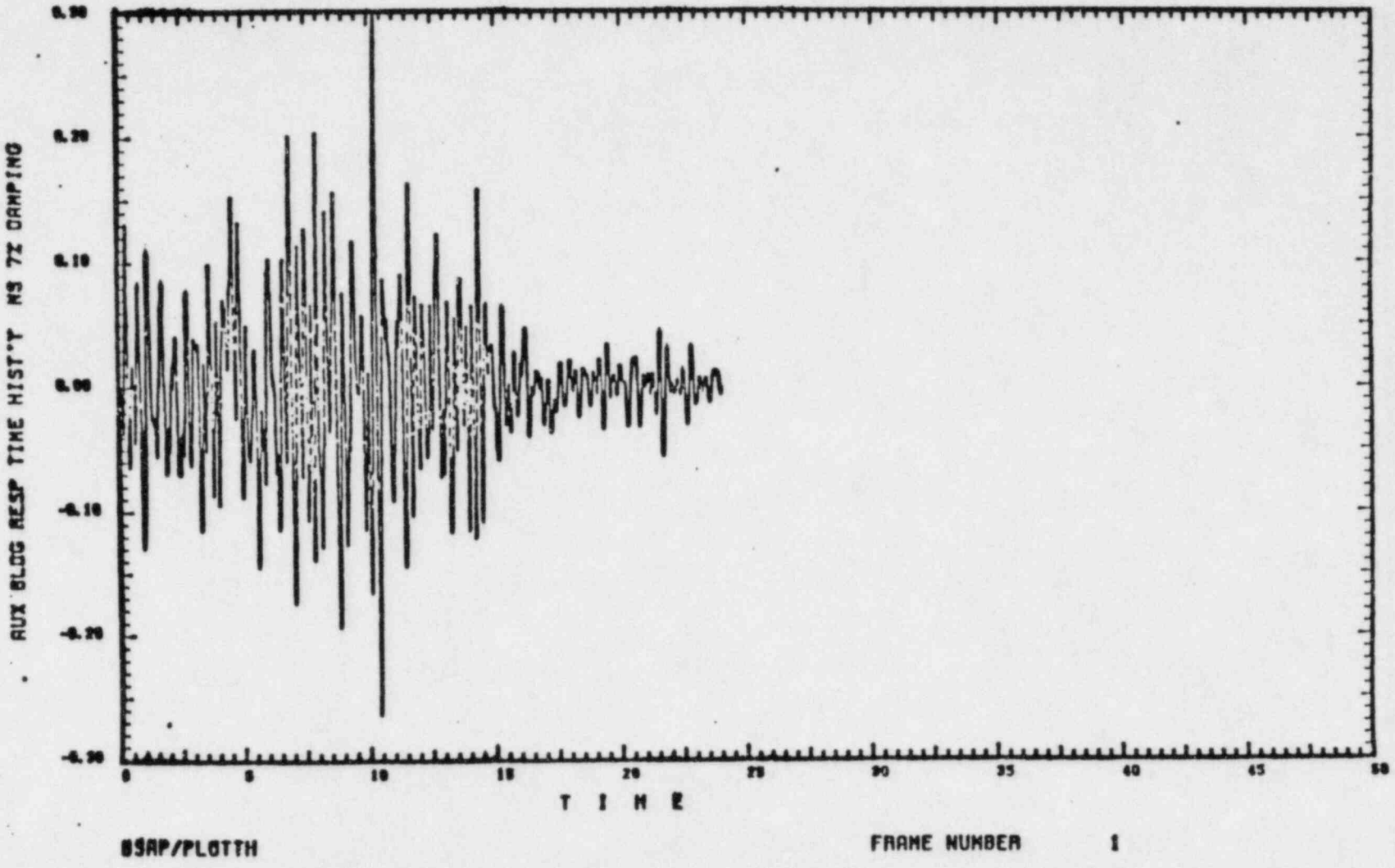

Figure 27 SEISMIC RESPONSE TIME HISTORY AT EL 166'-0" OF AUX BLDG SPENT FUEL POOL (HORIZONTAL N-S SSE 7% DAMPING)

CE201811-1 X3089 081382

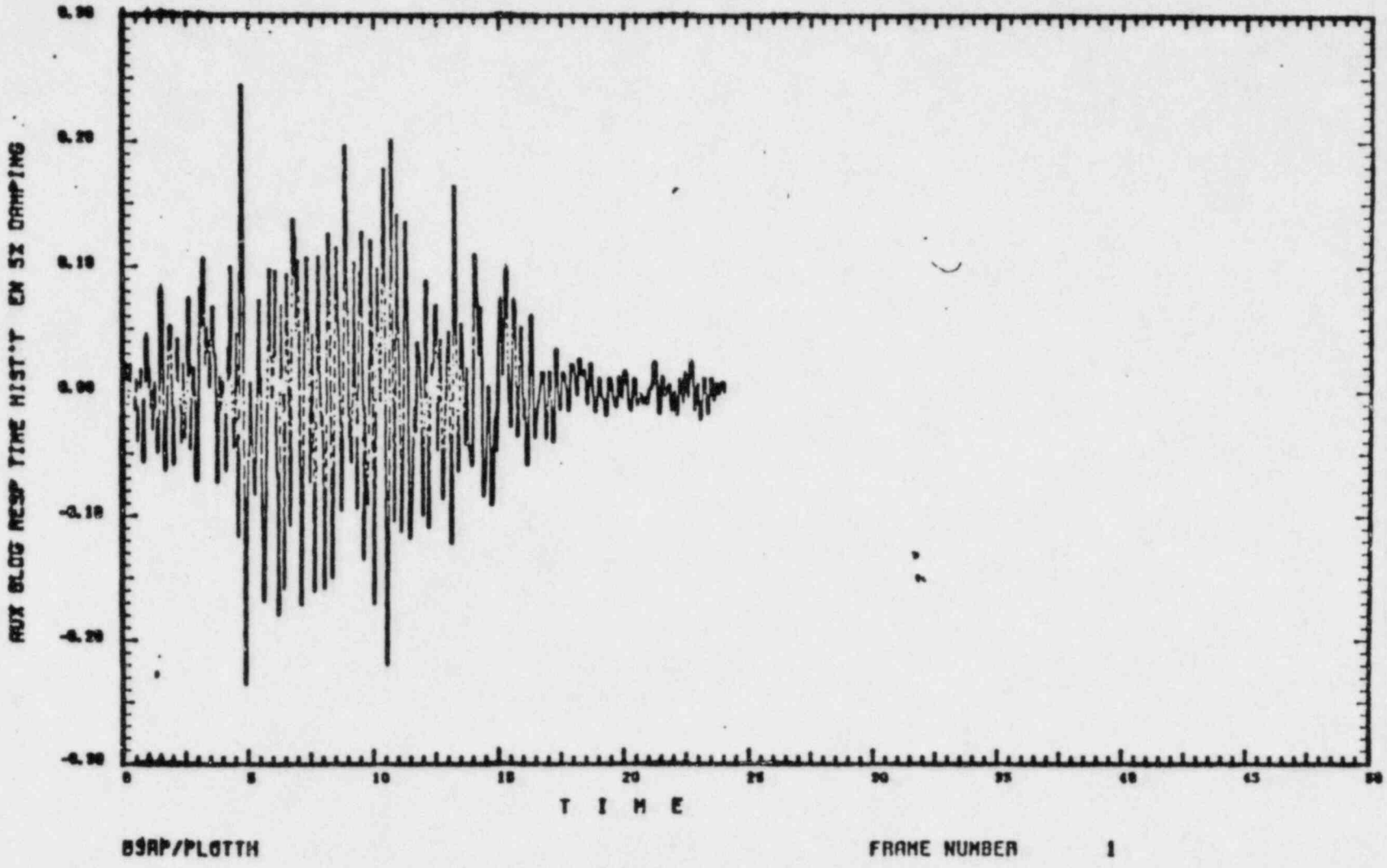

Figure 28 SEISMIC RESPONSE TIME HISTORY AT EL 166'-0" OF AUX BLDG SPENT FUEL POOL (HORIZONTAL E-W SSE 5% DAMPING)

CE201811-1 X3069 081382

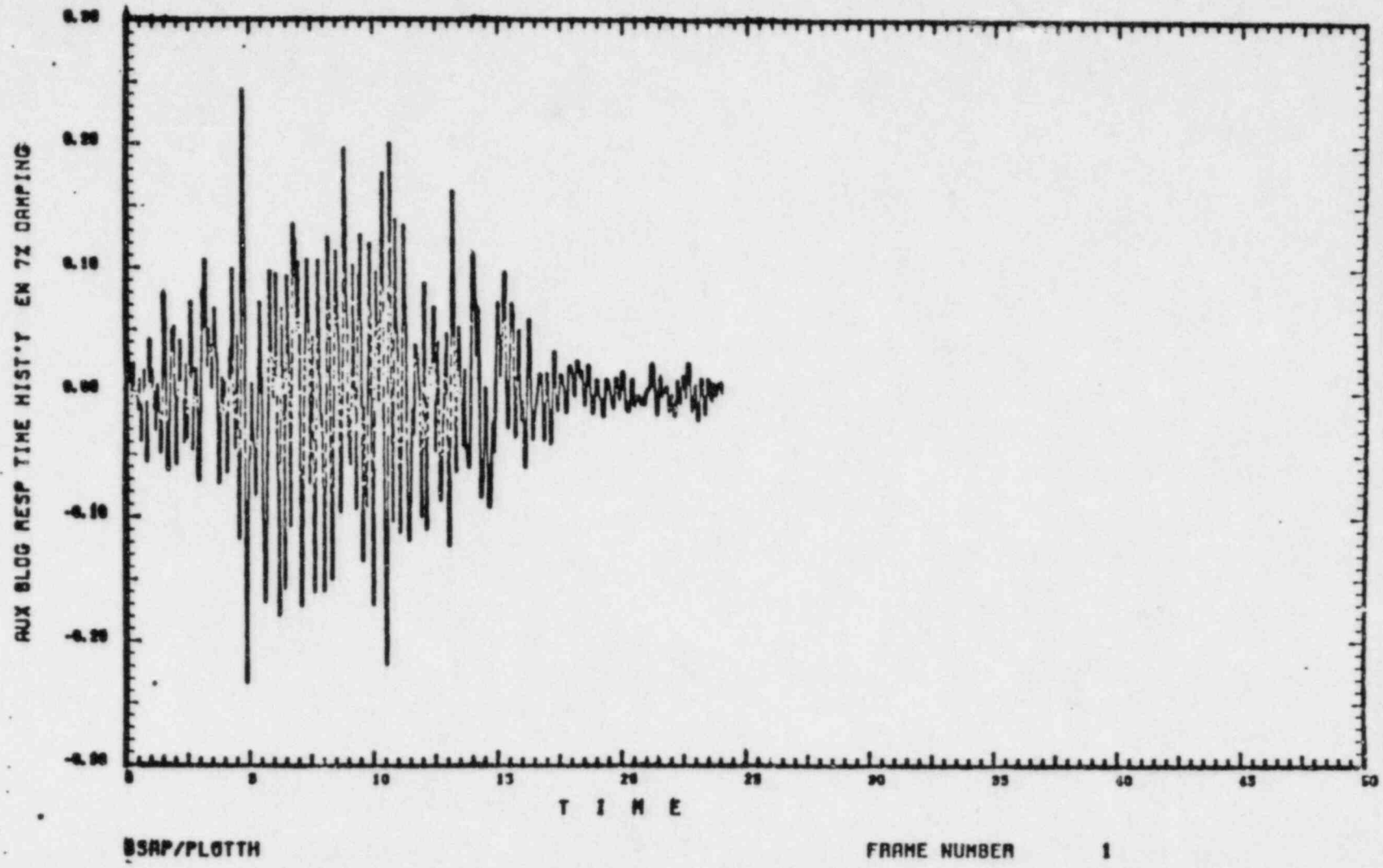

Figure 29 SEISMIC RESPONSE TIME HISTORY AT EL 166'-0" OF AUX BLDG SPENT FUEL POOL (HORIZONTAL E-W SSE 7% DAMPING)

CE201811-1 X3070 081382

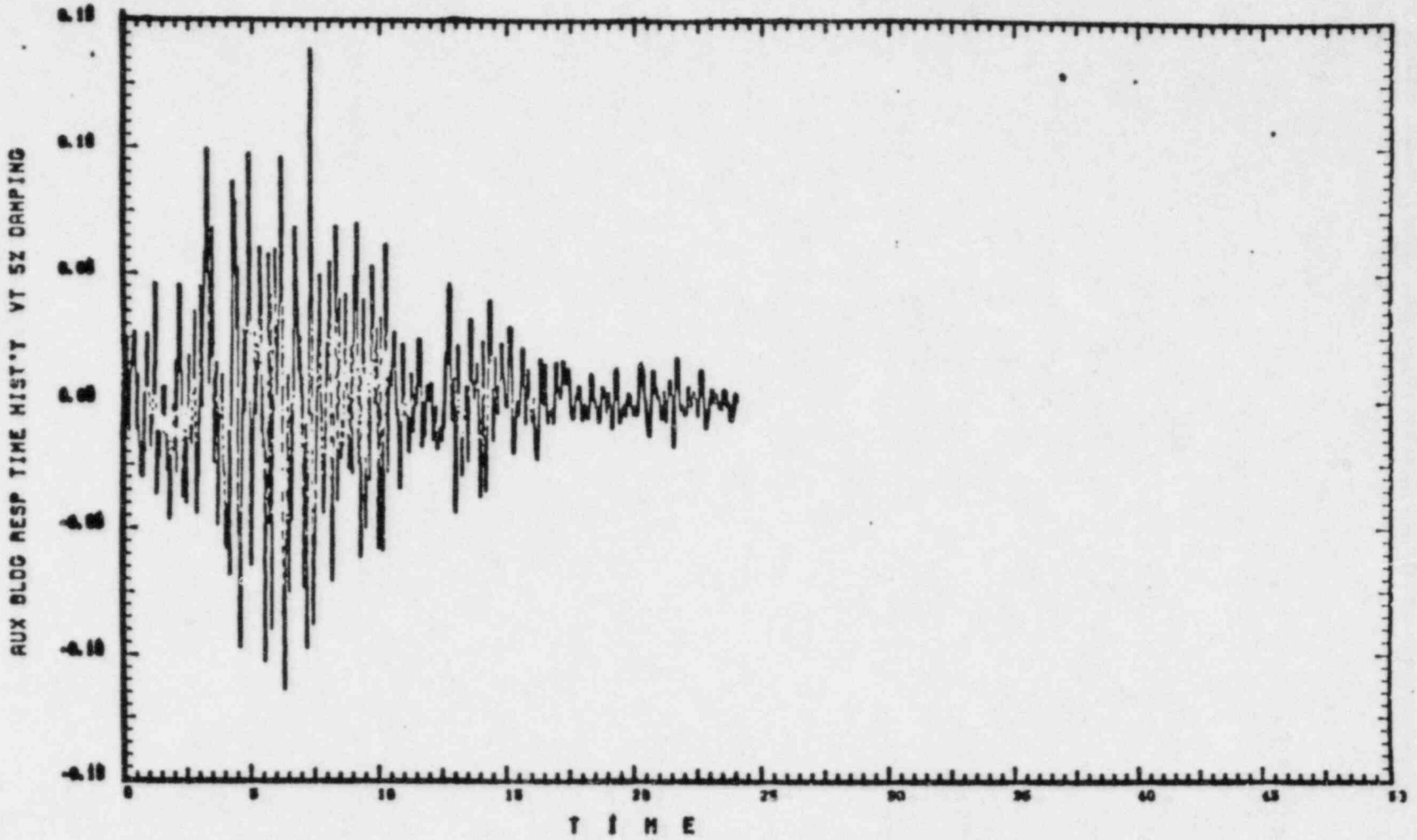

Figure 30 SEISMIC RESPONSE TIME HISTORY AT EL 166'-0" OF AUX BLDG SPENT FUEL POOL (VERTICAL SSE 5% DAMPING)

CE201811-1 X3071 081382

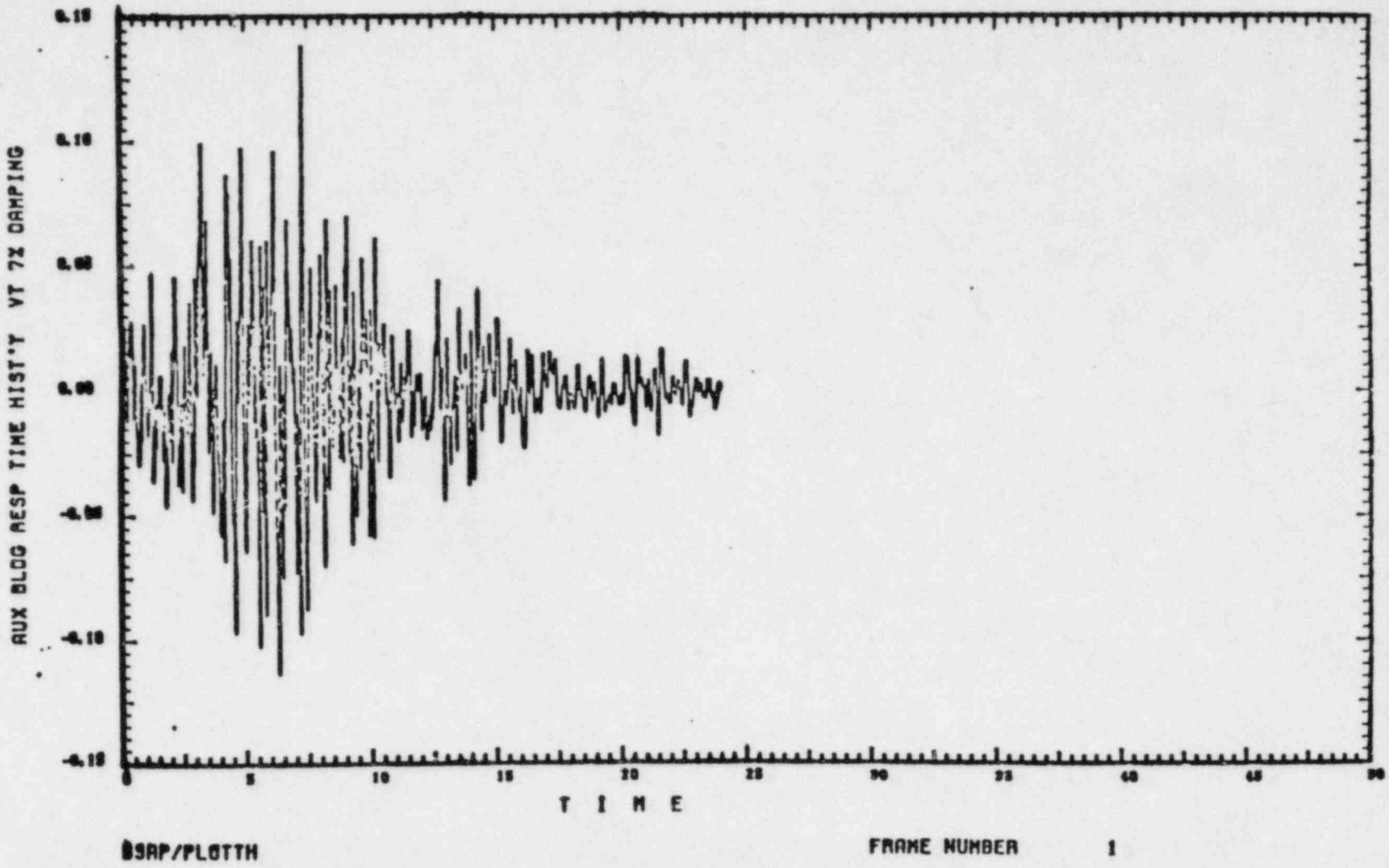

Figure 31 SEISMIC RESPONSE TIME HISTORY AT EL 166'-0" OF AUX BLDG SPENT FUEL POOL (VERTICAL SSE 7% DAMPING)

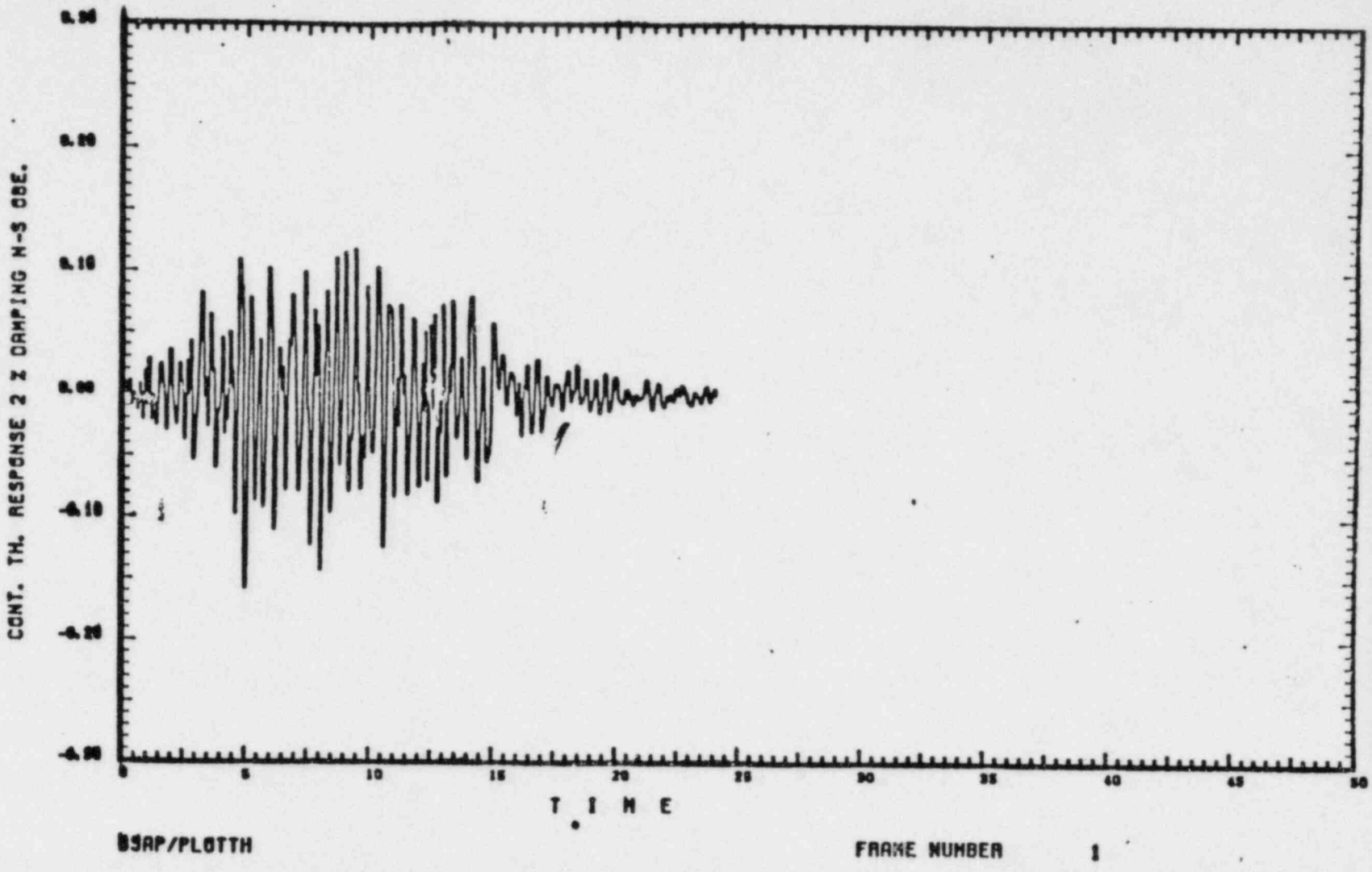

Figure 32 SEISMIC RESPONSE TIME HISTORY AT EL 161'-10" OF UPPER CONTAINMENT POOL HORIZONTAL N-S OBE 2% DAMPING

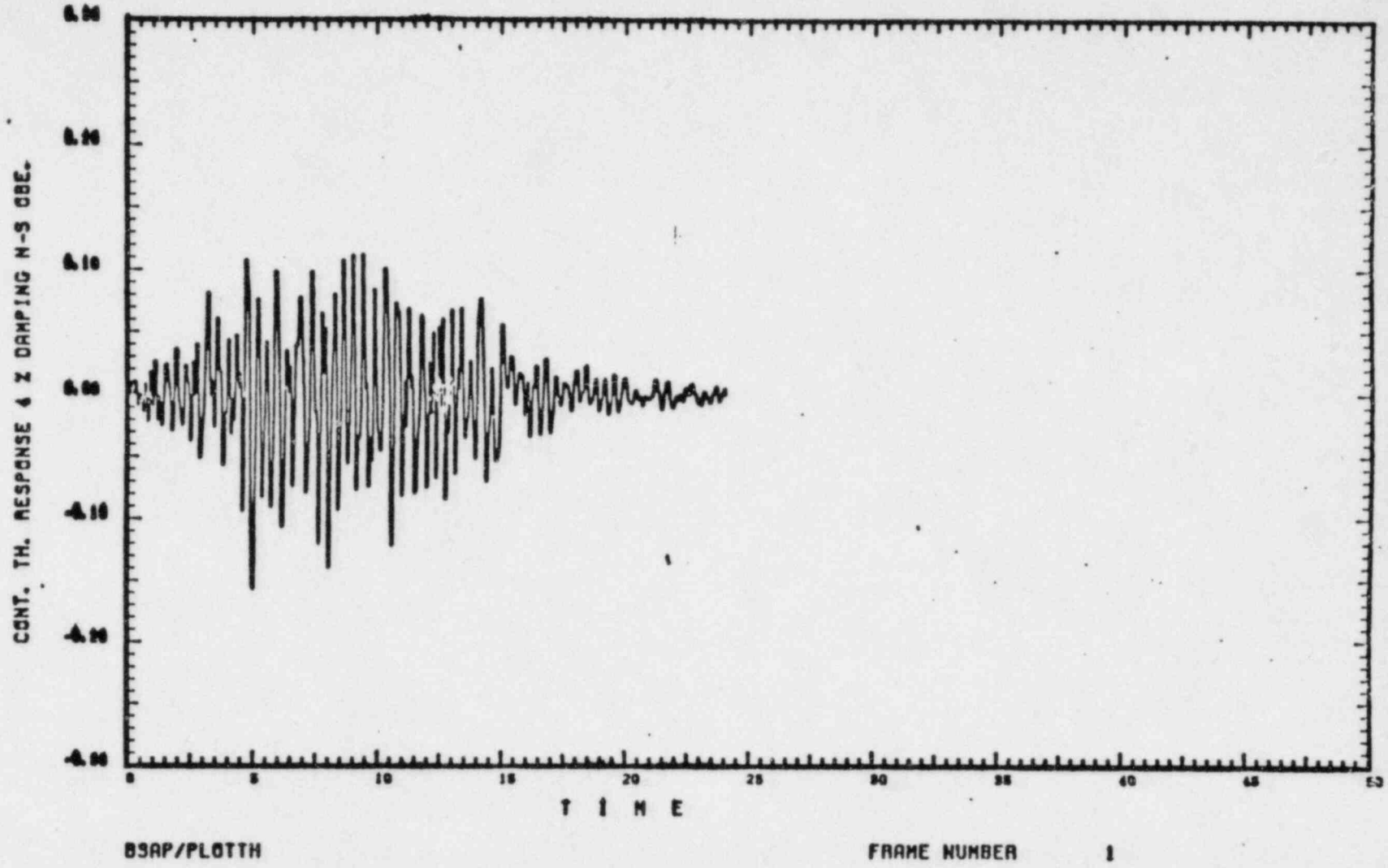

Figure 33 SEISMIC RESPONSE TIME HISTORY AT EL 161'-10" OF UPPER CONTAINMENT POOL HORIZONTAL N-S OBE 4% DAMPING

CE20I811-1 T70961 072782

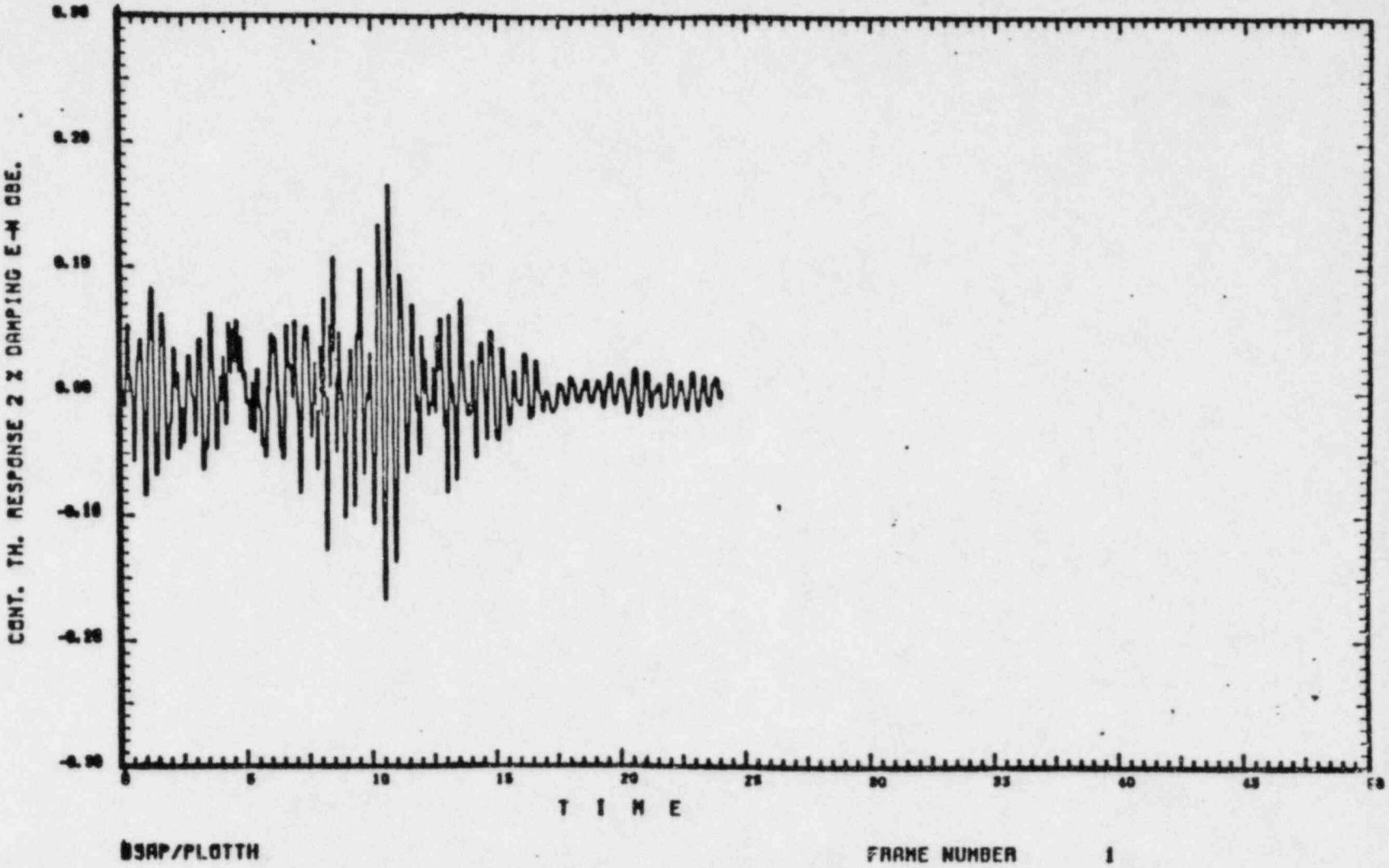

Figure 34 SEISMIC RESPONSE TIME HISTORY AT EL 161'-10" OF UPPER CONTAINMENT POOL HORIZONTAL E-W OBE 2% DAMPING

CE201811-1 T70381 072782

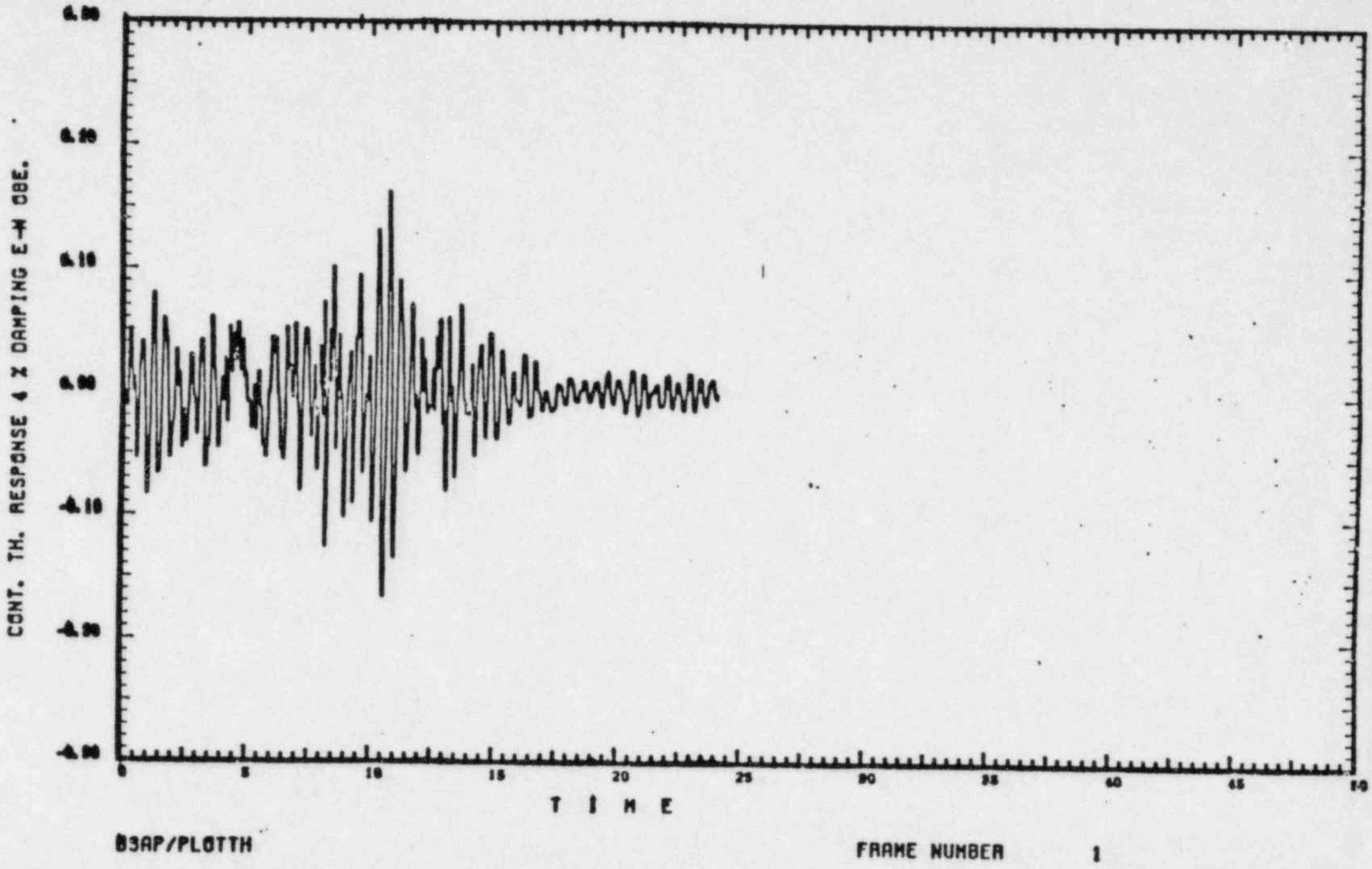

Figure 35 SEISMIC RESPONSE TIME HISTORY AT EL 161'-10" OF UPPER CONTAINMENT POOL HORIZONTAL E-W OBE 4% DAMPING

CE201811-1 T70381 072782

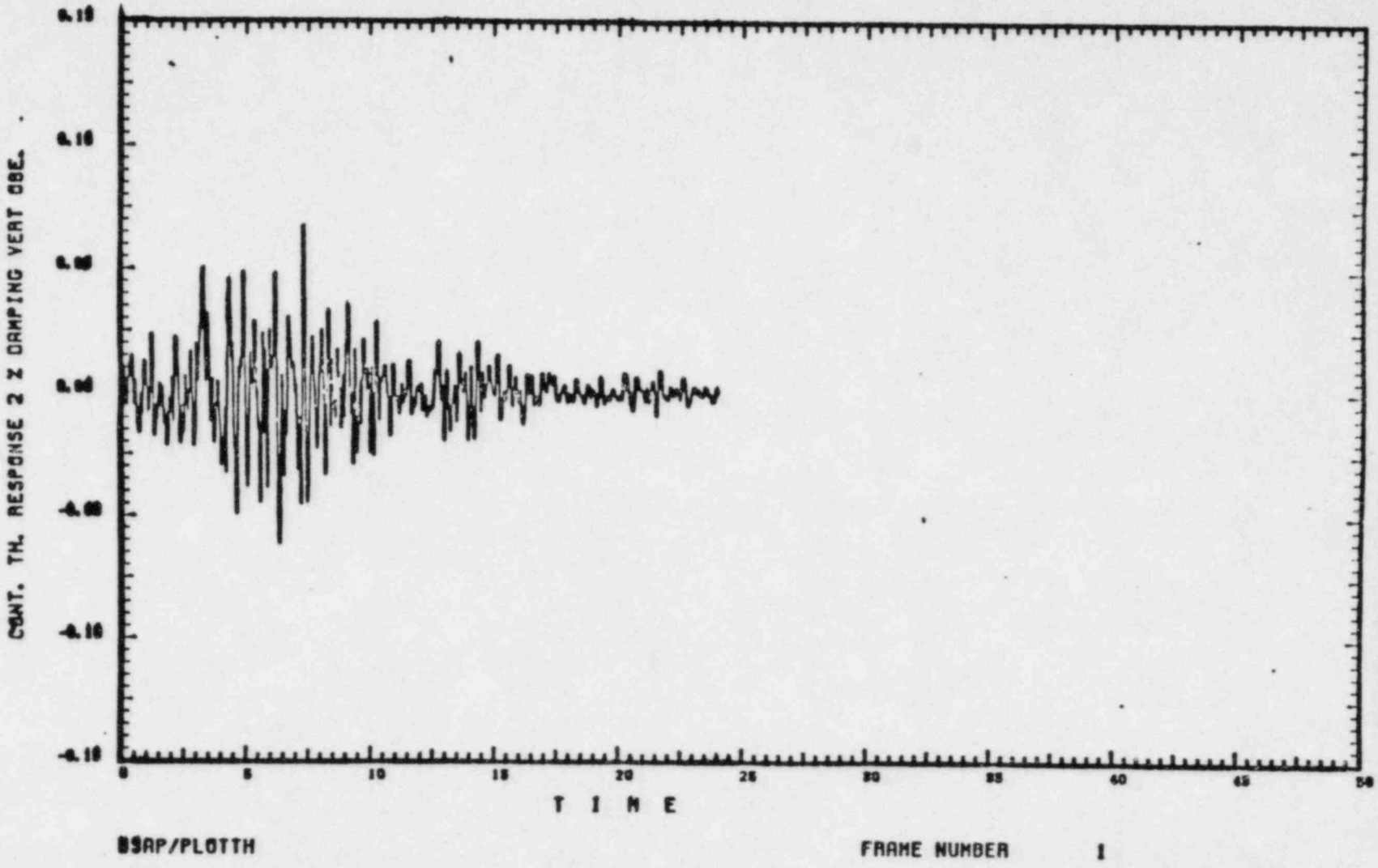

Figure 36 SEISMIC RESPONSE TIME HISTORY AT EL 161'-10" OF UPPER CONTAINMENT POOL VERTICAL OBE 2% DAMPING

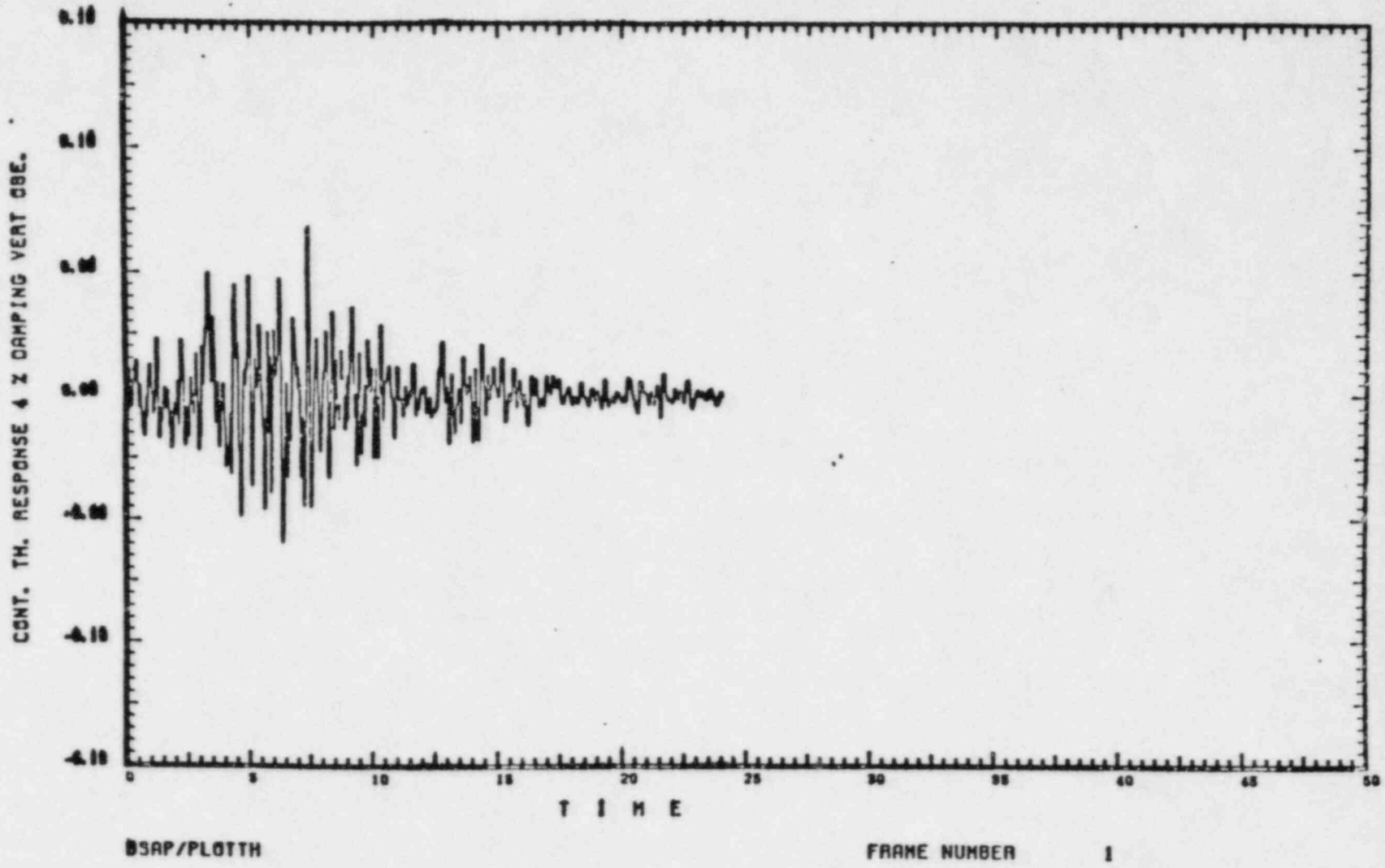

Figure 37 SEISMIC RESPONSE TIME HISTORY AT EL 161'-10" OF UPPER CONTAINMENT POOL VERTICAL OBE 4% DAMPING

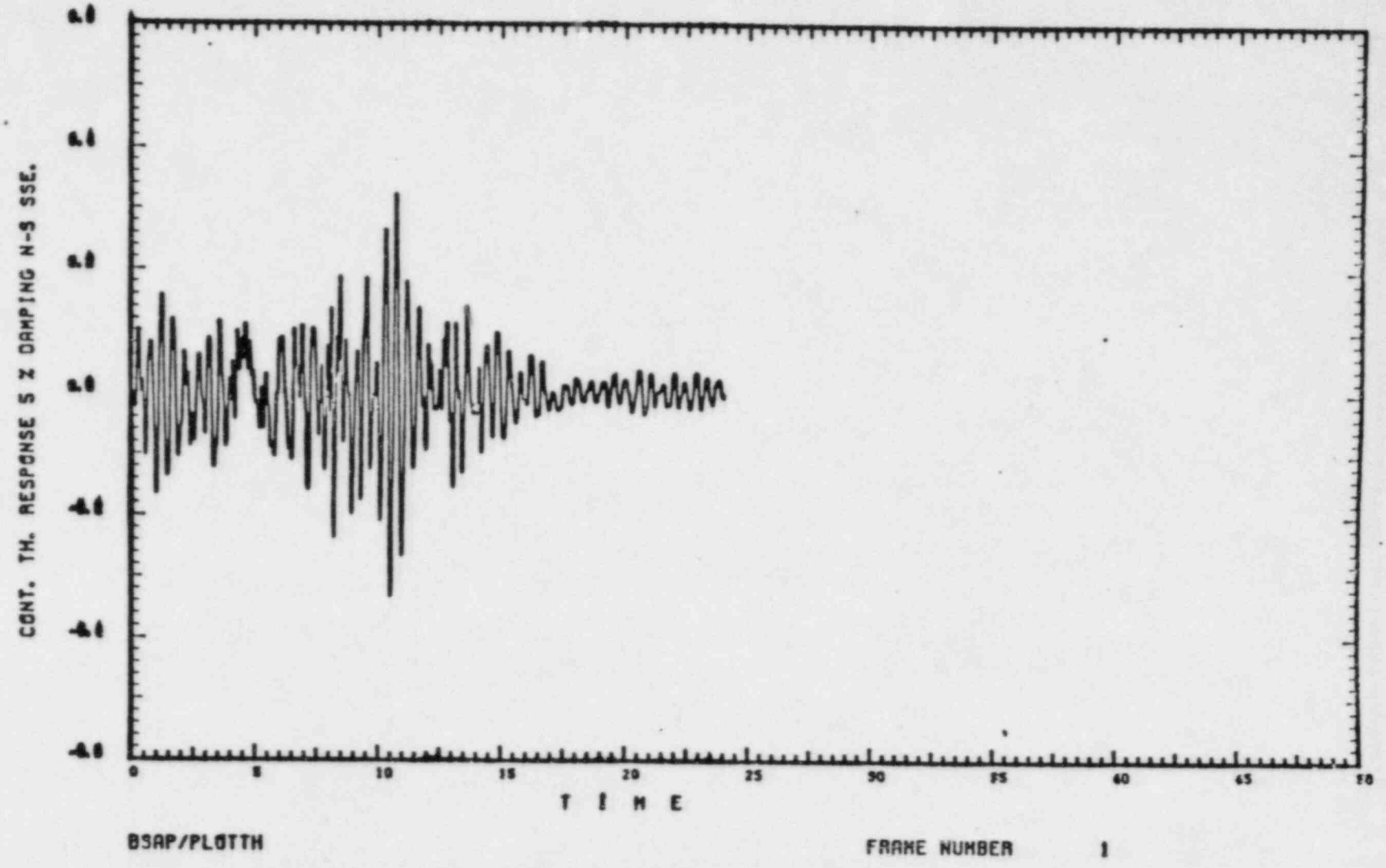

Figure 38 SEISMIC RESPONSE TIME HISTORY AT EL 161'-10" OF UPPER CONTAINMENT POOL HORIZONTAL N-S SSE 5% DAMPING

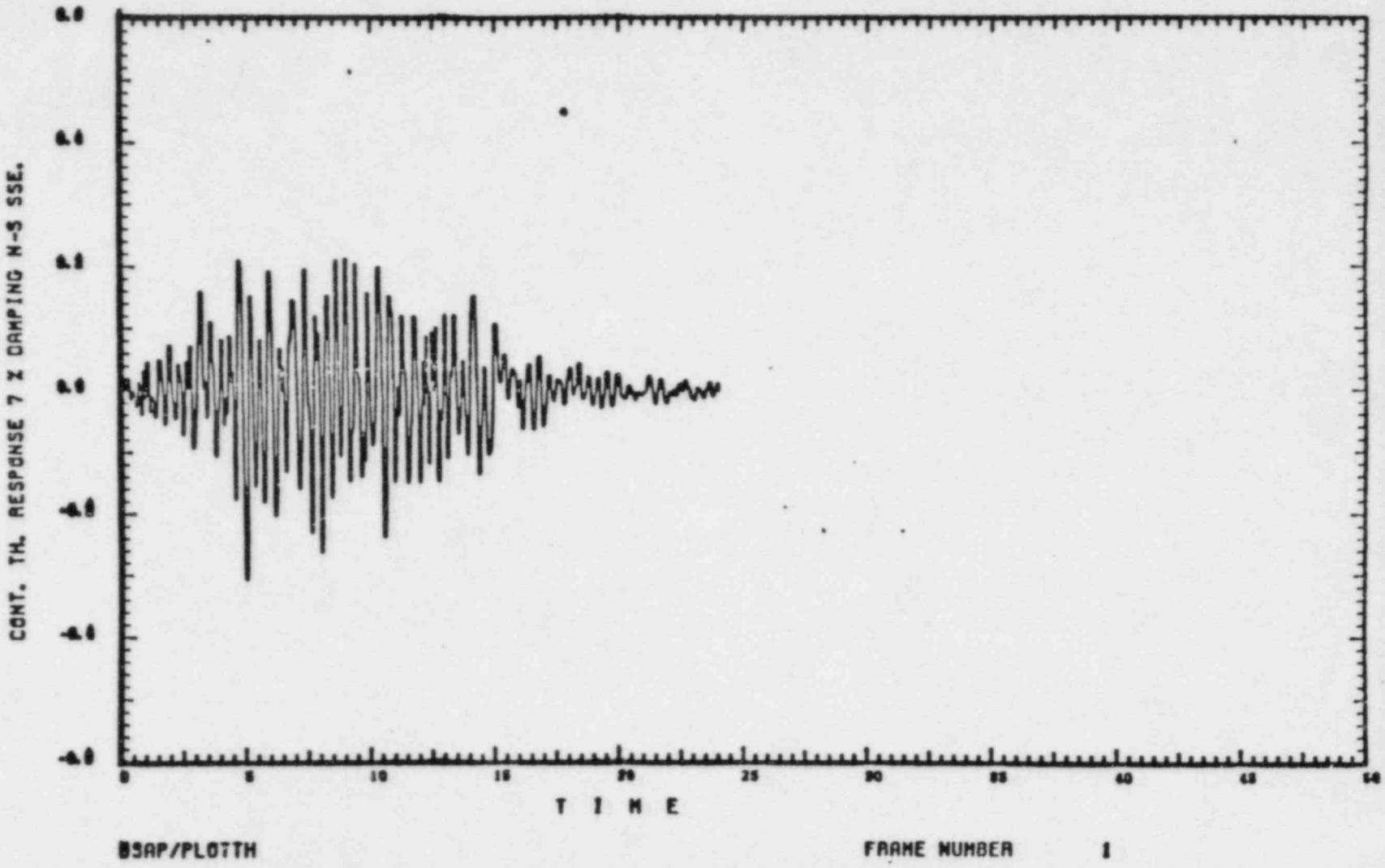

Figure 39 SEISMIC RESPONSE TIME HISTORY AT EL 161'-10" OF UPPER CONTAINMENT POOL HORIZONTAL N-S SSE 7% DAMPING

CE201811-1 T70981 072782

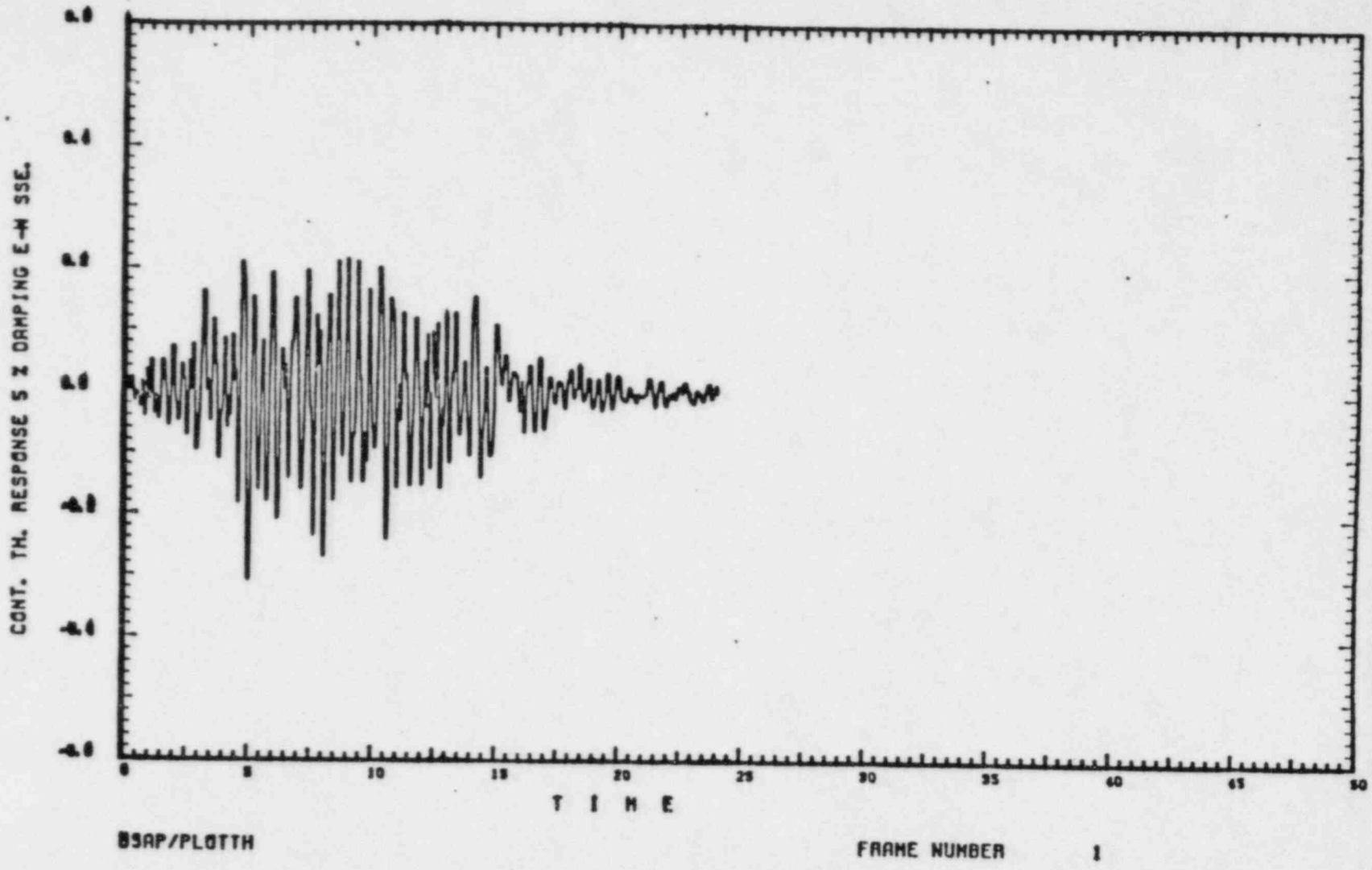

Figure 40 SEISMIC RESPONSE TIME HISTORY AT EL 161'-10" OF UPPER CONTAINMENT POOL HORIZONTAL E-W SSE 5% DAMPING

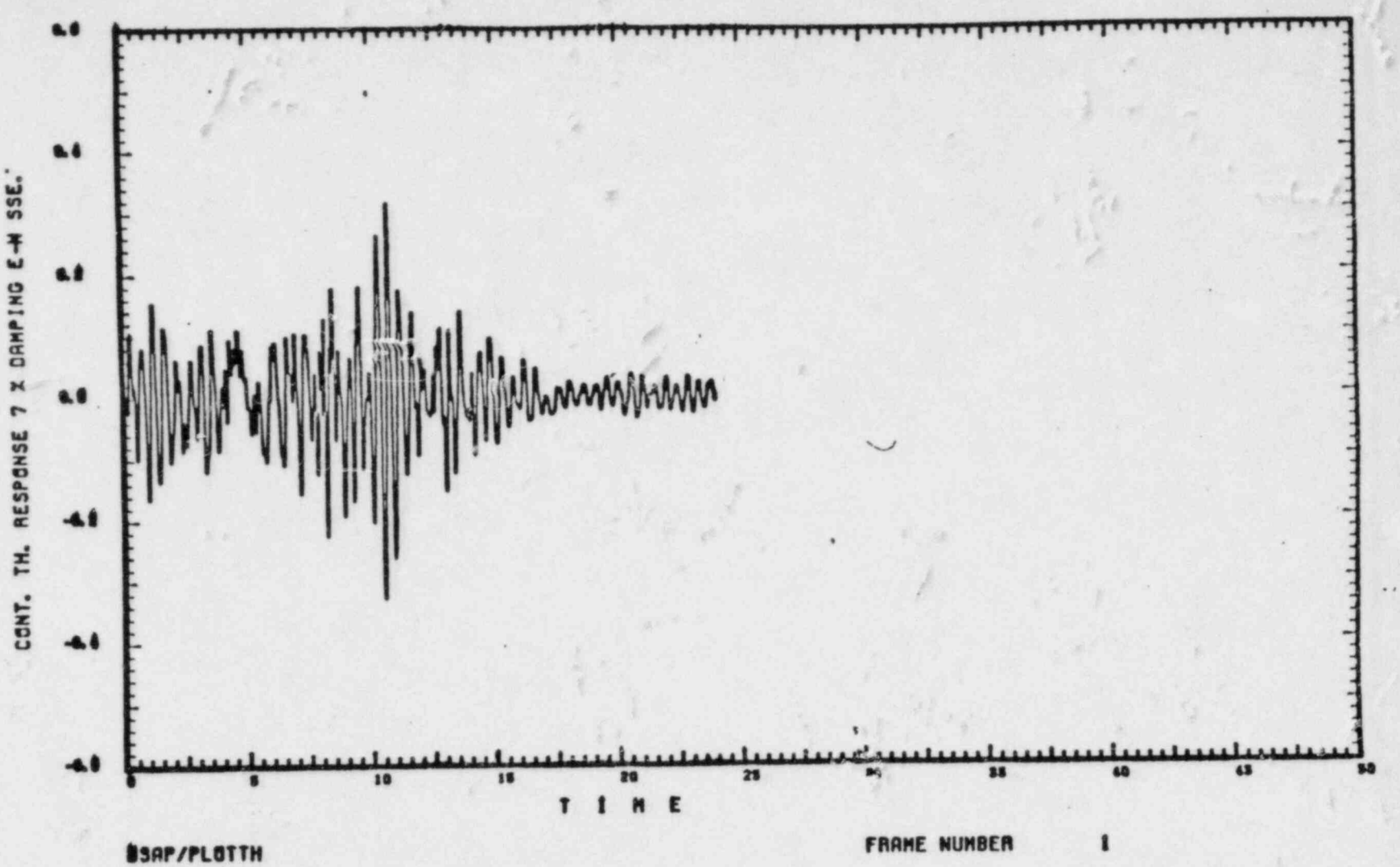

Figure 41 SEISMIC RESPONSE TIME HISTORY AT EL 161'-10" OF UPPER CONTAINMENT POOL HORIZONTAL E-W SSE 7% DAMPING

CE201811-1 T70581 072782

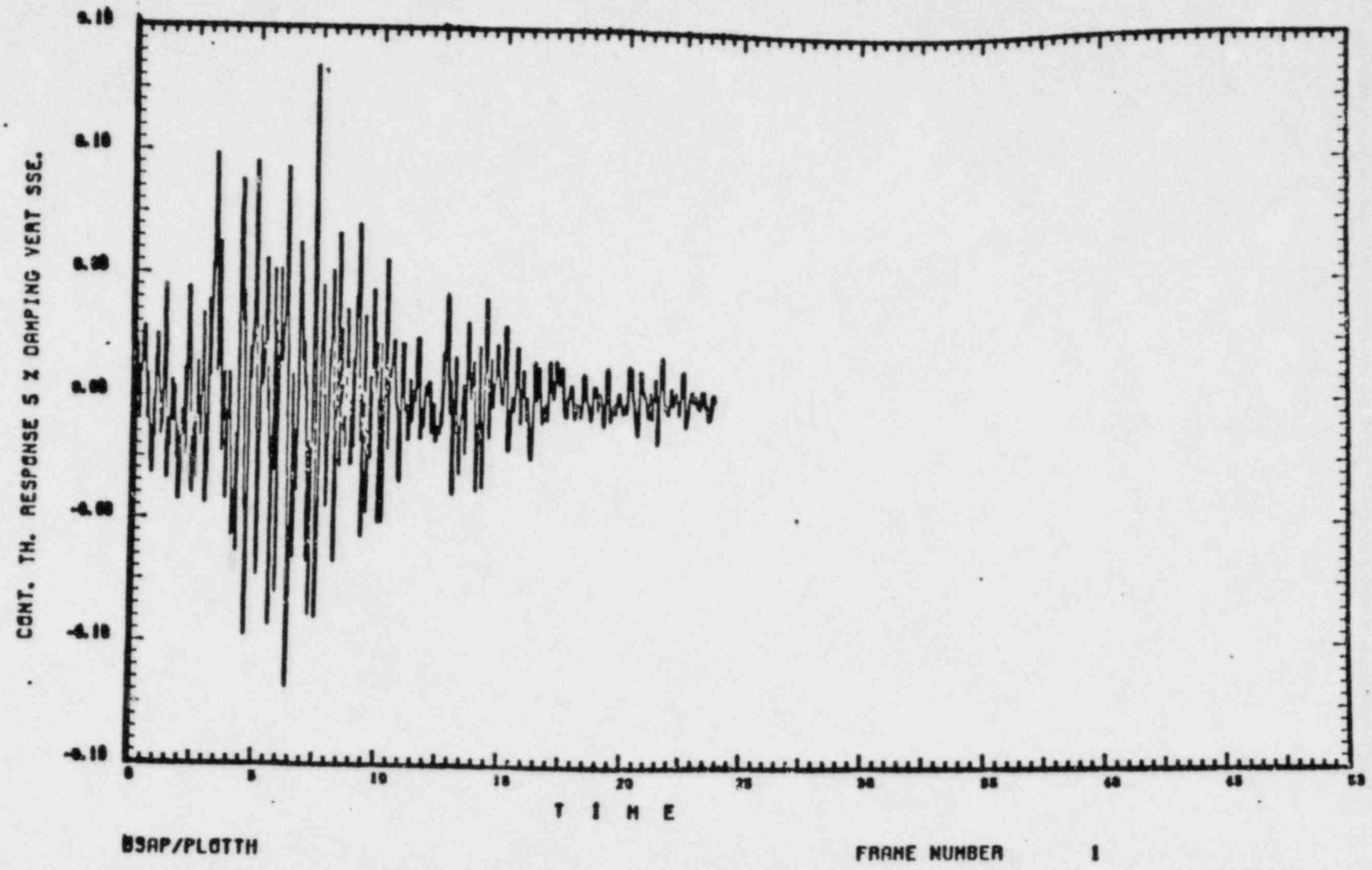

Figure 42 SEISMIC RESPONSE TIME HISTORY AT EL 161'-10" OF UPPER CONTAINMENT POOL VERTICAL SSE 5% DAMPING

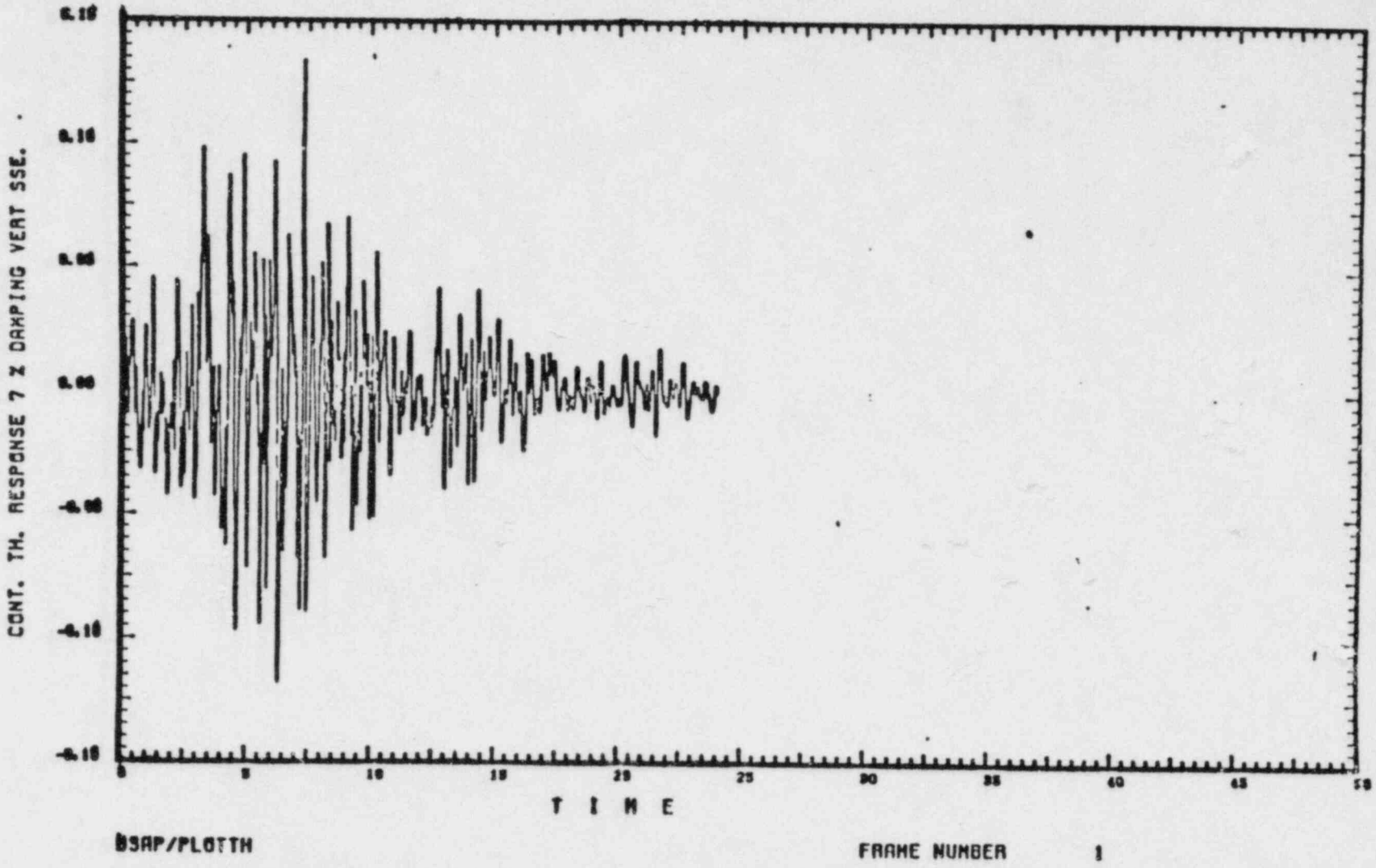

Figure 43 SEISMIC RESPONSE TIME HISTORY AT EL 161'-10" OF UPPER CONTAINMENT POOL VERTICAL SSE 7% DAMPING

Neutron Absorber Traceability

A general description of the Quality Assurance (QA) Program utilized by the Joseph Oat Corporation during the fabrication of the GGNS high density spent fuel racks (HDSFR) is described in Chapter 12 of the HDSFR Licensing Report. As described in Chapter 12, the Joseph Oat QA program was established to meet the intent of 10CFR50, Appendix B. In order to ensure proper implementation of the program requirements, MP&L's QA and Nuclear Plant Engineering organizations monitored various phases of the HDSFR construction and fabrication process.

The acceptance criteria for criticality calculations is that k_{eff} be less than or equal to 0.95, including all uncertainties. To meet this criteria, the minimum B10 areal density of 0.0175 g/cm^2 was established to determine the minimum acceptable specific gravity of the neutron absorber (Boraflex). This determination is explained in more detail in Section 4.4.3 of the HDSFR Licensing Report. During the manufacture of the Boraflex, testing was conducted on samples from each batch to establish that the minimum areal density was met.

The Boraflex test documentation for each batch, fabrication drawings, and shop travelers provide a basis for traceability of boron content throughout the rack manufacturing process. Thus, the Boraflex material used in each cruciform, "T" sub-assembly, and corner angle sub-assembly of the racks can be traced to this batch documentation.

Based on the above discussion, MP&L is confident that the HDSFR manufactured for GGNS meets the design criteria for boron content and criticality control.